Analysis of Crystallographic Texture Information by the Hyperspherical Harmonic Expansion

by

Jeremy K. Mason

S.B., Physics (2005)

Massachusetts Institute of Technology

MASSACHUSETTS INSTITUTE OF TECHNOLOGY
JUL 28 2009
LIBRARIES

ARCHIVES

Submitted to the Department of Materials Science and Engineering
in Partial Fulfillment of the Requirements for the Degree of
Doctor of Philosophy in Materials Science and Engineering

at the

Massachusetts Institute of Technology

June 2009

© 2009 Massachusetts Institute of Technology
All rights reserved

Signature of Author.....
Department of Materials Science and Engineering
May 18, 2009

Certified by .....
Christopher Schuh
Danae and Vasilios Salapatas Associate Professor of Metallurgy
Thesis Supervisor

Accepted by .....
Christine Ortiz
Chair, Departmental Committee on Graduate Students

Analysis of Crystallographic Texture Information by the Hyperspherical Harmonic Expansion

by

Jeremy K. Mason

Submitted to the Department of Materials Science and Engineering on May 18, 2009 in Partial Fulfillment of the Requirements for the Degree of Doctor of Philosophy in Materials Science and Engineering

Abstract

The field of texture analysis is fundamentally concerned with measuring and analyzing the distribution of crystalline orientations in a given polycrystalline material. Traditionally, the orientation distribution function describing crystallographic orientation information is written as a linear combination of the generalized spherical harmonics. Since the use of generalized spherical harmonics requires that orientations be described by sets of Euler angles, the field of texture analysis suffers from the inherent limitations of Euler angles. These include difficulty of presentation and interpretation, discontinuous changes in the description of a changing orientation, and singularities in many equations of Euler angles. An alternative expansion of the orientation distribution function as a linear combination of the hyperspherical harmonics is therefore proposed, with the advantage that this expansion allows rotations to be described by angles that directly relate to the axis and angle of a rotation. Apart from the straightforward and intuitive presentation of orientation statistics that this allows, the utility of the hyperspherical harmonic expansion rests on the fact that the orientation distribution function inherits the useful mathematical properties of the hyperspherical harmonics. The relationship of the hyperspherical harmonics to the three- and four-dimensional rotation groups is investigated, and expressions for the matrix elements of the irreducible representatives of these rotation groups as linear combinations of the hyperspherical harmonics are found. These expressions allow an addition formula for the hyperspherical harmonics to be derived, and provide the means to write a simple conversion between the generalized spherical harmonic and hyperspherical harmonic expansions. This allows results derived via the hyperspherical harmonic expansion to be related to the texture analysis literature. Furthermore, a procedure for calculating the symmetrized hyperspherical harmonics consistent with crystal and sample symmetries is indicated, and used to perform the expansion of an orientation distribution function significantly more efficiently. The capability of the hyperspherical harmonic expansion to provide results not traditionally accessible is demonstrated by the generalization of the Mackenzie distribution to arbitrary textures. Finally, further areas where the application of the hyperspherical harmonic expansion is expected to advance the field of texture analysis are discussed.

Thesis Supervisor: Christopher Schuh
Title: Danae and Vasilios Salapatas Associate Professor of Metallurgy

Table of Contents

List of Figures

Figure 7: A collection of discrete orientations from a copper textured material with cubic crystal symmetry, depicted in the fundamental zone of Rodrigues space. (a) The cubic fundamental zone containing the origin is a truncated cube with six octagonal faces and eight triangular faces. (b) The distribution is conventionally plotted in equidistant sections perpendicular to the r_3 axis.

Figure 8: A collection of discrete orientations from a copper textured material with cubic crystal symmetry, depicted in (a) the three dimensions inhabited by the vector part **q** of a quaternion q, and (b) in two dimensions as a collection of stereographic projections of concentric spherical shells of the space in (a). This presentation is naturally suited to the spherical shape of the space, and has the advantage that the rotation angle is constant within a given spherical shell, promoting an intuitive interpretation of points displayed in this format.

Figure 9: Definition of the orientation of a coordinate system, following the conventional interpretation of the Euler angles. The orientation is determined as the result of three consecutive rotations, performed about z, x', and z'' axes by the angles ϕ_1, Φ, and ϕ_2, respectively.

Figure 10: A collection of discrete orientations from a copper textured material with cubic crystal symmetry, depicted in Euler angle space. (a) The conventional volume used for cubic crystal symmetry and orthorhombic sample symmetry is bounded by planar surfaces, but contains three fundamental zones. (b) The distribution is conventionally plotted in equidistant sections perpendicular to the ϕ_2 axis.

Figure 11: {111} pole figures of the continuous pole distributions for (a) a cube texture, (b) a copper texture, and (c) a brass texture, corresponding to the respective discrete pole figures in Figure 4. The distribution functions are determined by Equation (15), with $l_{\max} = 15$. Regions of finite probability density appear in some areas that are empty in the corresponding discrete pole figures due to the use of a limited number of terms, while regions of negative probability density were removed by applying a positivity constraint.

Figure 12: Continuous Euler angle distribution for the crystal orientations in a copper textured material, corresponding to the collection of discrete orientations in Figure 10. The distribution function is determined by Equation (18), with $l_{\max} = 12$. (a) A single contour of the distribution function in the conventional volume used for cubic crystal symmetry and orthorhombic sample symmetry. (b) The distribution function, sectioned perpendicular to the ϕ_2 axis. Regions of finite probability density appear in some areas that are empty in Figure 10b due to the use of a limited number of terms, while regions of negative probability density were removed by applying a positivity constraint.

Figure 13: Relationship shared by the axis-angle parameterization of a rotation, the quaternion parameterization of a rotation, and the parameterization of a quaternion by three angles. (a) A three-dimensional rotation by the angle ω about the unit vector **n**, pointing along the axis of rotation. The direction of **n**

is specified by the angles θ and ϕ. (b) The vector part $\mathbf{q}$ of the quaternion q, corresponding to the rotation in (a). The vectors $\mathbf{q}$ and $\mathbf{n}$ point in the same direction, though the length of $\mathbf{q}$ is $\sin(\omega/2)$ rather than one.

Figure 14: Continuous quaternion distribution for the crystal orientations in a copper textured material, corresponding to the collection of discrete quaternions in Figure 8. The distribution function is determined by Equation (31), with $n_{\max} = 24$. (a) A single contour of the distribution function in the space of the vector part $\mathbf{q}$ of a quaternion q. (b) The distribution function, shown in two dimensions as stereographic projections of concentric spherical shells of the space in (a). Regions of finite probability density appear in some areas that are empty in Figure 8b due to the use of a limited number of terms, while regions of negative probability density were removed by applying a positivity constraint.

Figure 15: A random texture, corresponding to a uniform distribution of points on the surface of the unit four-dimensional sphere, presented using the volume-preserving (4D to 3D) and equal-area (3D to 2D) projections. The equal-area projection causes the uniformity of the distribution for a particular rotation angle, and the volume-preserving projection causes the uniformity of the distribution among the various rotation angles.

Figure 16: The physical interpretation and relationship of the quantities $T_l^{m'm}(\phi_1, \Phi, \phi_2)$, $D^l_{m'm}(\phi_1, \Phi, \phi_2)$, and $U^l_{m'm}(\omega, \theta, \phi)$. $T_l^{m'm}(\phi_1, \Phi, \phi_2)$ is considered to passively bring the coordinate system into coincidence with an oriented crystal. $D^l_{m'm}(\phi_1, \Phi, \phi_2)$ is considered to actively bring an oriented crystal into coincidence with the coordinate system; this is identical to the effect of $T_l^{m'm}(\phi_1, \Phi, \phi_2)$ from the perspective of an observer attached to the coordinate system. $U^l_{m'm}(\omega, \theta, \phi)$ is considered to actively bring a reference crystal into coincidence with the oriented crystal; this is the inverse of the effect of $D^l_{m'm}(\phi_1, \Phi, \phi_2)$.

Figure 17: The normal direction inverse pole figure of a copper sample, as measured experimentally by EBSD.

Figure 18: The ODF of the copper sample in Figure 17, expressed via the hyperspherical harmonic expansion given in Equation (96). Blue and red indicate regions of positive and negative probability density, respectively. (a) The coefficients of the expansion are calculated using Equation (97). (b) The coefficients of the expansion are calculated using Equations (95) and (122), i.e. by means of the coefficient conversion formulas. Inspection of the figures reveals that the expansions are identical.

Figure 19: The ODF given in Figure 18a, constrained to positive values by the procedure described in Section 4.6. Apart from the removal of the regions of negative probability density and a slight broadening of the peaks, the distribution function is identical.

Figure 20: An example of the reduction in the number of linearly independent harmonics required for the expansion of a function on the surface of a sphere with cubic point group symmetry; blue and red correspond to positive and negative values respectively. (a) The nine spherical harmonics defined by Equation (14) for $l = 4$. The value of the index m is indicated above the columns, with the harmonics Y_l^{mc} on the top and Y_l^{ms} on the bottom of a given column. (b) The single linear combination of the harmonics in (a) that satisfies the requirements of cubic point group symmetry.

Figure 21: Examples of the symmetrized hyperspherical harmonics, as calculated from the tables of coefficients in Appendix E. Specifically, these are sets of the three lowest-order, non-trivial symmetrized hyperspherical harmonics for orthorhombic sample symmetry and for the crystal point symmetries (a) 222, (b) 422, and (c) 432. In each of the projections, the z and x axes of the projections point out of the page and to the right, respectively.

Figure 22: Conventional methods of viewing a simulated cube texture. (a) The (100) and (b) (111) pole figures are presented in stereographic projection, with the z and x axes pointing out of the page and up the page, respectively. (c) The blue and red regions in the Euler angle space indicate regions of positive and negative probability density, respectively.

Figure 23: The current method of viewing a simulated cube texture. The z and x axes of the projections point out of the page and to the right, respectively. (a) Projection of the discrete quaternions corresponding to the simulated texture, including all of the rotations in the crystallographic point group 432. (b) ODF corresponding to the discrete distribution of part (a), calculated using the first thirty-seven hyperspherical harmonics of orthorhombic sample symmetry and cubic crystal symmetry. Blue and red regions indicate regions of positive and negative probability density, respectively.

Figure 24: Conventional methods of viewing a simulated copper texture. (a) The (100) and (b) (111) pole figures are presented in stereographic projection, with the z and x axes pointing out of the page and up the page, respectively. (c) The blue and red regions in the Euler angle space indicate regions of positive and negative probability density, respectively.

Figure 25: The current method of viewing a simulated copper texture. The z and x axes of the projections point out of the page and to the right, respectively. (a) Projection of the discrete quaternions corresponding to the simulated texture, including all of the orientations described in Ref. [89]. (b) ODF corresponding to the discrete distribution of part (a), calculated using the first thirty-seven hyperspherical harmonics of orthorhombic sample symmetry and cubic crystal symmetry. Blue and red regions indicate regions of positive and negative probability density, respectively.

Figure 26: The cubic orientation (light lines) and disorientation (bold lines) spaces, displayed in the orthographic projection of the quaternion space. The solid

points mark the intersection of the axes with the surface of the orientation space. The q_i are the components of the vector part of the quaternion.

Figure 27: {100} pole figure plots for simulated cube textures of varying degrees of sharpness, plotted in equal area projection. The angles indicate the maximum allowed disorientation angle of a cubic crystal from the reference orientation. The normal direction is out of the page, and the rolling direction is vertical in the plane of the page.

Figure 28: Disorientation angle distribution functions corresponding to simulated cube textures of varying degrees of sharpness (cf. Figure 27). Labels given in degrees indicate the maximum allowed disorientation angle of a cubic crystal from the reference orientation (smaller values denote sharper textures), while the heavy dark line corresponds to a material in which every misorientation is equally likely.

Figure 29: Disorientation angle distribution function for a copper texture, assuming the absence of correlations relating the orientations of neighboring grains or relating the orientation and shape of a single grain. The solid line is the result of our simulation, while the bars indicate the probability density for an experimental material with a similar texture, as measured by Mishin, Gertsman and Gottstein [106]. The dashed line corresponds to a material in which every misorientation is equally likely (i.e., the Mackenzie distribution).

Figure 30: Representative triple junction depicting the physical significance of the quantities ω and ϕ. Grain A is rotated by the angle ω_A and is located opposite the boundary with orientation ϕ_A; a similar geometry applies for grains B and C.

Figure 31: Comparison of the quantities used to define the state of a grain boundary. A single boundary is depicted in terms of (a) ω, ω' and ϕ and (b) θ and φ. Notice that in (b) the grains share the misorientation equally, resulting from a rotation of the system in (a).

Figure 32: Labeling scheme for the grain rotations ω and the quantities θ and φ around a triple junction. The misorientations θ are the rotations that bring the grain at the tail of the arrow into coincidence with the grain at the head. Our labeling scheme differs in sense from some similar examples in the literature [97].

Figure 33: Lattices of symmetrically equivalent points and corresponding unit cells for θ and φ at a single grain boundary. (a) θ and φ display independent periodicities of ω_s and $\omega_s/2$, respectively, resulting in a rectangular lattice and simply described boundaries. (b) θ and φ display joint periodicities, leading to a sparser lattice, an extended range of unique quantity pairs, and more complicated boundaries.

Figure 34: Lattices of symmetrically equivalent points and corresponding unit cells for θ_A, θ_B and θ_C at a triple junction. (a) θ_A, θ_B and θ_C each display independent periodicities of ω_s, resulting in a cubic lattice. The size of the markers indicates the relative positions of points residing in the three (111) type

planes shown. (b) The three misorientations display joint periodicities, such that the lattice resides entirely in the (111) plane and each lattice point satisfies the constraint $\theta_A + \theta_B + \theta_C = 0$.

Figure 35: Representation of the distribution functions for misorientations about a triple junction. Triple junctions are classified by the number of misorientations smaller in magnitude than θ_t; for this figure, $0 \le \theta_t < \omega_s/3$. Darker shading corresponds to more special boundaries, e.g., white is a J_0 region, and dark grey is a J_3 region. Solid lines indicate unit cell borders in the current representation, and dashed lines in the alternate representation. (a) Classification of triple junctions as defined by Equation (211). For clarity of representation, the distribution is projected into the plane spanned by θ_A and θ_B. This representation is preferred for integration due to the simplicity of the equations of the region boundaries. (b) Classification of the triple junction distribution defined by Equation (209). Bands of special boundaries occur in a high symmetry configuration, and classification is continued outside of the fundamental zone to emphasize this symmetry. The three regions in dashed lines correspond to the three parallel planes that intersect the unit cell appearing in Figure 34a.

Figure 36: Analytic solutions for the special fraction of boundaries in correlated boundary networks, for the specific case where ω is uniformly distributed on the interval $-\omega_{\max} \le \omega < \omega_{\max}$, and $\theta_t = \omega_s/6$ with ω_s the angle of rotational symmetry of the crystallites. Our exact solution (Equation (213)) is given by the solid black line, and is valid over the full range of $\omega_{\max}/\omega_s$. The vertical dashed lines appear at $\omega_{\max} = \theta_t/2$ and $\omega_{\max} = \omega_s/2 - \theta_t/2$. The solutions of Frary and Schuh [97] and Van Siclen [98] are represented by the dashed grey line, which deviates for $\omega_{\max} < \theta_t/2$ and excludes the effects of crystal symmetry for $\omega_s/2 - \theta_t/2 < \omega_{\max}$. A further result for $\omega_{\max} = \omega_s/2$, found by Van Siclen, is denoted by the black dot. Equation (222), our simplification for sharp textures, is shown by the series of grey points.

Figure 37: Triple junction fractions plotted as a function of the special boundary fraction in correlated boundary networks, for the specific case where ω is distributed uniformly on the interval $-\omega_{\max} \le \omega < \omega_{\max}$. For comparison, the dotted lines show the predicted triple junction fractions for a random (uncorrelated) spatial distribution of misorientations. Solutions by Frary and Schuh [97] and Van Siclen [98] for $\omega_{\max} < \omega_s/2 - \theta_t/2$ appear as the solid lines, and the specific case derived by Van Siclen for $\omega_{\max} = \omega_s/2$ is given by the dashed lines. Our solutions, presented in Appendix I, migrate continuously over the regions shaded in grey with changes in the values of ω_s and θ_t.

1. State of the Field[1]

The field of materials science and engineering is fundamentally concerned with manipulating the microstructure of materials in order to control their properties. Recent improvements in instrumentation, which include electron backscatter diffraction (EBSD), dramatically enhance our abilities in this regard by providing extensive crystallographic orientation information of a given two-dimensional section of a microstructure. As this technique has been developed and combined with chemical analysis and serial sectioning methods, it has become possible to access complete three-dimensional chemistry, phase, and crystal orientation information; in short, the microstructural state of a polycrystal may now be completely quantified.

While these techniques allow an unprecedented opportunity for examining the microstructure-property relationships of materials, in many cases the controlling physics depend on only a relatively small subset of the available information. For example, a variety of the effective tensor properties of materials (e.g. elasticity and transport coefficients) as well as inherently anisotropic, nonlinear properties at the single crystal level (e.g. plasticity and cracking) are governed primarily by the crystallographic texture, or the distribution of crystal orientations within a polycrystal. When properties of this type are of interest, it may be reasonable to simplify the analysis of a material by neglecting the spatial information of the microstructure and examining only the orientations of the crystalline grains.

Figure 1 illustrates schematically the process of abstraction that is useful when studying texture and the effects of texture on material properties. Figure 1a shows a complete microstructure, reconstructed from a progression of EBSD maps obtained through serial sectioning, where each grain is colored differently according to its orientation. The central purpose of texture representation is to preferentially examine the orientation of the crystallites without concern for their spatial characteristics, e.g. their arrangement, size and morphology; to this end, Figure 1b shows a schematic representation of the distribution of discrete orientations sampled from the polycrystal. Numerous alternatives exist for the representation of texture information, and these will

[1] The content of this chapter has previously been published in Ref. [1].

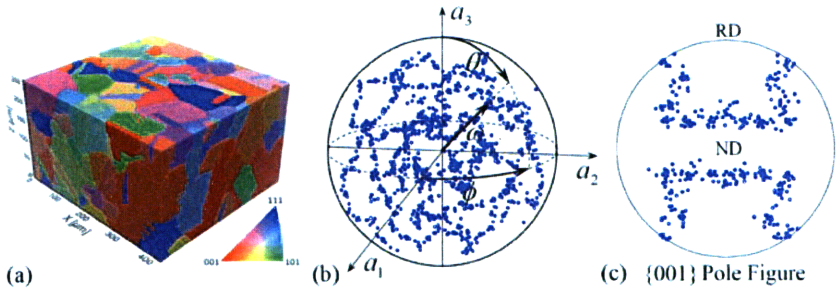

Figure 1: The progressive abstraction of microstructural information. (a) Three-dimensional reconstruction of the microstructure of a commercial austenitic stainless steel; reproduced from Figure 5 of Ref. [2], with kind permission of Springer Science and Business Media. (b) Axis-angle representation of the texture of a crystalline material, completely characterizing the crystallographic orientations present. (c) Stereographic projection indicating the orientation of {100} crystallographic planes of a material with a copper texture.

be covered at length later in this chapter. However, all of these alternatives, including that used in Figure 1b, significantly distill the dataset represented by Figure 1a. Even more selective presentation of texture information is not only sometimes feasible, but may be necessary; in certain situations, only a portion of the orientation information is relevant or readily accessible. For example, many properties depend predominantly on the orientation of a single crystallographic axis, as for the *c* axis in transversely isotropic crystals. The representation of these crystallographic axes, or poles, is illustrated in Figure 1c.

The paradigm of data reduction and distillation exemplified in Figure 1 is not only powerful, but necessary. The acquisition of increasing amounts of data, in and of itself, does not provide the insights that advance the field. These insights depend entirely upon the depth of our understanding, and therefore on the skillful and judicious refinement of the data to a form that is both transparent and useful. Unfortunately, as with many unintuitive subjects, the essential content may be unintentionally obscured, or even discarded, during the process of simplification; in the case of crystallographic texture, it is altogether too easy to abandon the most critical information in the interest of depicting the data in a familiar form.

We explore the abstractions of Figure 1 in this chapter, both in a general sense and with specific emphasis on forms common in the materials science community. Since

this chapter is intended as an overview of a complex and well-developed field, the reader is referred to various works in the literature for more complete mathematical treatments as the need arises, e.g., Morawiec [3] and Bunge [4].

1.1. Rotations and Orientations

EBSD measures the discrete crystallographic orientations of volume elements arranged in a regular manner on the surface of a material. The analysis of material texture therefore begins with an examination of the available methods to parameterize discrete crystallite orientations and present the accumulated orientation information in a clear and concise format. Of course, this requires the definition of an orientation, which in turn requires the definition of a rotation.

1.1.1. Defining a Rotation

While often not appreciated, a certain amount of precision is necessary in the definition of a rotation to be able to relate the rotation to the orientation of a particular object. For example, we may be provided with a rotation matrix, but unless the quantity on which the matrix acts and a method for applying the matrix are specified, the resulting orientation is obscured. One difficulty is that two conventions for defining a rotation appear in the literature, known as the active and passive conventions.

An active rotation is defined as a transformation of space relative to a stationary coordinate system. A rotation B then brings the vector $\mathbf{u}$ to the vector $\mathbf{u}'$, which is found to by left multiplying the column vector of the coordinates of $\mathbf{u}$ by a suitable matrix $\boldsymbol{B}$:

$$\mathbf{u}' = \boldsymbol{B}\mathbf{u}\,. \tag{1}$$

A second rotation of space A with respect to the same, stationary coordinate system similarly brings the vector $\mathbf{u}'$ to the vector $\mathbf{u}''$, found by left multiplying the coordinates of the vector $\mathbf{u}'$ with a suitable matrix $\boldsymbol{A}$:

$$\mathbf{u}'' = \boldsymbol{A}\mathbf{u}' = \boldsymbol{AB}\mathbf{u}\,. \tag{2}$$

By the associativity of matrix multiplication, the combined effect of these rotations on the vector $\mathbf{u}$ may instead be expressed as a left multiplication of $\mathbf{u}$ by the single matrix $\boldsymbol{AB}$; that is, the combined effect AB of two rotations, B and A, is still a rotation.

A rotation in the passive convention behaves rather differently, by leaving the space fixed and rotating the coordinate system by which points are identified. For an observer attached to the rotating coordinate system, space appears to rotate in the reverse sense to that of the active convention. For example, perform the same rotation B as above, but on the coordinate system rather than on the space. Then the coordinates of the stationary vector $\mathbf{v}$, relative to the rotated coordinate system, become

$$\mathbf{v}' = \boldsymbol{B}^{-1}\mathbf{v}, \tag{3}$$

the matrix $\boldsymbol{B}^{-1}$ performing the inverse operation of $\boldsymbol{B}$. This result is generalized to the following relationship: the matrix transforming the coordinates of a vector during a passive rotation is the inverse of the matrix transforming the coordinates of a vector during the corresponding active rotation. The rotation AB that transforms coordinates by the matrix $\boldsymbol{AB}$ in the active convention, then, transforms coordinates by the matrix $(\boldsymbol{AB})^{-1} = \boldsymbol{B}^{-1}\boldsymbol{A}^{-1}$ when interpreted in the passive convention; not only the sense of the individual rotations is reversed, but the *order of application* is reversed as well.

The difference between these conventions is demonstrated in Figure 2. The active convention is used in Figure 2a, where a vector initially on the x axis is aligned with the z axis by a rotation of $\pi/2$ about the z axis and a rotation of $\pi/2$ about the x axis. The equivalent operation to that in Figure 2a is performed in the passive convention in Figure 2b by applying the individual rotations to the coordinate system in the same sense, but

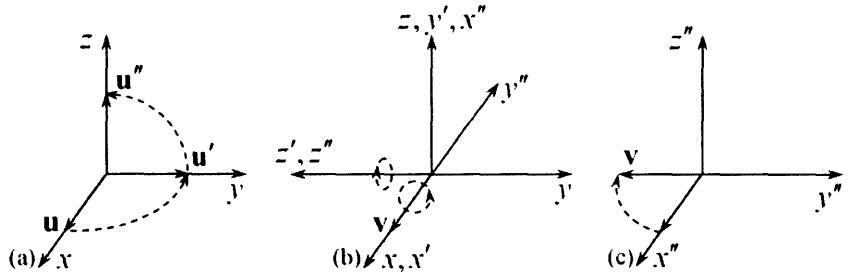

Figure 2: Comparison of rotations performed in the active and passive conventions. (a) Rotations in the active convention. A vector $\mathbf{u}$ is rotated by $\pi/2$ about the z axis to $\mathbf{u}'$, then by $\pi/2$ about the x axis to $\mathbf{u}''$. (b) Rotations in the passive convention. The coordinate system is rotated by $\pi/2$ about the x axis, then by $\pi/2$ about the z' axis. (c) Effect of the passive rotations in (b) on $\mathbf{v}$ from the viewpoint of an observer attached to the coordinate system. The vector $\mathbf{v}$ appears to be rotated by $-\pi/2$ about the x axis, then by $-\pi/2$ about the z' axis.

reversed in order; the coordinate system is rotated by $\pi/2$ about the x axis, then by $\pi/2$ about the resulting z' axis. This operation is equivalent to that in Figure 2a in the sense that the space in Figure 2a and the coordinate system in Figure 2b experience the same effective rotation by $2\pi/3$ about the $[1\,\bar{1}\,1]$ direction. Figure 2c demonstrates that from the viewpoint of an observer attached to the coordinate system, the apparent rotation in Figure 2b is exactly the inverse, namely, a rotation by $-2\pi/3$ about the $[1\,\bar{1}\,1]$ direction.

While equivalent in the sense that one may be transformed into the other, the interpretation of matrices expressed in these conventions is clearly different. The convention used must therefore be clearly specified for a discussion of rotations to be meaningful. We use the active convention in the majority of the present work, for the reason that we find it simpler to interpret a rotation performed relative to a stationary frame of reference than a rotation performed with respect to a frame of reference that changes with every operation.

1.1.2. Defining an Orientation

An orientation is simply the physical result of a sequence of rotations. Rotations must be performed with respect to a coordinate system, usually defined as that system with coordinate axes aligned along the edges (often assumed to be orthogonal) of the sample being examined. The orientation of a crystal is identified with an active rotation that brings a reference crystal aligned with the coordinate system into coincidence with the crystal embedded in the material. The matrix corresponding to this rotation is designated by $\boldsymbol{O}$, though there could be many equivalent such rotations. For example, the configuration resulting from an active rotation of a crystal by $\pi/2$ about the z axis is equivalent to that resulting from a rotation by $5\pi/2$ about the same axis. Some of this redundancy is eliminated by considering only rotations by angles between 0 and π, but there is additional ambiguity that depends on the symmetries of the system.

A reference crystal with cubic symmetry could be initially aligned with the coordinate system in any of twenty-four physically indistinguishable ways. Indicating the symmetry operations of the crystallographic point group by $\boldsymbol{C}_j$, all of the matrices $\boldsymbol{OC}_j$ describe equivalent orientations of the crystal. Furthermore, the sample often exhibits

statistical symmetry in the distribution of crystal orientations as a result of processing history. When this symmetry is present, any of the symmetry operations $\boldsymbol{S}_i$ can be applied to the sample without changing the observable characteristics, thereby expanding the set of rotations resulting in physically indistinguishable orientations to $\boldsymbol{S}_i\boldsymbol{O}\boldsymbol{C}_j$. A reasonable discussion of texture requires that an orientation be uniquely identified with just one of these rotations; usually, selecting the rotation with the minimum rotation angle about an axis lying in the standard stereographic triangle is sufficient. A discussion of more subtle cases, where this criterion does not uniquely identify the rotation, is given elsewhere [5].

1.2. Pole Figures

One of the conventional methods for representing a texture is by means of pole figures. These originated as a natural result of diffraction experiments, and reveal the orientations of particular crystallographic planes rather than of individual crystals. Despite the development of more sophisticated methods of texture representation, the use of pole figures persists for a number of reasons; these include the familiarity of the materials science community with this method of presentation, the relative simplicity of physically interpreting the information displayed in this format, and the existence of many situations in which the orientation of a particular crystallographic plane controls some property of interest.

The orientation of a particular crystallographic plane is completely specified by a single line, passing through the origin and oriented in the direction normal to the plane. This line intersects a unit sphere centered on the origin in two diametrically opposed points. Since the line passes through the origin, either one of these two points uniquely identifies the line. The orientation of a single crystallographic plane is then completely specified by the point of intersection of the normal vector to the plane with the positive hemisphere of the unit sphere; this point is referred to as the pole. (Incidentally, the pole is identical to the crystallographic axis with the same indices for cubic crystals). An example of a pole, p, corresponding to a given plane orientation is shown in Figure 3.

When the poles of a particular crystallographic plane are considered, and the hemisphere is projected into two dimensions, a *pole figure* is obtained. The most

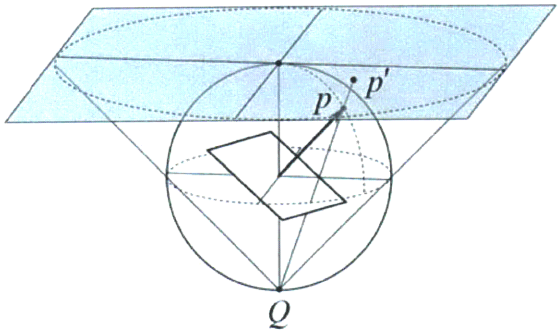

Figure 3: Indication of a crystallographic plane's orientation by a point on the surface of a sphere, projected onto a plane by stereographic projection. The stereographic projection of a point p may be performed by placing a light source at Q and observing the shadow cast by the point p onto the plane at p'.

common projection for this purpose is the stereographic projection, which preserves angles but not area; the angle between two lines drawn on the hemisphere is the same as the angle between their projections on the plane, though this comes at the price of changing the apparent density of the poles in the projection. Occasionally, an equal-area projection is useful instead of the stereographic; this projection preserves the apparent density of the poles, but distorts the angles between projected lines. While we use the stereographic projection for the present case, several discussions of the benefits of one projection or the other exist in the literature, e.g. Refs. [6, 7].

The stereographic projection of the point p in Figure 3 is given by the point of intersection of the unique line passing through Q and p with the plane of projection at $z = 1$. Mathematically, this projection is given by

$$x' = \frac{2x}{1+z}, \quad y' = \frac{2y}{1+z}, \tag{4}$$

where x, y, and z are the coordinates of the point p, and x' and y' are the coordinates of the point p'. Since they depend on the choice of the point Q and the plane of projection, other formulas for the stereographic projection may differ.

As the method delineated above permits a single pole to be represented as a point in the plane of projection, a distribution of poles can be represented as a collection of points in this plane. A complete description of the discrete poles in a polycrystalline sample is provided by depicting one point per crystal, or one point per volume element.

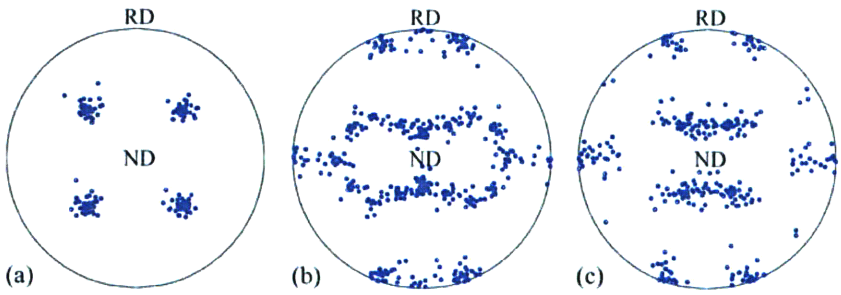

Figure 4: {111} pole figures for (a) a cube texture, (b) a copper texture, and (c) a brass texture. "ND" and "RD" correspond to the "normal direction" and the "rolling direction", respectively, of a sample deformed by rolling.

Schematic {111} pole figures for a number of commonly observed textures appear in Figure 4, including the cube, copper and brass textures. These projections are conventionally depicted in the plane parallel to that of a sheet sample, and the "normal direction" to this plane is labeled "ND". The transverse direction of highest symmetry is usually called the "rolling direction" and is labeled "RD", although this notation is used for non-rolled materials as well.

Since the geometry of the sample indicates a suitable set of axes for this projection, any sample symmetry is generally visible in the resulting pole figures; for example, samples with orthorhombic symmetry were used to generate the pole figures of Figure 4, meaning that a statistically identical pole figure could be reproduced from any one of the four quadrants. Although this symmetry is occasionally exploited and only a portion of the pole figure provided, it is quite common to find the entire pole figure in the literature.

The same is not true for so-called *inverse pole figures*. Whereas a pole figure shows sample directions aligned with a particular crystallographic pole, an inverse pole figure does the opposite, indicating the crystallographic poles aligned with a specified sample direction. This is often of interest for samples in which the processing history strongly identifies a single direction, e.g., the axis of a fiber or wire, or the growth direction of a thin film. The procedure for constructing an inverse pole figure is quite similar to that of a pole figure, with one exception; instead of projecting a crystallographic pole onto a plane determined by the sample geometry, the vector pointing along a given sample direction is projected onto planes determined by the local

crystallographic orientation. That is, the projection procedure illustrated in Figure 3 is performed for each crystal or volume element, with the frame of reference always given by the local crystallographic frame. An inverse pole figure is obtained by plotting the results of all of these projections together.

Figure 5 shows the normal-direction inverse pole figures for samples with the three textures shown in Figure 4, namely, the cube, copper and brass textures. Since the frame of reference for an inverse pole figure is always defined by the local crystal orientation, the symmetry of the crystals is reflected in the inverse pole figures. As indicated by the fine lines in Figures 5a, 5c and 5e, the cubic crystal symmetry of the samples with these textures divides the projections into twenty-four stereographic triangles, each containing identical orientation information. The crystal symmetry is exact, rather than statistical as is the case for sample symmetry, allowing the entire inverse pole figure to be recovered exactly from any one of the stereographic triangles. Hence, the twenty-four-fold redundancy strongly encourages presentation by a single stereographic triangle. The standard stereographic triangle of the cubic system is that

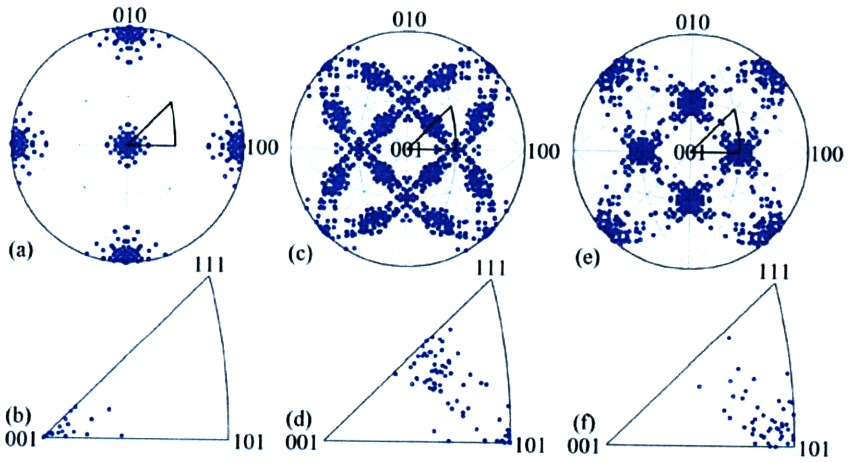

Figure 5: Normal-direction inverse pole figures for the three textures in Figure 4. The inverse pole figure at the top of a given column is divided into twenty-four stereographic triangles, with the standard stereographic triangle outlined. This triangle appears alone at the bottom of the column. Miller indices in the figure refer to directions in the local crystallographic frame. (a) A cube texture, and (b) the standard stereographic triangle of the cube texture. (c) A copper texture, and (d) the standard stereographic triangle of the copper texture. (e) A brass texture, and (f) the standard stereographic triangle of the brass texture.

containing the crystallographic directions $\{hkl\}$ for which $l \geq h \geq k \geq 0$, which we have outlined using bold lines in Figure 5. The usual presentation of an inverse pole figure provides only this standard stereographic triangle, as shown in Figures 5b, 5d and 5f.

It is important to remember that pole figures and inverse pole figures do not explicitly indicate the orientations of crystals in a polycrystalline sample, only the orientations of selected crystalline planes or directions. As suggested by Figure 1, these constructions represent only a fraction of the orientation information that is accessible via techniques that include EBSD. Occasionally, multiple pole figures, each of a different crystallographic axis, may be presented as a means of illustrating texture; however, there is no explicit means to identify the points on two pole figures originating from a single crystal. There do exist highly developed methods for determining the *most probable* crystal orientation distribution consistent with the pole figures of multiple crystallographic planes [4], but in general pole figures unnecessarily discard a great deal of the available orientation information. Therefore, methods of texture representation that accurately reflect the orientations of the crystals, rather than their planes, are frequently more useful than representation by pole figures.

1.3. Discrete Orientations

Any real, orthogonal, three-by-three matrix of determinant one corresponds to a proper rotation of space in the active convention. The group of rotation matrices with these properties is often considered to be the canonical parameterization of rotations, partly due to the simplicity of applying a rotation matrix to either a vector or to another rotation matrix via the matrix product. As a result, rotation matrices are quite convenient for the algebraic manipulation of discrete orientations; on the other hand, the visualization of a collection of orientations via rotation matrices is rather difficult.

A unique description of an orientation in three dimensions only requires three independent parameters [8]. If these can be identified, they can be taken as coordinates of a three-dimensional group space in which individual orientations appear as points. In the case of rotation matrices, each matrix contains nine components. While the direct use of these nine components to form a nine-dimensional group space is unreasonable, there is no obvious way to use only three of the matrix components to represent an orientation

(though there is some motivation for using six [9, 10]). A related difficulty lies in interpreting the physical effect of a rotation matrix; at least to the current authors, this is not transparent except in the simplest cases. The regrettable result is that the use of this convenient and familiar parameterization of rotations is sharply restricted to the algebraic manipulation of discrete orientations, rather than to their visualization.

Partly for this reason, the materials science community employs a number of other parameterizations side by side with rotation matrices, each with their own particular advantages and weaknesses. The analysis of texture information requires familiarity with the most common parameterizations in order to be able to select the most appropriate one for the application at hand. We provide a brief overview of these parameterizations in this section, with particular emphasis on their relative strengths.

1.3.1. Axis-Angle Parameters

A theorem due to Euler states that every displacement of a sphere with a fixed center is equivalent to some rotation of that sphere about an axis by an angle [11]. Although this description of a rotation requires four parameters, three for the coordinates of the unit vector **n** pointing along the axis of rotation and one for the angle ω, it has the advantage that the physical effect of a rotation described by an axis and angle is easily visualized (see Figure 6a). These four parameters may be reduced to three without loss of information by observing that the constraint on the length of **n** allows only two of its three coordinates to be chosen independently. For instance, **n** may be expressed in terms of the spherical coordinates θ and ϕ, at the expense of introducing an asymmetry into the parameters which is inherent to the spherical coordinate system. As pointed out by Frank [12], a more symmetric method for combining these four parameters into three is to multiply **n** by a simple function $f(\omega)$:

$$\mathbf{s} = \mathbf{n} f(\omega). \tag{5}$$

Varying the function $f(\omega)$ converts the quantity **s** into various *neo-Eulerian mappings*. The close relationship between the axis and angle of a rotation and the corresponding point in the group space of one of these neo-Eulerian mappings is illustrated in Figure 6.

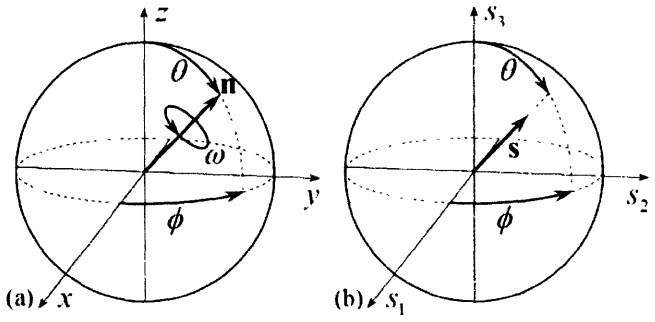

Figure 6: Relationship of the vector **n** and angle ω to the parameters of a neo-Eulerian mapping. (a) The result of any series of rotations is equivalent to some rotation, performed about an axis parallel to **n** by an angle ω. The vector **n** can be written in terms of the spherical angles θ and ϕ. (b) The corresponding point in the group space of a neo-Eulerian mapping with parameters $\mathbf{s} = \mathbf{n}f(\omega)$. The result is nearly as straightforward to interpret as the description using **n** and ω directly.

The simplest function of this type is the rotation angle itself. The vector **a** then points in the same direction as the axis of rotation and scales linearly in length with the rotation angle:

$$\mathbf{a} = \mathbf{n}\omega . \tag{6}$$

We refer to the components of **a**, and not the four parameters of the separate axis and angle of rotation, as the axis-angle parameters because their behaviour is more reasonable for small rotations and because they appear more often in the literature. Since **n** may point in any direction and ω is constrained to the values $0 \le \omega \le \pi$, the group space of these parameters is a solid ball of radius π. Each point on the interior of this ball corresponds to a unique rotation, and diametrically opposed points on the surface correspond to the same two-fold rotation. While the redundant points can be removed by excluding certain portions of the surface [13], the topological properties of the space nevertheless allow small variations in a physical orientation to correspond to discontinuous changes in the axis-angle parameters as a point jumps from one part of the group space to another. This behaviour is rather inconvenient from the standpoint of numerical calculations.

A more serious drawback of the axis-angle parameterization is the complexity of the multiplication law, or the formula required to calculate the single rotation equivalent to two rotations performed in succession. This difficulty may be addressed by more

deliberate selection of the function multiplying **n**, which provides neo-Eulerian parameterizations with simpler combination laws and certain other useful properties. As a result, the simplicity of the axis-angle parameterization is useful when introducing certain ideas concerning the rotation group, but this parameterization is rarely used for the representation of texture due to the existence of more attractive alternatives.

1.3.2. Rodrigues Vectors

The Rodrigues vector parameterization is a neo-Eulerian mapping introduced into the discussion of texture by Frank [12]. The three parameters of a Rodrigues vector are constructed by multiplying **n** by the tangent of half of ω:

$$\mathbf{r} = \mathbf{n}\tan(\omega/2). \tag{7}$$

As with all of the neo-Eulerian parameterizations, this vector points in the same direction as the axis of rotation and increases monotonically in length with the rotation angle ω for angles $0 \le \omega \le \pi$. Hence, the interpretation of a Rodrigues vector, as with the axis-angle parameters, is nearly as simple as that of the axis and angle of a rotation directly. One disadvantage of this parameterization, though, is that the magnitude of a Rodrigues vector diverges as the rotation angle approaches π, meaning that a binary rotation cannot be represented with a Rodrigues vector. Furthermore, the unbounded group space brings into question the feasibility of visualizing a texture as a collection of points distributed throughout an infinite volume.

Nevertheless, certain properties of Rodrigues vectors make this parameterization quite favorable for the presentation of texture information. These may be derived from the multiplication law for rotations expressed as Rodrigues vectors; the result of a rotation $\mathbf{r}_B$ followed by a rotation $\mathbf{r}_A$ is determined by [14]

$$\mathbf{r}_A\mathbf{r}_B = \frac{\mathbf{r}_A + \mathbf{r}_B + \mathbf{r}_A \times \mathbf{r}_B}{1 - \mathbf{r}_A \cdot \mathbf{r}_B}, \tag{8}$$

which is a slight rearrangement of the form appearing in the literature. Apart from its relative simplicity, the particular advantage of this multiplication law is that it may be used to show that the trajectory for a continuing rotation about a single axis is a straight

line in the Rodrigues space, regardless of the orientation of the reference frame; similarly, any change of the reference frame transforms a line into another line, and a plane into another plane [12]. The benefit of these properties becomes apparent when considering the effect of symmetry on the group space.

The presence of sample or crystal symmetry partitions the group space into distinct regions known as fundamental zones, defined by the requirement that they contain a unique point for every physically distinguishable orientation of a crystal. That is, a given fundamental zone contains only one of the points corresponding to the set of symmetrically equivalent rotations $\boldsymbol{S}_i\boldsymbol{O}\boldsymbol{C}_j$. The presence of symmetry thereby reduces the matter of visualizing the group space to that of a single fundamental zone, since all of the texture information is contained in each fundamental zone. While for most parameterizations the surfaces of these fundamental zones are curved, it follows from Equation (8) that the boundaries of the fundamental zones in Rodrigues space are always planar [12]. The specific forms of these fundamental zones have been derived for a variety of crystal and sample symmetries, and are generally finite and bounded by planar surfaces [14, 15]. For materials with sufficiently high crystal symmetry, this has encouraged the presentation of texture information in two dimensions by equidistant

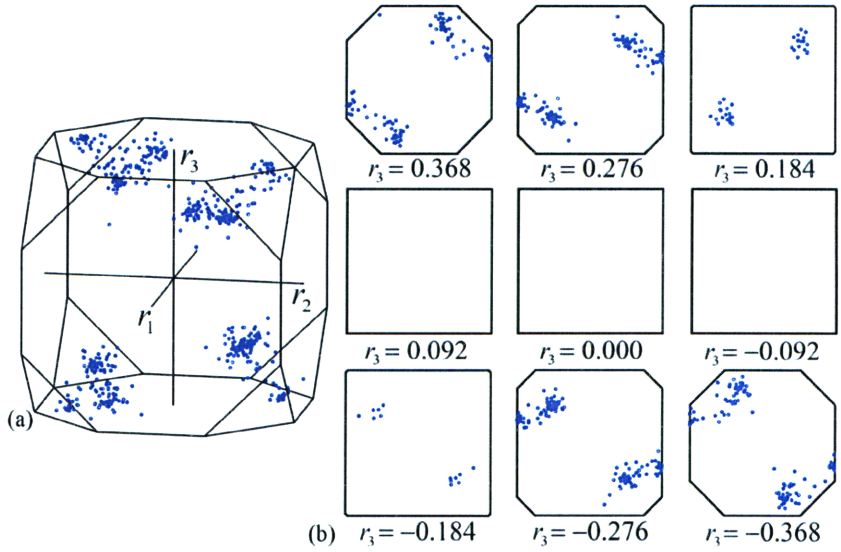

Figure 7: A collection of discrete orientations from a copper textured material with cubic crystal symmetry, depicted in the fundamental zone of Rodrigues space. (a) The cubic fundamental zone containing the origin is a truncated cube with six octagonal faces and eight triangular faces. (b) The distribution is conventionally plotted in equidistant sections perpendicular to the r_3 axis.

planar sections of the fundamental zone. This presentation is used in Figure 7 for a collection of orientations from a copper textured material with cubic crystal symmetry. Figure 7a displays the orientations in the cubic fundamental zone, and Figure 7b gives the conventional sections of this space in two dimensions.

1.3.3. Quaternions

Although quaternions often receive less notice than other parameterizations, their attractive mathematical properties have proven indispensable for a number of subjects with particular relevance to the analysis of orientation information. Specifically, quaternions have been used for texture analysis [12, 16-19], disorientation and mean orientation calculations [5, 15, 20-25], expression of certain specific textures [26-28], and in connection with the equations of texture evolution [29, 30]. Quaternions appear in related fields of materials science as well, as in the development of the theory of coincident site lattices [21, 31, 32] and in the investigation of the symmetry groups for modulated crystals and quasicrystals [33].

A quaternion q is often interpreted as a vector in four-dimensional space. For the study of rotations, the quaternions of interest satisfy the normalization constraint $q_0^2 + q_1^2 + q_2^2 + q_3^2 = 1$, which is assumed throughout the remainder of this document. A quaternion is then related to the quantities $\mathbf{n}$ and ω of a rotation by

$$q = (q_0, \mathbf{q}) = [\cos(\omega/2), \mathbf{n}\sin(\omega/2)], \tag{9}$$

where q_0 and $\mathbf{q}$ are conventionally referred to as the scalar and vector parts of the quaternion, respectively. While the description of a three-dimensional rotation requires three parameters and a quaternion contains four, we observe that a rotation is completely specified by just the vector part $\mathbf{q}$, which may be interpreted as a neo-Eulerian mapping. Although the scalar part q_0 appears redundant, the properties of this four-component parameterization strongly encourage the use of the parameter q_0 as well, at the price of a little redundancy.

As normalized vectors in four-dimensional space, quaternions inhabit the region defined as the set of points at a distance of one from the origin, i.e. the unit sphere in four dimensions (or S^3, for those familiar with this notation). Exactly as for a sphere in three

dimensions, there is no closed path on the unit sphere in four dimensions that contains a discontinuous change in the values of the quaternion components; the discontinuous change in the values of the axis-angle and Rodrigues vector parameters for rotations in the vicinity of $\omega = \pi$ is simply not present. By including all of the quaternions on this hypersphere, though, every physical orientation is represented twice. Equation (9) indicates that given a quaternion $+q$, increasing ω by 2π results in the antipodal quaternion $-q$ with the signs of all the components reversed. Although these quaternions correspond to distinct rotations, they clearly result in the same physical orientation (meaning that one may consider the space inhabited by orientations as RP^3). This may be interpreted as resulting from the trivial symmetry of three-dimensional space, that is, a rotation by 2π about any axis results in an indistinguishable orientation. As in Rodrigues space, the presence of symmetry partitions the quaternion group space into distinct fundamental zones (actually, Heinz and Neumann derived the boundaries of these regions in Rodrigues space from the properties of the quaternion group space [15]). The symmetry through a rotation by 2π identifies the fundamental zones as one half of the unit sphere, and we select the half with positive values of q_0 for the representation of textures. Hence, the parameterization of a single orientation by two quaternions is not a particularly serious obstacle.

The advantage of writing the quaternion in Equation (9) in terms of half-angle trigonometric functions (and thereby introducing the redundancy in $+q$ and $-q$) rather than full-angle functions is that this form permits the multiplication law to be written in an exceptionally simple form; a rotation expressed by the quaternion q_B followed by q_A results in the quaternion given by [13]

$$[q_{A0}, \mathbf{q}_A][q_{B0}, \mathbf{q}_B] = [q_{A0}q_{B0} - \mathbf{q}_A \cdot \mathbf{q}_B, q_{A0}\mathbf{q}_B + q_{B0}\mathbf{q}_A + \mathbf{q}_A \times \mathbf{q}_B], \tag{10}$$

where quaternions operate to the right. The simplicity of this multiplication law lies in the fact that the components of the resulting quaternion are all linear functions of the components of q_B and q_A. Although this is a feature of other parameterizations as well (e.g. rotation matrices), the quaternion parameterization is the parameterization of smallest dimension with this property [10]. With respect to numerical calculations, this

type of multiplication law tends to be efficient and robust, and there is some indication that quaternions may even be preferable to rotation matrices for this purpose [34].

There remains the matter of visualizing a collection of points embedded in a four-dimensional space, i.e., of the necessity of projecting from four dimensions to three, and from three dimensions to two. While there are many projections of the quaternion group space with $q_0 \geq 0$ into three dimensions, we mention only the orthographic and gnomic projections at the moment (stereographic and equal-volume projections into three dimensions should generally be considered as well, though the formulas for these are slightly more complex [6, 12]). The first, the orthographic projection, follows from the observation that the vector part **q** of a quaternion q resembles a neo-Eulerian mapping, for which all orientations may be plotted in the analog of the representative spherical volume in Figure 6b. This method is attractive because there is little additional computation involved, and knowledge of the vector part allows the final component of the quaternion to be quickly reconstructed by applying the normalization constraint. An

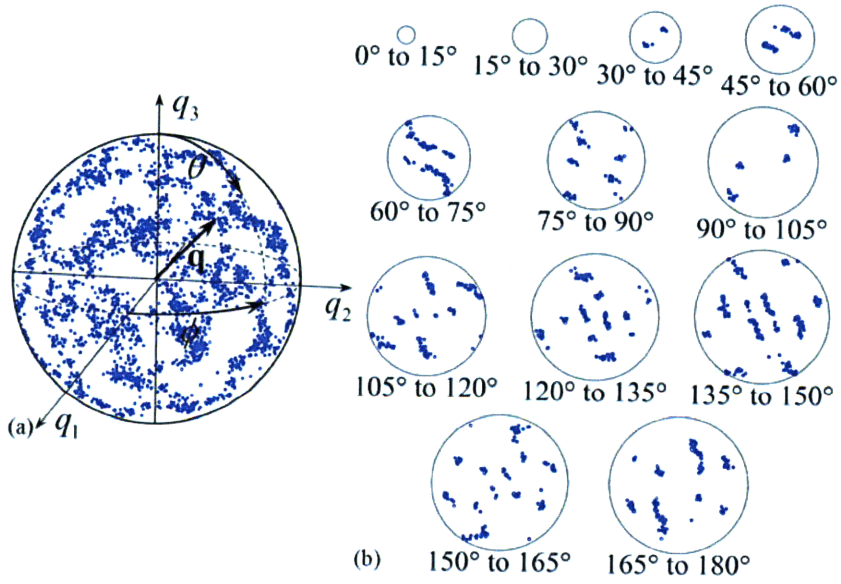

Figure 8: A collection of discrete orientations from a copper textured material with cubic crystal symmetry, depicted in (a) the three dimensions inhabited by the vector part **q** of a quaternion q, and (b) in two dimensions as a collection of stereographic projections of concentric spherical shells of the space in (a). This presentation is naturally suited to the spherical shape of the space, and has the advantage that the rotation angle is constant within a given spherical shell, promoting an intuitive interpretation of points displayed in this format.

example of this representation for the crystal orientations in a copper textured material with cubic crystal symmetry is shown in Figure 8a.

Meanwhile, the gnomic projection converts a quaternion into the corresponding Rodrigues vector. The projection is performed simply by dividing the vector part of a quaternion by the scalar part, or $\mathbf{r} = \mathbf{q}/q_0$. This suggests that orientation measurements may be analyzed as quaternions and projected into the Rodrigues space as a final step for the purpose of visualization.

The parameterizations resulting from the projections suggested above are clearly neo-Eulerian, meaning that a vector within the three-dimensional group space points along the axis of rotation and scales monotonically with the rotation angle. In particular, the value of the rotation angle is constant within a given spherical shell centered on the origin of any neo-Eulerian parameterization. This suggests that the axis and angle of rotations represented by points in any neo-Eulerian group space will be easily identified when the space is sectioned into concentric spherical shells at constant intervals of rotation angle. We use this presentation in Figure 8b by sectioning the orthographic projection of Figure 8a into concentric spherical shells. Since the symmetry of this texture renders the upper and lower hemispheres identical, we use the stereographic projection (given by Equation (4)) to project only the upper hemispheres into two dimensions. When this symmetry is not present, the upper and lower hemispheres may be plotted side by side. Points within a given stereographic projection in Figure 8b correspond to a particular interval of rotation angle, and their location within the projection indicates the orientation of the rotation axis.

The quaternion parameterization offers some notable advantages, at the price of requiring four parameters instead of three. For example, the quaternion group space includes points for all distinct orientations, and does not contain discontinuities in the parameter values along any trajectory through the space; these cannot simultaneously be properties of any three-dimensional parameterization [10]. Furthermore, the bilinearity of the multiplication law markedly simplifies many functions of orientations when expressed in the quaternion coordinates. The primary obstacle to the use of quaternions is the perceived difficulty in visualizing the group space, though as shown in Figure 8, this is not actually as difficult as might be expected. While several other reasons strongly

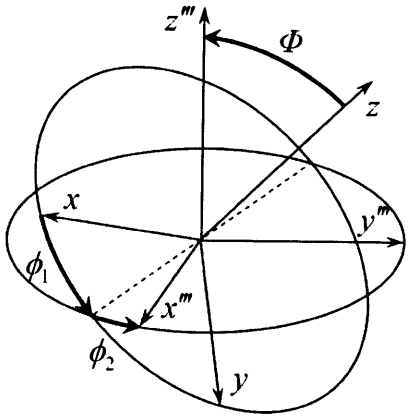

Figure 9: Definition of the orientation of a coordinate system, following the conventional interpretation of the Euler angles. The orientation is determined as the result of three consecutive rotations, performed about z, x', and z'' axes by the angles ϕ_1, Φ, and ϕ_2, respectively.

supporting the use of quaternions in the field of texture analysis exist, these will be become apparent only in subsequent chapters.

1.3.4. Euler Angles

Of the options enumerated in this chapter, the Euler angle parameterization is the one most conventionally used for the analysis and presentation of texture information. Instead of deriving from an axis and angle of rotation, this parameterization describes the relative orientation of two coordinate systems with three passive rotations (we follow the passive convention with the Euler angles in order to conform to the majority of the literature on the subject). These rotations are performed about the z, x', and z'' axes, with rotation angles given by the three Euler angles ϕ_1, Φ, and ϕ_2, respectively [4]. Applying these rotations in the determined sense and order brings one of the coordinate systems into coincidence with the other, as indicated in Figure 9. Meanwhile, plotting the Euler angles on orthogonal axes forms a group space that is 2π-periodic along all three axes. Since, in this space, a cube of edge length 2π contains two points for every orientation, the Euler angles are generally restricted to the values $0 \le \phi_1 < 2\pi$, $0 \le \Phi \le \pi$ and $0 \le \phi_2 < 2\pi$ to remove the redundant points. Cubic crystal symmetry and orthorhombic sample symmetry reduce the fundamental zone still further, though the resulting surface in Euler angle space is invariably curved. For this reason, the region defined by

$0 \le \phi_1 \le \pi/2$, $0 \le \Phi \le \pi/2$ and $0 \le \phi_2 \le \pi/2$ is often selected instead for these symmetries, despite the fact that this region contains three points for every orientation [7]. The benefit of this choice is that the planar surfaces permit a natural presentation in two dimensions by a series of parallel sections, conventionally selected perpendicular to the ϕ_2 axis. This is the method used in Figure 10 for a collection of orientations from a copper textured material with cubic crystal symmetry, where Figure 10a displays the orientations in the Euler angle group space, and Figure 10b presents the corresponding conventional two-dimensional sections.

One conspicuous feature of this definition is its asymmetry [12]. While the neo-Eulerian parameterizations do not single out any particular direction in space, the Euler angles more naturally describe rotations about the *x* and *z* axes than about the *y* axis. The asymmetry has a number of repercussions, among which is the presence of a singularity in the definition of certain rotations and therefore a singularity in the group space [10, 35]. This occurs for rotations about the *z* axis, for which $\Phi = 0$. When this Euler angle

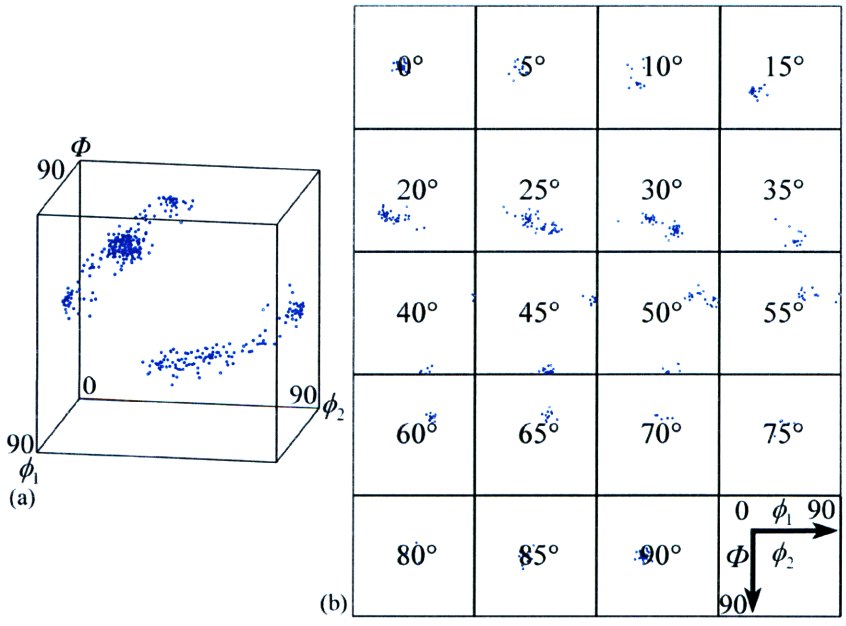

Figure 10: A collection of discrete orientations from a copper textured material with cubic crystal symmetry, depicted in Euler angle space. (a) The conventional volume used for cubic crystal symmetry and orthorhombic sample symmetry is bounded by planar surfaces, but contains three fundamental zones. (b) The distribution is conventionally plotted in equidistant sections perpendicular to the ϕ_2 axis.

vanishes, all ϕ_1 and ϕ_2 for which $\phi_1 + \phi_2$ is a constant result in the same orientation. What is particularly concerning is that this non-uniqueness applies to the identity operation (the non-rotation) as well; the rotation group is a Lie group, and this requires any proper parameterization of the rotation group be reasonably behaved in the region around the identity [36]. The singularity often appears in functions of orientations parameterized by the Euler angles as well; for example, the multiplication law for Euler angles [37] and the kinematic equations [10] each contain a singularity when $\Phi = 0$.

More pragmatically, interpreting an orientation parameterized by Euler angles is not as simple as for the neo-Eulerian parameterizations. One of the reasons for this difficulty is that instead of a single rotation, as for the alternatives outlined in the previous sections, the Euler angles require one to envision the result of three consecutive rotations. Furthermore, the effect of any of these rotations is not specified by a single Euler angle, but depends on the preceding rotations due to the use of the passive convention. The situation is mollified slightly by recognizing that the first two Euler angles can be interpreted as a variety of spherical coordinates for the z''' axis with respect to the initial coordinate system. The x''' axis may then be established by following the construction given by, e.g., Wenk and Kocks [7]. Despite this interpretation, though, the author finds the neo-Eulerian parameterizations to be far simpler.

1.4. Orientation Distribution Functions

Traditionally, diffraction techniques lacked the spatial resolution to measure the orientations of individual crystals; instead, a diffraction pattern provided probabilistic information about the orientations of many grains within the diffracting region. This information could be used to construct an *orientation distribution function*, indicating the probability of finding a volume element within the material with a particular crystalline orientation. Often, a continuous probability distribution of this type is actually more useful for the analysis of texture information than discrete orientation measurements. More specifically, given a set of continuous functions with a few particular properties, any collection of discrete orientation measurements may be accurately approximated as a linear combination of these functions. The coefficients in this expansion then give an efficient and compact expression of a texture. Indeed, this relatively simple principle is

the foundation for the whole of classical texture analysis [4] and continues to motivate recent developments as well, including, e.g., microstructure sensitive design [38, 39].

1.4.1. Circular Harmonics

The expansion of an arbitrary, square-integrable function $f(\phi)$ defined on the unit circle as an infinite linear combination of sines and cosines, i.e. as a Fourier series, is well-known. The normalized, real circular harmonics may be written as

$$\begin{aligned} X_{mc} &= \frac{1}{\sqrt{\pi}}\cos(m\phi) \\ X_{ms} &= \frac{1}{\sqrt{\pi}}\sin(m\phi), \end{aligned} \tag{11}$$

with integer index $1 \le m$; for $m = 0$, X_{0s} vanishes and $X_{0c} = 1/\sqrt{2\pi}$. This notation allows the expansion of $f(\phi)$ to be written in the form

$$f(\phi) = a_0 X_{0c} + \sum_{m=1}^{\infty}\left(a_m X_{mc} + b_m X_{ms}\right), \tag{12}$$

where the coefficients are determined by the inner product of the function $f(\phi)$ with the corresponding basis function, or

$$\begin{aligned} a_m &= \int_0^{2\pi} f(\phi) X_{mc}\, d\phi \\ b_m &= \int_0^{2\pi} f(\phi) X_{ms}\, d\phi . \end{aligned} \tag{13}$$

Our purpose in reproducing these formulas is not to instruct in the principles of their use, but rather to provide a sense of continuity with the other harmonics currently used for the representation of texture, namely, the spherical and generalized spherical harmonics.

1.4.2. Spherical Harmonics

Whereas a point on a unit circle is specified by a single angle ϕ, a point on a unit sphere is specified by two, the polar $0 \le \theta \le \pi$ and azimuthal $0 \le \phi < 2\pi$ angles. Now, since the transition from two dimensions to three involves the addition of the z axis, and a

sphere may be considered as a progression of circles centered on and perpendicular to the z axis, one expects the spherical harmonics to be constructed from circular harmonics modulated by a function of z. This is exactly the case, as is clear from the real spherical harmonics[2]

$$\begin{aligned} Y_l^{mc} &= (-1)^m \sqrt{\frac{2l+1}{2}\frac{(l-m)!}{(l+m)!}} P_l^m(\cos\theta) X_{mc} \\ Y_l^{ms} &= (-1)^m \sqrt{\frac{2l+1}{2}\frac{(l-m)!}{(l+m)!}} P_l^m(\cos\theta) X_{ms}, \end{aligned} \tag{14}$$

with integer indices $0 \le l$ and $1 \le m \le l$; when $m = 0$, Y_l^{0s} vanishes and Y_l^{0c} is divided by $\sqrt{2}$ to preserve the normalization. These functions contain the circular harmonics from Equation (11), an associated Legendre function P_l^m [40, 41], and a normalizing coefficient. With the spherical harmonics, any square-integrable function $f(\theta,\phi)$ on the surface of a sphere may be written as a linear combination in the form

$$f(\theta,\phi) = \sum_{l=0}^{\infty}\left[a_l^0 Y_l^{0c} + \sum_{m=1}^{l}\left(a_l^m Y_l^{mc} + b_l^m Y_l^{ms}\right)\right], \tag{15}$$

where the coefficients are determined by the inner product of the function $f(\theta,\phi)$ with the corresponding basis function, or

$$\begin{aligned} a_l^m &= \int_0^{2\pi}\int_0^{\pi} f(\theta,\phi) Y_l^{mc} \sin\theta d\theta d\phi \\ b_l^m &= \int_0^{2\pi}\int_0^{\pi} f(\theta,\phi) Y_l^{ms} \sin\theta d\theta d\phi. \end{aligned} \tag{16}$$

While Equation (15) is an exact expansion for $f(\theta,\phi)$, the calculation of an infinite number of coefficients is not particularly practical. Instead, the expansion is always performed with a finite number of terms by limiting the index l to values less than or equal to $l_{\max}$; this smoothes the resulting approximation, although limiting the number of terms occasionally introduces spurious peaks or valleys as well.

[2] Please forgive the shift in notation. The placing of the indices in Equation (11) is more consistent with the eventual notation for the hyperspherical harmonics, while the placing of the indices in Equation (14) is fixed by convention.

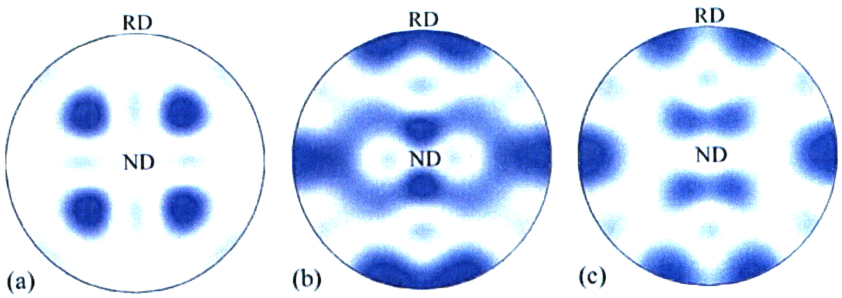

Figure 11: {111} pole figures of the continuous pole distributions for (a) a cube texture, (b) a copper texture, and (c) a brass texture, corresponding to the respective discrete pole figures in Figure 4. The distribution functions are determined by Equation (15), with $l_{\max} = 15$. Regions of finite probability density appear in some areas that are empty in the corresponding discrete pole figures due to the use of a limited number of terms, while regions of negative probability density were removed by applying a positivity constraint.

The smoothing performed by limiting the number of terms makes this expansion a convenient method for finding an approximation to a collection of points on the surface of a sphere, as, for instance, the discrete poles for a given crystallographic plane. When normalized, the resulting function is interpreted as the probability density function of observing a pole in a particular area of the sphere's surface. We follow this procedure to calculate the probability density functions for the three {111} pole figures of Figure 4, and plot the results in stereographic projection in Figure 11.

1.4.3. Generalized Spherical Harmonics

Bunge, often thought of as the founder of modern texture analysis, considered textures as probability distribution functions in Euler angle space [4]. Since the definition of the Euler angles precludes their interpretation as angular coordinates on the surface of a familiar geometrical shape, the basis functions for the Euler angles are generally considered to reside in the space formed by placing the three Euler angles on orthogonal coordinate axes, as in Figure 10a. These functions, known as the generalized spherical harmonics, resemble the product of two complex spherical harmonics with a shared index l and polar angle Φ, and are given by [4]

$$T_l^{mn} = e^{im\phi_2} P_l^{mn}(\cos\Phi) e^{in\phi_1}, \tag{17}$$

with integer indices $0 \le l$, $-l \le m \le l$ and $-l \le n \le l$. The function P_l^{mn} is occasionally referred to as a generalized associated Legendre function (a definition and derivation of a closely related function are provided elsewhere [42]). One practical point to consider is that while the generalized spherical harmonics defined in Equation (17) are complex, a probability distribution function of orientations is real. This means that the expansion of a probability distribution function over the generalized spherical harmonics generally requires complex expansion coefficients containing redundant information.

A square-integrable function $f(\phi_1, \Phi, \phi_2)$ defined within the Euler angle space is expanded as [4]

$$f(\phi_1, \Phi, \phi_2) = \sum_{l=0}^{\infty} \sum_{m=-l}^{l} \sum_{n=-l}^{l} t_l^{mn} T_l^{mn}, \tag{18}$$

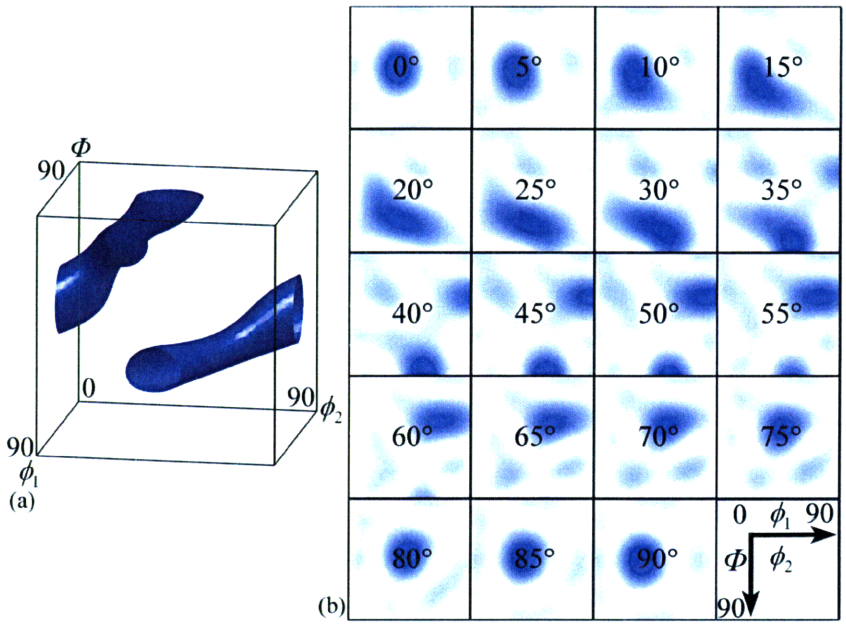

Figure 12: Continuous Euler angle distribution for the crystal orientations in a copper textured material, corresponding to the collection of discrete orientations in Figure 10. The distribution function is determined by Equation (18), with $l_{\max} = 12$. (a) A single contour of the distribution function in the conventional volume used for cubic crystal symmetry and orthorhombic sample symmetry. (b) The distribution function, sectioned perpendicular to the ϕ_2 axis. Regions of finite probability density appear in some areas that are empty in Figure 10b due to the use of a limited number of terms, while regions of negative probability density were removed by applying a positivity constraint.

with complex coefficients t_l^{mn}. The coefficients of this expansion are found by taking the inner product of the function with the appropriate generalized spherical harmonic [4]

$$t_l^{m'm} = \frac{2l+1}{8\pi^2} \int_0^{2\pi} \int_0^{\pi} \int_0^{2\pi} f(\phi_1, \Phi, \phi_2) T_l^{m'm*} \sin \Phi d\phi_1 d\Phi d\phi_2 , \tag{19}$$

where $(2l+1)$ arises from the fact that the inner product of a generalized spherical harmonic with itself depends on the value of l, $8\pi^2$ is a normalization factor, and the * indicates the complex conjugate. The labor required to calculate these coefficients is reduced to practical limits by including in the expansion only terms with l less than or equal to some $l_{\max}$, at the expense of some accuracy.

A normalized, real-valued and positive function $f(\phi_1, \Phi, \phi_2)$ may always be interpreted as the probability density of an orientation occurring in the region of ϕ_1, Φ, and ϕ_2 in Euler angle space. The expansion of Equation (18) was applied to the discrete orientations given as points in Euler angle space in Figure 10, and the result is shown in Figure 12. The single contour of the distribution function in Figure 12a makes clear the interpretation of the copper texture as a "tube" through Euler angle space, while the two-dimensional format used in Figure 12b is the traditional means of reporting a texture graphically in the literature.

1.5. Problem Statement

The various representations outlined in this chapter should be considered as methods for the communication of textures, presumably of materials with advantageous properties or resulting from particular processing procedures. That is, the representation of texture is fundamentally a means to an end, though one that is inherently subject to the properties of the accompanying mathematical framework. Specifically, the measurement and subsequent analysis of orientation information is usually performed within the Euler angle parameterization of orientations. In a sense, this is the foundation upon which the entire field of texture measurement, representation and engineering is built; every aspect of this field benefits from the enormous effort invested by the scientific community in

developing the mathematical aspects of orientation analysis using the Euler angles, and is constrained by the inevitable difficulties of working with this formulation as well.

Although three parameters suffice to characterize a rotation, the topological properties of $SO(3)$ preclude the existence of a three-dimensional parameterization that covers every orientation and is simultaneously nonsingular [10]. This is manifested in the Euler angles by the well-known degeneracy wherein certain orientations, including the identity, are represented by an infinite number of points in the group space [4, 8, 43]. A distortion of the metric tensor [29], the related degeneracy of the invariant volume element [4], and singularities in the equations of motion [10, 43] follow as a result. This severe non-uniqueness causes some small changes in a physical orientation to correspond to abrupt jumps in the values of the Euler angles, posing an inconvenient complication to the calculation of disorientations and the tracking of orientations during texture evolution. Furthermore, the present author along with other researchers [14, 23, 30] find that the Euler angles are not intuitive; a particular physical orientation does not intuitively relate to a triplet of Euler angles, partly due to the difficulty of visualizing three successive rotations, and partly to the asymmetric treatment of the coordinate axes [12, 23, 30]. The calculation of grain misorientations, by extension, suffers from the same complexities, and requires equations involving trigonometric functions, inverse trigonometric functions and singularities [35, 44].

Despite the achievements of the field using the Euler angles (e.g., Refs. [4, 45, 46]), the shortcomings outlined above render them either difficult or impractical to use for certain situations in the analysis of crystallographic texture. Hence, a mathematical framework for the analysis of orientation information that has all the same capabilities as the existing one using Euler angles, but in a different parameterization, would be valuable. A few specific properties that would be convenient for this parameterization to exhibit include

i. a simple multiplication rule for combining successive rotations,
ii. an intuitive physical interpretation,
iii. the absence of singular orientations, and
iv. the ability to express distribution functions in an explicit mathematical form.

1.6. Structure of this Thesis

As discussed in Section 1.3.3, the quaternion parameterization already displays the first three characteristics outlined above. The purpose of this thesis is therefore to provide and develop the utility of a series expansion for the representation of orientation information within the context of the quaternion parameterization. Specifically:

- An orientation distribution function is mapped to a square-integrable function on the surface of a unit sphere in four dimensions, and then expressed as a linear combination of the hyperspherical harmonics. A discussion of the means by which to visualize an orientation distribution function in this form is provided as well.
- The mathematical connections relating the hyperspherical harmonic functions to rotations in three and four dimensions are investigated.
- Formulas to convert from the generalized spherical harmonic expansion to the hyperspherical harmonic expansion are found by considering the mutual relationship of the generalized spherical harmonics and the hyperspherical harmonics to the three-dimensional rotation group.
- Sets of symmetrized hyperspherical harmonics that satisfy the sample and crystal point group symmetries identically are found, and provide an alternate basis for the expansion of an orientation distribution function.
- The Mackenzie distribution is generalized to materials with arbitrary textures for the first time by expressing the misorientation distribution function in the form of the hyperspherical harmonic expansion.

2. Hyperspherical Harmonics[3]

The central purpose of this chapter is to provide the formulas required to express an arbitrary orientation distribution in the form of a series expansion over the hyperspherical harmonics, defined below. This expansion does not appear to be known within the materials science literature, despite the fact that at least since a seminal paper by Fock [48], the hyperspherical harmonics and the related series expansion have frequently been used in other contexts, e.g. Refs. [49-56]. Indeed, as will be explained in more detail, the hyperspherical harmonic expansion is a natural extension of the more familiar expansions of functions on the unit circle and the unit sphere, as discussed in Sections 1.4.1 and 1.4.2, respectively.

2.1. Quaternions

The motivation for the hyperspherical harmonic expansion depends closely on the representation of rotations by normalized quaternions. An overview of the properties of quaternions that reproduces and expands on the material presented in Section 1.3.3 is therefore provided in this section. For reference, the quaternion parameterization is more completely described in, e.g. Refs. [13, 36].

A quaternion q is often represented as a vector in a four-dimensional vector space over the field of real numbers, that is,

$$q = q_0 + q_1 i + q_2 j + q_3 k, \tag{20}$$

where the unit quaternions 1, i, j and k form the basis of the vector space. Hereafter, the word "quaternion" will refer specifically to a normalized quaternion, i.e. one that satisfies the condition $q_0^2 + q_1^2 + q_2^2 + q_3^2 = 1$ and describes a point on the surface of the unit sphere S^3 in four dimensions. Exactly as a point on a circle is conveniently described by an angle, and a point on a sphere by a pair of angles, a quaternion residing on S^3 is parameterized by a triplet of angles; namely, the hyperspherical angle $\omega/2$ and the spherical angles θ and ϕ, constrained to the values $0 \le \omega/2 \le \pi$, $0 \le \theta \le \pi$ and

[3] The content of this chapter has previously been published in Ref. [47].

$0 \le \phi \le 2\pi$. These relate to the coordinates of four-dimensional space by the relations [49, 53, 56, 57]

$$\begin{aligned} q_0 &= \cos(\omega/2) \\ q_1 &= \sin(\omega/2)\sin\theta\cos\phi \\ q_2 &= \sin(\omega/2)\sin\theta\sin\phi \\ q_3 &= \sin(\omega/2)\cos\theta . \end{aligned} \tag{21}$$

Recognizing ω as a rotation angle and the angles θ and ϕ as spherical angles that indicate the direction of a rotation axis **n**, a quaternion may instead be expressed in the form

$$q = (q_0, \mathbf{q}) = [\cos(\omega/2), \mathbf{n}\sin(\omega/2)], \tag{22}$$

where q_0 is conventionally referred to as the scalar part, and **q** as the vector part. The relationship between the axis-angle and quaternion parameterizations appearing in Equation (22) is depicted explicitly in Figure 13. Exactly as changing the sign of the components of **n** in the axis-angle parameterization inverts a rotation, changing the sign of the components of **q** of a quaternion q forms the quaternion corresponding to the inverse rotation, or more simply the inverse quaternion q^{-1}. On the other hand, while increasing the angle of a rotation by 2π results in an orientation of three-dimensional space that is indistinguishable from the original one, Equation (22) indicates that this

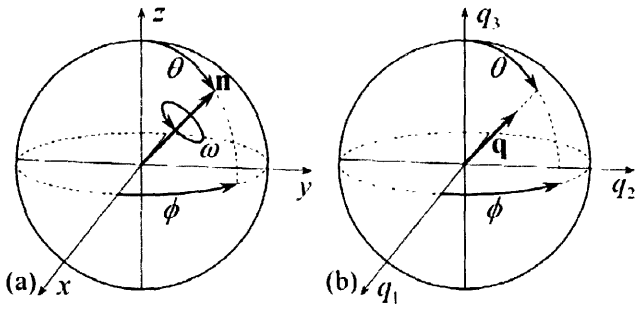

Figure 13: Relationship shared by the axis-angle parameterization of a rotation, the quaternion parameterization of a rotation, and the parameterization of a quaternion by three angles. (a) A three-dimensional rotation by the angle ω about the unit vector **n**, pointing along the axis of rotation. The direction of **n** is specified by the angles θ and ϕ. (b) The vector part **q** of the quaternion q, corresponding to the rotation in (a). The vectors **q** and **n** point in the same direction, though the length of **q** is $\sin(\omega/2)$ rather than one.

increase in rotation angle changes the sign of every component of q. More explicitly, a particular orientation of three-dimensional space corresponds to two distinct rotation operations that differ in rotation angle by 2π, and to two distinct quaternions $+q$ and $-q$. Therefore, although rotation angles in the domain $0 \le \omega \le \pi$ are sufficient to describe every unique orientation of three-dimensional space, the above construction requires the domain $0 \le \omega \le 2\pi$ to describe the rotation operations corresponding to every distinct quaternion.

The multiplication law for quaternions follows directly from the definition of multiplication for the basis quaternions 1, i, j and k, and is a linear function with respect to all of the quaternion parameters [13]. While other parameterizations exhibit a bilinear composition rule, the quaternion parameterization is the representation of smallest dimension for which this is the case [10]. The composition rule is often written as a vector equation containing the dot and cross products in the form

$$[p_0, \mathbf{p}][q_0, \mathbf{q}] = [p_0 q_0 - \mathbf{p} \cdot \mathbf{q}, p_0 \mathbf{q} + q_0 \mathbf{p} + \mathbf{p} \times \mathbf{q}], \tag{23}$$

and provides the single rotation equivalent to the rotation q followed by the rotation p.[4] As defined, quaternions operate in the same order as rotation matrices, from right to left. The unusual bilinearity of this composition allows the formulation of equivalent expressions using four-by-four orthogonal matrices of unit determinant [58], a fact that will be of considerable importance presently.

Contrasting markedly with other parameterizations currently in use, the quaternion parameterization includes no singular points [10]. Since the quaternion parameterization handles rotations about all three axes equally in the sense of having a complete set of infinitesimal generators [35], quaternions avoid the singularity in the vicinity of the identity operation that is present for the Euler angles. Meanwhile, the singularities and discontinuities in the values of the axis-angle and Rodrigues parameters in the vicinity of rotations by π do not appear in the quaternion parameterization. This is actually intimately related to the correspondence of two quaternions to a single orientation; specifically, the quaternion group is isomorphic to the simply connected

[4] "The rotation q" is occasionally written as an abbreviation for "the rotation corresponding to the quaternion q".

covering group $SU(2)$, and is related to $SO(3)$ by a 2-to-1 homomorphism [36]. More pragmatically, the absence of singularities is not only convenient, but is practically important for numerical calculations.

2.2. Defining the Hyperspherical Harmonic Expansion

One advantage of expressing a rotation using the four components of a quaternion is that every quaternion resides on the unit sphere in four-dimensional space. That is, a collection of three-dimensional rotations is mapped to a collection of points on the four-dimensional unit sphere. Analogous to the expansion of an arbitrary square-integrable function defined on the unit circle using a Fourier series and the expansion of an arbitrary square-integrable function defined on the three-dimensional unit sphere using the spherical harmonics, an arbitrary square-integrable function on the four-dimensional unit sphere may be expanded as an infinite linear combination of harmonic functions restricted to this space. We refer to these functions as the hyperspherical harmonics, and indicate them in complex form by the symbol Z_{lm}^{n}. Since the hyperspherical harmonics are defined on the four-dimensional unit sphere, and any point on the four-dimensional unit sphere may be written as functions of the angles ω, θ, and ϕ by Equation (21), the hyperspherical harmonics may be written as explicit functions of these angles as well. A definition consistent with many of those appearing in the literature [49, 53, 56, 59] is[5]

$$Z_{lm}^{n}(\omega,\theta,\phi) = (-i)^{l}\frac{2^{l+1/2}\,l!}{2\pi}\sqrt{(2l+1)\frac{(l-m)!}{(l+m)!}\frac{(n+1)(n-l)!}{(n+l+1)!}}\sin^{l}(\omega/2)C_{n-l}^{l+1}[\cos(\omega/2)] \times P_{l}^{m}(\cos\theta)e^{im\phi}, \tag{24}$$

with integer indices $0 \le n$, $0 \le l \le n$, and $-l \le m \le l$, and where C_{n-l}^{l+1} and P_{l}^{m} stand for a Gegenbauer polynomial and an associated Legendre function, respectively; definitions of these functions consistent with the current usage appear in Appendix A. Of some significance is that these harmonics cleanly separate into the product of functions each of a single angular coordinate. The remaining coefficient ensures that the hyperspherical

[5] The arrangement of indices on the hyperspherical harmonics differs from that elsewhere [47] due to the consideration that the index n identifies the set of hyperspherical harmonics that form a basis for an irreducible representation of $SO(4)$, while the indices l and m identify individual members of this set; this difference in significance encourages the separation of n from l and m.

harmonics are normalized and form an orthonormal set with respect to the inner product, i.e.

$$\int_0^{2\pi}\int_0^{\pi}\int_0^{\pi} Z_{l'm'}^{n'} Z_{lm}^{n} \sin^2(\omega/2) d(\omega/2) \sin\theta d\theta d\phi = \delta_{mm'}\delta_{ll'}\delta_{nn'}, \tag{25}$$

where δ is the Kronecker delta. The expansion of an orientation distribution function f that reflects a distribution of quaternions on the unit sphere in four-dimensional space is given as a linear combination of the hyperspherical harmonics above by

$$f(\omega,\theta,\phi) = \sum_{n=0,2..}^{\infty} \sum_{l=0}^{n} \sum_{m=-l}^{l} c_{lm}^{n} Z_{lm}^{n}, \tag{26}$$

where the index n is restricted to even integers by the trivial symmetry of three-dimensional space. The complex coefficients c_{lm}^{n} of this expansion may be calculated from the inner product (which behaves exactly like a projection operator) of f with the appropriate hyperspherical harmonic Z_{lm}^{n}, or

$$c_{lm}^{n} = \int_0^{2\pi}\int_0^{\pi}\int_0^{\pi} Z_{lm}^{n*} f \sin^2(\omega/2) \sin\theta d(\omega/2) d\theta d\phi. \tag{27}$$

One distinct advantage of the complex form of the hyperspherical harmonic expansion is simplicity of mathematical notation. Nevertheless, the use of complex functions and coefficients is not necessarily ideal for the expansion of a real-valued probability distribution of orientations. Instead, the expansion is potentially simpler as a linear combination of real functions with real coefficients. We define the real hyperspherical harmonics Z_{lmc}^{n} and Z_{lms}^{n} for $m \neq 0$ in terms of the complex hyperspherical harmonics by the unitary transformation

$$\begin{aligned} Z_{lmc}^{n} &= i^{l} \left[(-1)^{m} Z_{lm}^{n} + Z_{l-m}^{n}\right]/\sqrt{2} \\ Z_{lms}^{n} &= i^{l-1} \left[(-1)^{m} Z_{lm}^{n} - Z_{l-m}^{n}\right]/\sqrt{2}. \end{aligned} \tag{28}$$

Although this construction is straightforward, these real forms do not, to our knowledge, appear in the literature. Explicitly, the real hyperspherical harmonics are given by

$$
\begin{aligned}
Z^n_{lmc}(\omega,\theta,\phi) &= (-1)^m \frac{2^l l!}{\pi}\sqrt{(2l+1)\frac{(l-m)!}{(l+m)!}\frac{(n+1)(n-l)!}{(n+l+1)!}}\sin^l(\omega/2)C^{l+1}_{n-l}[\cos(\omega/2)] \\
&\quad \times P_l^m(\cos\theta)\cos(m\phi) \\
Z^n_{lms}(\omega,\theta,\phi) &= (-1)^m \frac{2^l l!}{\pi}\sqrt{(2l+1)\frac{(l-m)!}{(l+m)!}\frac{(n+1)(n-l)!}{(n+l+1)!}}\sin^l(\omega/2)C^{l+1}_{n-l}[\cos(\omega/2)] \\
&\quad \times P_l^m(\cos\theta)\sin(m\phi),
\end{aligned}
\tag{29}
$$

with integer indices $0 \le n$, $0 \le l \le n$, and $1 \le m \le l$; for $m = 0$, Z^n_{l0s} vanishes and Z^n_{l0c} is defined as $Z^n_{l0c} = i^l Z^n_{l0}$. Since the transformation performed in Equation (28) is unitary, the functions Z^n_{lmc} and Z^n_{lms} inherit the advantageous property that they are normalized and form an orthonormal basis with respect to the inner product, i.e.

$$
\int_0^{2\pi}\int_0^{\pi}\int_0^{\pi} Z^{n'}_{l'm'i'} Z^n_{lmi} \sin^2(\omega/2) d(\omega/2)\sin\theta d\theta d\phi = \delta_{ii'}\delta_{mm'}\delta_{ll'}\delta_{nn'},
\tag{30}
$$

where the index i stands for either c or s. Analogous to Equation (26), the expansion of an orientation distribution function f, or a distribution of quaternions on the unit sphere in four dimensions, is written as a linear combination of the real hyperspherical harmonics above with real coefficients a^n_{lm} and b^n_{lm} by

$$
f(\omega,\theta,\phi) = \sum_{n=0,2}^{\infty}\sum_{l=0}^{n}\left[a^n_{l0}Z^n_{l0c} + \sum_{m=1}^{l}\left(a^n_{lm}Z^n_{lmc} + b^n_{lm}Z^n_{lms}\right)\right].
\tag{31}
$$

Suitable coefficients for the expansion are determined by the inner product of f with the appropriate harmonic. Explicitly, the coefficient a^n_{lm} of the even basis function Z^n_{lmc} and the coefficient b^n_{lm} of the odd basis function Z^n_{lms} are provided by

$$
\begin{aligned}
a^n_{lm} &= \int_0^{2\pi}\int_0^{\pi}\int_0^{\pi} Z^n_{lmc} f(\omega,\theta,\phi)\sin^2(\omega/2)d(\omega/2)\sin\theta d\theta d\phi \\
b^n_{lm} &= \int_0^{2\pi}\int_0^{\pi}\int_0^{\pi} Z^n_{lms} f(\omega,\theta,\phi)\sin^2(\omega/2)d(\omega/2)\sin\theta d\theta d\phi .
\end{aligned}
\tag{32}
$$

While preferable from the standpoint of numerical calculations, the real hyperspherical harmonic expansion is given in a less convenient mathematical form. For this reason, many of the derivations in the following chapters are performed using the complex

hyperspherical harmonic expansion, though the results of these derivations are readily expressed in the form of the real hyperspherical harmonic expansion with reference to the conversion formulas provided in Appendix B.

As a basic examination of the degree to which Equation (31) is able to reproduce the details of a discrete orientation distribution, we apply the expansion to the collection of discrete quaternions in Figure 8 of Section 1.3.3. The result appearing in Figure 14 employs the orthographic and stereographic projections described in Chapter 1, and indicates that despite the inevitable inaccuracies introduced by limiting the number of terms, the probability density function reflects the distribution of the orientation measurements quite accurately. Though the expression for a texture as a hyperspherical harmonic expansion has only recently been presented [47], the principle follows naturally from the more familiar expansions of functions on the unit circle and unit sphere.

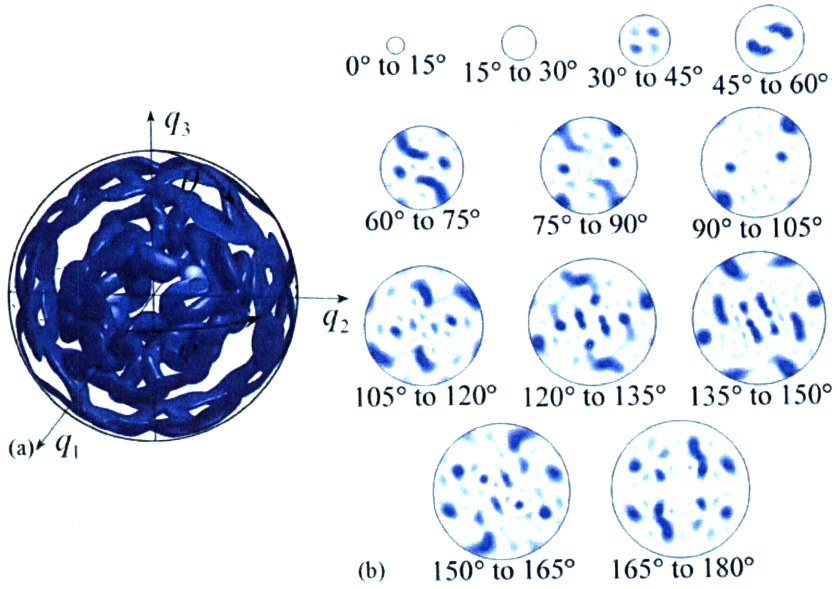

Figure 14: Continuous quaternion distribution for the crystal orientations in a copper textured material, corresponding to the collection of discrete quaternions in Figure 8. The distribution function is determined by Equation (31), with $n_{\max} = 24$. (a) A single contour of the distribution function in the space of the vector part $\mathbf{q}$ of a quaternion q. (b) The distribution function, shown in two dimensions as stereographic projections of concentric spherical shells of the space in (a). Regions of finite probability density appear in some areas that are empty in Figure 8b due to the use of a limited number of terms, while regions of negative probability density were removed by applying a positivity constraint.

2.3. Projections of a Quaternion Distribution Function

While the orthographic and stereographic projections used in Figure 8 and Figure 14 provide a convenient means to represent a quaternion distribution function in two-dimensions, there nevertheless remains the question of whether this presentation is the most suitable one. Since quaternions and the hyperspherical harmonics reside on the surface of a unit sphere in four-dimensional space, projections from a four-dimensional space into a three-dimensional space and from a three-dimensional space into a two-dimensional space are necessary in order to display orientation statistics in a format suitable for the printed page. We consider these projections separately.

Of the projections appearing in the literature which may be used to project the four-dimensional unit sphere into three dimensions, the current section mentions only three. The outstanding feature of the first of these, the stereographic projection, is that it preserves the angles of intersection. While this makes the stereographic projection useful to depict crystallographic directions and to measure the angles between them, the benefit of preserving the angles of intersection of paths on the surface of the four-dimensional unit sphere is not clear. A second projection that has been the subject of considerable interest is the geodesic projection, defined as the projection that maps great circles on the four-dimensional unit sphere onto straight lines in three-dimensional space. More simply, this projection maps a quaternion onto the corresponding Rodrigues vector with the benefit that the orientation and disorientation spaces of symmetric objects are bounded by planar surfaces. Since the stereographic and geodesic projections are not used extensively in the following, the reader is referred to, e.g., Refs. [3, 6, 60] for explicit formulas and descriptions of the properties of the resulting parameterizations.

The third projection, and the one that is used most frequently in the following, is the volume-preserving projection (otherwise known as the homochoric projection in Refs. [3, 12, 30]). The outstanding feature of this projection is that the invariant measure of the three-dimensional volume projected from the four-dimensional unit sphere is unity. That is, the density of points within a particular volume of the projected group space is directly proportional to the volume of crystalline material with that orientation. The projection maps a point with angular coordinates ω, θ, and ϕ on the surface of the four-

dimensional unit sphere to a point with Cartesian coordinates x, y and z in the interior of a three-dimensional solid ball by the relations

$$\begin{aligned} x &= r\sin\theta\cos\phi \\ y &= r\sin\theta\sin\phi \\ z &= r\cos\theta, \end{aligned} \tag{33}$$

where $r = (3/4)^{1/3}(\omega - \sin\omega)^{1/3}$. Alternatively, the projected coordinates may be written as functions of the quaternion coordinates q_i by means of Equation (21).

With the usual limits on ω, θ, and ϕ, the projection of Equation (33) maps the positive hemisphere of the four-dimensional unit sphere to a solid three-dimensional ball of radius $r = (3\pi/4)^{1/3}$. Since the vector from the origin to a point defined by x, y and z within this ball points in the direction of the axis of rotation and increases monotonically in length with the rotation angle, the values of the projected orientation distribution on a spherical shell of radius r indicates the distribution of rotation axes for rotations by a specific angle ω. The sectioning of the projected group space into concentric spherical shells therefore allows the orientation distribution to be viewed as a series of distributions of rotation axes for particular rotation angles, thereby holding one of the physically relevant quantities constant and simplifying the interpretation.

As for the projection of a three-dimensional spherical shell onto two-dimensions, the equal-area projection is used for the same reason that the volume-preserving projection is used above. That is, the density of points within a particular projected area is directly proportional to the volume of crystalline material with the specified orientation. The area-preserving projection maps a point with coordinates r, θ, and ϕ on the surface of a three-dimensional spherical shell to a point with coordinates X and Y on a solid two-dimensional disk by the relations

$$\begin{aligned} X &= R\cos\phi \\ Y &= R\sin\phi, \end{aligned} \tag{34}$$

where $R = r\sqrt{2(1-|\cos\theta|)}$. As above, the projected coordinates may be written as functions of the coordinates x, y and z or the quaternion coordinates q_i by means of Equations (33) and (21). Since the hemispheres of the three-dimensional spherical shells

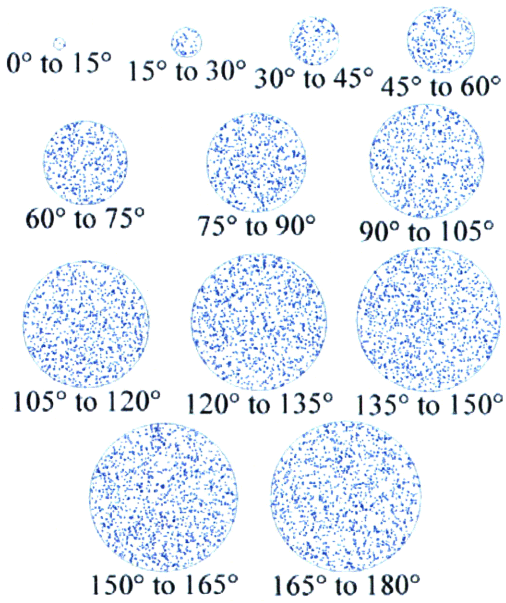

Figure 15: A random texture, corresponding to a uniform distribution of points on the surface of the unit four-dimensional sphere, presented using the volume-preserving (4D to 3D) and equal-area (3D to 2D) projections. The equal-area projection causes the uniformity of the distribution for a particular rotation angle, and the volume-preserving projection causes the uniformity of the distribution among the various rotation angles.

defined by $0 \le \theta \le \pi/2$ and $\pi/2 \le \theta \le \pi$ generally contain distinct information for orthorhombic samples and crystal symmetry of 6 or lower, these hemispheres should be presented as separate projections. However, for the common situation of orthorhombic samples and crystal symmetry of 222 or higher, the hemispheres contain identical information and a projection of the positive hemisphere alone is sufficient.

The benefit of using this method of presentation is demonstrated in Figure 15. This figure depicts a random texture, i.e. the projection of a uniform distribution of points on the surface of the four-dimensional sphere to a two-dimensional figure, for rotation angles from 0° to 180° in 15° increments. Inspection reveals that the apparent density of rotation axes is uniform not only within the projection of a spherical shell corresponding to a particular rotation angle, but amongst the projections of all the rotation angles as well; these properties result from the equal-area projection of Equation (34), and from the volume-preserving projection of Equation (33), respectively. This projection therefore simplifies the identification of the physical significance of orientation information.

3. Hyperspherical Harmonics and the Rotation Groups[6]

While the expansion of an ODF as a linear combination of basis functions gives an analytical expression to an otherwise arbitrary square-integrable function, the main motivation for this technique is that the expanded function inherits the properties of the basis functions. That is, the expansion allows the established properties of the basis functions to be used in the analysis of an experimental ODF. Therefore, there is some need to improve our understanding of the properties of the hyperspherical harmonics and thereby to more completely realize the utility of the expansion in Equation (26). Within this context, an investigation of the properties of the hyperspherical harmonics as they relate to the rotation groups in three and four dimensions is found to be particularly useful. Although the following is not intended as a general discussion of group theory, some results indispensable for the development of the hyperspherical harmonic expansion will be presented in this section. For a more complete presentation of group theory and representation theory in general refer to, e.g. Ref. [8].

3.1. Three-Dimensional Rotations

The orientations of the individual crystallites in a sample are generally described by a three-dimensional rotation of a crystal in a reference orientation that brings the reference crystal into coincidence with the actual crystallite. Since a three-dimensional rotation of the sample as a whole effectively changes the reference orientation, this operation changes the ODF of the sample and the hyperspherical harmonic expansion of the ODF as well. The study of the three-dimensional proper rotation group, referred to as $SO(3)$, is therefore pertinent to the study of the properties of the hyperspherical harmonics and the related series expansion.

3.1.1. Irreducible Representatives of SO(3)

The study of $SO(3)$ requires an analytical realization of the group to give the elements an explicit form. Any realization to a set of matrices is more specifically called

[6] Much of the content of this chapter has previously been published in Refs. [47, 61].

a representation of the group, and given a particular rotation g_i, the matrix $\boldsymbol{R}(g_i)$ is called the corresponding representative. We note that matrix multiplication proceeds from right to left, and adopt the same convention for the result of rotation g_j followed by g_i:

$$g_i g_j = g_k \Rightarrow \boldsymbol{R}(g_i)\boldsymbol{R}(g_j) = \boldsymbol{R}(g_k). \tag{35}$$

We further note that a similarity transformation of the representation, with matrices $\boldsymbol{S}^{-1}\boldsymbol{R}(g_i)\boldsymbol{S}$ formed from $\boldsymbol{R}(g_i)$ and the invertible linear transformation $\boldsymbol{S}$, is considered to be a change of basis of the representation. The canonical realization of $SO(3)$ is to the group of real, three-by-three orthogonal matrices with unit determinant, but the frequency of this representation does not preclude the existence of representations by matrices of a different dimension. Indeed, an infinite number of representations exist, but the majority may be decomposed into a direct sum of representations of smaller dimension. The representations for which decomposition is not possible are said to be irreducible, and possess a number of quite useful properties.

Irreducible representations for $SU(2)$, the covering group of $SO(3)$, exist for all integer dimensions. A formula for the matrix elements of these representatives is given by [8, 13, 45]

$$R^{l}_{m'm}(a,b) = \sqrt{(l+m')!(l-m')!(l+m)!(l-m)!}\cdot\sum_{k}\frac{a^{l+m-k}(a^*)^{l-m'-k}b^{m'-m+k}(-b^*)^{k}}{(l+m-k)!(l-m'-k)!(m'-m+k)!k!}, \tag{36}$$

though the cited references differ subtly in the use and meaning of this representative. We follow the interpretation of Altmann [13]. That is, a rotation operation is considered as an active rotation of configuration space, rather than a passive rotation of the coordinate system. An irreducible representative left-multiplies the column vector of the coordinates of a point, and right-multiplies the row vector of the components of the basis. The dimension of the representative given in Equation (36) is $(2l+1)$, where l is restricted to positive integer or half-integer values. The index m' labels the rows of the matrix sequentially from l to $-l$, and m labels the columns sequentially from l to $-l$. The index k ranges over all values for which the factorials are finite. The proper rotation corresponding to the representative above is identified by the Cayley-Klein parameters a and b, related to the components of the corresponding quaternion q by [13]

$$a = q_0 - iq_3$$
$$b = -q_2 - iq_1 . \tag{37}$$

Finally, the operation * indicates the complex conjugate. Equation (36) then gives an infinite number of equally valid representatives of all integer dimensions for a single rotation, corresponding to the quaternion q.

However, in Equation (21) the quaternion q is written as an explicit function of the angles ω, θ and ϕ rather than of the Cayley-Klein parameters a and b. This suggests that the formula for the matrix element in row m' and column m of a $(2l+1)$-dimensional irreducible representative of $SU(2)$ may equivalently be written as $U^l_{m'm}(\omega,\theta,\phi)$ instead of $R^l_{m'm}(a,b)$, provided that conversion formulas from the Cayley-Klein parameters to the angles ω, θ and ϕ are found. This is accomplished by introducing Equation (21) into Equation (37), with the result

$$a = \cos(\omega/2) - i\sin(\omega/2)\cos(\theta)$$
$$b = -i\sin(\omega/2)\sin(\theta)e^{-i\phi} . \tag{38}$$

One more result is required before the conversion of Equation (36). The reader is invited to confirm that the substitution of the quantities a^* and $-b$ into Equation (36) in the place of a and b provides the relation

$$R^l_{m'm}(a^*,-b) = (-1)^{m-m'} R^l_{-m-m'}(a,b) \tag{39}$$

for the matrix elements of the inverse of $\boldsymbol{R}^l(a,b)$. This actually holds for the irreducible representatives of $SO(3)$ in other forms as well, meaning that

$$U^l_{m'm}(-\omega,\theta,\phi) = (-1)^{m-m'} U^l_{-m-m'}(\omega,\theta,\phi) \tag{40}$$

is an equivalent relation for the matrix elements of the inverse of $\boldsymbol{U}^l(\omega,\theta,\phi)$. While there are other symmetries of the irreducible representatives, Equation (40) shall be of particular use in the following.

Although an expression for the functions $U^l_{m',m}(\omega,\theta,\phi)$ may be found by direct substitution of Equation (38) into Equation (36), a more elegant expression is given by considering the operation described by the representative $\boldsymbol{U}^l(\omega,\theta,\phi)$ to be the result of

three distinct rotations [62]. The first rotation, described by the representative $\boldsymbol{U}^{l}(\theta,\pi/2,\phi-\pi/2)$, brings the point on the sphere described by the spherical angles θ and ϕ into coincidence with the z axis. The second rotation, described by the representative $\boldsymbol{U}^{l}(\omega,0,0)$, performs a rotation by the angle ω about the z axis. The third rotation, described by the representative $\boldsymbol{U}^{l}(\theta,\pi/2,\phi+\pi/2)$, brings the point on the z axis into coincidence with the point on the sphere described by the spherical angles θ and ϕ, and is the inverse of the first rotation. The representative $\boldsymbol{U}^{l}(\omega,\theta,\phi)$ is then constructed from the product of three representatives by

$$U^{l}_{m'm}(\omega,\theta,\phi)=\sum_{m'''}\sum_{m''}U^{l}_{m'm'''}(\theta,\pi/2,\phi+\pi/2)U^{l}_{m'''m''}(\omega,0,0)U^{l}_{m''m}(\theta,\pi/2,\phi-\pi/2), \tag{41}$$

with integer or half-integer indices $-l\le m'''\le l$ and $-l\le m''\le l$. Observing that the third representative is the inverse of the first, a symmetry relation equivalent to Equation (40) is used to find

$$U^{l}_{m'm}(\omega,\theta,\phi)=\sum_{m'''}\sum_{m''}(-1)^{m'''-m'}U^{l}_{m'''m'}(\omega,0,0)U^{l}_{-m''-m'}(\theta,\pi/2,\phi-\pi/2)U^{l}_{m'''m}(\theta,\pi/2,\phi-\pi/2). \tag{42}$$

Since two of the representatives in Equation (42) share the same arguments, the product of these representatives may be expanded in a series using the Clebsch-Gordan coefficients [8, 44, 45, 63]. This gives

$$U^{l}_{m'm}(\omega,\theta,\phi)=\sum_{m'''}\sum_{m''}(-1)^{m'''-m'}U^{l}_{m'''m'}(\omega,0,0)\sum_{\lambda}\sum_{\nu,\mu}C^{\lambda\nu}_{l-m'''lm'}U^{\lambda}_{\nu\mu}(\theta,\pi/2,\phi-\pi/2)C^{\lambda\mu}_{l-m'lm}, \tag{43}$$

with integer indices $0\le\lambda\le 2l$, $-\lambda\le\nu\le\lambda$ and $-\lambda\le\mu\le\lambda$, and where the properties of the Clebsch-Gordan coefficients $C^{jm}_{j_1m_1j_2m_2}$ constrain the remaining summation indices to the values $\nu=-m'''+m''$ and $\mu=-m'+m$. Appendix C provides a definition of the Clebsch-Gordan coefficients, while Refs. [8, 44, 45, 63] offer discussions of the properties of these quantities. Our notation for the Clebsch-Gordan coefficients follows that of Ref. [63].

The quantity $U^{l}_{m'''m''}(\omega,0,0)$ is evaluated by referring to Equation (38) to find that $a=e^{-i\omega/2}$ and $b=0$ for these values of θ and ϕ. Inserting these quantities into Equation

(36) reveals that the individual terms of the summation therein vanish for $k \neq 0$, and that $U^{l}_{m'''m''}(\omega,0,0)$ vanishes for $m''' \neq m''$. Simplification of the remaining quantity provides the expected result, namely, that

$$U^{l}_{m'''m''}(\omega,0,0) = \delta_{m'''m''} e^{-\imath m''\omega}. \tag{44}$$

With this, the expression for $U^{l}_{m'm}(\omega,\theta,\phi)$ becomes

$$U^{l}_{m'm}(\omega,\theta,\phi) = \sum_{m''} (-1)^{m''-m'} e^{-\imath m''\omega} \sum_{\lambda}\sum_{\mu} C^{\lambda 0}_{l-m''lm''} U^{\lambda}_{0\mu}(\theta,\pi/2,\phi-\pi/2) C^{\lambda\mu}_{l-m'lm}. \tag{45}$$

The quantity $U^{\lambda}_{0\mu}(\theta,\pi/2,\phi-\pi/2)$ is evaluated similarly. Reference to Equation (38) indicates that, for this representative, $a = \cos(\theta/2)$ and $b = \sin(\theta/2)e^{-\imath\phi}$. Substitution of these quantities into Equation (36) yields

$$\begin{aligned} U^{\lambda}_{0\mu}(\theta,\pi/2,\phi-\pi/2) = (-1)^{\mu}\sqrt{\frac{(\lambda+\mu)!}{(\lambda-\mu)!}}\Bigg[(-1)^{\mu}\lambda!(\lambda-\mu)!\left(\frac{1+\cos\theta}{2}\right)^{\lambda}\left(\frac{1-\cos\theta}{1+\cos\theta}\right)^{-\mu/2} \\ \times\sum_{k}\frac{(-1)^{k}}{(\lambda+\mu-k)!(\lambda-k)!(-\mu+k)!k!}\left(\frac{1-\cos\theta}{1+\cos\theta}\right)^{k}\Bigg]e^{\imath\mu\phi}, \end{aligned} \tag{46}$$

after some rearrangement and collection of terms. The trigonometric functions of half-angles in this equation have been converted to functions of full angles. Recognizing the quantity in brackets as the associated Legendre function $P^{-\mu}_{\lambda}(\cos\theta)$ [44], the function $U^{\lambda}_{0\mu}(\theta,\pi/2,\phi-\pi/2)$ is instead written as

$$U^{\lambda}_{0\mu}(\theta,\pi/2,\phi-\pi/2) = \sqrt{\frac{(\lambda-\mu)!}{(\lambda+\mu)!}} P^{\mu}_{\lambda}(\cos\theta) e^{\imath\mu\phi}. \tag{47}$$

The expression for $U^{l}_{m'm}(\omega,\theta,\phi)$ then becomes

$$U^{l}_{m'm}(\omega,\theta,\phi) = \sum_{\lambda}\sum_{\mu}(-1)^{-m'} C^{\lambda\mu}_{l-m'lm}\sqrt{\frac{(\lambda-\mu)!}{(\lambda+\mu)!}} P^{\mu}_{\lambda}(\cos\theta) e^{\imath\mu\phi}\sum_{m''}(-1)^{m''} C^{\lambda 0}_{l-m''lm''} e^{-\imath m''\omega}. \tag{48}$$

The symmetry properties of the Clebsch-Gordan coefficients [44, 45, 63] allow the factors of $(-1)^{-m'}$ and $(-1)^{m''}$ to be cancelled by rearranging the indices, giving

$$U^{l}_{m'm}(\omega,\theta,\phi)=\sum_{\lambda}\sum_{\mu}(-i)^{\lambda}C^{lm}_{lm'\lambda\mu}\frac{2\lambda+1}{2l+1}\sqrt{\frac{(\lambda-\mu)!}{(\lambda+\mu)!}}P^{\mu}_{\lambda}(\cos\theta)e^{i\mu\phi}\left[i^{\lambda}\sum_{m''}C^{lm''}_{lm'\lambda 0}e^{-im''\omega}\right]. \quad (49)$$

The quantity in brackets is referred to as the generalized character of the irreducible representations of the rotation group, and is written as $\chi^{l}_{\lambda}(\omega)$. An alternate expression for this function is [63]

$$\chi^{l}_{\lambda}(\omega)=2^{\lambda}\lambda!\sqrt{\frac{(2l+1)(2l-\lambda)!}{(2l+\lambda+1)!}}\sin^{\lambda}(\omega/2)C^{\lambda+1}_{2l-\lambda}[\cos(\omega/2)], \quad (50)$$

where $C^{\lambda+1}_{2l-\lambda}$ is a Gegenbauer polynomial, as defined in Appendix A. Substitution of Equation (50) into Equation (49) and some rearrangement yields

$$\begin{aligned}U^{l}_{m'm}(\omega,\theta,\phi)=\sum_{\lambda}\sum_{\mu}\frac{\sqrt{2(2\lambda+1)\pi}}{2l+1}C^{lm}_{lm'\lambda\mu}\Bigg[&(-i)^{\lambda}\frac{2^{\lambda+1/2}\lambda!}{2\pi}\sqrt{(2\lambda+1)\frac{(\lambda-\mu)!}{(\lambda+\mu)!}}\\&\times\sqrt{\frac{(2l+1)(2l-\lambda)!}{(2l+\lambda+1)!}}\sin^{\lambda}(\omega/2)C^{\lambda+1}_{2l-\lambda}[\cos(\omega/2)]P^{\mu}_{\lambda}(\cos\theta)e^{i\mu\phi}\Bigg].\end{aligned} \quad (51)$$

The quantity in brackets is the hyperspherical harmonic $Z^{2l}_{\lambda\mu}(\omega,\theta,\phi)$, as defined by Equation (24). This allows a compact expression for the matrix elements in the form

$$U^{l}_{m'm}(\omega,\theta,\phi)=\sum_{\lambda}\sum_{\mu}\frac{\sqrt{2(2\lambda+1)\pi}}{2l+1}C^{lm}_{lm'\lambda\mu}Z^{2l}_{\lambda\mu}(\omega,\theta,\phi). \quad (52)$$

Although this result is identical to the one obtained for the $U^{l}_{m'm}(\omega,\theta,\phi)$ as defined in Refs. [62, 63], this derivation is meant to verify that Equation (52) is consistent with the current conventions.

The elements of the irreducible representatives of *SU*(2) defined by Equation (52) are equivalent to those defined by Equation (36), though in a different parameterization. However, the purpose of this section is to determine the irreducible representatives of *SO*(3), not of *SU*(2), in terms of the angles ω, θ and ϕ. Since *SO*(3) is a subgroup of *SU*(2), the irreducible representatives of *SO*(3) must appear among the irreducible representatives of *SU*(2). Specifically, they are found by restricting l to integer values. Equation (52) therefore provides the desired formula for the irreducible representatives of *SO*(3) as well.

3.1.2. An Addition Theorem

With a formulation for the matrix elements of the irreducible representatives of $SO(3)$ in hand, an addition theorem for the hyperspherical harmonics may now be derived. Practically speaking, the addition theorem simplifies the summation of products of the hyperspherical harmonics, and allows the convolution of ODFs as is required to calculate distribution functions of orientation differences. We point out that restricted forms of the addition theorem for the hyperspherical harmonics appear in the quantum mechanics literature [50, 52, 55]. Nevertheless, these results are generally presented in the literature without an explicit (or, in some cases, consistent) set of conventions. To the author's knowledge, this addition theorem does not appear elsewhere in the literature in a form that is consistent with the current conventions, particularly as they apply to the field of texture analysis and to the expansion of the ODF as in Equation (26).

The addition theorem for the hyperspherical harmonics is analogous to the addition theorems for, e.g., the Gegenbauer polynomials or the associated Legendre functions. The formula derives from the observation that if a rotation described by the angles ω_1, θ_1 and ϕ_1 is followed by a rotation described by the angles ω_2, θ_2 and ϕ_2, then the result is equivalent to that of some single rotation described by the parameters ω, θ and ϕ. This is equivalent to the matrix multiplication of the corresponding irreducible representatives, or

$$U^l_{m'm}(\omega,\theta,\phi) = \sum_{m''} U^l_{m'm''}(\omega_2,\theta_2,\phi_2) U^l_{m''m}(\omega_1,\theta_1,\phi_1). \tag{53}$$

Although Equation (53) may be expanded by means of Equation (52), the procedure is simplified somewhat by applying some of the symmetry properties of the Clebsch-Gordan coefficients to Equation (52) to obtain

$$U^l_{m'm}(\omega,\theta,\phi) = \sum_{\lambda}\sum_{\mu}(-1)^{-\lambda+l-m'} \frac{\sqrt{2\pi}}{\sqrt{2l+1}} C^{\lambda\mu}_{l-m'lm} Z^{2l}_{\lambda\mu}(\omega,\theta,\phi). \tag{54}$$

This is substituted into Equation (53) to give

$$\sum_{\lambda}\sum_{\mu}(-1)^{-\lambda+l-m'}\frac{\sqrt{2}\pi}{\sqrt{2l+1}}C^{\lambda\mu}_{l-m'lm}Z^{2l}_{\lambda\mu}=\sum_{m''}\sum_{\lambda_2}\sum_{\mu_2}(-1)^{-\lambda_2+l-m'}\frac{\sqrt{2}\pi}{\sqrt{2l+1}}C^{\lambda_2\mu_2}_{l-m'lm''}Z^{2l}_{\lambda_2\mu_2}$$
$$\times\sum_{\lambda_1}\sum_{\mu_1}(-1)^{-\lambda_1+l-m''}\frac{\sqrt{2}\pi}{\sqrt{2l+1}}C^{\lambda_1\mu_1}_{l-m''lm}Z^{2l}_{\lambda_1\mu_1}, \tag{55}$$

where $Z^{2l}_{\lambda_i\mu_i}$ is written for $Z^{2l}_{\lambda_i\mu_i}(\omega_i,\theta_i,\phi_i)$ for the sake of brevity. After multiplying by the Clebsch-Gordan coefficient $C^{\lambda'\mu'}_{l-m'lm}$ and summing over the indices $-m'$ and m, this becomes

$$\sum_{\lambda}\sum_{\mu}(-1)^{-\lambda}Z^{2l}_{\lambda\mu}\left[\sum_{-m'}\sum_{m}C^{\lambda'\mu'}_{l-m'lm}C^{\lambda\mu}_{l-m'lm}\right]=\frac{\sqrt{2}\pi}{\sqrt{2l+1}}\sum_{\lambda_2}\sum_{\mu_2}\sum_{\lambda_1}\sum_{\mu_1}(-1)^{-\lambda_2-\lambda_1}Z^{2l}_{\lambda_2\mu_2}Z^{2l}_{\lambda_1\mu_1}$$
$$\times\left[\sum_{m''}\sum_{-m'}\sum_{m}(-1)^{l-m''}C^{\lambda'\mu'}_{l-m'lm}C^{\lambda_2\mu_2}_{l-m'lm''}C^{\lambda_1\mu_1}_{l-m''lm}\right]. \tag{56}$$

The quantity in brackets on the left is $\delta_{\lambda'\lambda}\delta_{\mu'\mu}$ by the unitarity of the Clebsch-Gordan coefficients, where δ is the Kronecker delta, while the quantity in brackets on the right is found to be [63]

$$\sum_{m''}\sum_{-m'}\sum_{m}(-1)^{l-m''}C^{\lambda\mu}_{l-m'lm}C^{\lambda_2\mu_2}_{l-m'lm''}C^{\lambda_1\mu_1}_{l-m''lm}=(-1)^{-\lambda}\sqrt{2\lambda_2+1}\sqrt{2\lambda_1+1}C^{\lambda\mu}_{\lambda_2\mu_2\lambda_1\mu_1}\begin{Bmatrix}\lambda & \lambda_2 & \lambda_1\\ l & l & l\end{Bmatrix}. \tag{57}$$

The quantity in braces is the Wigner 6*j* symbol, and is defined in, e.g., Refs. [8, 63]. Simplification of the left side of Equation (56) and substitution of Equation (57) into the right side of Equation (56) gives

$$Z^{2l}_{\lambda\mu}=\frac{\sqrt{2}\pi}{\sqrt{2l+1}}\sum_{\lambda_2}\sum_{\mu_2}\sum_{\lambda_1}\sum_{\mu_1}(-1)^{-\lambda_2-\lambda_1}\sqrt{2\lambda_2+1}\sqrt{2\lambda_1+1}Z^{2l}_{\lambda_2\mu_2}Z^{2l}_{\lambda_1\mu_1}C^{\lambda\mu}_{\lambda_2\mu_2\lambda_1\mu_1}\begin{Bmatrix}\lambda & \lambda_2 & \lambda_1\\ l & l & l\end{Bmatrix} \tag{58}$$

as an addition theorem for the hyperspherical harmonics. This is closely related to an addition theorem for the generalized characters of the irreducible representations of the rotation group as reported in Refs. [62, 64], and is a generalization of the more restricted addition theorems reported in Refs. [50, 52, 55]. The corresponding generalized spherical harmonic addition theorem enables the convolution of ODFs expressed in the

generalized spherical harmonic expansion, and as indicated in the subsequent sections, the hyperspherical harmonic addition theorem serves a similar purpose.

3.1.3. Bases of the Irreducible Representatives of SO(3)

The significance of the irreducible representatives of $SO(3)$, as with any set of matrices, is defined only to the extent that the nature and behavior of the corresponding bases is established. The literature on the subject indicates that a suitable orthonormal basis for the $(2l+1)$-dimensional representatives of $SO(3)$ is formed by the set of $(2l+1)$ complex spherical harmonics Y_l^m with a specific value of $0 \le l$ [13, 45]. The convention followed above suggests that the relationship of the spherical harmonics to the irreducible representatives of $SO(3)$ is such that a rotation of the spherical harmonics is performed by right multiplying a row vector formed by the spherical harmonics by the representative $\boldsymbol{U}^l$. Since the basis of the representative is formed from the set of spherical harmonics with a particular value of l, the rotation transforms a linear combination of harmonics of a given value of l into a different linear combination of harmonics with the same value of l, and no others. This is more commonly expressed in the physics literature as the principle of conservation of angular momentum [8, 13, 45]. The purpose of this section is to establish a mathematical notation that will be useful in subsequent sections in the context of these considerations.

The principle that an arbitrary square-integrable function on the unit sphere in three dimensions may be expressed as an infinite linear combination of the complex spherical harmonics is well-known. Specifically, an arbitrary complex square-integrable function $f(\theta,\phi)$ is expanded using the complex equivalent of Equation (15) as

$$f(\theta,\phi) = \sum_{l=0}^{\infty} \sum_{m=-l}^{l} c_l^m Y_l^m = \sum_{l=0}^{\infty} \left\langle Y_l^l \ldots Y_l^{-l} \middle| c_l^l \ldots c_l^{-l} \right\rangle, \tag{59}$$

where the c_l^m are the complex coefficients of the expansion. Although an unusual use of the notation, the symbol $\left\langle Y_l^l \ldots Y_l^{-l} \right|$ stands for a row vector of the complex spherical harmonics Y_l^m with a specific value of l arranged in decreasing values of m, and the symbol $\left| c_l^l \ldots c_l^{-l} \right\rangle$ indicates the column vector of the corresponding complex coefficients

arranged similarly. The inner product of these vectors, expressed by $\langle Y_l^l \ldots Y_l^{-l} | c_l^l \ldots c_l^{-l} \rangle$, is equivalent to the summation over m in Equation (59). Although the definitions of the complex spherical harmonics vary subtly with the field in which they are used, we follow the definitions provided in Refs. [13, 45].

The application of a rotation operation to a vector may be considered as giving either a linear combination of the transformed basis vectors with the original coefficients, or a linear combination of the original basis vectors with transformed coefficients. With regard to the expansion in Equation (59), this implies that the result of an active rotation of the function f may either be written as the product of the transformed basis functions $\langle Y_l^l \ldots Y_l^{-l} | \boldsymbol{U}^l$ with the original coefficients $| c_l^l \ldots c_l^{-l} \rangle$, or as a linear combination of the original basis functions $\langle Y_l^l \ldots Y_l^{-l} |$ with the transformed coefficients $\boldsymbol{U}^l | c_l^l \ldots c_l^{-l} \rangle$. This is equivalent to the statement that the matrix equation

$$Rf(\theta,\phi) = \sum_{l=0}^{\infty} \langle Y_l^l \ldots Y_l^{-l} | \boldsymbol{U}^l | c_l^l \ldots c_l^{-l} \rangle \tag{60}$$

is invariant with regard to the order of operations. When necessary, Equation (60) is interpreted as a transformation of the coefficients. The symbol R, written without indices, indicates a rotation operator in this section. Notice that any set of coefficients that is unchanged by the application of $\boldsymbol{U}^l$ describes a function that is invariant to that rotation operation, i.e. a function that displays the corresponding symmetry.

While Equation (59) is natural for complex-valued functions, functions that are known to be real-valued, e.g. the probability distribution of crystalline axes, may be expanded more efficiently as a linear combination of the real spherical harmonics with real coefficients by means of Equation (15). Analogous to Equation (28), the conversion from the complex to the real spherical harmonic is effected by a unitary transformation

$$\begin{aligned} Y_l^{mc} &= \left[(-1)^m Y_l^m + Y_l^{-m}\right]/\sqrt{2} \\ Y_l^{ms} &= -i\left[(-1)^m Y_l^m - Y_l^{-m}\right]/\sqrt{2} \end{aligned} \tag{61}$$

for harmonics with integer indices $0 \le l$ and $1 \le m \le l$, and by $Y_l^{0c} = Y_l^0$ for $m = 0$. If the complex spherical harmonics with a specific value of l are written as a row vector,

then this unitary transformation may be written as the unitary matrix $\boldsymbol{T}^l$ that transforms the basis functions into a row vector of the corresponding real spherical harmonics, i.e.

$$\left\langle Y_l^l \ldots Y_l^{-l} \right| \boldsymbol{T}^l = \left\langle Y_l^{lc}, Y_l^{ls} \ldots Y_l^{0c} \right|. \tag{62}$$

The invariance of the function f with respect to expansion over the basis of the complex or real spherical harmonics requires that

$$\begin{aligned} f(\theta,\phi) &= \sum_{l=0}^{\infty} \left\langle Y_l^l \ldots Y_l^{-l} \middle| c_l^l \ldots c_l^{-l} \right\rangle \\ &= \sum_{l=0}^{\infty} \left\langle Y_l^l \ldots Y_l^{-l} \middle| \boldsymbol{T}^l \boldsymbol{T}^{l\dagger} \middle| c_l^l \ldots c_l^{-l} \right\rangle \\ &= \sum_{l=0}^{\infty} \left\langle Y_l^{lc}, Y_l^{ls} \ldots Y_l^{0c} \middle| a_l^l, b_l^l \ldots a_l^0 \right\rangle, \end{aligned} \tag{63}$$

where $\boldsymbol{T}^{l\dagger}$ is the adjoint of $\boldsymbol{T}^l$, or the complex conjugate transpose. This indicates that that the corresponding transformation of the coefficients from the complex expansion to the real expansion is effected by

$$\boldsymbol{T}^{l\dagger} \left| c_l^l \ldots c_l^{-l} \right\rangle = \left| a_l^l, b_l^l \ldots a_l^0 \right\rangle. \tag{64}$$

The irreducible representative in the basis of the real spherical harmonics is therefore $\boldsymbol{T}^{l\dagger} \boldsymbol{U}^l \boldsymbol{T}^l$, since

$$\begin{aligned} \boldsymbol{R}f(\theta,\phi) &= \sum_{l=0}^{\infty} \left\langle Y_l^l \ldots Y_l^{-l} \middle| \boldsymbol{U}^l \middle| c_l^l \ldots c_l^{-l} \right\rangle \\ &= \sum_{l=0}^{\infty} \left\langle Y_l^l \ldots Y_l^{-l} \middle| \boldsymbol{T}^l \boldsymbol{T}^{l\dagger} \boldsymbol{U}^l \boldsymbol{T}^l \boldsymbol{T}^{l\dagger} \middle| c_l^l \ldots c_l^{-l} \right\rangle \\ &= \sum_{l=0}^{\infty} \left\langle Y_l^{lc}, Y_l^{ls} \ldots Y_l^{0c} \middle| \boldsymbol{T}^{l\dagger} \boldsymbol{U}^l \boldsymbol{T}^l \middle| a_l^l, b_l^l \ldots a_l^0 \right\rangle \end{aligned} \tag{65}$$

While a change of the phase of the real spherical harmonics or of the ordering of the rows and columns of $\boldsymbol{T}^l$ does not change the meaning of the result, the convention followed above causes the three-by-three matrix $\boldsymbol{T}^{1\dagger} \boldsymbol{U}^1 \boldsymbol{T}^1$ to correspond exactly to the canonical real three-by-three rotation matrix.

The material included in this section has followed, for the most part, from well-known results and methods of representation theory. In what follows, we will use this

notation and extend these techniques to the less familiar irreducible representatives of $SO(4)$, the group of proper four-dimensional rotations.

3.2. Four-Dimensional Rotations

As observed in the introduction to Section 3.1, a three-dimensional rotation of a given sample effectively changes the reference orientation of the individual crystallites, and therefore the ODF of the sample and the hyperspherical harmonic expansion of the ODF as well. The nature of the effect on the hyperspherical harmonic expansion is determined by the following line of reasoning. A particular set of quaternions residing on the four-dimensional unit sphere describes the initial crystal orientations within the sample. Since a change of reference orientation maps this set to a different set of quaternions in the same space, this operation is a mapping of the four-dimensional unit sphere onto itself. That is, a three-dimensional rotation of the sample effects a four-dimensional rotation of the hyperspherical harmonic basis of the expansion. The effect of this rotation on the hyperspherical harmonics is given in matrix form by the irreducible representatives of $SO(4)$, the group of proper four-dimensional rotations. Hence, an explicit expression for the irreducible representatives is not only of mathematical interest, but imparts practical benefits as well. These include, for example, the ability to change the reference orientation of a collection of orientation measurements to clearly reveal any statistical sample symmetry introduced by the processing history.

3.2.1. Relating SO(3) and SO(4)

By analogy with the canonical form of the irreducible representatives of $SO(3)$, the canonical form of the irreducible representatives of $SO(4)$ is expected to be given by real orthogonal four-by-four matrices of unit determinant. The requirements that these matrices be real and orthogonal indicate that a general four-dimensional rotation is determined by six independent parameters [36]. This suggests that a general four-dimensional rotation may be related in some manner to two three-dimensional rotations, determined by three independent parameters each. The existence and nature of this relationship is established below by considering the multiplication law for quaternions.

For clarity, the investigation is performed within the context of symmetry operations applied to a crystal.

Our convention is that a crystallographic orientation is described by an active rotation q of a reference crystal from a reference orientation, aligned with the sample, to the orientation of the observed crystal. Since an initial rotation of the reference crystal by a crystal symmetry operation r must result in a symmetrically indistinguishable initial orientation of the crystal, the composition of the rotation q with the prior symmetry operation r results in the symmetrically equivalent rotation u given by the quaternion product $[q_0,\mathbf{q}][r_0,\mathbf{r}]=[u_0,\mathbf{u}]$. While this multiplication may be evaluated with Equation (23), it is more convenient for the present purpose to write the quaternion product in matrix form as the product of an orthogonal four-by-four matrix of unit determinant with the vector formed by the quaternion components of q [58]:

$$\begin{bmatrix} r_0 & -r_1 & -r_2 & -r_3 \\ r_1 & r_0 & r_3 & -r_2 \\ r_2 & -r_3 & r_0 & r_1 \\ r_3 & r_2 & -r_1 & r_0 \end{bmatrix} \begin{bmatrix} q_0 \\ q_1 \\ q_2 \\ q_3 \end{bmatrix} = \begin{bmatrix} u_0 \\ u_1 \\ u_2 \\ u_3 \end{bmatrix}. \tag{66}$$

Once the crystal is oriented, a subsequent rotation of the sample by a sample symmetry operation p must result in a statistically indistinguishable final orientation of the crystal, since every orientation of this type occurs with equal frequency in the sample. That is, the composition of the rotation q with the subsequent symmetry operation p results in the symmetrically equivalent rotation v, given by $[p_0,\mathbf{p}][q_0,\mathbf{q}]=[v_0,\mathbf{v}]$. This may be written as a multiplication by a similar orthogonal four-by-four matrix of unit determinant, though with the signs of the off-diagonal components of the lower three-by-three section reversed [58]:

$$\begin{bmatrix} p_0 & -p_1 & -p_2 & -p_3 \\ p_1 & p_0 & -p_3 & p_2 \\ p_2 & p_3 & p_0 & -p_1 \\ p_3 & -p_2 & p_1 & p_0 \end{bmatrix} \begin{bmatrix} q_0 \\ q_1 \\ q_2 \\ q_3 \end{bmatrix} = \begin{bmatrix} v_0 \\ v_1 \\ v_2 \\ v_3 \end{bmatrix}. \tag{67}$$

As orthogonal four-by-four matrices with unit determinants, the matrices for the rotations r and p appearing in Equations (66) and (67) perform restricted rigid rotations of four-

dimensional space. That these rotations are not general is reflected by the fact that each matrix is determined by only three independent parameters, e.g. the angles ω, θ, and ϕ. Nevertheless, the product of these matrices *does* produce a general real orthogonal four-by-four matrix of unit determinant [65, 66]. That is, the quaternion w as calculated from $[p_0, \mathbf{p}][q_0, \mathbf{q}][r_0, \mathbf{r}] = [w_0, \mathbf{w}]$ is related to the quaternion q by a single four-dimensional rotation which subsumes the crystal symmetry operation r and the sample symmetry operation p. Since formulas for the irreducible representatives of $SO(3)$ are provided in Section 3.1, and the relationship of three- to four-dimensional rotations is known, these results now may be used to determine explicit formulas for the irreducible representatives of $SO(4)$.

3.2.2. Irreducible Representations of SO(4)

The procedure by which we find the irreducible representations of $SO(4)$ requires a well-known theorem from group theory. For a certain set of conditions, when the elements g_i of one group of transformations commute with the elements h_j of a second group of transformations, the set of products $g_i h_j$ formed by combinations of these elements form a group as well, known as the direct product group. Given the irreducible representatives $\boldsymbol{G}(g_i)$ and $\boldsymbol{H}(h_j)$ of the elements g_i and h_j, respectively, the direct product $\boldsymbol{G}(g_i) \otimes \boldsymbol{H}(h_j)$ of these matrices forms an irreducible representative of the element $g_i h_j$ of the direct product group [8, 66].

For some quaternion q, consider prior multiplication by the quaternion r and subsequent multiplication by the quaternion p as distinct transformations. Then the associativity of quaternion multiplication requires that the quaternion w, resulting from q by $[p_0, \mathbf{p}][q_0, \mathbf{q}][r_0, \mathbf{r}] = [w_0, \mathbf{w}]$, not depend on the order of application of r and p; that is, the associativity of quaternion multiplication requires that the transformations performed by r and p commute. As found in Section 3.2.1, the combination of right multiplication by r and left multiplication by p corresponds to a single four-dimensional rotation of q, and Equation (52) provides the irreducible representatives $\boldsymbol{U}^l$ of $SU(2)$ corresponding to r and p separately. The above theorem then indicates that the irreducible representatives of the proper four-dimensional rotation group are uniquely determined, up to a similarity

transformation, by the direct product of two of the irreducible representatives $\boldsymbol{U}^l$, one corresponding to the quaternion r and the other to the quaternion p. This is equivalent to the statement that the direct product group $SU(2)\otimes SU(2)$ is locally isomorphic to the group $SO(4)$, as is widely recognized in the literature on the four-dimensional rotation group [49, 50, 53, 65]. That is, the direct product group is related to $SO(4)$ by a 2-to-1 homomorphism, due to the ambiguity in the common sign of the $\boldsymbol{U}^l$ [66, 67].

While the direct product of irreducible representatives of $SU(2)$ does provide the irreducible representatives of $SO(4)$, the bases of these representatives do not initially correspond to the either the complex hyperspherical harmonics defined in Equation (24) or the real hyperspherical harmonics defined in Equation (29). For that reason, they may not initially be used to perform a rotation of a function in the form of Equation (26) or in the form of Equation (31). A suitable similarity transformation of the representatives is first necessary to bring them into the appropriate basis. This similarity transformation is determined by investigating the properties of the irreducible representatives of $SU(2)$.

A rotation r transforms a square-integrable function $f^{(r)}$ defined on the unit sphere in three-dimensional dual vector space into the function $R(r)f^{(r)}$, where the operator $R(r)$ is a function of the quaternion components of r and where duality is interpreted to mean that the space transforms in the opposite sense to the usual vector space. The parenthesized superscript (r) is a label denoting that $f^{(r)}$ resides in the three-dimensional dual vector space on which r operates. Since $f^{(r)}$ is defined on the unit sphere, it may be expanded as an infinite linear combination of the complex spherical harmonics $Y_l^{m(r)}$ with complex coefficients $c_l^{m(r)}$, as in Equation (59). This allows the rotated function $R(r)f^{(r)}$ to be given in terms of the coefficients of the expansion and the irreducible representatives $\boldsymbol{U}^{l\dagger}(r)$ of the rotation r, as in Equation (60):

$$R(r)f^{(r)} = \sum_{l=0}^{\infty} \left\langle Y_l^{l(r)} \ldots Y_l^{-l(r)} \left| \boldsymbol{U}^{l\dagger}(r) \right| c_l^{l(r)} \ldots c_l^{-l(r)} \right\rangle . \tag{68}$$

Similarly, the rotation p transforms a square-integrable function $f^{(p)}$ defined on the unit sphere in three-dimensional vector space into the function $R(p)f^{(p)}$. As before, the

parenthesized superscript (p) indicates that $f^{(p)}$ resides in the three-dimensional vector space on which p operates. If the function $f^{(p)}$ is expanded as a linear combination of the complex spherical harmonics $Y_{l'}^{m'(p)}$ with complex coefficients $c_{l'}^{m'(p)}$, then the rotated function $R(p)f^{(p)}$ may be written in terms of the coefficients of this expansion and the irreducible representatives $\boldsymbol{U}^{l'}(p)$ of the rotation p as

$$R(p)f^{(p)} = \sum_{l'=0}^{\infty} \left\langle Y_{l'}^{l'(p)} \ldots Y_{l'}^{-l'(p)} \left| \boldsymbol{U}^{l'}(p) \right| c_{l'}^{l'(p)} \ldots c_{l'}^{-l'(p)} \right\rangle. \tag{69}$$

Since only the $\boldsymbol{U}^{l}$ with integer values of l appear in these expansions, the restriction of the irreducible representatives of $SU(2)$ to the irreducible representatives of $SO(3)$ follows naturally from this construction.

The commutation of r and p, in the sense discussed above, indicates that $R(r)$ and $R(p)$ operate on distinct functions residing in distinct spaces, as is emphasized by the use of the superscripts (r) and (p) and the differentiation of the indices by the use of a prime. Therefore, the meaning of the symbol $f^{(r)}f^{(p)}$ must not be interpreted as the product of $f^{(r)}$ and $f^{(p)}$ in the usual sense. Rather, this must be interpreted as a single function, one part of which is operated on by $R(r)$ and the other part of which is operated on by $R(p)$. Since $f^{(r)}f^{(p)}$ defines values at points in distinct spaces operated on by distinct transformations, this function must be expanded over a similar set of basis functions $Y_l^{m(r)}Y_{l'}^{m'(p)}$, where $Y_l^{m(r)}$ resides in the space operated on by the rotation r, and $Y_{l'}^{m'(p)}$ resides in the space operated on by the rotation p. The corresponding coefficients are denoted by $c_l^{m(r)}c_{l'}^{m'(p)}$. The expansion of the transformed function $R(r)R(p)f^{(r)}f^{(p)}$ is then given in terms of the expansion of $f^{(r)}f^{(p)}$ and the irreducible representatives formed by the direct product of $\boldsymbol{U}^{l\dagger}(r)$ and $\boldsymbol{U}^{l'}(p)$, *vis-à-vis* the above theorem, by

$$\begin{aligned} R(r)R(p)f^{(r)}f^{(p)} = \sum_{l=0}^{\infty}\sum_{l'=0}^{\infty} \Big\langle Y_l^{l(r)}Y_{l'}^{l'(p)} \ldots Y_l^{-l(r)}Y_{l'}^{-l'(p)} \Big| \boldsymbol{U}^{l\dagger}(r) \otimes \boldsymbol{U}^{l'}(p) \Big| \\ \times \Big| c_l^{l(r)}c_{l'}^{l'(p)} \ldots c_l^{-l(r)}c_{l'}^{-l'(p)} \Big\rangle, \end{aligned} \tag{70}$$

where the basis functions $Y_l^{m(r)}Y_{l'}^{m'(p)}$ and coefficients $c_l^{m(r)}c_{l'}^{m'(p)}$ are ordered in decreasing values of m, and in decreasing values of m' for a particular value of m. Although perfectly reasonable representatives $\boldsymbol{U}^{l\dagger}(r)\otimes\boldsymbol{U}^{l'}(p)$ may be formed with independent values of l and l', the complex hyperspherical harmonics form the basis of only those irreducible representatives given by a similarity transformation of the $\boldsymbol{U}^{l\dagger}(r)\otimes\boldsymbol{U}^{l'}(p)$ with $l=l'$ [49, 50, 53, 68]. We therefore apply this constraint to the function in Equation (70), and the double summation becomes a single summation.

If the three-dimensional spaces in which the functions $f^{(r)}$ and $f^{(p)}$ reside are considered to be distinct, then it is expected that they be operated on by distinct three-dimensional rotations. On the other hand, if the three-dimensional spaces in which they reside are considered to be projections of a single four-dimensional space, then it is expected that a single four-dimensional rotation operate on them simultaneously. The change of basis necessary to emphasize this point of view is accomplished by a similarity transformation involving the Clebsch-Gordan coefficients $C^{jm}_{j_1m_1j_2m_2}$ [49, 53], as defined in Appendix C. The Clebsch-Gordan coefficients relate the basis of Equation (70), where each basis function $Y_l^{m(r)}Y_{l'}^{m'(p)}$ is given by a pair of spherical harmonics, to the coupled basis, where each basis function $Z^n_{\lambda\mu}$ is a single hyperspherical harmonic:

$$\left\langle Y_l^{l(r)}Y_{l'}^{l'(p)}\ldots Y_l^{-l(r)}Y_{l'}^{-l'(p)}\right|\boldsymbol{C}_{ll'}=\left\langle Z^n_{00}\ldots Z^n_{nn}\ldots Z^n_{n-n}\right|. \tag{71}$$

The complex spherical harmonics are ordered in increasing values of λ, and in decreasing values of μ for a particular value of λ, with $n=l+l'$. $\boldsymbol{C}_{ll'}$ is the unitary matrix formed by arranging the Clebsch-Gordan coefficients in accordance with the ordering of the row vectors in Equation (71). Following the procedure used in Equation (63), we find that the corresponding transformation of the coefficients is

$$\boldsymbol{C}^{\dagger}_{ll'}\left|c_l^{l(r)}c_{l'}^{l'(p)}\ldots c_l^{-l(r)}c_{l'}^{-l'(p)}\right\rangle=\left|c^n_{00}\ldots c^n_{nn}\ldots c^n_{n-n}\right\rangle, \tag{72}$$

where the coefficients are ordered similarly to the hyperspherical harmonics in Equation (71). Equations (71) and (72) and a procedure analogous to that of Equation (65) indicate

that the reformulation of Equation (70) as a four-dimensional rotation of a function f, written as a linear combination of the complex spherical harmonics, is given by

$$R(r,p)f = \sum_{n=0,2.}^{\infty} \left\langle Z^n_{00} \ldots Z^n_{nn} \ldots Z^n_{n-n} \left| \boldsymbol{C}^{\dagger}_{ll'} \boldsymbol{U}^{l\dagger}(r) \otimes \boldsymbol{U}^{l'}(p) \boldsymbol{C}_{ll'} \right| c^n_{00} \ldots c^n_{nn} \ldots c^n_{n-n} \right\rangle, \tag{73}$$

where the direct product $\boldsymbol{U}^{l\dagger}(r) \otimes \boldsymbol{U}^{l'}(p)$ is evaluated before right multiplication by $\boldsymbol{C}_{ll'}$ and left multiplication by $\boldsymbol{C}^{\dagger}_{ll'}$, and $R(r,p)$ is the operator that performs a single four-dimensional rotation equivalent to the action of $R(r)R(p)$. Notice that n in Equation (73) ranges over only the non-negative even integers, as is required by the relations $n = l + l'$ and $l = l'$ for integer l and l'. This may be viewed as a consequence of performing transformations with elements of $SO(3)$, rather than with elements of $SU(2)$, in Equations (68) and (69). Alternatively, we may consider that the hyperspherical harmonics with odd values of n do not remain invariant under a four-dimensional rotation corresponding to a three-dimensional rotation by 2π. Since this is a basic requirement of an orientation distribution function, the coefficients of these hyperspherical harmonics must vanish identically and the expansion in Equation (73) does not include the odd values of n.

Comparing Equation (73) with Equation (60) reveals that if $R(r,p)$ is considered to be a four-dimensional rotation operation, then the matrices appearing in the middle of Equation (73) are the irreducible representatives of $SO(4)$ corresponding to this operator. Therefore, the formula for the elements of the irreducible representatives of $SO(4)$ is given in index notation by

$$R^n_{\lambda'\mu'\lambda\mu}(\omega_2,\theta_2,\phi_2,\omega_1,\theta_1,\phi_1) = \sum_{m_2'} \sum_{m_2} \sum_{m_1'} \sum_{m_1} C^{\lambda'\mu'}_{lm_2lm_1'} U^{l*}_{m_2'm_2}(\omega_2,\theta_2,\phi_2) U^{l}_{m_1'm_1}(\omega_1,\theta_1,\phi_1) C^{\lambda\mu}_{lm_2'lm_1}, \tag{74}$$

where the rotation p is expressed with the angles ω_1, θ_1 and ϕ_1, the rotation r is expressed with the angles ω_2, θ_2 and ϕ_2, and the element in the $\lambda'\mu'$ row and in the $\lambda\mu$ column of the $(n+1)^2$-dimensional irreducible representative of $SO(4)$ is considered to be a function of these angles. Since the basis of the irreducible representative of Equation (74) is formed from a set of the complex hyperspherical harmonics, this formula allows the rotation of a function written in the form of Equation (26).

For the rotation of a function written in the form of Equation (31), a similarity transformation of Equation (73) must be performed to convert the basis functions into a set of the real hyperspherical harmonics. The necessary transformation, already provided in Equation (28), is written as a unitary matrix $\boldsymbol{T}^n$ such that the application of this matrix to a row vector of the complex hyperspherical harmonics gives

$$\left\langle Z_{00}^n \ldots Z_{mn}^n \ldots Z_{n-n}^n \right| \boldsymbol{T}^n = \left\langle Z_{00c}^n \ldots Z_{mnc}^n, Z_{mns}^n \ldots Z_{n0c}^n \right|. \tag{75}$$

As demonstrated by the procedure of Equation (63), the corresponding transformation of the coefficients is given by

$$\boldsymbol{T}^{n\dagger} \left| c_{00}^n \ldots c_{mn}^n \ldots c_{n-n}^n \right\rangle = \left| a_{00}^n \ldots a_{mn}^n, b_{mn}^n \ldots a_{n0}^n \right\rangle. \tag{76}$$

The basis functions and coefficients of Equations (75) and (76) are ordered in increasing values of λ, and in decreasing values of μ for a particular value of λ, with c before s for a particular value of μ. Following the procedure of Equation (65) to apply this unitary transformation to Equation (73) results in

$$\begin{aligned} R(r,p)f = \sum_{n=0,2\ldots}^{\infty} & \left\langle Z_{00c}^n \ldots Z_{nnc}^n, Z_{nns}^n \ldots Z_{n0c}^n \right| \boldsymbol{T}^{n\dagger} \boldsymbol{C}_{ll'}^{\dagger} \boldsymbol{U}^{l\dagger}(r) \otimes \boldsymbol{U}^{l'}(p) \boldsymbol{C}_{ll'} \boldsymbol{T}^n \Big| \\ & \times \left| a_{00}^n \ldots a_{nn}^n, b_{nn}^n \ldots a_{n0}^n \right\rangle. \end{aligned} \tag{77}$$

The $(n+1)^2$-dimensional irreducible representative of $SO(4)$ appearing in Equation (77) is interpreted as performing the necessary transformation of the expansion coefficients, and is given in index notation by

$$\begin{aligned} R_{\lambda'\mu'\nu'\lambda\mu}^n(\omega_2,\theta_2,\phi_2,\omega_1,\theta_1,\phi_1) = & \sum_{\lambda_2\mu_2} \sum_{m_2 m_1' m_2' m_1 \lambda_1\mu_1} \sum \sum T_{\lambda_2\mu_2\lambda'\mu'\nu'}^{n*} C_{lm_2'lm_1'}^{\lambda_2\mu_2} U_{m_2'm_2}^{l*}(\omega_2,\theta_2,\phi_2) \\ & \times U_{m_1'm_1}^{l}(\omega_1,\theta_1,\phi_1) C_{lm_2'lm_1}^{\lambda_1\mu_1} T_{\lambda_1\mu_1\lambda\mu}^n, \end{aligned} \tag{78}$$

where the usual notation for summations is condensed for the sake of brevity. Whereas the irreducible representative of $SO(3)$ changed a linear combination of the $(2l+1)$ spherical harmonics for a particular value of l into a different linear combination of the same harmonics, the irreducible representative of $SO(4)$ changes a linear combination of the $(n+1)^2$ hyperspherical harmonics for a particular value of n into a different linear combination of the same harmonics.

While a change in the phase of the hyperspherical harmonics or the ordering of the rows and columns of the various transformations performed in this section does not change the significance of the result, following the current convention causes the matrix $\boldsymbol{T}^{n\dagger}\boldsymbol{C}^{\dagger}_{ll'}\boldsymbol{U}^{l\dagger}(r)\otimes\boldsymbol{U}^{l'}(p)\boldsymbol{C}_{ll'}\boldsymbol{T}^{n}$ for $n=1$ to correspond the matrix form of the quaternion r in Equation (66) when p is the identity, and to the matrix form of the quaternion p in Equation (67) when r is the identity. Apart from aesthetic considerations, the reason for this choice will be made clear in the following sections.

3.2.3. An Alternate Formula for the Irreducible Representations of SO(4)

The purpose of this section is to find an alternative expression for the $(2l+1)^2$-dimensional irreducible representatives of $SO(4)$, the elements $R^{2l}_{\lambda'\mu'\lambda\mu}$ of which are found in the preceding section to be

$$R^{2l}_{\lambda'\mu'\lambda\mu}(\omega_2,\theta_2,\phi_2,\omega_1,\theta_1,\phi_1)=\sum_{m'_2}\sum_{m_2}\sum_{m'_1}\sum_{m_1}C^{\lambda'\mu'}_{lm_2lm'_1}U^{l*}_{m'_2m_2}(\omega_2,\theta_2,\phi_2)U^{l}_{m'_1m_1}(\omega_1,\theta_1,\phi_1)C^{\lambda\mu}_{lm'_2lm_1}\,, \tag{79}$$

with integer or half-integer index $0\le l$, and integer indices $0\le\lambda'\le 2l$, $-\lambda'\le\mu'\le\lambda'$, $0\le\lambda\le 2l$, and $-\lambda\le\mu\le\lambda$. The indices λ' and μ' label the rows of the representative in increasing values of λ' and in decreasing values of μ' for a particular value of λ', while the indices λ and μ label the columns of the representative in increasing values of λ and in decreasing values of μ for a particular value of λ. The summation indices m'_2, m_2, m'_1, and m_1 range from $-l$ to l, subject to the constraints $m_2+m'_1=\mu'$ and $m'_2+m_1=\mu$. For the moment, the author simply asserts that the irreducible representative in Equation (79) correctly transforms the hyperspherical harmonics in Equation (24), and that the phases of the quantities defined in these equations are consistent.

The irreducible representatives of $SU(2)$ in Equation (79) may be expanded by means of Equation (52) to find

$$R^{2l}_{\lambda'\mu'\lambda\mu} = \sum_{m_2'}\sum_{m_2}\sum_{m_1'}\sum_{m_1} C^{\lambda'\mu'}_{lm_2lm_1'} C^{\lambda\mu}_{lm_2'lm_1} \sum_{\lambda_2}\sum_{\mu_2} \frac{\sqrt{2(2\lambda_2+1)}\pi}{2l+1} C^{lm_2}_{lm_2'\lambda_2\mu_2} Z^{2l*}_{\lambda_2\mu_2} \times \sum_{\lambda_1}\sum_{\mu_1} \frac{\sqrt{2(2\lambda_1+1)}\pi}{2l+1} C^{lm_1}_{lm_1'\lambda_1\mu_1} Z^{2l}_{\lambda_1\mu_1}, \tag{80}$$

where $Z^{2l}_{\lambda_t\mu_t}$ and $R^{2l}_{\lambda'\mu'\lambda\mu}$ are written for $Z^{2l}_{\lambda_t\mu_t}(\omega_t,\theta_t,\phi_t)$ and $R^{2l}_{\lambda'\mu'\lambda\mu}(\omega_2,\theta_2,\phi_2,\omega_1,\theta_1,\phi_1)$ for the sake of brevity. Since complex conjugation of Equation (24) reveals that

$$Z^{n*}_{lm}(\omega,\theta,\phi) = (-1)^{l+m} Z^{n}_{l-m}(\omega,\theta,\phi), \tag{81}$$

some rearrangement of Equation (80) and substitution of Equation (81) gives

$$R^{2l}_{\lambda'\mu'\lambda\mu} = \frac{2\pi^2}{(2l+1)^2} \sum_{\lambda_2}\sum_{\mu_2}\sum_{\lambda_1}\sum_{\mu_1} (-1)^{\lambda_2+\mu_2} \sqrt{2\lambda_2+1}\sqrt{2\lambda_1+1} Z^{2l}_{\lambda_2-\mu_2} Z^{2l}_{\lambda_1\mu_1} \times \sum_{m_2'}\sum_{m_2}\sum_{m_1'}\sum_{m_1} C^{\lambda'\mu'}_{lm_2lm_1'} C^{\lambda\mu}_{lm_2'lm_1} C^{lm_2}_{lm_2'\lambda_2\mu_2} C^{lm_1}_{lm_1'\lambda_1\mu_1}. \tag{82}$$

The symmetry properties of the Clebsch-Gordan coefficients, along with substitution of the index $-\mu_2$ for μ_2, allow Equation (82) to be written as

$$R^{2l}_{\lambda'\mu'\lambda\mu} = \frac{2\pi^2}{(2l+1)^2} \sum_{\lambda_2}\sum_{\mu_2}\sum_{\lambda_1}\sum_{\mu_1} (-1)^{\lambda_2-\mu_2+\mu_1} \sqrt{2\lambda_2+1}\sqrt{2\lambda_1+1} Z^{2l}_{\lambda_2\mu_2} Z^{2l}_{\lambda_1\mu_1} \times \left[\sum_{m_2'}\sum_{m_2}\sum_{m_1'}\sum_{m_1} C^{\lambda'\mu'}_{lm_2lm_1'} C^{\lambda\mu}_{lm_2'lm_1} C^{lm_2}_{lm_2'\lambda_2-\mu_2} C^{lm_1'}_{lm_1\lambda_1-\mu_1} \right]. \tag{83}$$

The quantity in brackets is found to be [63]

$$\sum_{m_2'}\sum_{m_2}\sum_{m_1'}\sum_{m_1} C^{\lambda'\mu'}_{lm_2lm_1'} C^{\lambda\mu}_{lm_2'lm_1} C^{lm_2}_{lm_2'\lambda_2-\mu_2} C^{lm_1'}_{lm_1\lambda_1-\mu_1} = \sum_{k}\sum_{\kappa} (2l+1)\sqrt{2\lambda+1}\sqrt{2k+1} \times C^{k\kappa}_{\lambda_2-\mu_2\lambda_1-\mu_1} C^{\lambda'\mu'}_{\lambda\mu k\kappa} \begin{Bmatrix} \lambda' & l & l \\ \lambda & l & l \\ k & \lambda_2 & \lambda_1 \end{Bmatrix}, \tag{84}$$

where the quantity in braces in Equation (84) is the Wigner 9*j* symbol, and is defined in, e.g., Refs. [8, 63]. With this, the expression for the matrix element of the irreducible representative becomes

$$R^{2l}_{\lambda'\mu'\lambda\mu} = \frac{2\pi^2\sqrt{2\lambda+1}}{2l+1}\sum_{\lambda_2}\sum_{\mu_2}\sum_{\lambda_1}\sum_{\mu_1}(-1)^{\lambda_2-\mu_2+\mu_1}\sqrt{2\lambda_2+1}\sqrt{2\lambda_1+1}Z^{2l}_{\lambda_2\mu_2}Z^{2l}_{\lambda_1\mu_1}$$
$$\times\sum_{k}\sum_{\kappa}\sqrt{2k+1}C^{k\kappa}_{\lambda_2-\mu_2\lambda_1-\mu_1}C^{\lambda'\mu'}_{\lambda\mu k\kappa}\begin{Bmatrix}\lambda' & l & l\\ \lambda & l & l\\ k & \lambda_2 & \lambda_1\end{Bmatrix}, \tag{85}$$

which is an alternative form for the elements of the irreducible representatives of $SO(4)$ described by Equation (79).

The utility of Equation (85) is that some of the properties of the irreducible representatives of $SO(4)$ follow more readily from this form than from Equation (79). For instance, consider the elements of the row labeled by the indices $\lambda' = 0$ and $\mu' = 0$. Applying this restriction to the indices in Equation (85) gives

$$R^{2l}_{00\lambda\mu} = \frac{2\pi^2\sqrt{2\lambda+1}}{2l+1}\sum_{\lambda_2}\sum_{\mu_2}\sum_{\lambda_1}\sum_{\mu_1}(-1)^{\lambda_2-\mu_2+\mu_1}\sqrt{2\lambda_2+1}\sqrt{2\lambda_1+1}Z^{2l}_{\lambda_2\mu_2}Z^{2l}_{\lambda_1\mu_1}$$
$$\times\sum_{k}\sum_{\kappa}\sqrt{2k+1}C^{k\kappa}_{\lambda_2-\mu_2\lambda_1-\mu_1}C^{00}_{\lambda\mu k\kappa}\begin{Bmatrix}0 & l & l\\ \lambda & l & l\\ k & \lambda_2 & \lambda_1\end{Bmatrix}. \tag{86}$$

Since the Clebsch-Gordan coefficient $C^{00}_{\lambda\mu k\kappa}$ is equal to $(-1)^{\lambda-\mu}\delta_{\lambda k}\delta_{\mu-\kappa}/\sqrt{2\lambda+1}$, this simplifies to

$$R^{2l}_{00\lambda\mu} = \frac{2\pi^2\sqrt{2\lambda+1}}{2l+1}\sum_{\lambda_2}\sum_{\mu_2}\sum_{\lambda_1}\sum_{\mu_1}(-1)^{\lambda+\lambda_2}\sqrt{2\lambda_2+1}\sqrt{2\lambda_1+1}Z^{2l}_{\lambda_2\mu_2}Z^{2l}_{\lambda_1\mu_1}C^{\lambda-\mu}_{\lambda_2-\mu_2\lambda_1-\mu_1}$$
$$\times\begin{Bmatrix}0 & l & l\\ \lambda & l & l\\ \lambda & \lambda_2 & \lambda_1\end{Bmatrix}, \tag{87}$$

where the requirement that $\mu = \mu_1 + \mu_2$, as enforced by the remaining Clebsch-Gordan coefficient, cancels several of the factors of (-1). This expression is simplified further by observing that the 9*j* symbol where one of the arguments vanishes may be reduced to a 6*j* symbol by the relation [63]

$$\begin{Bmatrix} 0 & l & l \\ \lambda & l & l \\ \lambda & \lambda_2 & \lambda_1 \end{Bmatrix} = \frac{(-1)^{\lambda+\lambda_2}}{\sqrt{2l+1}\sqrt{2\lambda+1}} \begin{Bmatrix} \lambda & \lambda_2 & \lambda_1 \\ l & l & l \end{Bmatrix}. \tag{88}$$

This allows Equation (87) to be written as

$$R^{2l}_{00\lambda\mu} = \frac{2\pi^2}{(2l+1)^{3/2}} \sum_{\lambda_2}\sum_{\mu_2}\sum_{\lambda_1}\sum_{\mu_1} \sqrt{2\lambda_2+1}\sqrt{2\lambda_1+1} Z^{2l}_{\lambda_2\mu_2} Z^{2l}_{\lambda_1\mu_1} C^{\lambda-\mu}_{\lambda_2-\mu_2\lambda_1-\mu_1} \begin{Bmatrix} \lambda & \lambda_2 & \lambda_1 \\ l & l & l \end{Bmatrix}, \tag{89}$$

or, once more using the symmetry properties of the Clebsch-Gordan coefficients,

$$\begin{aligned} R^{2l}_{00\lambda\mu} = (-1)^{-\lambda} \frac{\sqrt{2}\pi}{2l+1} \Bigg[\frac{\sqrt{2}\pi}{\sqrt{2l+1}} \sum_{\lambda_2}\sum_{\mu_2}\sum_{\lambda_1}\sum_{\mu_1} (-1)^{\lambda_2+\lambda_1} \sqrt{2\lambda_2+1}\sqrt{2\lambda_1+1} Z^{2l}_{\lambda_2\mu_2} Z^{2l}_{\lambda_1\mu_1} \\ \times C^{\lambda\mu}_{\lambda_2\mu_2\lambda_1\mu_1} \begin{Bmatrix} \lambda & \lambda_2 & \lambda_1 \\ l & l & l \end{Bmatrix} \Bigg]. \end{aligned} \tag{90}$$

The quantity in brackets, by the addition theorem provided in Equation (58), is one of the hyperspherical harmonics. That is, the expression for the elements of the row identified by the indices $\lambda' = 0$ and $\mu' = 0$ of the irreducible representative of $SO(4)$ defined in Equation (79) is given by

$$R^{2l}_{00\lambda\mu}(\omega_2,\theta_2,\phi_2,\omega_1,\theta_1,\phi_1) = (-1)^{\lambda} \frac{\sqrt{2}\pi}{2l+1} Z^{2l}_{\lambda\mu}(\omega,\theta,\phi), \tag{91}$$

where the arguments ω, θ and ϕ of the hyperspherical harmonic describe the rotation resulting from following a rotation described by ω_1, θ_1 and ϕ_1 by a rotation described by ω_2, θ_2 and ϕ_2. Similar considerations reveal that the elements of the column of the irreducible representative identified by the indices $\lambda = 0$ and $\mu = 0$ may be written as

$$R^{2l}_{\lambda'\mu'00}(\omega_2,\theta_2,\phi_2,\omega_1,\theta_1,\phi_1) = \frac{\sqrt{2}\pi}{2l+1} Z^{2l*}_{\lambda'\mu'}(\omega,\theta,\phi), \tag{92}$$

where the arguments ω, θ and ϕ of the hyperspherical harmonic describe the rotation resulting from following a rotation described by ω_2, θ_2 and ϕ_2 by a rotation described by ω_1, θ_1 and ϕ_1. The author emphasizes that these results are obtained much more simply from Equation (85) than from Equation (79).

Equation (85) is an analytical form for the irreducible representatives of $SO(4)$ that does not require prior construction of the irreducible representatives of $SU(2)$. As indicated above, this formulation allows the properties of the irreducible representatives of $SO(4)$ to be more easily observed, and provides a route to a deeper understanding of the matrices required to change the reference orientation for an ODF in the form of Equation (26).

3.2.4. Bases of the Irreducible Representatives of SO(4)

While definitions of the hyperspherical harmonics appear throughout the literature [49, 50, 52, 59], there is no general agreement on the phase. Since changing the phase of the hyperspherical harmonics amounts to a similarity transformation of the irreducible representatives of $SO(4)$ for which these form a basis, some care should be exercised to ensure that the phase of the hyperspherical harmonics is consistent with the explicit formula for the irreducible representatives of $SO(4)$. Otherwise, these representatives do not transform the elements of the basis correctly. We specifically follow the phase convention of the complex-valued definitions of the hyperspherical harmonics in Refs. [49, 53, 56, 57], and provide some evidence in this section that our formulas for the irreducible representatives of $SO(4)$ are consistent with this choice.

Let us return, for the moment, to the matter of the phase of the irreducible representatives of $SO(3)$. While not necessarily obvious, the irreducible representatives of $SO(3)$ as presented in the literature are entirely compatible with the canonical representation of three-dimensional rotations by real three-by-three orthogonal matrices of determinant one. That is, there exists a similarity transformation that brings the complex three-by-three irreducible representative of $SO(3)$ into the familiar canonical form. Furthermore, the linear transformation effecting this similarity transformation, when right multiplying the row vector of the basis elements of the three-by-three irreducible representative, simultaneously brings the basis into a form that behaves identically to the usual basis vectors of three-dimensional space. Although merely requiring that this similarity transformation exist places a certain constraint on the relationship of the irreducible representative to the basis elements, the ability to freely select the similarity transformation permits an infinite number of consistent forms for the

irreducible representatives and the basis elements. Fortunately, Condon-Shortley phase convention uniquely determines a standard similarity transformation, and allows the irreducible representatives of $SO(3)$ to be given in a consistent form throughout the literature.

The situation is rather different with irreducible representatives of $SO(4)$ and the hyperspherical harmonics. There does not appear to be any counterpart to the Condon-Shortley phase convention to uniquely specify the form of the irreducible representatives of $SO(4)$ and the phase of the hyperspherical harmonics, as is reflected in the variety of phases for the hyperspherical harmonics appearing in the literature [49, 50, 52, 59]. Nevertheless, requiring that the four-by-four irreducible representative of $SO(4)$ and the four hyperspherical harmonics for which $n = 1$ be related in the manner described above is certainly reasonable. That is, we require that there exist an invertible linear transformation of the hyperspherical harmonics which makes the resulting basis behave identically to the orthogonal unit vectors along the w-, x-, y-, and z-axes of Euclidean four-dimensional space, and that simultaneously defines a similarity transformation of the four-by-four irreducible representative which brings the representative into the canonical form.

Of course, this raises the question of the canonical form for the representatives of $SO(4)$, which is generally speaking not as familiar as for $SO(3)$. We propose that the canonical form for these representatives may be considered as deriving from the multiplication rule for normalized quaternions. As indicated in Section 3.2.1, the effect of a prior rotation r on some rotation q may be represented as a multiplication of the column vector of the quaternion components of q by a real four-by-four orthogonal matrix $\boldsymbol{R}$ formed from the quaternion components of r. Similarly, the effect of a subsequent rotation p on some rotation q may be represented as a multiplication of the column vector of the quaternion components of q by a different real four-by-four orthogonal matrix $\boldsymbol{P}$ formed from the quaternion components of p. While the matrices $\boldsymbol{R}$ and $\boldsymbol{P}$ separately perform distinct, constrained four-dimensional rotations, the matrix formed by their product is a general real four-by-four orthogonal matrix of determinant one and performs a general four-dimensional rotation. Since $\boldsymbol{R}$ and $\boldsymbol{P}$ commute, the order

of application of these matrices does not change the result. This provides a canonical form for four-dimensional rotations.

Consider the four-by-four irreducible representative of $SO(4)$ with elements given by Equation (74). The basis of this representative is formed by the four hyperspherical harmonics for which $n=1$. The proposed condition on the phase of the hyperspherical harmonics is that there exists an invertible linear transformation $\boldsymbol{T}^1$ of the hyperspherical harmonics which defines functions that behave analogously to the unit vectors along the w-, x-, y-, and z-axes of Euclidian four-dimensional space, and that $\boldsymbol{T}^1$ simultaneously defines a similarity transformation which brings the irreducible representative into canonical form. A suitable linear transformation exists, and is defined by the relation

$$\begin{bmatrix} Z^1_{00} & Z^1_{11} & Z^1_{10} & Z^1_{1-1} \end{bmatrix} \boldsymbol{T}^1 = \begin{bmatrix} Z^1_{00} & i\left(-Z^1_{11}+Z^1_{1-1}\right)/\sqrt{2} & -\left(Z^1_{11}+Z^1_{1-1}\right)/\sqrt{2} & iZ^1_{10} \end{bmatrix}. \qquad (93)$$

The basis functions on the right of Equation (93) behave exactly as required, differing only by a constant positive coefficient from the four components of a vector in this space as defined by Equation (21). Actually, Equation (93) is identical to Equation (75) for the case $n=1$, since $\boldsymbol{T}^1$ in the current section is identical to the $\boldsymbol{T}^1$ of Section 3.2.2. As remarked at the end of that section, the similarity transformation effected by $\boldsymbol{T}^1$ brings the four-by-four irreducible representative of $SO(4)$ into the canonical form as well. Therefore, while this is not intended to be a rigorous justification for the choice of phase for the hyperspherical harmonics, the hyperspherical harmonics as defined in Equation (24) and the irreducible representatives of $SO(4)$ as defined in Equation (74) appear to be reasonable insofar as they satisfy the compatibility condition outlined above.

4. Conversion to and from the Generalized Spherical Harmonic Expansion

The introductory section of this chapter contains a discussion of numerous ideas and formulas presented in earlier sections of this thesis, which are reproduced here for the reader's convenience. The reader to whom this material is already familiar is encouraged to pass over the current introduction and continuing at the beginning of Section 4.1.

The availability of an analytical form for an orientation distribution function (ODF), which describes a distribution of crystal orientations, is fundamental to the field of texture analysis. Analytical forms of the ODF are used, for example, in extracting orientation statistics from diffraction measurements [69], in studying the effect of processing history on the statistical evolution of microstructures [70], as an input to crystal plasticity finite element methods that examine the effect of mechanical anisotropy during deformation [71], and in the design of materials using spectral methods to identify a desired ODF on the basis of the properties of interest [72]. Nevertheless, the current mathematical treatment of the ODF has remained essentially the same for more than forty years, since the introduction of the generalized spherical harmonic expansion for this purpose [73, 74]. This situation appears to be principally due to the propagation of conventions followed by Bunge in his seminal contributions to the field of texture analysis [4]. These conventions notably include the description of an orientation by the Euler angles ϕ_1, Φ, and ϕ_2, and the consequent expression of the ODF as a linear combination of generalized spherical harmonics $T_l^{m'm}(\phi_1,\Phi,\phi_2)$ in the form

$$f(\phi_1,\Phi,\phi_2)=\sum_{l=0}^{\infty}\sum_{m'=-l}^{l}\sum_{m=-l}^{l}t_l^{m'm}T_l^{m'm}(\phi_1,\Phi,\phi_2), \tag{94}$$

where the coefficients of the expansion are determined by the inner product

$$t_l^{m'm}=\frac{2l+1}{8\pi^2}\int_0^{2\pi}\int_0^{\pi}\int_0^{2\pi}f(\phi_1,\Phi,\phi_2)T_l^{m'm*}(\phi_1,\Phi,\phi_2)\sin\Phi d\phi_1 d\Phi d\phi_2 . \tag{95}$$

Despite the utility of this expansion, the use of Euler angles as a parameterization of rotations is not necessarily ideal. For example, one inevitable difficulty with this method

is the existence of certain singular orientations that do not correspond to a unique set of Euler angles [10]. These orientations correspond to an infinite number of points in the orientation space, and give rise to singularities in the equations of motion [10] and in the formulas used to determine the result of sequential rotations [35, 44]. Furthermore, the description for the boundaries of the asymmetric domains in the orientation space is notably more complex for the Euler angle parameterization [75] than for some of the alternatives [5, 14, 15].

These disadvantages of Euler angles are certainly not inherent to the study of orientation information; to be convinced of this, one needs merely to consider the properties of the normalized quaternion parameterization of rotations [13]. The rotation corresponding to a quaternion is readily apparent from the final three components, which form a vector that points along the axis of rotation and scales monotonically in length with the rotation angle [12]. This close relationship of a quaternion with the axis and angle of a rotation further permits the construction of an orientation space which is substantially simpler to visualize and interpret than that of the Euler angle parameterization, as is described in Section 2.3. With regard to the manipulation of orientation information, the most familiar example of the advantage of quaternions is given by the formula for the multiplication of rotations, which involves only a bilinear combination of the quaternion components [58]. Other instances where the use of quaternions simplifies calculations related to the analysis of orientation information appear throughout the literature [5, 10, 24, 29].

Despite these advantages, a significant portion of the crystallography community continues to use Euler angles instead of quaternions to describe crystallographic texture. While this preference for Euler angles may historically be attributed to the absence of an analytical expression by which to represent an ODF in the quaternion group space, the hyperspherical harmonic expansion provides exactly this alternative. The motivation for this expansion relies on the observation that normalized quaternions may be considered as vectors identifying points on S^3 (the unit sphere in four-dimensional space). Analogous to the expansion of a square-integrable function on S^2 (the unit sphere in three-dimensional space) as an infinite linear combination of the spherical harmonics, a

square-integrable function on S^3 may be expanded as an infinite linear combination of the hyperspherical harmonics $Z_{lm}^{n}(\omega,\theta,\phi)$, or

$$f(\omega,\theta,\phi)=\sum_{n=0,2\ldots}^{\infty}\sum_{l=0}^{n}\sum_{m=-l}^{l}c_{lm}^{n}Z_{lm}^{n}(\omega,\theta,\phi), \tag{96}$$

where the coefficients of the expansion are found from the inner product

$$c_{lm}^{n}=\int_{0}^{2\pi}\int_{0}^{\pi}\int_{0}^{\pi}f(\omega,\theta,\phi)Z_{lm}^{n}(\omega,\theta,\phi)\sin^{2}(\omega/2)\sin\theta d(\omega/2)d\theta d\phi, \tag{97}$$

and n is restricted to even integers by the trivial symmetry of three-dimensional space. This expansion is discussed in more detail in Chapter 2.

Since the physical significance of orientation information does not depend on the means by which it is described, the expansions given in Equations (94) and (96) may in principle be used interchangeably. However, there is presently no means of converting an ODF expressed in the form of the generalized spherical harmonic expansion of Equation (94) to one in the form of the hyperspherical harmonic expansion of Equation (96). With this in mind, the purpose of this chapter is principally to provide continuity with the existing literature by deriving a simple linear transformation to relate the coefficients of these two expansions. Our expectation is that this will allow extant published results in texture analysis to be converted to, and presented in, a more intuitive and accessible form. This result is then harnessed to apply a mathematical technique in common use with the generalized spherical harmonic expansion to the hyperspherical harmonic expansion as well.

4.1. Overview of the Conversion Method

The group of primary concern to the study of crystallographic orientations is *SO*(3), the group of rotations of three-dimensional space. While the importance of this group to the physical sciences has encouraged many authors to investigate its properties, the resulting treatments do not always follow a consistent set of conventions [8, 13, 44, 45]. At least for the current authors, this situation has caused a certain degree of confusion and inconvenience, as the conventions used in deriving many of the results

available in the literature are not always explicitly stated. To our knowledge, the results contained in this paper do not appear anywhere else in the literature with a consistent set of conventions.

We follow the same conventions in the interpretation and use of a rotation matrix as those of Altmann [13]. That is, a rotation operation is viewed as an active rotation of configuration space rather than as a passive rotation of the coordinate system, unless explicitly stated otherwise. A rotation matrix left-multiplies the column vector of the coordinates of a point, and right-multiplies the row vector of the components of a basis. This interpretation allows one to identify a crystal orientation with the rotation operation required to bring a reference crystal into coincidence with the actual crystal. The ODF is then interpreted as a function of rotations of three-dimensional space, or more often as a function of some set of parameters that clearly define a rotation.

This chapter makes use of two parameterizations. The first of these is the Euler angles ϕ_1, Φ, and ϕ_2, which define a general rotation as the result of three consecutive active rotations by the angles $-\phi_1$, $-\Phi$, and $-\phi_2$ about the z-, x-, and z-axes, respectively (from the point of view of an observer attached to the coordinate system, this active rotation sequence is identical to the passive rotation sequence defining the Euler angles as described by Bunge [4]). The second rotation parameterization is by the angles ω, θ, and ϕ, as described in Chapter 2. The relationship of the Euler angles to the angles ω, θ, and ϕ is established by the conversion formulas provided in Appendix D.

The analytical form of the ODF used by the majority of the crystallography community is provided in Equation (94), where rotations are parameterized by sets of Euler angles. This equation actually derives from one of the consequences of the Peter-Weyl theorem, namely, that the matrix elements of the irreducible representatives of $SO(3)$ provide a complete, orthogonal basis for the expansion of a square-integrable function of three-dimensional rotations [76]. While many expressions for the irreducible representatives of $SO(3)$ appear in the literature, they often differ from one another by similarity transformations [8, 13, 44, 45]. Once a set of conventions is specified and a consistent expression is found, the Peter-Weyl theorem allows the ODF to be written as an infinite linear combination of the matrix elements of these irreducible representatives. For example, the expansion in Equation (94) is found by following the phase convention

of Bunge [4], expressing the matrix elements of the irreducible representatives of $SO(3)$ as functions of the Euler angles, and denoting the matrix element in row m' and column m of the $(2l+1)$-dimensional irreducible representative by $T_l^{m'm}(\phi_1, \Phi, \phi_2)$.

The expansion provided in Equation (96) follows more directly from a consideration of $SO(4)$, the group of rotations of four-dimensional space. A well-known result of group theory states that the basis elements of the irreducible representatives of a group of operators provide a complete, orthogonal basis for the expansion of a function to which an operation of that group may be applied [8]. Since sets of the hyperspherical harmonics $Z_{lm}^{n}(\omega, \theta, \phi)$ transform as the bases of the irreducible representatives of $SO(4)$, the hyperspherical harmonics form a complete, orthogonal basis for the expansion of a square-integrable function on S^3. Considering points on S^3 to correspond to normalized quaternions, Equation (21) suggests that the angles ω, θ, and ϕ identify points on S^3 in a manner analogous to that of the spherical angles on S^2. That is, exactly as a function on S^2 is more naturally written as a function of the spherical angles than Cartesian coordinates, a function on S^3 is more naturally written as a function of the angles ω, θ, and ϕ than of quaternion coordinates. The angles ω, θ, and ϕ are therefore entirely compatible with the interpretation of the ODF as a square-integrable function on S^3, which allows the ODF to be written as an infinite linear combination of the hyperspherical harmonics in Equation (96).

Regardless of the different motivations for the generalized spherical harmonic and the hyperspherical harmonic expansions, they contain the same orientation information. As such, there must be a method to convert from one expansion to the other. This conversion is found by comparing the expressions for the matrix elements of the irreducible representatives of $SO(3)$ as functions of the Euler angles and the angles ω, θ, and ϕ. When written using the Euler angles, the expression for these matrix elements gives the formula for the generalized spherical harmonics. When written using the angles ω, θ, and ϕ, the same expression becomes a linear combination of the hyperspherical harmonics. Equating these forms gives the conversion of the basis functions in Equation (94) to the basis functions in Equation (96), and the conversion from the coefficients in

Equation (94) to the coefficients in Equation (96) as well. We develop this approach further in the following.

4.2. Rotation Conventions and the Generalized Spherical Harmonics

There are many mathematical results in the literature that are useful and relevant to the present task. However, incorporating or referring to them without establishing a consistent set of conventions is quite hazardous. In particular, the conversion from the generalized spherical harmonics to the hyperspherical harmonics is nonsensical unless a consistent set of conventions is used to derive the expressions for the matrix elements of the irreducible representatives of $SO(3)$ as functions of the Euler angles and the angles ω, θ, and ϕ. We therefore devote a significant portion of this chapter to the consideration of this issue.

The definition of the generalized spherical harmonics most frequently used by the crystallography community is [4]

$$T_l^{m'm}(\phi_1,\Phi,\phi_2) = e^{im'\phi_2} P_l^{m'm}(\cos\Phi) e^{im\phi_1}, \tag{98}$$

where the function $P_l^{m'm}(\cos\Phi)$ is defined as

$$\begin{aligned} P_l^{m'm}(\cos\Phi) = \frac{(-1)^{l-m'} i^{m-m'}}{2^l} \sqrt{\frac{(l+m)!}{(l-m')!(l+m')!(l-m)!}} (1-\cos\Phi)^{(m'-m)/2} \\ \times (1+\cos\Phi)^{-(m'+m)/2} \frac{d^{l-m}}{d(\cos\Phi)^{l-m}} \left[(1-\cos\Phi)^{l-m'} (1+\cos\Phi)^{l+m'} \right]. \end{aligned} \tag{99}$$

The generalized spherical harmonic may be considered as the matrix element in row m' and column m of the $(2l+1)$-dimensional irreducible representative of $SO(3)$. Therefore, Equation (98) depends implicitly on the conventions adopted by Bunge [4] during the construction of the irreducible representatives. Generally speaking, the range of conventions that must be specified include the selection of the basis elements, the choice of the active or passive rotation convention, and the parameterization used to write the formulas for the resulting matrix elements.

The vast majority of literature on the subject, including that by Bunge [4] and the current document, selects the set of spherical harmonics with a particular value of l as the

basis elements of the $(2l+1)$-dimensional irreducible representatives of $SO(3)$. Since the basis is consistent throughout, the issue is not discussed further. As for the remaining conventions enumerated above, Bunge [4] uses the passive convention and the Euler angle parameterization, while we use the active convention and the angles ω, θ, and ϕ. The comparison of matrix elements apparently requires that the relationship of the representatives constructed following these different conventions be clearly established. We address these differences individually for the sake of clarity, with the difference in rotation convention first and the difference in parameterization second.

4.2.1. Determination of the Functions $D^{l}_{m'm}(\phi_1,\Phi,\phi_2)$

Regarding the difference in rotation convention, consider that a rotation matrix's elements depend only on the selection of an initial coordinate system and the apparent rotation of space from the perspective of an observer rigidly attached to that coordinate system. If two matrices that effect the same apparent transformation of space share a single basis, then corresponding matrix elements of the two matrices should be the same, independent of the rotation convention followed. In particular, sequential active rotations by $-\phi_1$ about the z axis, $-\Phi$ about the x axis, and $-\phi_2$ about the z axis effect the same apparent transformation of space as sequential passive rotations by ϕ_1 about the z axis, by Φ about the x' axis, and by ϕ_2 about the z'' axis. Therefore, the elements of the matrix describing the active rotation sequence should be the same as the elements of the matrix describing the passive rotation sequence.

Throughout the literature, the generalized spherical harmonic $T_l^{m'm}(\phi_1,\Phi,\phi_2)$ is considered to be the matrix element in row m' and column m of the $(2l+1)$-dimensional irreducible representative of $SO(3)$ that describes the passive rotation sequence of the preceding paragraph. Define the function $D^{l}_{m'm}(\phi_1,\Phi,\phi_2)$ as the corresponding matrix element in row m' and column m of the $(2l+1)$-dimensional irreducible representative of $SO(3)$ that describes the active rotation sequence of the preceding paragraph. Since this function differs from the generalized spherical harmonic $T_l^{m'm}(\phi_1,\Phi,\phi_2)$ only in the sense

in which the irreducible representative is interpreted, these functions should be identical, i.e. $T_l^{m'm}(\phi_1,\theta,\phi_2)=D_{m'm}^l(\phi_1,\Phi,\phi_2)$. Curiously, this is not found to be the case.

The functions $D_{m'm}^l(\phi_1,\Phi,\phi_2)$ may be found by converting an existing expression for the matrix elements of the $(2l+1)$-dimensional irreducible representatives of $SU(2)$ in terms of the Cayley-Klein parameters into an equivalent expression in terms of the Euler angles ϕ_1, Φ, and ϕ_2. The matrix elements of the irreducible representatives of $SU(2)$ as functions of the Cayley-Klein parameters are given by [8, 13, 44, 45]

$$R_{m'm}^l(a,b)=\sqrt{(l+m')!(l-m')!(l+m)!(l-m)!}\cdot\sum_k\frac{a^{l+m-k}(a^*)^{l-m'-k}b^{m'-m+k}(-b^*)^k}{(l+m-k)!(l-m'-k)!(m'-m+k)!k!}, \tag{100}$$

as in Equation (36). The meaning and use of the representative constructed from these matrix elements varies among the cited references; our interpretation follows that of Ref. [13]. The dimension of the representative is $(2l+1)$, where l is restricted to non-negative integral or half-integral (half of an odd integer) values. Restricting l to integral values gives the representatives of $SO(3)$. The index m' labels the rows of the matrix sequentially from l to $-l$, and m labels the columns sequentially from l to $-l$. The index k ranges over all values for which the factorials are finite.

Converting Equation (100) into a function of the Euler angles requires that the relationship of the Cayley-Klein and Euler angle parameterizations be known. Their relationship is found by comparing the matrix elements of the complex two-by-two irreducible representatives of $SU(2)$ written in the Cayley-Klein and Euler angle parameterizations, which are provided by Equations (184) and (186) of Appendix D. This comparison yields the relations $a=\cos(\Phi/2)e^{i(\phi_1+\phi_2)/2}$ and $b=i\sin(\Phi/2)e^{-i(\phi_1-\phi_2)/2}$. Substituting these into Equation (100) and rearranging the result provides

$$D_{m'm}^l(\phi_1,\Phi,\phi_2)=\left[i^{m'-m}\sqrt{(l+m')!(l-m')!(l+m)!(l-m)!}\left(\frac{1+\cos\Phi}{2}\right)^l\left(\frac{1-\cos\Phi}{1+\cos\Phi}\right)^{(m'-m)/2}\right.$$
$$\left.\times\sum_k\frac{(-1)^k}{(l+m-k)!(l-m'-k)!(m'-m+k)!k!}\left(\frac{1-\cos\Phi}{1+\cos\Phi}\right)^k\right]e^{im'\phi_2}e^{im\phi_1}. \tag{101}$$

The quantity in brackets (or a closely related quantity) appears in Refs. [8, 42, 44, 45], though there is considerable variation in the phase and notation, and none of these references provide this quantity with a name. This quantity is in fact exactly equal to one appearing in Ref. [44], where it is denoted as the function $P^{l}_{m'm}(\cos\Phi)$.

One of the symmetries of the function $P^{l}_{m'm}(\cos\Phi)$ is revealed by introducing $k' = k - m$ as the summation index instead of k in Equation (101). Inspection of the result indicates that $P^{l}_{m'm}(\cos\Phi)$ is symmetric with respect to the exchange of the indices m' and m, or that $P^{l}_{m'm}(\cos\Phi) = P^{l}_{mm'}(\cos\Phi)$. An alternate expression for $P^{l}_{m'm}(\cos\Phi)$ that is provided in Ref. [44] is

$$P^{l}_{m'm}(\cos\Phi) = \frac{(-1)^{l-m'} i^{m'-m}}{2^{l}} \sqrt{\frac{(l+m')!}{(l-m)!(l+m)!(l-m')!}} (1+\cos\Phi)^{-(m'+m)/2} (1-\cos\Phi)^{-(m'-m)/2} \times \frac{d^{l-m'}}{d(\cos\Phi)^{l-m'}} \left[(1-\cos\Phi)^{l-m} (1+\cos\Phi)^{l+m} \right]. \tag{102}$$

Exchanging the indices m' and m in this expression and comparing with the function $P_{l}^{m'm}(\cos\Phi)$ of Equation (99) reveals that

$$P^{l}_{m'm}(\cos\Phi) = (-1)^{m'-m} P_{l}^{m'm}(\cos\Phi). \tag{103}$$

With this equivalence, the function $D^{l}_{m'm}(\phi_1, \Phi, \phi_2)$ may be written as

$$D^{l}_{m'm}(\phi_1, \Phi, \phi_2) = (-1)^{m'-m} \left[e^{im'\phi_2} P_{l}^{m'm}(\cos\Phi) e^{im\phi_1} \right]. \tag{104}$$

The quantity in brackets is the generalized spherical harmonic $T_{l}^{m'm}(\phi_1, \Phi, \phi_2)$ of Equation (98), providing the relation

$$D^{l}_{m'm}(\phi_1, \Phi, \phi_2) = (-1)^{m'-m} T_{l}^{m'm}(\phi_1, \Phi, \phi_2). \tag{105}$$

That is, the representatives of $SU(2)$ consistent with the current conventions differ from those used by Bunge [4], and by the texture community in general, by a similarity transformation.

4.2.2. Phase of the Generalized Spherical Harmonics

As indicated by Equation (105), the relationship between the two nominally equivalent expressions for the matrix elements of the irreducible representatives is found to be

$$T_l^{m'm}(\phi_1,\Phi,\phi_2) = (-1)^{m-m'} D_{m'm}^l(\phi_1,\Phi,\phi_2), \tag{106}$$

where there is an unexpected difference of phase between the two functions. Unfortunately, it is not possible to directly compare the derivations of these expressions in order to identify the source of the disparity, since Bunge [4] does not provide a derivation of the formula for the generalized spherical harmonics. Rather, he indicates that more detailed accounts of the representations and properties of the generalized spherical harmonics appear in Gelfand, Minlos and Shapiro [42], Vilenkin [44], and Wigner [8], though this is not precisely true. While functions related to the generalized spherical harmonics do appear in these references, none of these is identical to his definition of the generalized spherical harmonics. These authors indicate their assorted expressions for the matrix elements of the irreducible representatives of $SO(3)$ by $T_{m'm}^l(\phi_1,\theta,\phi_2)$ [42], $t_{m'm}^l(\phi,\theta,\psi)$ [44], and $\boldsymbol{D}^{(l)}(\{\alpha,\beta,\gamma\})_{m'm}$ [8], respectively. Inserting ϕ_1, Φ, and ϕ_2 for the angles of the first, second, and third rotations of these functions, we find that their relationships to the generalized spherical harmonics $T_l^{m'm}(\phi_1,\Phi,\phi_2)$ are

$$T_l^{m'm}(\phi_1,\Phi,\phi_2) = (-1)^{m'-m} T_{m'm}^{l*}(\phi_1,\Phi,\phi_2) = t_{m'm}^{l*}(\phi_2,\Phi,\phi_1) = i^{m-m'} \boldsymbol{D}^{(l)}(\{\phi_2,\Phi,\phi_1\})_{m'm}, \tag{107}$$

where * is the complex conjugate. Examining Equation (107), we see that none of these expressions matches the form provided by Bunge. That is, Bunge neither provides a derivation of the expression he uses for the generalized spherical harmonics, nor provides a reference to a derivation consistent with the conventions he followed. The difference between $T_l^{m'm}(\phi_1,\Phi,\phi_2)$ and $D_{m'm}^l(\phi_1,\Phi,\phi_2)$ in Equation (106) therefore appears to have developed from an internal inconsistency in his work [4], though it is difficult to verify the presence of an error without clearly establishing the source of the generalized spherical harmonics.

Whether or not the equation for the generalized spherical harmonics is internally consistent with the conventions followed by Bunge [4], the expansion in Equation (94) remains a valid expansion of the ODF; changing the generalized spherical harmonics by a constant factor amounts to pulling a constant factor out of the coefficients in the expansion. Since Bunge used the generalized spherical harmonics almost exclusively in the context of Equation (94), the question of the constant factor appearing in Equation (106) is virtually irrelevant to his subsequent results. For the purposes of the present chapter, however, a constant factor represents a change in the values of the matrix elements of the irreducible representatives of $SO(3)$. Equating expressions for the matrix elements in different parameterizations certainly gives nonsensical results when the expressions are not equal. Therefore, the functions $D^{l}_{m'm}(\phi_1,\Phi,\phi_2)$ will be considered as more fundamental from the standpoint of calculations within this section, though the majority of our equations will be formulated using the functions $T_l^{m'm}(\phi_1,\Phi,\phi_2)$ in order to relate our results more directly to the literature.

4.3. Relating the Irreducible Representatives

With the relationship of the generalized spherical harmonics $T_l^{m'm}(\phi_1,\Phi,\phi_2)$ to the functions $D^{l}_{m'm}(\phi_1,\Phi,\phi_2)$ provided by Equation (106), the conversion formulas relating $T_l^{m'm}(\phi_1,\Phi,\phi_2)$ to the hyperspherical harmonics may be formulated once the relationship of the hyperspherical harmonics to the intermediate functions $D^{l}_{m'm}(\phi_1,\Phi,\phi_2)$ is known. The current convention is to define the hyperspherical harmonics as in Equation (24), that is,

$$Z^{n}_{lm}(\omega,\theta,\phi) = (-i)^{l}\frac{2^{l+1/2}\,l!}{2\pi}\sqrt{(2l+1)\frac{(l-m)!}{(l+m)!}\frac{(n+1)(n-l)!}{(n+l+1)!}}\sin^{l}(\omega/2)C^{l+1}_{n-l}[\cos(\omega/2)] \times P_l^{m}(\cos\theta)e^{im\phi}, \tag{108}$$

with integer indices $0 \le n$, $0 \le l \le n$, and $-l \le m \le l$. As indicated by Equation (52) of Section 3.1.1, the matrix element in row m' and column m of the $(2l+1)$-dimensional irreducible representative of $SO(3)$ may be written as a linear combination of the hyperspherical harmonics in the form

$$U^{l}_{m'm}(\omega,\theta,\phi)=\sum_{\lambda}\sum_{\mu}C^{lm}_{lm'\lambda\mu}\frac{\sqrt{2(2\lambda+1)}\pi}{2l+1}Z^{2l}_{\lambda\mu}(\omega,\theta,\phi). \tag{109}$$

The question of the relationship of the hyperspherical harmonics to the functions $D^{l}_{m'm}(\phi_1,\Phi,\phi_2)$ is therefore equivalent to the question of the relationship of the functions $U^{l}_{m'm}(\omega,\theta,\phi)$ to the $D^{l}_{m'm}(\phi_1,\Phi,\phi_2)$.

For this, a consideration of the physical significance of the rotation operations

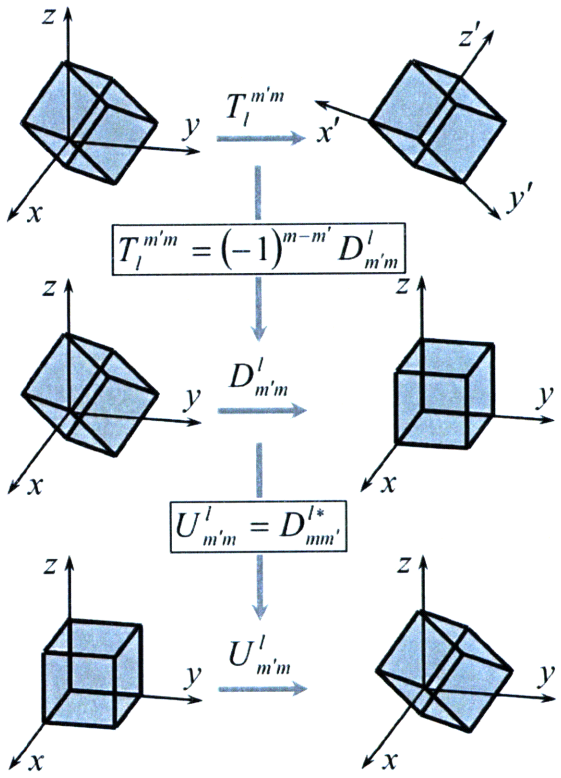

Figure 16: The physical interpretation and relationship of the quantities $T_l^{m'm}(\phi_1,\Phi,\phi_2)$, $D^{l}_{m'm}(\phi_1,\Phi,\phi_2)$, and $U^{l}_{m'm}(\omega,\theta,\phi)$. $T_l^{m'm}(\phi_1,\Phi,\phi_2)$ is considered to passively bring the coordinate system into coincidence with an oriented crystal. $D^{l}_{m'm}(\phi_1,\Phi,\phi_2)$ is considered to actively bring an oriented crystal into coincidence with the coordinate system; this is identical to the effect of $T_l^{m'm}(\phi_1,\Phi,\phi_2)$ from the perspective of an observer attached to the coordinate system. $U^{l}_{m'm}(\omega,\theta,\phi)$ is considered to actively bring a reference crystal into coincidence with the oriented crystal; this is the inverse of the effect of $D^{l}_{m'm}(\phi_1,\Phi,\phi_2)$.

corresponding to $T_l^{m'm}(\phi_1,\Phi,\phi_2)$, $D_{m'm}^l(\phi_1,\Phi,\phi_2)$ and $U_{m'm}^l(\omega,\theta,\phi)$ is useful. According to Bunge [4], $T_l^{m'm}(\phi_1,\Phi,\phi_2)$ describes a crystal orientation by the passive rotation which brings the coordinate system initially aligned with the sample into alignment with the crystal, where the crystal is aligned with the actual orientation throughout. This operation is shown at the top of Figure 16. As discussed in Section 4.2.1, $D_{m'm}^l(\phi_1,\Phi,\phi_2)$ describes a crystal orientation by the active rotation which brings the crystal initially aligned with the actual orientation into alignment with the reference orientation, where the coordinate system is aligned with the sample throughout. This operation is shown in the middle of Figure 16, and is the active counterpart to the traditional description. Finally, $U_{m'm}^l(\omega,\theta,\phi)$ by definition describes a crystal orientation by the active rotation which brings the crystal initially aligned with the reference orientation into alignment with the actual orientation, where the coordinate system is aligned with the sample throughout. This operation is shown at the bottom of Figure 16.

Reference to Figure 16 clearly indicates that the active rotation corresponding to $D_{m'm}^l(\phi_1,\Phi,\phi_2)$ is the inverse of the active rotation corresponding to $U_{m'm}^l(\omega,\theta,\phi)$. That is, the unitary matrix constructed from $D_{m'm}^l(\phi_1,\Phi,\phi_2)$ is the inverse of the unitary matrix constructed from $U_{m'm}^l(\omega,\theta,\phi)$, or

$$D_{m'm}^l(\phi_1,\Phi,\phi_2)=U_{mm'}^{l*}(\omega,\theta,\phi). \tag{110}$$

Applying Equation (106) to Equation (110) gives

$$T_l^{m'm}(\phi_1,\Phi,\phi_2)=(-1)^{m-m'}U_{mm'}^{l*}(\omega,\theta,\phi). \tag{111}$$

This equation relates $T_l^{m'm}(\phi_1,\Phi,\phi_2)$, formulated with the passive convention and the Euler angle parameterization, to $U_{m'm}^l(\omega,\theta,\phi)$, formulated with the active convention and the axis-angle parameterization, and is the basis for the conversion formulas presented in the subsequent section.

4.4. Conversion Formulas

The conversion from the generalized spherical harmonics to the hyperspherical harmonics proceeds according to the prescription mentioned Section 4.1 of the current chapter; since the value of the matrix elements of the irreducible representatives of $SO(3)$ must be independent of the parameterization, the formulas for these matrix elements as functions of the Euler angles and of the angles ω, θ, and ϕ may be equated. Inverting Equation (111) and inserting Equation (109) reveals that

$$(-1)^{m-m'} T_l^{mm'*}(\phi_1, \Phi, \phi_2) = \sum_{\lambda} \sum_{\mu} C_{lm'\lambda\mu}^{lm} \frac{\sqrt{2(2\lambda+1)}\pi}{2l+1} Z_{\lambda\mu}^{2l}(\omega, \theta, \phi). \tag{112}$$

After relabeling the indices m and m', complex conjugating both sides and applying Equation (81), this becomes

$$T_l^{m'm}(\phi_1, \Phi, \phi_2) = \sum_{\lambda} \sum_{\mu} (-1)^{\lambda+\mu+m-m'} C_{lm\lambda\mu}^{lm'} \frac{\sqrt{2(2\lambda+1)}\pi}{2l+1} Z_{\lambda-\mu}^{2l}(\omega, \theta, \phi). \tag{113}$$

Changing the summation over μ to a summation over $-\mu$ and applying the symmetry properties of the Clebsch-Gordan coefficients gives the result

$$T_l^{m'm}(\phi_1, \Phi, \phi_2) = \sum_{\lambda} \sum_{\mu} (-1)^{\lambda+m-m'} C_{lm'\lambda\mu}^{lm} \frac{\sqrt{2(2\lambda+1)}\pi}{2l+1} Z_{\lambda\mu}^{2l}(\omega, \theta, \phi). \tag{114}$$

This establishes the formula to convert from the generalized spherical harmonics to the hyperspherical harmonics.

The inverse expression is found by exploiting the unitarity relations of the Clebsch-Gordan coefficients. This procedure is simplified by initially applying the symmetry properties of the Clebsch-Gordan coefficients to obtain

$$T_l^{m'm}(\phi_1, \Phi, \phi_2) = \sum_{\lambda} \sum_{\mu} (-1)^{l+m} C_{l-m'lm}^{\lambda\mu} \frac{\sqrt{2}\pi}{\sqrt{2l+1}} Z_{\lambda\mu}^{2l}(\omega, \theta, \phi). \tag{115}$$

Multiplying through by $C_{l-m'lm}^{\lambda'\mu'}$, summing over the indices $-m'$ and m, and rearranging the summations then gives

$$\sum_{-m'}\sum_{m}(-1)^{-l-m}C^{\lambda'\mu'}_{l-m'lm}\frac{\sqrt{2l+1}}{\sqrt{2\pi}}T_l^{m'm}(\phi_1,\Phi,\phi_2)=\sum_{\lambda}\sum_{\mu}Z^{2l}_{\lambda\mu}(\omega,\theta,\phi)\times\left[\sum_{-m'}\sum_{m}C^{\lambda'\mu'}_{l-m'lm}C^{\lambda\mu}_{l-m'lm}\right]. \tag{116}$$

The quantity in brackets is $\delta_{\lambda'\lambda}\delta_{\mu'\mu}$ by the unitarity of the Clebsch-Gordan coefficients, simplifying the equation to

$$Z^{2l}_{\lambda\mu}(\omega,\theta,\phi)=\sum_{-m'}\sum_{m}(-1)^{-l-m}C^{\lambda\mu}_{l-m'lm}\frac{\sqrt{2l+1}}{\sqrt{2\pi}}T_l^{m'm}(\phi_1,\Phi,\phi_2). \tag{117}$$

Applying the symmetry properties of the Clebsch-Gordan coefficients and replacing the summation over $-m'$ with a summation over m' gives

$$Z^{2l}_{\lambda\mu}(\omega,\theta,\phi)=\sum_{m'}\sum_{m}(-1)^{\lambda+m'-m}C^{lm}_{lm'\lambda\mu}\frac{\sqrt{2\lambda+1}}{\sqrt{2\pi}}T_l^{m'm}(\phi_1,\Phi,\phi_2), \tag{118}$$

where the indices of summation satisfy the constraint $m-m'=\mu$. This is the counterpart to Equation (114), and establishes the formula to convert from the hyperspherical harmonics to the generalized spherical harmonics.

The ability to convert the basis functions of Equation (94) into those of Equation (96) is not as useful as the ability to convert the expansion coefficients directly, though. Calculation of these formulas requires one to account for the fact that the values of the ODFs as expressed by Equation (94) and Equation (96) are different. This is simplest to observe for the case of a uniform distribution, for which the value of the ODF in Equation (94) is unity everywhere, while the value of the ODF in Equation (96) is $1/2\pi^2$ everywhere. As with the matrix elements of the irreducible representatives of $SO(3)$, equating expansions of the ODF when the values of the ODFs at corresponding points are not equal is nonsensical. This disparity is resolved by multiplying one of the expansions by the appropriate coefficient, or

$$f(\phi_1,\Phi,\phi_2)=2\pi^2 f(\omega,\theta,\phi). \tag{119}$$

Multiplying this by the complex conjugate of Equation (114) and integrating by means of Equation (190) in Appendix D results in

$$\int_0^{2\pi}\int_0^{\pi}\int_0^{2\pi} f(\phi_1,\Phi,\phi_2)T_l^{m'm*}\sin\Phi d\phi_1 d\Phi d\phi_2 = \sum_{\lambda}\sum_{\mu}(-1)^{\lambda+m-m'} C_{lm'\lambda\mu}^{lm}\frac{8\pi^3\sqrt{2(2\lambda+1)}}{2l+1} \times \int_0^{2\pi}\int_0^{\pi}\int_0^{\pi} f(\omega,\theta,\phi)Z_{\lambda\mu}^{2l*}\sin^2(\omega/2)\sin\theta d(\omega/2)d\theta d\phi\,, \tag{120}$$

where an additional factor of 1/2 is introduced on the right side to account for the fact that every orientation is included in the integrated volume twice. The integrals may be evaluated by means of Equation (95) and Equation (97), and simplification gives

$$t_l^{m'm} = \sum_{\lambda}\sum_{\mu}(-1)^{\lambda+m-m'} C_{lm'\lambda\mu}^{lm}\pi\sqrt{2(2\lambda+1)}c_{\lambda\mu}^{2l}\,. \tag{121}$$

The inverse expression may be found either by a similar integration, or by inverting Equation (121) directly, with the result that

$$c_{\lambda\mu}^{2l} = \sum_{m'}\sum_{m}(-1)^{\lambda+m'-m} C_{lm'\lambda\mu}^{lm}\frac{\sqrt{2\lambda+1}}{\sqrt{2}\pi(2l+1)}t_l^{m'm}\,. \tag{122}$$

Equations (121) and (122) provide the linear transformations to convert an ODF written in the form of Equation (94) directly into the form of Equation (96), and *vice-versa*; the required Clebsch-Gordan coefficients are given in Appendix C.

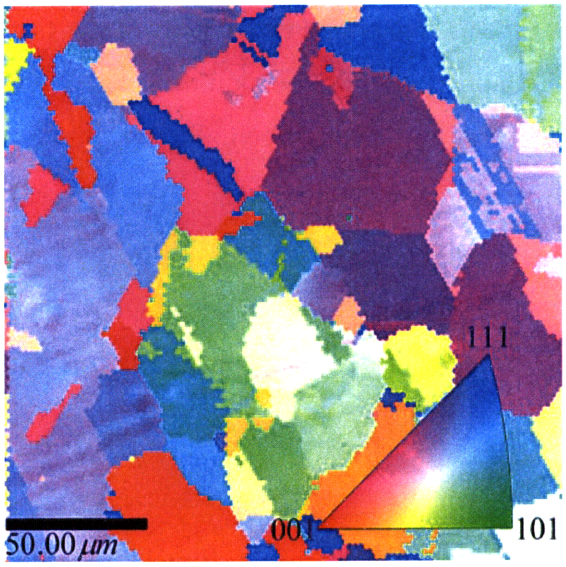

Figure 17: The normal direction inverse pole figure of a copper sample, as measured experimentally by EBSD.

4.5. Implementation of the Conversion

In this section we validate the results of the previous sections of the chapter by applying them to the ODF of a copper sample, as determined experimentally by electron backscatter diffraction (EBSD). For reference, the normal direction inverse pole figure map of the measured area is given in Figure 17. We validate the conversion formulas by comparing the coefficients c_{lm}^{n} of the hyperspherical harmonic expansion as calculated directly from fitting the experimental data with Equation (97), and as calculated by first fitting for the coefficients $t_{l}^{m'm}$ of the generalized spherical harmonic expansion from Equation (95) and then converting them to the c_{lm}^{n} using Equation (122). The analytical expression for an ODF should be independent of the calculation method used, so the equivalence of these sets of coefficients provides evidence for the accuracy of the formulas derived in the preceding sections.

The expansion of the ODF given by the coefficients calculated directly from the

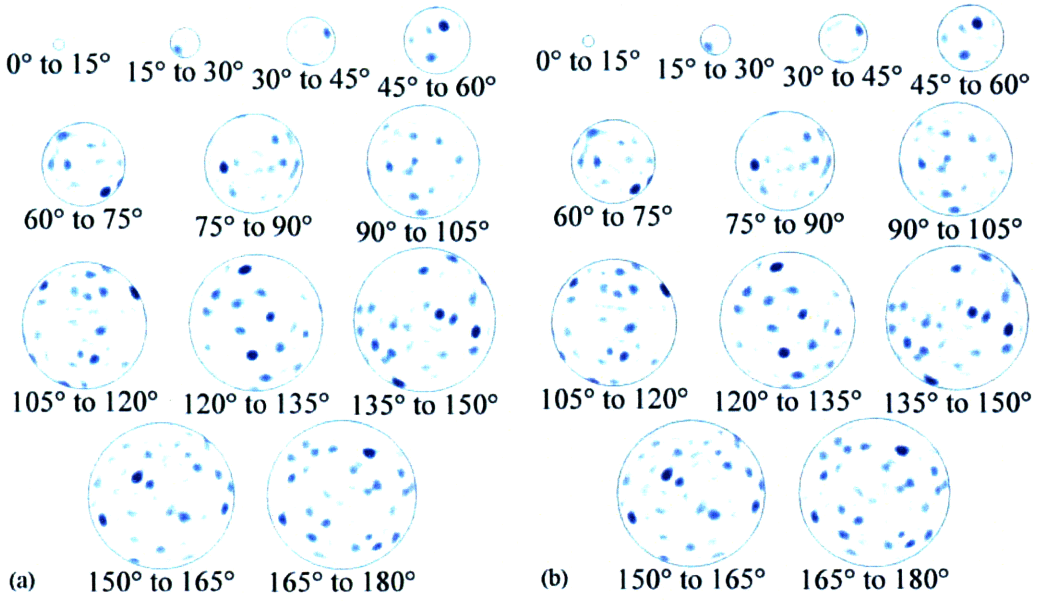

Figure 18: The ODF of the copper sample in Figure 17, expressed via the hyperspherical harmonic expansion given in Equation (96). Blue and red indicate regions of positive and negative probability density, respectively. (a) The coefficients of the expansion are calculated using Equation (97). (b) The coefficients of the expansion are calculated using Equations (95) and (122), i.e. by means of the coefficient conversion formulas. Inspection of the figures reveals that the expansions are identical.

experimental data appears in Figure 18a, and that given by the coefficients calculated indirectly through conversion from the generalized spherical harmonics using Equation (122) appears in Figure 18b. The infinite summation in the hyperspherical harmonic expansion of Equation (96) is limited to $n \leq 30$, and the procedure used to display the hyperspherical harmonic expansions graphically is described in Section 2.3. Blue and red regions correspond to positive and negative probability density, respectively. The presence of a few clearly distinguishable probability density peaks reflects that the observed region contained only a few grains, while the resemblance of Figure 18a to Figure 18b indicates that the directly calculated coefficients match well with those calculated by means of the conversion formulas. Although not practical to present in print, we have directly compared the numerical values of the 5456 coefficients in the two expansions as well, and they are equal to within one part per 10^8, i.e., to within the error of the numerical calculations. These results convincingly validate the conclusions in the preceding sections.

4.6. The Positivity Constraint

We anticipate that the conversion formulas presented above will allow existing texture information to be translated easily into the new hyperspherical harmonic-based representation. Beyond texture information, however, the conversion formulas carry the broader implication that mathematical methods and tools developed for use with the generalized spherical harmonics do not need to be re-derived for the hyperspherical harmonics. One example is provided by the positivity method for the correction of the ghost error, which has been handled in the context of the generalized spherical harmonic expansion by prior researchers [77-79].

The regions of negative probability density appearing in Figure 18 are unphysical, and result from the truncation of the infinite expansion to a finite number of terms. Historically speaking, regions of negative probability density often appeared in the generalized spherical harmonic expansion of the ODF, though this phenomenon was generally attributed to the inherent limitations on information obtained from conventional diffraction experiments (i.e., the so-called "ghost error") rather than truncation error. Many of the same techniques developed in the literature to correct for the ghost error may

be used to correct for the truncation error as well. Roughly, these include the positivity method [77-79], the quadratic method [80, 81], and the maximum entropy method [82-85]. Of these, the positivity method is arguably the simplest to implement. This method traditionally involves finding an approximation for the odd l coefficients in Equation (94) by enforcing the non-negativity of the ODF.

Explicitly, given a reduced ODF $f_0(g)$ that is calculated using only the even l coefficients, define a function

$$\hat{f}_{l+1}(g)=\begin{cases}-f_l(g) & f_l(g)<0\\ 0 & \text{otherwise}\end{cases}. \tag{123}$$

Find the expansion coefficients of $\hat{f}_1(g)$ from Equation (95), and use the even l coefficients of $f_0(g)$ and the odd l coefficients of $\hat{f}_1(g)$ to define the function $f_1(g)$. From this point on, the positivity method follows an iterative procedure. Insert $f_l(g)$ into Equation (123) to define a function $\hat{f}_{l+1}(g)$, and find the expansion coefficients of this function from Equation (95). Define the function $f_{l+1}(g)$ from the even l coefficients of $f_l(g)$ and the sum of the odd l coefficients of $\hat{f}_{l+1}(g)$ and $f_l(g)$, and repeat the procedure until the magnitude of the negative probability density in $f_{l+1}(g)$ falls below a set threshold. The function $f_{l+1}(g)$ is called the complete ODF.

The same general principle, with minor modifications, may be used to reduce the extent of the truncation error in Figure 18. Indicate the hyperspherical harmonic expansion of the ODF by $f_0(g)$. Insert this function into Equation (123) to find $\hat{f}_1(g)$, and calculate the expansion coefficients of $\hat{f}_1(g)$ from Equation (97). Form the sum of every coefficient of $f_0(g)$ with the corresponding coefficient of $\hat{f}_1(g)$, and normalize the result by multiplying each coefficient by the constant that brings c_{00}^0 to the value $1/\sqrt{2\pi}$. This collection of coefficients defines the function $f_1(g)$, which is a normalized approximation to $f_0(g)+\hat{f}_1(g)$. This procedure is iteratively repeated, using Equation (123) to find $\hat{f}_{l+1}(g)$ from $f_l(g)$, until the magnitude of the negative probability density

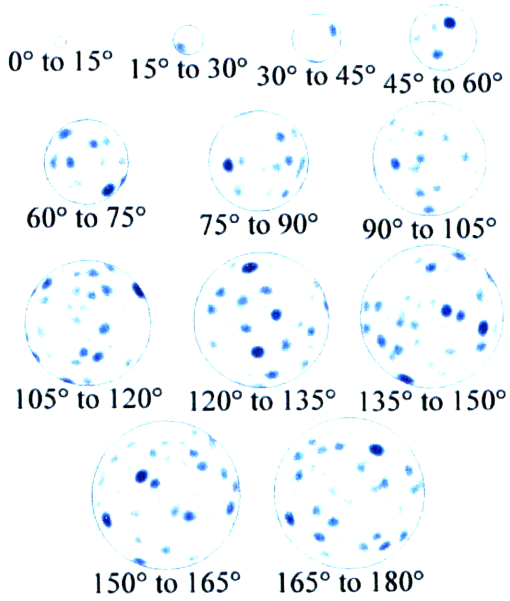

Figure 19: The ODF given in Figure 18a, constrained to positive values by the procedure described in Section 4.6. Apart from the removal of the regions of negative probability density and a slight broadening of the peaks, the distribution function is identical.

in $f_{i+1}(g)$ falls below a set threshold. The primary difference of this method from the positivity method outlined above is that the majority of current orientation measurement techniques provide information about all the coefficients in the expansion. This property removes the need to preserve the values of some coefficients while selectively changing others.

This positivity method is applied to the hyperspherical harmonic expansion of the ODF appearing in Figure 18, with the result shown in Figure 19. The procedure markedly reduces the magnitude of the negative probability density regions, though at the inevitable price of broadening the peaks in the probability distribution function.

4.7. Conclusion

While the importance of the generalized spherical harmonic expansion of an ODF to the historical development of texture analysis is undeniable, exclusive reliance on a single particular expansion is inherently limiting. This is quite clear from an examination of the literature, where discrete orientations are routinely manipulated with multiple parameterizations (rotation matrices, Rodrigues vectors, Euler angles, etc.) to leverage

their complementary strengths, but orientation distributions in the past benefited from only this single representation. The absence of an alternative to the generalized spherical harmonic expansion required that every operation on the ODF be performed in the Euler angle parameterization, regardless of its suitability. The hyperspherical harmonic expansion of an ODF provides the missing alternative, though the utility of this expansion relies on the existence of a means by which to efficiently and easily convert from one representation to the other; this chapter provides the equations effecting this conversion for the first time.

The ramifications of these conversion formulas are expected to extend further than the ability to express a particular ODF in the axis-angle parameterization. Specifically, these formulas provide continuity of the hyperspherical harmonic expansion with the existing literature, and allow mathematical results derived using the generalized spherical harmonic expansion (or programs written using this expansion) to be used with a minimum of modification. As a simple example, the fact that the conversion of the expansion coefficients is a linear transformation enables one of the procedures existing in the literature to enforce a positivity condition on the generalized spherical harmonic expansion of the ODF to be applied directly to the hyperspherical harmonic expansion of the ODF. We hope that these results significantly increase the accessibility and utility of the hyperspherical harmonic expansion in the field of texture analysis.

5. Symmetrization of the Hyperspherical Harmonics[7]

While the expansion of functions on a unit circle and a unit sphere (as performed with Equations (12) and (15), respectively) and the hyperspherical harmonic expansion (as performed with Equation (31)) may be applied to any square-integrable function defined on the appropriate space, the functions of practical interest are usually not arbitrary. For example, an orientation distribution function must reflect the crystal and sample symmetries of the material being considered. The knowledge that the function being considered is subject to certain symmetries is quite valuable, since it allows one to use significantly fewer terms in the expansion than for the general case. The essential idea is that it is only necessary to use the *symmetrized harmonics*, or those linear combinations of harmonics that reflect the symmetries of the system. Any linear combination of the symmetrized harmonics must reflect these same symmetries, and furthermore, any square-integrable function with these symmetries may be decomposed into a linear combination of the symmetrized harmonics. Since the number of symmetrized harmonics is usually just a fraction of the number of general harmonics (and decreases further as the symmetry increases), the reduction in the number of coefficients to calculate is often considerable.

As an example, consider the rotation of a circle about an axis perpendicular to the plane of the circle and passing through its center. If this is a k-fold axis, then the symmetrized circular harmonics are given by Equation (11) with m restricted to integer multiple of k. Requiring a function on the circle to conform to this symmetry causes the coefficients of its expansion to vanish for all except these values of m, meaning that the number of coefficients to be calculated is reduced by a factor of k.

The situation is more complicated for the spherical harmonics, since the increase in dimension allows a particular point group symmetry to include multiple rotations performed about different axes. While the theory underlying the procedure is more involved (refer to, e.g., Refs. [86, 87]), the reduction in the number of coefficients to calculate is considerable, as the example given in Figure 20 indicates. Of all the linear

[7] The content of this chapter has previously been published in Refs. [1, 47].

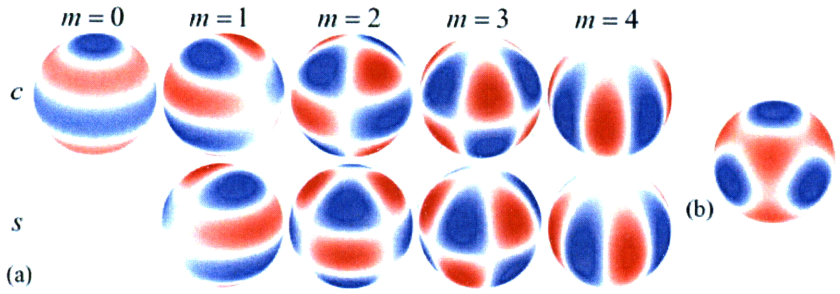

Figure 20: An example of the reduction in the number of linearly independent harmonics required for the expansion of a function on the surface of a sphere with cubic point group symmetry; blue and red correspond to positive and negative values respectively. (a) The nine spherical harmonics defined by Equation (14) for $l = 4$. The value of the index m is indicated above the columns, with the harmonics Y_l^{mc} on the top and Y_l^{ms} on the bottom of a given column. (b) The single linear combination of the harmonics in (a) that satisfies the requirements of cubic point group symmetry.

combinations of the nine spherical harmonics for $l = 4$ (Figure 20a), only one combination satisfies the symmetry of the cubic point group (Figure 20b). Furthermore, the ability to derive the symmetrized spherical harmonics is not necessary to reap this benefit, since tables are available that list the symmetrized spherical harmonics [88].

Of course, the symmetrization of the hyperspherical harmonics to enforce crystal and sample symmetry is of particular interest, due to the utility of these functions in the expression of texture. Following Bunge [4], the symmetrized hyperspherical harmonics are defined as linear combinations of the real hyperspherical harmonics. Provided that the symmetrizing coefficients of these linear combinations satisfy certain conditions, the symmetrized hyperspherical harmonics constitute a set of orthonormal functions over which an orientation distribution with the appropriate symmetry may be expanded significantly more efficiently. While our method to derive the symmetrizing coefficients is quite general, we have explicitly determined the symmetrized harmonics only for samples with orthorhombic symmetry and for crystals with the Laue symmetry groups. Despite our use of well-known group theoretical techniques, certain aspects of our symmetrization procedure, as well as the symmetrized harmonics themselves, appear to be unique within the literature.

5.1. Eigenvectors of the Irreducible Representatives

A function f on the surface of the unit sphere in four dimensions may be written in the form of a real hyperspherical harmonic expansion, as in Equation (31). As indicated in Section 3.2.2, a four-dimensional rotation $R(r,p)$ of the function f is equivalent to a transformation of the expansion coefficients such that the result is written in the form

$$R(r,p)f = \sum_{n=0,2}^{\infty} \left\langle Z^n_{00c} \ldots Z^n_{mnc}, Z^n_{mns} \ldots Z^n_{n0c} \left| \boldsymbol{T}^{n\dagger} \boldsymbol{C}^{\dagger}_{ll'} \boldsymbol{U}^{l\dagger}(r) \otimes \boldsymbol{U}^{l'}(p) \boldsymbol{C}_{ll'} \boldsymbol{T}^{n} \right| \right. \\ \left. \times \left| a^n_{00} \ldots a^n_{mn}, b^n_{mn} \ldots a^n_{n0} \right\rangle \right., \tag{124}$$

where the irreducible representatives of $SO(4)$ corresponding to $R(r,p)$ are functions of the sample symmetry operation p and the crystal symmetry operation r. A symmetrized function f may now be defined as one that is invariant to the application of every distinct four-dimensional rotation corresponding to the simultaneous action of a crystal and a sample symmetry operation. From Equation (124), one finds that a function is invariant to the application of a particular four-dimensional rotation only when the sets formed from expansion coefficients with particular values of n are invariant to the application of the corresponding $(n+1)^2$-dimensional irreducible representatives of $SO(4)$. That is, a function is invariant to a four-dimensional rotation only when the sets of expansion coefficients form eigenvectors of eigenvalue one of the irreducible representatives.

An inspection of Equation (124) indicates that any four-dimensional rotation operation may be considered to transform the hyperspherical harmonics for a particular value of n into linear combinations of the hyperspherical harmonics for the same value of n, and no others. Since the symmetrized hyperspherical harmonics are defined to be linear combinations of the hyperspherical harmonics that are invariant to certain four-dimensional rotation operations, they may be constructed as linear combinations of only the hyperspherical harmonics with a particular value of n. Let $\Lambda(n)$ indicate the number of linearly independent combinations of the hyperspherical harmonics for a particular value of n that are invariant to all the four-dimensional rotation operations corresponding to the application of distinct pairs of crystal and sample symmetries. The expression for the λth of these linearly independent combinations is written as

$$\ddot{\dot{Z}}^n_\lambda = \left\langle Z^n_{00c} \ldots Z^n_{nnc}, Z^n_{nns} \ldots Z^n_{n0c} \middle| \ddot{\dot{a}}^n_{00\lambda} \ldots \ddot{\dot{a}}^n_{nn\lambda}, \ddot{\dot{b}}^n_{nn\lambda} \ldots \ddot{\dot{a}}^n_{n0\lambda} \right\rangle, \tag{125}$$

where the $\ddot{\dot{a}}^n_{lm\lambda}$ and $\ddot{\dot{b}}^n_{lm\lambda}$ are referred to as the symmetrizing coefficients. Since the symmetrized basis functions are square integrable functions on the surface of the unit sphere in four dimensions, a general four-dimensional rotation of $\ddot{\dot{Z}}^n_\lambda$ may be expanded using the hyperspherical harmonic expansion and written as

$$\begin{aligned} R(r,p)\ddot{\dot{Z}}^n_\lambda = \left\langle Z^n_{00c} \ldots Z^n_{nnc}, Z^n_{nns} \ldots Z^n_{n0c} \middle| \boldsymbol{T}^{n\dagger} \boldsymbol{C}^\dagger_{ll'} \boldsymbol{U}^{l\dagger}(r) \otimes \boldsymbol{U}^{l'}(p) \boldsymbol{C}_{ll'} \boldsymbol{T}^n \right| \\ \times \left| \ddot{\dot{a}}^n_{00\lambda} \ldots \ddot{\dot{a}}^n_{nn\lambda}, \ddot{\dot{b}}^n_{nn\lambda} \ldots \ddot{\dot{a}}^n_{n0\lambda} \right\rangle, \end{aligned} \tag{126}$$

which is simply a specific instance of Equation (124). If the four-dimensional rotation operation $R(r,p)$ is constructed from a sample symmetry operation and a crystal symmetry operation, then the definition of the symmetrized hyperspherical harmonics requires that

$$R(r,p)\ddot{\dot{Z}}^n_\lambda = \ddot{\dot{Z}}^n_\lambda . \tag{127}$$

Introducing Equation (125) on the right and Equation (126) on the left of Equation (127) reveals that for the $\ddot{\dot{Z}}^n_\lambda$ to be a symmetrized hyperspherical harmonic, the symmetrizing coefficients must satisfy the condition

$$\boldsymbol{T}^{n\dagger} \boldsymbol{C}^\dagger_{ll'} \boldsymbol{U}^{l\dagger}(r) \otimes \boldsymbol{U}^{l'}(p) \boldsymbol{C}_{ll'} \boldsymbol{T}^n \left| \ddot{\dot{a}}^n_{00\lambda} \ldots \ddot{\dot{a}}^n_{nn\lambda}, \ddot{\dot{b}}^n_{nn\lambda} \ldots \ddot{\dot{a}}^n_{n0\lambda} \right\rangle = \left| \ddot{\dot{a}}^n_{00\lambda} \ldots \ddot{\dot{a}}^n_{nn\lambda}, \ddot{\dot{b}}^n_{nn\lambda} \ldots \ddot{\dot{a}}^n_{n0\lambda} \right\rangle. \tag{128}$$

That is, the symmetrizing coefficients of the λth linearly independent symmetrized hyperspherical harmonic for a particular value of n must form a simultaneous eigenvector of eigenvalue one of all the $(n+1)^2$-dimensional irreducible representatives of $SO(4)$ corresponding to the application of distinct pairs of crystal and sample symmetries.

The implementation of the condition given by Equation (132) is simplified by considering only the simultaneous eigenvectors of eigenvalue one of all the $(n+1)^2$-dimensional irreducible representatives of $SO(4)$ corresponding to distinct pairs of the *generators* of the crystal and sample point groups, rather than the point groups themselves. This gives an identical result because any operation of the point group may

be constructed from some combination of the generators. Therefore, a function that is invariant to the four-dimensional rotation corresponding to these generators will remain invariant under the application of any four-dimensional rotation corresponding to the full rotation groups.

For the purpose of clarity, the calculation of the symmetrizing coefficients of the symmetrized hyperspherical harmonics is performed via the following steps:

i. Enumerate the generators of the crystal proper point group symmetry and the sample proper point group symmetry.
ii. Form a pair of rotation operations by combining one of the generators from step i with the identity, and find the $(n+1)^2$-dimensional irreducible representative of $SO(4)$ corresponding to this pair. Repeat for every generator from step i. The necessary form of the representatives appears in Equation (78).
iii. Calculate the simultaneous eigenvectors with eigenvalues of one for every representative found in step ii.
iv. Construct an orthonormal basis from the linearly independent eigenvectors. The components of the basis vectors provide the coefficients necessary to find the symmetrized hyperspherical harmonics from Equation (125).

We have used this procedure to calculate the symmetrized harmonics for samples with orthorhombic symmetry and crystals with the proper rotational symmetries of all the Laue groups, such as would be required to describe textures in rolled sheet materials. The symmetrizing coefficients necessary to construct at least thirty of the symmetrized hyperspherical harmonics for each of these symmetries in provided Appendix E.

Since the calculation and use of these functions constitute the central aim of this chapter, it is worthwhile to briefly examine a few of the symmetrized hyperspherical harmonics. In Figure 21 appear the first three non-trivial symmetrized hyperspherical harmonics with orthorhombic sample symmetry and the crystal point group symmetries 222 (Figure 21a), 422 (Figure 21b), and 432 (Figure 21c). The specific nature of the symmetry present in these harmonics is not necessarily obvious due to the fact that rotations do not combine linearly. For example, a symmetry rotation about the z axis moves the point corresponding to the identity along the z axis, but rotates certain of the points corresponding to 180° rotations about the z axis. When combined with different

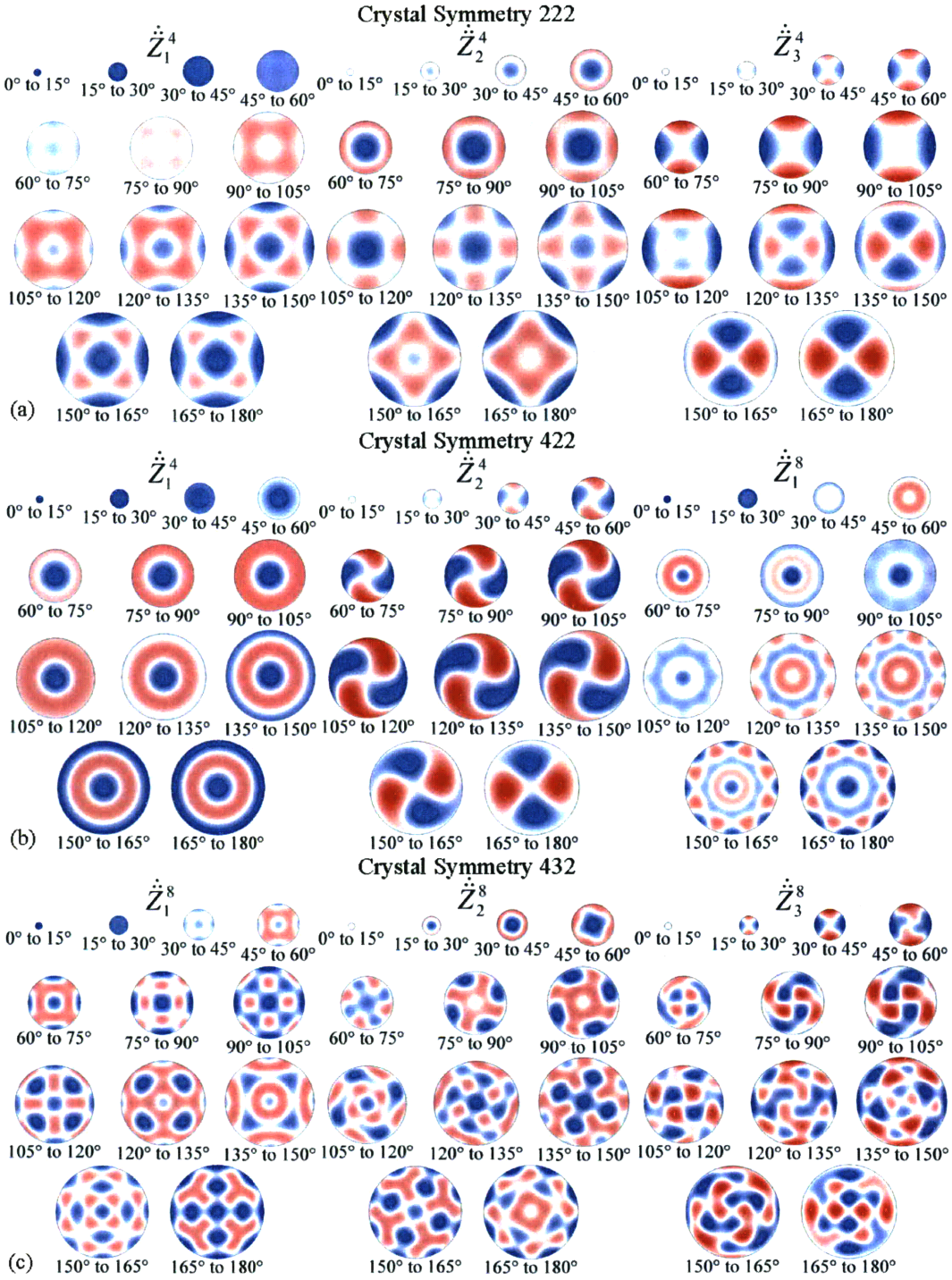

Figure 21: Examples of the symmetrized hyperspherical harmonics, as calculated from the tables of coefficients in Appendix E. Specifically, these are sets of the three lowest-order, non-trivial symmetrized hyperspherical harmonics for orthorhombic sample symmetry and for the crystal point symmetries (a) 222, (b) 422, and (c) 432. In each of the projections, the z and x axes of the projections point out of the page and to the right, respectively.

sample and crystal symmetries, and the absence of an inversion center in the quaternion group space, this results in the marked chirality of some of the images. The exception to this difficulty though is the identification of regions corresponding to transformations of the identity by symmetry operations. This allows one to identify the point group 222 in the first harmonic of Figure 21a, the point group 422 in the third harmonic of Figure 21b, and the point group 432 in the first harmonic of Figure 21c.

5.2. Symmetrized Hyperspherical Harmonic Expansion

While the λth linearly independent simultaneous eigenvector for a particular value of n may be constructed from Equation (125), this equation may instead be written as

$$\dot{\ddot{Z}}^n_\lambda = \sum_{l=0}^{n}\left[\ddot{a}^n_{l0\lambda} Z^n_{l0c} + \sum_{m=1}^{l}\left(\ddot{a}^n_{lm\lambda} Z^n_{lmc} + \ddot{b}^n_{lm\lambda} Z^n_{lms}\right)\right]. \tag{129}$$

With the symmetrizing coefficients calculated by the procedure provided above, the symmetrized hyperspherical harmonics form an orthonormal system of functions, i.e.

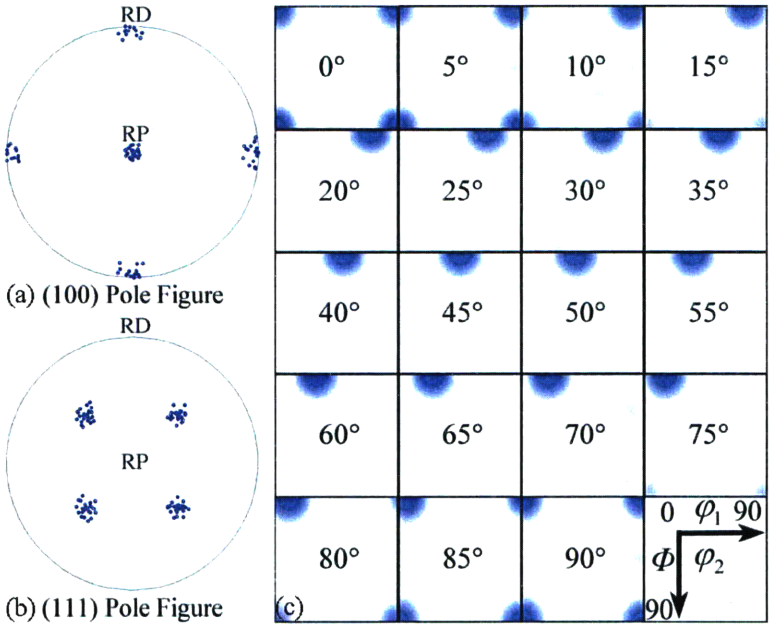

Figure 22: Conventional methods of viewing a simulated cube texture. (a) The (100) and (b) (111) pole figures are presented in stereographic projection, with the z and x axes pointing out of the page and up the page, respectively. (c) The blue and red regions in the Euler angle space indicate regions of positive and negative probability density, respectively.

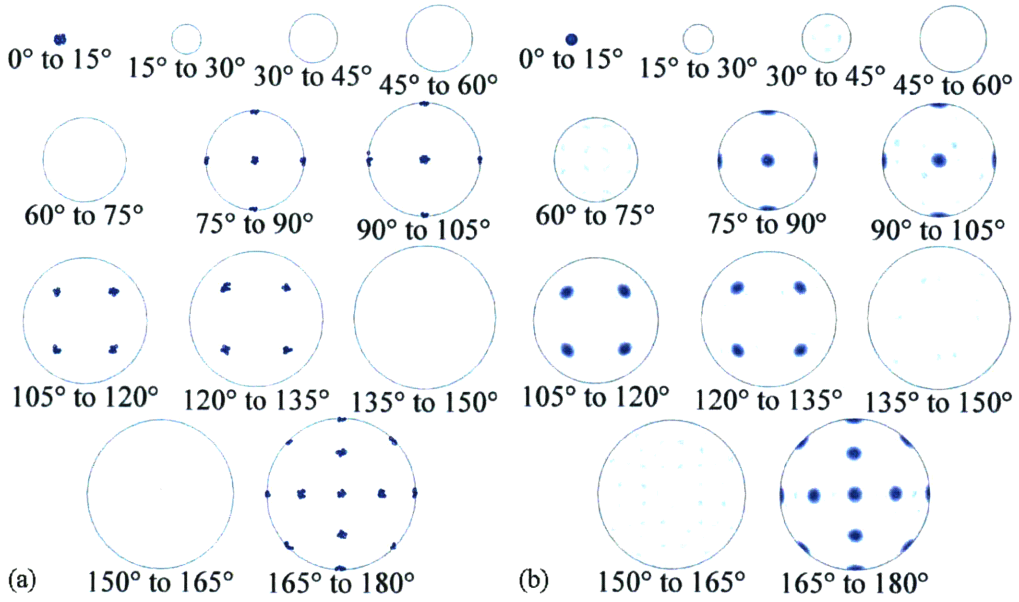

Figure 23: The current method of viewing a simulated cube texture. The z and x axes of the projections point out of the page and to the right, respectively. (a) Projection of the discrete quaternions corresponding to the simulated texture, including all of the rotations in the crystallographic point group 432. (b) ODF corresponding to the discrete distribution of part (a), calculated using the first thirty-seven hyperspherical harmonics of orthorhombic sample symmetry and cubic crystal symmetry. Blue and red regions indicate regions of positive and negative probability density, respectively.

$$\int_0^{2\pi}\int_0^{\pi}\int_0^{\pi} \dddot{Z}^{n'}_{\lambda'} \dddot{Z}^{n}_{\lambda} \sin^2(\omega/2) d(\omega/2) \sin\theta d\theta d\phi = \delta_{nn'}\delta_{\lambda\lambda'}. \tag{130}$$

Any orientation distribution function f that satisfies the necessary crystal and sample symmetries may be uniquely expressed as a linear combination of the symmetrized hyperspherical harmonics in the form

$$f(\omega,\theta,\phi) = \sum_{n=0,2\ldots}^{\infty} \sum_{\lambda=1}^{\Lambda(n)} s^n_\lambda \dddot{Z}^n_\lambda . \tag{131}$$

Meanwhile, the coefficients s^n_λ of this expansion are found from the inner product of the appropriate symmetrized hyperspherical harmonic with f, or

$$f^n_\lambda = \int_0^{2\pi}\int_0^{\pi}\int_0^{\pi} \dddot{Z}^n_\lambda f(\omega,\theta,\phi) \sin^2(\omega/2) d(\omega/2) \sin\theta d\theta d\phi . \tag{132}$$

5.3. *Representation of Textures with Symmetry*

As a demonstration of the ability of the symmetrized harmonics to accurately reproduce ODFs, we now consider two simulated textures for cubic polycrystals in samples of orthorhombic symmetry. We begin with a "cube" texture, which is presented in Figure 22 by the conventional means of (100) and (111) pole figures (Figure 22a,b) and an orientation distribution function in the Euler angle parameterization (Figure 22c), where the blue and red regions indicate positive and negative probability density, respectively. Although the physical meaning of the high probability density regions in the Euler angle space is not intuitively clear, the texture in Figure 22c may be identified as a cube texture by reference to a legend of common texture elements, for example, Ref. [3]. Figure 23a displays the discrete orientations of the simulated cube texture as projected quaternions, with the corresponding orientation distribution function appearing in Figure 23b. The orientation distribution is calculated from Equation (131) using the first thirty-seven symmetrized hyperspherical harmonics with orthorhombic sample and cubic crystal symmetry, as presented Appendix E. Although a depiction of actual

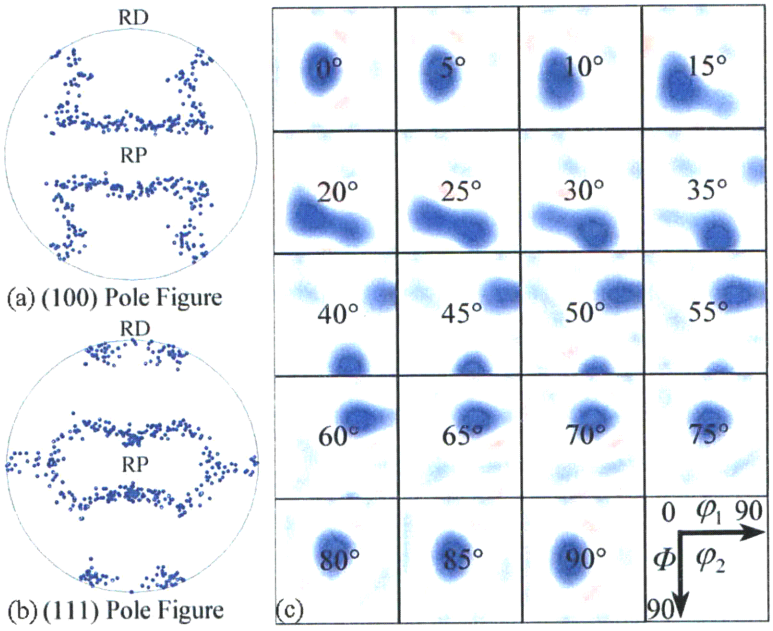

Figure 24: Conventional methods of viewing a simulated copper texture. (a) The (100) and (b) (111) pole figures are presented in stereographic projection, with the z and x axes pointing out of the page and up the page, respectively. (c) The blue and red regions in the Euler angle space indicate regions of positive and negative probability density, respectively.

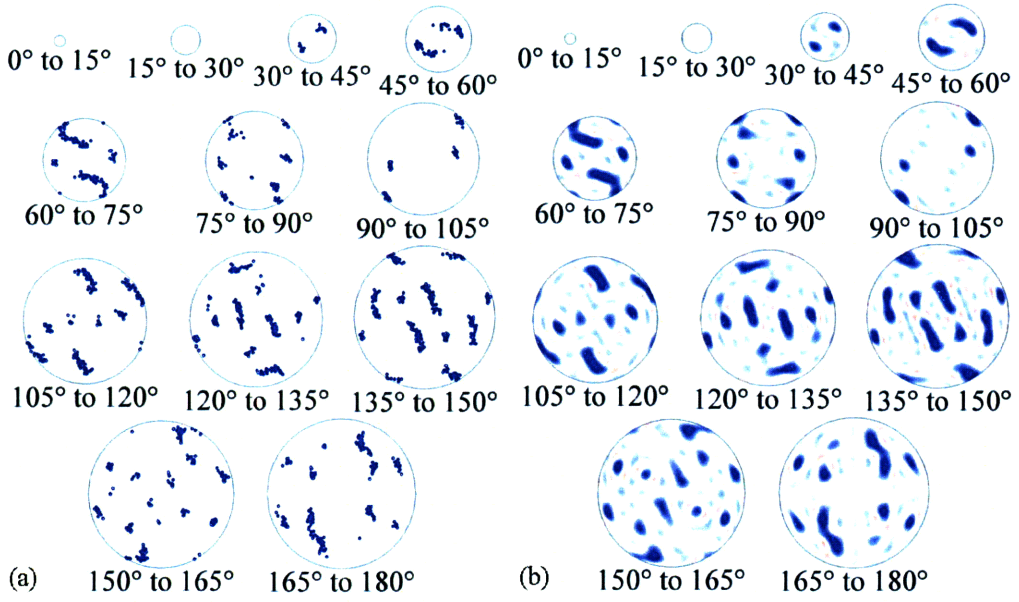

Figure 25: The current method of viewing a simulated copper texture. The z and x axes of the projections point out of the page and to the right, respectively. (a) Projection of the discrete quaternions corresponding to the simulated texture, including all of the orientations described in Ref. [89]. (b) ODF corresponding to the discrete distribution of part (a), calculated using the first thirty-seven hyperspherical harmonics of orthorhombic sample symmetry and cubic crystal symmetry. Blue and red regions indicate regions of positive and negative probability density, respectively.

orientation statistics would probably use finer sections and only cover the asymmetric unit, the full representation is used to emphasize the symmetry; inspection of the figure reveals the presence of the expected 90° rotations about $\langle 100 \rangle$ axes, 120° rotations about $\langle 111 \rangle$ axes, and 180° rotations about $\langle 100 \rangle$ and $\langle 110 \rangle$ axes.

We consider a more complex texture as well, the "copper" texture, conventional and current representations of which appear in Figure 24 and Figure 25, respectively. Whereas the symmetry of the cube texture permits an expansion in terms of a relatively small number of harmonics, including the first harmonic of Figure 21c, the copper texture is considerably more asymmetric and therefore more thoroughly reflects the ability of the symmetrized hyperspherical harmonic expansion to represent arbitrary textures with the requisite symmetry; notice the close agreement between the discrete orientation distribution of Figure 25a and the ODF of Figure 25b, calculated as before with the first thirty-seven hyperspherical harmonics with orthorhombic sample and cubic crystal symmetry.

5.4. Conclusion

While the real hyperspherical harmonic expansion in Equation (31) may be applied to an arbitrary square-integrable function on the surface of the unit sphere in four dimensions, an ODF mapped onto this surface by the quaternion parameterization is certainly not arbitrary. Apart from the purely mathematical constraint that a probability density function should be real and positive valued, the ODF must reflect the physical properties of the sample being characterized. This notably includes the symmetries that are inherent to the crystallites considered individually and the statistical symmetries of the crystallites considered collectively, i.e. the crystal and sample point group symmetries must be reflected in the ODF. Since these symmetry operations as performed in three-dimensional space leave the sample in a symmetrically equivalent state, the reflection of these symmetry operations in four-dimensional space should leave the ODF in a symmetrically equivalent state as well.

The effect of a three-dimensional rotation on the four-dimensional quaternion group space is determined by the irreducible representatives of $SO(4)$, as provided in Section 3.2.2. The irreducible representatives of $SO(4)$ provide the means to find the linear combinations of the real hyperspherical harmonics that remain invariant to the application of the crystal and sample symmetries. These linear combinations, called the symmetrized harmonics, satisfy the symmetry requirements of the ODF identically, and provide a set of basis function over which the expansion of the ODF may be performed significantly more efficiently. This section provides an explicit procedure to calculate the symmetrized hyperspherical harmonics for any set of sample and crystal proper point group symmetries. Furthermore, the coefficients necessary to construct the symmetrized hyperspherical harmonics for orthorhombic sample symmetry and for the proper rotation groups corresponding to each of the Laue groups are calculated and provided for use by the reader or the broader community in Appendix E.

6. A Generalized Mackenzie Distribution

The study of disorientations between neighboring crystals begins with the so-called "Mackenzie distribution" [90], which gives the probability density of observing a particular disorientation angle between randomly oriented cubic crystals. This distribution is one of the simplest and most widely known results involving three-dimensional geometrical probabilities in materials science. While the direct applicability of the Mackenzie distribution is sharply restricted to a small class of microstructures, it is nevertheless frequently used to measure the deviation of experimental disorientation angle distributions from the random case. Such comparisons are useful because the properties and behaviors of grain boundaries are in many cases related to the magnitude of the disorientation angle [91, 92]. The disorientation angle distribution is often used to quantify changes in the grain boundary network resulting from various processing procedures as well [93, 94], and therefore continues to be a function of direct engineering significance.

It is an interesting historical fact that, concurrently with Mackenzie's work, Handscomb [20] developed an analogous solution to the problem using a different mathematical framework. The near-simultaneous appearance of Refs. [90] and [20] suggests that the "Mackenzie distribution" is more aptly named the "Handscomb-Mackenzie distribution", but it also highlights an important theme for the present work. Whereas Mackenzie's derivation proceeded using rotation matrices to describe orientations and misorientations, Handscomb worked in the framework of quaternions. The unique and beneficial properties of the quaternion parameterization led Handscomb to a short and transparent analytical solution in only four pages, whereas the Mackenzie derivation required twelve. A close analogy to this situation is addressed in the present chapter, where we consider the generalization of the Handscomb-Mackenzie problem from simple random textures to the case of arbitrary textures. Whereas this problem has remained intractable for the past 50 years when relying on orientation distributions expressed as functions of the Euler angles, by once more exploiting the properties of the quaternion parameterization we are able to achieve an explicit solution.

The Handscomb-Mackenzie function is a distribution of disorientation angles. As such, it is essentially a projection of the more general misorientation distribution function (MDF), which provides the probability of measuring a particular relative misorientation of adjacent grains. Although the literature provides general formulations by which to express an arbitrary orientation distribution function (ODF) or MDF analytically [4], there does not appear to be any means by which to describe the simpler disorientation angle distribution function explicitly. There are only two exceptions of which we are aware. The first exception is the case addressed by Handscomb [20] and Mackenzie [90] for materials with randomly oriented crystals, i.e., for materials with perfectly uniform ODFs. Although their solutions apply specifically for crystals of cubic point symmetry, their approach has more recently been extended to materials of arbitrary crystal symmetry [95, 96]. The second exception is for ensembles of two-dimensional crystals where the only allowed rotations are in the plane of the material, for which disorientation distributions have been derived for some specific textures in the literature, [97, 98], and for more general families of textures in Appendix F. Nevertheless, a general explicit formula for the disorientation angle distribution function that begins from an arbitrary ODF or MDF of an inherently three-dimensional material does not appear to exist. As noted above, we ascribe this to the nature of the current mathematical treatment of the ODF and the MDF.

For historical reasons, the prevailing treatment of orientation information is based on the description of a rotation by Euler angles, and of the ODF and MDF as linear combinations of functions of Euler angles [4]. In principle, the disorientation angle distribution function could be found by expressing the Euler angles as functions of the axis and angle of rotation, substituting these formulas into the existing analytical description of the MDF, and integrating out the axis information. However, the conversion formulas from the Euler angle to the axis-angle description of a rotation are unwieldy enough to effectively preclude the application this method. This purely mathematical obstacle would be removed if, instead of expressing the ODF and MDF as functions of Euler angles and then converting them to the axis-angle description, the ODF and MDF were expanded as linear combinations of functions of the axis and angle of

rotation directly. Then the reduction of the MDF to the disorientation angle distribution function would be as simple as integrating out the axis information.

This alternative expansion of the ODF and MDF as linear combinations of functions simply related to the axis-angle description of rotations is provided by the hyperspherical harmonic expansion. In parallel to the work of Handscomb [20], this expansion is constructed in Section 2 with reference to the unique properties of quaternions. It consequently offers certain advantages and simplifications with regard to the presentation, interpretation, and manipulation of orientation distributions as compared to treatments based on the Euler angles. As a result, the derivation of a general, explicit form for the disorientation angle distribution function is now practicable for the first time. We present this derivation for materials with cubic crystal symmetry in the current paper, along with some related results.

6.1. Quaternions and the hyperspherical harmonics

The section reproduces many of the formulas presented in Section 2 of this thesis for the reader's convenience. For those to whom this material is already familiar, the discussion of new material continues in Section 6.2.

A crystal orientation may be described by a rotation operation that brings a reference crystal into coincidence with the actual crystal. Similarly, a misorientation between two crystals may be described by a rotation operation that brings one of the crystals into coincidence with the other. The MDF and ODF therefore share a common mathematical framework as functions describing probability distributions of rotations. The primary description of rotations followed throughout this document is by the triplet of angles ω, θ, and ϕ, where $0 \le \omega \le 2\pi$ is the rotation angle and $0 \le \theta \le \pi$ and $0 \le \phi < 2\pi$ are the spherical angles of the axis of rotation. The components of a quaternion corresponding to a given active rotation may be constructed from these angles by the formulas [13]

$$
\begin{aligned}
q_0 &= \cos(\omega/2) \\
q_1 &= \sin(\omega/2)\sin\theta\cos\phi \\
q_2 &= \sin(\omega/2)\sin\theta\sin\phi \\
q_3 &= \sin(\omega/2)\cos\theta,
\end{aligned}
\tag{133}
$$

where the four components satisfy the normalization condition $q_0^2 + q_1^2 + q_2^2 + q_3^2 = 1$.

As discussed in Section 2, the advantage of expressing a rotation in this way is that every normalized quaternion resides on the unit sphere in four dimensions. That is, a collection of three-dimensional rotations is mapped to a collection of points on the four-dimensional unit sphere. Meanwhile, an arbitrary square-integrable function on the four-dimensional unit sphere may be expanded as an infinite linear combination of harmonic functions restricted to this space. These functions are the hyperspherical harmonics, indicated by the symbol Z_{lm}^n. Since the hyperspherical harmonics are defined on the four-dimensional unit sphere, and any point on the four-dimensional unit sphere may be written as functions of the angles ω, θ, and ϕ via Equation (133), the hyperspherical harmonics may be written as explicit functions of these angles as well [49, 50]:

$$
\begin{aligned}
Z_{lm}^n(\omega,\theta,\phi) = (-i)^l \frac{2^{l+1/2}\, l!}{2\pi} \sqrt{(2l+1)\frac{(l-m)!}{(l+m)!}\frac{(n+1)(n-l)!}{(n+l+1)!}}\, \sin^l(\omega/2) C_{n-l}^{l+1}[\cos(\omega/2)] \\
\times P_l^m(\cos\theta) e^{im\phi},
\end{aligned}
\tag{134}
$$

with integer indices $0 \le n$, $0 \le l \le n$, and $-l \le m \le l$, and where C_{n-l}^{l+1} and P_l^m stand for a Gegenbauer polynomial and an associated Legendre function, respectively [40, 41]. The hyperspherical harmonics provide a complete, orthonormal basis for the expansion of a square-integrable function f on the four-dimensional unit sphere in the form

$$
f(\omega,\theta,\phi) = \sum_{n=0,2\ldots}^{\infty} \sum_{l=0}^{n} \sum_{m=-l}^{l} c_{lm}^n Z_{lm}^n .
\tag{135}
$$

The complex coefficients c_{lm}^n of this expansion may be calculated from the inner product of f with the appropriate hyperspherical harmonic Z_{lm}^n, or

$$c_{lm}^{n} = \int_{0}^{2\pi}\int_{0}^{\pi}\int_{0}^{\pi} Z_{lm}^{n*} f \sin^2(\omega/2)\sin\theta d(\omega/2)d\theta d\phi, \tag{136}$$

where * indicates the complex conjugate. Using the above equations, the ODF and MDF may be expressed as analytic functions of quantities relating directly to the axis-angle description of a rotation. While this analysis is presented in more detail in other sections, the formulas provided above will be sufficient for the present purpose.

6.2. Uncorrelated Misorientation Distribution Function

Generally, the MDF is calculated by analyzing the spatial variations of local crystallographic orientation as determined by, e.g., electron back-scatter diffraction measurements. If the necessary spatial information is not available, then the MDF may be approximated from the ODF by making certain assumptions. This is necessary because while the MDF depends on the ODF [99-102], the ODF is not the only contributing factor. In particular, the presence of correlations relating the orientations of neighboring grains or correlations relating the orientation and shape of a single grain may have a strong effect on the misorientations present in a material [103]. Nevertheless, if these correlations are assumed absent, then one is able to predict an "uncorrelated MDF" from the ODF alone. Although derivations of the uncorrelated MDF from the ODF within the framework of the generalized spherical harmonic expansion have been presented elsewhere in the literature [104, 105], we present this derivation within the framework of the hyperspherical harmonic expansion for the first time.

Assume that two crystals are in the reference orientation, and that their relative misorientation is described by the identity rotation. Act on the first crystal with the rotation Δg, with the result that the misorientation of the crystals is described by the same Δg. Now, act on the pair of crystals with the further rotation g. The final orientation of the first crystal is described by $g \cdot \Delta g$, where $\cdot$ denotes the rotation multiplication operation with the order of operations running from right to left, and the final orientation of the second crystal is described simply by g. Since the relative misorientation of the crystals is still described by Δg, the relative misorientation is clearly independent of the choice of g. Therefore, the probability density of observing a relative crystal misorientation of Δg

is given by the probability density of observing crystals with orientations described by $g \cdot \Delta g$ and g, integrated over all g. That is,

$$M'(\Delta g) = \int f^*(g) f(g \cdot \Delta g) dg, \tag{137}$$

where f is the ODF, M' is the uncorrelated MDF, and * indicates the complex conjugate. Writing f in Equation (137) in the form of Equation (135) gives

$$M'(\Delta g) = \int \sum_{n''} \sum_{n'} \sum_{l''} \sum_{l'} \sum_{m''} \sum_{m'} c_{l''m''}^{n''*} c_{l'm'}^{n'} Z_{l''m''}^{n''*}(g) Z_{l'm'}^{n'}(g \cdot \Delta g) dg. \tag{138}$$

Since the integration is only with respect to g, separating the dependence of $Z_{l'm'}^{n'}$ on g and Δg would allow the integral to be evaluated and Equation (138) to be simplified. The desired decomposition of $Z_{l'm'}^{n'}$ is permitted by means of the hyperspherical harmonic addition theorem in Equation (58), with the result

$$\begin{aligned} M'(\Delta g) = \int \sum_{n''} \sum_{n'} \sum_{l''} \sum_{l'} \sum_{m''} \sum_{m'} c_{l''m''}^{n''*} c_{l'm'}^{n'} Z_{l''m''}^{n''*}(g) \frac{\sqrt{2}\pi}{\sqrt{n'+1}} \sum_{l'''} \sum_{l} \sum_{m'''} \sum_{m} \sqrt{2l'''+1}\sqrt{2l+1} \\ \times (-1)^{-l'''-l} Z_{l'''m'''}^{n'}(g) Z_{lm}^{n'}(\Delta g) C_{l'''m'''lm}^{l'm'} \begin{Bmatrix} l' & l''' & l \\ n'/2 & n'/2 & n'/2 \end{Bmatrix} dg. \end{aligned} \tag{139}$$

Collecting the quantities that do not depend on g outside the integral and rearranging the summations yields

$$\begin{aligned} M'(\Delta g) = \sum_{n'} \sum_{l} \sum_{m} Z_{lm}^{n'}(\Delta g) \frac{\sqrt{2}\pi}{\sqrt{n'+1}} \sqrt{2l+1} \sum_{n''} \sum_{l'''} \sum_{l''} \sum_{l'} \sqrt{2l'''+1} \begin{Bmatrix} l' & l''' & l \\ n'/2 & n'/2 & n'/2 \end{Bmatrix} \\ \times (-1)^{-l'''-l} \sum_{m'''} \sum_{m''} \sum_{m'} C_{l'''m'''lm}^{l'm'} c_{l''m''}^{n''*} c_{l'm'}^{n'} \int Z_{l''m''}^{n''*}(g) Z_{l'''m'''}^{n'}(g) dg. \end{aligned} \tag{140}$$

The integral here is equal to $\delta_{n''n'} \delta_{l''l'} \delta_{m''m'}$ by the orthogonality of the hyperspherical harmonics (as is visible from Equation (25)), where δ is the Kronecker delta. Simplifying the indices and relabeling the index n' as n gives

$$\begin{aligned} M'(\Delta g) = \sum_{n} \sum_{l} \sum_{m} Z_{lm}^{n}(\Delta g) \Bigg[(-1)^{-l} \frac{\sqrt{2}\pi}{\sqrt{n+1}} \sqrt{2l+1} \sum_{l''} \sum_{l'} (-1)^{-l''} \sqrt{2l''+1} \begin{Bmatrix} l' & l'' & l \\ n/2 & n/2 & n/2 \end{Bmatrix} \\ \times \sum_{m''} \sum_{m'} C_{l''m''lm}^{l'm'} c_{l''m''}^{n*} c_{l'm'}^{n} \Bigg], \end{aligned}$$

(141)

where the expression for M' is observed to be in the form of the hyperspherical harmonic expansion of Equation (135). That is, we may write:

$$M'(\Delta g) = \sum_{n} \sum_{l} \sum_{m} m'^{n}_{lm} Z^{n}_{lm}(\Delta g). \tag{142}$$

Comparing Equation (141) with Eq. (142) indicates that

$$m'^{n}_{lm} = (-1)^{-l} \frac{\sqrt{2}\pi}{\sqrt{n+1}} \sqrt{2l+1} \sum_{l''} \sum_{l'} (-1)^{-l''} \sqrt{2l''+1} \begin{Bmatrix} l' & l'' & l \\ n/2 & n/2 & n/2 \end{Bmatrix} \sum_{m''} \sum_{m'} C^{l'm'}_{l''m''lm} c^{n*}_{l''m''} c^{n}_{l'm'} \tag{143}$$

is the relation determining the expansion coefficients m'^{n}_{lm} of the uncorrelated MDF from the expansion coefficients c^{n}_{lm} of the ODF. Along with Equation (142), the coefficients of Equation (143) allow a prediction of the MDF to be found for cases where the ODF characterizing the grains is available, but the measured MDF is not.

6.3. Disorientation Angle Distribution Function

The procedure for finding the disorientation angle distribution function assumes that the MDF be known. If the actual MDF of the material is not known, then the uncorrelated MDF may be calculated from the ODF by the method given in the previous section. The derivation of the disorientation angle distribution function further assumes that the MDF is written as an expansion over the complex hyperspherical harmonics, as in Equation (135). If the MDF is instead written as an expansion over the real or symmetrized hyperspherical harmonics (as defined in Sections 2.2 and 5.1), then this expansion may be converted into the form of Equation (135) by means of the conversion formulas provided in Appendix B. If the MDF is written as an expansion over the generalized spherical harmonics, then the conversion formulas available in Section 4.4 may be used to bring the MDF into the required form. Hence, the expansion of the misorientation distribution function M may always be given as

$$M(\omega,\theta,\phi) = \sum_{n=0,2,\ldots}^{\infty} \sum_{l=0}^{n} \sum_{m=-l}^{l} m^{n}_{lm} Z^{n}_{lm}. \tag{144}$$

Generally speaking, the disorientation angle distribution function, $p(\omega)$, is found from M by integrating over the angular coordinates relating to the axis information, or

$$p(\omega) = \int_{\Omega(\omega)} \sum_n \sum_l \sum_m m_{lm}^n Z_{lm}^n d\Omega, \tag{145}$$

where $d\Omega = \sin^2(\omega/2)\sin\theta d\theta d\phi$. Substituting Equation (134) into Equation (145) gives

$$p(\omega) = \sum_n \sum_l \sum_m m_{lm}^n (-i)^l 2^l l! \sqrt{\frac{2}{\pi}\frac{(n+1)(n-l)!}{(n+l+1)!}} \sin^l(\omega/2) C_{n-l}^{l+1}[\cos(\omega/2)] \int_{\Omega(\omega)} Y_l^m(\theta,\phi) d\Omega, \tag{146}$$

leaving just the specification of the limits of integration $\Omega(\omega)$, and where Y_l^m is one of the spherical harmonics describing the distribution of rotation axes. Since this depends on the disorientation space of the MDF and therefore on the point symmetry group of the crystallites, Equation (146) is the simplest presentation of the disorientation angle distribution function for arbitrary materials.

6.3.1. Solution for Cubic Crystals

Given that many engineering materials exhibit cubic point group symmetry, we derive a more explicit formula for the disorientation angle distribution function for this case in the following. The orientation space, or the region within the quaternion group space containing one point for every unique orientation of a cubic crystal, is defined by the relations [15, 21]

$$\begin{aligned} &(\sqrt{2}-1)q_0 \geq \pm q_i \\ &q_0 \geq \pm q_1 \pm q_2 \pm q_3, \end{aligned} \tag{147}$$

where the subscript i stands for 1, 2, or 3. The disorientation space, or the region within the quaternion group space containing one point for every unique relative orientation of a pair of cubic crystals, is defined from the orientation space by an additional restriction placed on the allowable rotation axes. This restriction is written as [15, 21]

$$q_1 \geq q_2 \geq q_3 \geq 0. \tag{148}$$

While relations among the four quaternion components are convenient for describing the boundaries of the orientation and disorientation spaces mathematically, relations among three of the components are more suitable for the visualization of these regions. The normalization condition on the four quaternion components may be used to eliminate q_0 from Equations (147) and (148), and the resulting formulas give the description of the orientation and disorientation spaces used to construct Figure 26. This procedure is sometimes referred to as an orthographic projection of the orientation and disorientation spaces from the quaternion space. (Alternatively, a gnomic projection of the orientation and disorientation spaces from the quaternion space returns the analogous figures in the Rodrigues space [12]; this explains the similarity of Figure 26 to the more well-known view of the orientation space constructed in terms of Rodrigues vectors.)

Equation (133) indicates that the distance of a point from the origin in Figure 26 is $\sin(\omega/2)$, meaning that a surface of constant ω is a sphere in this space. Returning to Equation (146), we find that the integration should be performed over the area of intersection of the disorientation space with a sphere of radius $\sin(\omega/2)$ centered at the identity, where the disorientation space is used to avoid the inclusion of multiple symmetrically equivalent regions. Nevertheless, given that the disorientation space is defined from the orientation space by a restriction placed on the axis of rotation, and that the integral in Equation (146) removes the dependence on the axis of rotation anyway, performing the integration over the area of intersection of the sphere with the orientation

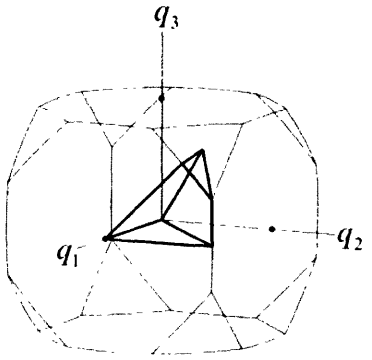

Figure 26: The cubic orientation (light lines) and disorientation (bold lines) spaces, displayed in the orthographic projection of the quaternion space. The solid points mark the intersection of the axes with the surface of the orientation space. The q_i are the components of the vector part of the quaternion.

space rather than the disorientation space changes $p(\omega)$ by nothing more than a multiplicative constant. The advantage of using the orientation space instead of the disorientation space is that this choice simplifies the formulas for $p(\omega)$.

An inspection of Figure 26 indicates that the area of intersection of the orientation space with a sphere centered at the identity is a piecewise function of ω. While the appropriate intervals of ω may be calculated from Equation (147), the relevant calculations have been reported in detail by other authors [20, 90, 96]. We describe the intervals of ω with reference to Figure 26 by visualizing the interaction of the boundary of the orientation space with an expanding sphere of radius $\sin(\omega/2)$ centered at the origin.

i. If $0 \le \tan(\omega/2) \le \sqrt{2}-1$, then the sphere is contained within the orientation space. At the upper limit of this region, the sphere contacts the centers of the six octagonal faces.

ii. If $\sqrt{2}-1 \le \tan(\omega/2) \le \sqrt{3}/3$, then spherical caps extend beyond each octagonal face. At the upper limit of this region, the sphere contacts the centers of the eight triangular faces.

iii. If $\sqrt{3}/3 \le \tan(\omega/2) \le 2-\sqrt{2}$, then spherical caps extend beyond each triangular face as well. At the upper limit of this region, the spherical caps extending beyond each face contact the spherical caps of neighboring faces at the center of the shared edges.

iv. If $2-\sqrt{2} \le \tan(\omega/2) \le \sqrt{23-16\sqrt{2}}$, then the spherical caps extending beyond each face overlap with the spherical caps of the neighboring faces. At the upper limit of this region, the sphere contains the entire orientation space.

The area of integration in Equation (146) and the disorientation angle distribution function $p(\omega)$ must be evaluated independently for each of these intervals of ω.

For the first interval (*i*) of ω, the integration in Equation (146) is performed over the entire ranges of the angles θ and ϕ. The integral is found to be

$$\sin^2(\omega/2)\int_0^{2\pi}\int_0^{\pi} Y_l^m(\theta,\phi)\sin\theta d\theta d\phi = 2\sqrt{\pi}\sin^2(\omega/2)\delta_{l0}\delta_{m0} \tag{149}$$

by the orthogonality of the spherical harmonics. Substitution of this result into Equation (146) gives

$$p_1(\omega) = 2\sqrt{2}\sum_n m_{00}^n \sin^2(\omega/2) C_n^1[\cos(\omega/2)] \tag{150}$$

for the disorientation angle distribution function in the first interval of ω.

For the second interval (*ii*) of ω, the integration in Equation (146) is performed over the entire sphere except for the six spherical caps extending beyond octagonal faces. Evaluation of Equation (146) over this area is equivalent to the result found by subtracting from Equation (150) the contribution from the area subtended by the spherical caps. By the symmetry of the MDF, the contribution of any one of these spherical caps is identical to that for any other. Therefore, the formula for the disorientation angle distribution function in this interval is found by subtracting from Equation (150) six times the result S_1 of evaluating Equation (146) over the spherical cap extending beyond the face in the positive q_3 direction in Figure 26, or

$$p_2(\omega) = p_1(\omega) - 6S_1(\omega). \tag{151}$$

This spherical cap is defined from Equation (147) by $\left(\sqrt{2}-1\right)q_0 \le q_3$, which provides the integration limits $0 \le \theta \le \cos^{-1}\left[\left(\sqrt{2}-1\right)\cot(\omega/2)\right]$ with reference to Equation (133). At the same time, the solid angle subtended by the spherical cap includes the entire range of ϕ. Writing $\theta_1(\omega)$ for the upper limit of θ, the relevant integral is then

$$\sin^2(\omega/2)\int_0^{2\pi\theta_1(\omega)}\int_0^{\pi} Y_l^m(\theta,\phi)\sin\theta d\theta d\phi = \sqrt{(2l+1)\pi}\sin^2(\omega/2)\delta_{m0}\int_{\cos[\theta_1(\omega)]}^{1} P_l(x)dx, \tag{152}$$

where the change of variable $x = \cos\theta$ has been performed. The integral over x may be evaluated for a lower limit of $\cos\theta$ as

$$\int_{\cos(\theta)}^{1} P_l(x)dx = \begin{cases} 1-\cos\theta & l=0 \\ \sin(\theta)P_l^{-1}(\cos\theta) & l\neq 0 \end{cases}, \tag{153}$$

though we consider the form in Equation (152) to be simpler from a notational standpoint. Substitution of Equation (152) into Equation (146) gives

$$S_1(\omega) = \sqrt{2}\sin^2(\omega/2)\sum_n\sum_l m_{l0}^n(-i)^l 2^l l!\sqrt{(2l+1)\frac{(n+1)(n-l)!}{(n+l+1)!}}\sin^l(\omega/2) \times C_{n-l}^{l+1}[\cos(\omega/2)]\int_{\cos[\theta_1(\omega)]}^{1} P_l(x)dx. \tag{154}$$

The solution for $p(\omega)$ in the second interval of ω is then given by direct substitution of Equation (154) into Equation (151).

For the third interval (*iii*) of ω, by similar reasoning, the contribution from the eight spherical caps extending beyond triangular faces must be subtracted from Equation (151). Since there are eight of these spherical caps, and by the symmetry of the MDF they all make the same contribution S_2 to Equation (146), the disorientation angle distribution function is

$$p_3(\omega) = p_1(\omega) - 6S_1(\omega) - 8S_2(\omega) \tag{155}$$

in the third interval of ω.

To evaluate S_2, we select the spherical cap extending beyond the triangular face in the positive octant of Figure 26. Since the integrand appearing in Equation (146) is a spherical harmonic, the symmetry of the spherical cap may be exploited to simplify the integration by initially performing a three-dimensional rotation $\boldsymbol{R}(\omega',\theta',\phi')$ of the integrand to bring the point corresponding to the triangular face's center into coincidence with a point corresponding to the q_3-axis in Figure 26. The rotation of a spherical harmonic is generally performed by writing the rotated spherical harmonic $\boldsymbol{R}(\omega',\theta',\phi')Y_l^m(\theta,\phi)$ as a linear combination of spherical harmonics with the same value of l, or [13]

$$\boldsymbol{R}(\omega',\theta',\phi')Y_l^m(\theta,\phi) = \sum_{m'=-l}^{l} Y_l^{m'}(\theta,\phi)U_{m'm}^l(\omega',\theta',\phi'). \tag{156}$$

The matrix $U_{m'm}^l$ is one of the $(2l+1)$-dimensional irreducible representatives of $SO(3)$ defined by Equation (52), while ω', θ' and ϕ' indicate the angle and axis of the rotation

being performed. In this case, the arguments of the irreducible representative are determined by the initial coordinates of the triangular face's center. From Equation (147), this triangular face is defined by the equation $q_0 = q_1 + q_2 + q_3$, which becomes $\cot(\omega/2) = (\sin\phi + \cos\phi)\sin\theta + \cos\theta$ with reference to Equation (133). Since the center is the point on this face closest to the origin, minimizing ω with respect to θ and ϕ gives $\phi = \pi/4$ and $\theta = \cos^{-1}\left(\sqrt{3}/3\right)$ for the angular coordinates of the center point. Therefore, the appropriate values for the arguments ω', θ' and ϕ' of the irreducible representative are $\cos^{-1}\left(\sqrt{3}/3\right)$, $\pi/2$, and $7\pi/4$, respectively.

We now require the solid angle subtended by the spherical cap in the rotated position. The equation for the rotated triangular face must be of the same form as the equation for the octagonal face in the positive q_3 direction, but modified to reflect the increased distance of the triangular face from the origin. These considerations give $\left(\sqrt{3}/3\right)q_0 \le q_3$ for the equation of the rotated face, or $0 \le \theta \le \cos^{-1}\left[\left(\sqrt{3}/3\right)\cot(\omega/2)\right]$ with reference to Equation (133). Meanwhile, the integration is performed over the entire range of ϕ. On substituting Equation (156) for the integrand in Equation (146) and writing $\theta_2(\omega)$ for the upper limit of θ, the integral in Equation (146) over the rotated spherical cap is found to be

$$\begin{aligned}\sin^2(\omega/2)\int_0^{2\pi}\int_0^{\theta_2(\omega)}\sum_{m'=-l}^{l} Y_l^{m'}(\theta,\phi)U_{m'm}^{l}\left[\cos^{-1}\left(\sqrt{3}/3\right),\pi/2,7\pi/4\right]\sin\theta\,d\theta\,d\phi \\ = \sqrt{(2l+1)\pi}\,\sin^2(\omega/2)U_{0m}^{l}\left[\cos^{-1}\left(\sqrt{3}/3\right),\pi/2,7\pi/4\right]\int_{\cos[\theta_2(\omega)]}^{1} P_l(x)\,dx,\end{aligned} \tag{157}$$

where the factor of $\delta_{m'0}$ arising from integration over the complete range of ϕ causes all but one term of the summation over m' to vanish. Applying Equation (157) to Equation (146) gives

$$\begin{aligned}S_2(\omega) = \sqrt{2}\sin^2(\omega/2)\sum_n\sum_l\sum_m m_{lm}^{n}(-i)^l 2^l l!\sqrt{(2l+1)\frac{(n+1)(n-l)!}{(n+l+1)!}}\sin^l(\omega/2) \\ \times C_{n-l}^{l+1}[\cos(\omega/2)]U_{0m}^{l}\left[\cos^{-1}\left(\sqrt{3}/3\right),\pi/2,7\pi/4\right]\int_{\cos[\theta_2(\omega)]}^{1} P_l(x)\,dx\end{aligned} \tag{158}$$

for the contribution that must be subtracted from the disorientation angle distribution function to account for a single spherical cap extending beyond a triangular face. Substitution into Equation (155) now gives the solution for the third interval of ω.

Finally, for the fourth interval (*iv*) of ω, the contribution from the six spherical caps extending beyond octagonal faces and the eight spherical caps extending beyond triangular faces must still be removed, but with a correction to account for the area excluded twice by the overlap of neighboring spherical caps. Two distinct types of these regions occur, one typified by the area common to the spherical caps extending beyond the neighboring octagonal faces in the positive q_1 and positive q_2 directions in Figure 26, and the other by the area common to the spherical caps extending beyond the octagonal face in the positive q_3 direction and the triangular face in the positive octant of Figure 26. By the symmetry of the MDF, the contribution T_1 from first of these regions is symmetrically equivalent to the contribution from any of the overlaps at the twelve edges joining neighboring octagonal faces, while the contribution T_2 from the second of these regions is symmetrically equivalent to the contribution from any of the overlaps at the twenty-four edges joining neighboring octagonal and triangular faces. Accordingly, the disorientation angle distribution function is written as

$$p_4(\omega) = p_1(\omega) - 6S_1(\omega) - 8S_2(\omega) + 12T_1(\omega) + 24T_2(\omega) \tag{159}$$

in the fourth interval of ω.

Consider the overlap of the spherical caps extending beyond the octagonal faces in the positive q_1 and positive q_2 directions first. From Equation (147), the equations defining these spherical caps are $\left(\sqrt{2}-1\right)q_0 \le q_1$ and $\left(\sqrt{2}-1\right)q_0 \le q_2$, respectively, which become $\left(\sqrt{2}-1\right)\cot(\omega/2) \le \sin\theta\cos\phi$ and $\left(\sqrt{2}-1\right)\cot(\omega/2) \le \sin\theta\cos\phi$ with reference to Equation (133). The limits of ϕ are found as functions of θ by solving these for ϕ, which gives $\sin^{-1}\left[\left(\sqrt{2}-1\right)\cot(\omega/2)\csc\theta\right] \le \phi \le \cos^{-1}\left[\left(\sqrt{2}-1\right)\cot(\omega/2)\csc\theta\right]$. Meanwhile, inspection of Figure 26 indicates that the maximum and minimum values of θ occur within the overlap region at $\phi = \pi/4$. Inserting this value for ϕ and solving for θ gives $\sin^{-1}\left[\left(2-\sqrt{2}\right)\cot(\omega/2)\right] \le \theta \le \pi - \sin^{-1}\left[\left(2-\sqrt{2}\right)\cot(\omega/2)\right]$ for the limits of θ. These limits

may now be used to evaluate Equation (146) over the area common to a pair of spherical caps on neighboring octagonal faces, with the result

$$T_1(\omega)=\sqrt{2/\pi}\sin^2(\omega/2)\sum_n\sum_l\sum_m m_{lm}^n(-i)^l 2^l l!\sqrt{\frac{(n+1)(n-l)!}{(n+l+1)!}}\sin^l(\omega/2)$$
$$\times C_{n-l}^{l+1}[\cos(\omega/2)]\int_{\theta_3(\omega)}^{\theta_4(\omega)}\int_{\phi_1(\omega,\theta)}^{\phi_2(\omega,\theta)}Y_l^m(\theta,\phi)d\phi\sin\theta d\theta, \tag{160}$$

where $\phi_2(\omega,\theta)$ and $\phi_1(\omega,\theta)$ stand for the upper and lower limits of ϕ, and $\theta_4(\omega)$ and $\theta_3(\omega)$ stand for the upper and lower limits of θ, respectively.

As for the overlap of the spherical caps beyond the octagonal face in the positive q_3 direction and the triangular face in the positive octant, Equation (147) indicates that these spherical caps are defined by the equations $(\sqrt{2}-1)q_0 \le q_3$ and $q_0 \le q_1+q_2+q_3$, respectively. Reference to Equation (133) allows these to be written in angular coordinates as $(\sqrt{2}-1)\cot(\omega/2)\le\cos\theta$ and $\cot(\omega/2)\le\cos\theta+\sqrt{2}\sin\theta\cos(\phi-\pi/4)$. The limits of ϕ are found as functions of θ by solving this second equation for ϕ, giving $\pi/4-\cos^{-1}\{[\cot(\omega/2)\csc\theta-\cot\theta]/\sqrt{2}\}\le\phi\le\cos^{-1}\{[\cot(\omega/2)\csc\theta-\cot\theta]/\sqrt{2}\}+\pi/4$. As before, inspection of Figure 26 indicates that the maximum and minimum values of θ occur within the overlap region at $\phi=\pi/4$. Inserting this value for ϕ and solving for θ gives $\cos^{-1}(\sqrt{3}/3)-\cos^{-1}[\sqrt{3}\cot(\omega/2)/3]\le\theta\le\cos^{-1}[(\sqrt{2}-1)\cot(\omega/2)]$ for the limits of θ. With the boundary of the area shared by these neighboring spherical caps defined in angular coordinates, Equation (146) is evaluated to determine the contribution from this region of overlap as

$$T_2(\omega)=\sqrt{2/\pi}\sin^2(\omega/2)\sum_n\sum_l\sum_m m_{lm}^n(-i)^l 2^l l!\sqrt{\frac{(n+1)(n-l)!}{(n+l+1)!}}\sin^l(\omega/2)$$
$$\times C_{n-l}^{l+1}[\cos(\omega/2)]\int_{\theta_5(\omega)}^{\theta_6(\omega)}\int_{\phi_3(\omega,\theta)}^{\phi_4(\omega,\theta)}Y_l^m(\theta,\phi)d\phi\sin\theta d\theta, \tag{161}$$

where $\phi_4(\omega,\theta)$ and $\phi_3(\omega,\theta)$ stand for the upper and lower limits of ϕ, and $\theta_6(\omega)$ and $\theta_5(\omega)$ stand for the upper and lower limits of θ, respectively.

Unfortunately, there does not appear to be any means to evaluate the integrals appearing in Equations (177) and (178) in closed form, and we resort to numerical integration methods. Nevertheless, since the contributions from the overlapping regions are given in an explicit form, we are able to write the disorientation angle distribution function explicitly as well, by introducing Equations (177) and (178) into Equation (159).

This completes the derivation of the explicit form for the disorientation angle distribution function for materials with cubic crystal symmetry. The disorientation angle distribution function $p(\omega)$ is defined in a piecewise fashion, with the solutions in the four distinct intervals of ω given by Equations (150), (151), (155), and (159). Although not normalized in the form given above, we now derive the normalization factor for $p(\omega)$. Since the MDF is a probability distribution function, this must be a normalized quantity, or

$$1 = \int_0^{2\pi}\int_0^{\pi}\int_0^{\pi} M(\omega,\theta,\phi)\sin^2(\omega/2)\sin\theta\, d(\omega/2)\, d\theta\, d\phi\,. \tag{162}$$

The cubic point group contains twenty-four elements, meaning that there are forty-eight points in the quaternion space that are symmetrically equivalent to the identity (antipodal pairs of quaternions represent identical rotations) and a corresponding forty-eight regions that are symmetrically equivalent to the orientation space. Making use of the notation in Equation (145), this allows Equation (162) to be written as

$$1 = 48\int_0^{\omega_{\max}/2}\int_{\Omega(\omega)} M(\omega,\theta,\phi)\, d\Omega\, d(\omega/2) = 48\int_0^{\omega_{\max}/2} p(\omega)\, d(\omega/2), \tag{163}$$

where $\omega_{\max}$ is the largest rotation angle contained in the orientation space. If $p(\omega)d\omega$ is considered as the probability of sampling a disorientation angle in the range $d\omega$, then Equation (163) is more conveniently written in the form

$$1 = 24\int_0^{\omega_{\max}} p(\omega)\, d\omega, \tag{164}$$

which indicates that multiplying the formulas for $p_i(\omega)$ derived above by a factor of 24 is sufficient to ensure normalization.

6.3.2. Solution for random grain orientations

For a material with completely random grain orientations (and no correlations in grain orientations), the misorientations relating neighboring grains will be completely random as well. The MDF for this type of material is therefore uniform. This MDF may be expanded by Equation (144), with the result that all the expansion coefficients vanish except for $m_{00}^{0} = 1/\sqrt{2}\pi$. Hence, the comparison of the results of Section 6.3.1 with the Handscomb-Mackenzie distribution for random textures is in principle as simple as evaluating our formulas for these coefficients and comparing the result to that given in the literature [20, 90]. For convenience, we apply the normalization constraint to the disorientation angle distribution functions in this section.

For the first interval of ω, the formula for the disorientation angle distribution function is given by Equation (150). Substitution of the appropriate coefficients causes all of the terms in the summation to vanish except for $n = 0$, or

$$p_1(\omega) = 48\sqrt{2}\frac{1}{\sqrt{2}\pi}\sin^2(\omega/2)C_0^1[\cos(\omega/2)]. \tag{165}$$

Simplifying Equation (165) and recognizing that $C_0^n = 1$ allows this to be written as

$$p_1(\omega) = \frac{48}{\pi}\sin^2(\omega/2) = \frac{24}{\pi}(1-\cos\omega) \tag{166}$$

in the first interval of ω, which is identical to the known result.

For the second interval of ω, the formula for the disorientation angle distribution function is given by introducing Equation (154) into Equation (151). Substitution of the appropriate coefficients causes all of the terms in the summations to vanish except for $n = 0$ and $l = 0$, or

$$p_2(\omega) = \frac{24}{\pi}(1-\cos\omega) - 148\sqrt{2}\sin^2(\omega/2)\frac{1}{\sqrt{2}\pi}C_0^1[\cos(\omega/2)]\int_{\cos[\theta_1(\omega)]}^{1} P_l(x)dx. \tag{167}$$

Evaluating the integral with reference to Equation (153) and simplifying the remainder gives

$$p_2(\omega)=\frac{24}{\pi}(1-\cos\omega)\left[3\left(\sqrt{2}-1\right)\cot(\omega/2)-2\right] \tag{168}$$

in the second interval of ω, which is also identical to the known result.

For the third interval of ω, the formula for the disorientation angle distribution function is found by introducing Equations (154) and (158) into Equation (155). Substitution of the appropriate coefficients causes all of the terms in the summations to vanish except for $n=0$ and $l=0$, or

$$\begin{aligned} p_3(\omega)=\frac{24}{\pi}(1-\cos\omega)\left[3\left(\sqrt{2}-1\right)\cot(\omega/2)-2\right]-192\sqrt{2}\sin^2(\omega/2)\frac{1}{\sqrt{2}\pi} \\ \times C_0^1\left[\cos(\omega/2)\right]U_{00}^0\left[\cos^{-1}\left(\sqrt{3}/3\right),\pi/2,7\pi/4\right]\int_{\cos[\theta_2(\omega)]}^{1}P_l(x)dx. \end{aligned} \tag{169}$$

The matrix U_{00}^0, as the irreducible representative of $SO(3)$ for a basis of a single element, is identically unity. As before, evaluating the integral with reference to Equation (153) and simplifying the remainder gives

$$p_3(\omega)=\frac{24}{\pi}(1-\cos\omega)\left\{\left[3\left(\sqrt{2}-1\right)+4/\sqrt{3}\right]\cot(\omega/2)-6\right\}. \tag{170}$$

for the disorientation angle distribution function in the third interval of ω, which is identical to the known result.

Finally, we consider the fourth interval of ω. Since there does not appear to be any means to evaluate the integrals in Equations (160) and (161) in closed form, even for constant integrands, these formulas do not simplify for the case of uniform texture. However, numerical evaluation of these integrals yields exactly the expected form; in the following section we provide graphical evidence to this effect.

6.4. Examples of disorientation angle distributions

We apply the above formulas to calculate the disorientation angle distributions for several simulated microstructures with textures of practical interest. We begin by considering simulated materials with cube textures of varying degrees of sharpness, with no spatial correlations among the grains. These materials are constructed by rotating

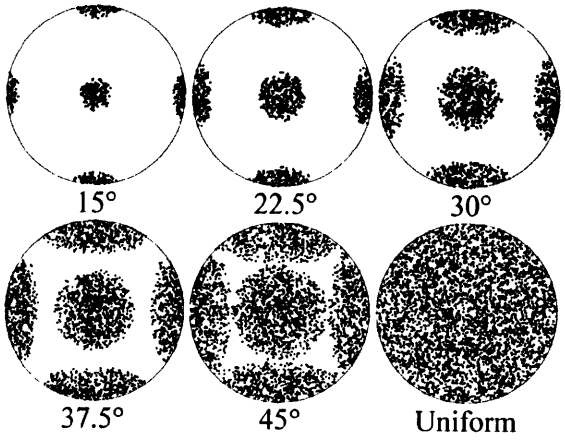

Figure 27: {100} pole figure plots for simulated cube textures of varying degrees of sharpness, plotted in equal area projection. The angles indicate the maximum allowed disorientation angle of a cubic crystal from the reference orientation. The normal direction is out of the page, and the rolling direction is vertical in the plane of the page.

individual crystals from the reference orientation, with any rotation by ω equal to or less than a prescribed threshold angle being equally probable. A set of disorientations is then constructed by sampling many randomly selected pairs of crystals, and subsequently finding a finite expansion of the MDF in the form of Equation (144). For reference, the {100} pole figures for the textures that were examined are presented in Figure 27, for several values of the allowed threshold rotation. The corresponding disorientation angle distributions are presented in Figure 28, where each curve is labeled with the prescribed threshold rotation.

These disorientation angle distributions appear essentially as expected on the basis of physical considerations. Roughly speaking, the ODF of any material of this family is nonzero only within spheres of uniform probability density centered on points in the quaternion space that are symmetrically equivalent to the identity. First consider the material with a threshold rotation angle of 15°. For this material, the boundaries of the spheres of uniform probability density are distant enough that the disorientation angle distribution only contains information relating one part of a given sphere to another part of the same sphere, resulting in a maximum observable disorientation angle of 30°. The situation is similar for a material with a threshold rotation angle of 22.5°, apart from the

maximum observable disorientation angle being increased to 45°. For a material with a threshold rotation angle of 30°, the situation is quite different though. The disorientations relating points in neighboring spheres of uniform probability density fall within the disorientation space and make a noticeable contribution to the disorientation angle distribution for large angles. This contribution introduces a marked asymmetry into the peak in probability density that was absent from the disorientation angle distributions of the sharper textures. This behavior becomes more significant for the material with a threshold rotation angle of 37.5°, and for the material with a threshold rotation angle of 45° the spheres of uniform probability density actually make contact with one another (cf. Figure 27). While the ODF continues to change as the angular threshold is increased beyond 45°, these changes become less noticeable from the standpoint of the disorientation angle distribution which continues to approach that of a uniform ODF. The heavy dark line in Figure 28 corresponds to this final disorientation angle distribution as calculated by the method of Section 6.3, and is in perfect agreement with the results of Handscomb [20] and Mackenzie [90].

As expected, the disorientation angle distribution function of all of these textures

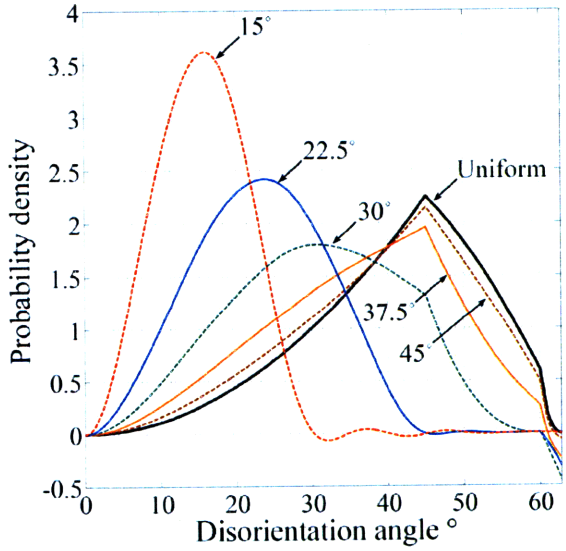

Figure 28: Disorientation angle distribution functions corresponding to simulated cube textures of varying degrees of sharpness (cf. Figure 27). Labels given in degrees indicate the maximum allowed disorientation angle of a cubic crystal from the reference orientation (smaller values denote sharper textures), while the heavy dark line corresponds to a material in which every misorientation is equally likely.

generally converges to zero at $\omega = 0^\circ$ and $\omega = 62.8^\circ$, since the area of intersection of the orientation space with a sphere of radius $\sin(\omega/2)$ centered at the identity vanishes either when the sphere vanishes or when the sphere extends beyond the orientation space. That this does not always occur at the upper limit of ω in Figure 28 indicates a potentially significant truncation error or numerical integration round-off error. Meanwhile, the oscillations that are visible for the material with a threshold rotation angle of 15° are clearly due to a truncation error, since they occur outside the region where numerical integration is performed. These sources of error result in areas of unphysical negative probability density, though they may be addressed either by increasing the number of terms in the expansion, or by dealing strictly with textures that do not contain sharp discontinuities that are difficult to capture with a finite-order series expansion (as in the present case where we have prescribed a sharp threshold rotation angle within which all orientations must lie).

Figure 29 shows the disorientation angle distributions for a simulated material and

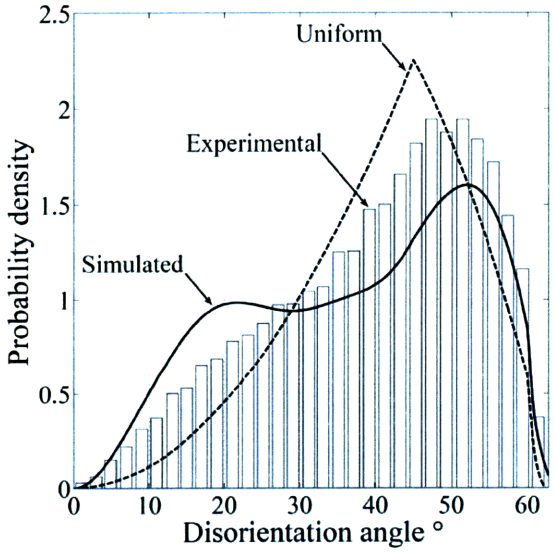

Figure 29: Disorientation angle distribution function for a copper texture, assuming the absence of correlations relating the orientations of neighboring grains or relating the orientation and shape of a single grain. The solid line is the result of our simulation, while the bars indicate the probability density for an experimental material with a similar texture, as measured by Mishin, Gertsman and Gottstein [106]. The dashed line corresponds to a material in which every misorientation is equally likely (i.e., the Mackenzie distribution).

for an experimental material (as measured by Mishin et al. [106]) with strong copper textures, in the absence of correlations relating the orientations of neighboring grains and relating the orientation and shape of a single grain. A comparison of the disorientation angle distributions presented in Figure 29 is encouraging. Specifically, the experimental result deviates from the reference distribution in the direction of the simulated result, which is expected since the simulated texture is sharper than the experimental one.

6.5. Conclusion

The disorientation angle distribution is a common and straightforward method to characterize some features of the grain boundary network, and benefits from a marked simplicity of measurement and presentation in experimental situations. Despite the use of the disorientation angle distribution function in the literature spanning several decades, the authors are aware of analytical formulas reported for this function only for materials where every misorientation of neighboring grains is equally likely [20, 90, 95, 96], or where the problem is restricted to inherently two-dimensional materials [97, 98, 107]. We attribute the absence of a more general formulation to certain difficulties inherent to the customary treatment of rotation distributions as linear combinations of the generalized spherical harmonics [4]. In particular, because the generalized spherical harmonics are written as functions of Euler angles, they cannot be easily transcribed into a form permitting analytical separation of rotation axis and angle.

On the other hand, the recently proposed alternative for the expansion of a rotation distribution function as a linear combination of the hyperspherical harmonics [47] is given as a function of quantities relating directly to the axis and angle of rotation. Writing the MDF of a material in this form immediately allows one to find a general, explicit formula for the misorientation angle distribution function, as is provided here in Equation (146). The current paper applies this formula more specifically to materials with cubic crystal symmetry, for which the misorientation angle distribution function must be defined in a piecewise fashion over four intervals. The explicit solutions in each of these intervals are reported in Equations (150), (151), (155), and (159). These expressions reduce properly to the well-known solutions of Mackenzie [90] and

Handscomb [20] when grains are randomly oriented, but generalize the result to arbitrary textures.

7. Conclusion

The field of modern texture analysis is to a certain extent founded on the seminal contributions of Bunge [4], and particularly on his realization of the significance of an analytical expression for textures by a series expansion. He established the conventions of parameterizing orientations as triplets of Euler angles and representing an orientation distribution function by a linear combination of the generalized spherical harmonics, conventions which remain established within the materials science community.

The recent increase in the availability of orientation statistics due to the marked improvement of measurement techniques and automated instrumentation provides an unprecedented wealth of orientation information, the extent of which is only now being realized by the texture analysis community. Furthermore, the emergence of advanced analytical methods to relate local or global orientation information to materials properties has increased the importance of texture analysis to the engineering community as a whole, and has extended the range of situations to which texture analysis is being applied. These developments bring the inevitable difficulties of working with Euler angles into sharp relief, and reveal that further advances in the field of texture analysis are limited by the continued use of Euler angles and generalized spherical harmonics.

Within this context, the current thesis proposes that a radically different approach to the analysis of orientation information is necessary, one that is based on the quaternion parameterization of rotations. Since quaternions may be considered as residing on the surface of a unit sphere in four dimensions, a collection of crystal orientations may be mapped to a collection of points on this sphere. Hence, this parameterization serves to motivate the expansion of an orientation distribution function as a linear combination of harmonic functions restricted to this space, namely, the hyperspherical harmonics. This expansion not only allows rotations to be expressed by the angles ω, θ, and ϕ, but is found to simplify the visualization and interpretation of an orientation distribution function as well.

The main motivation behind the expansion of an orientation distribution function though is that the expansion inherits the beneficial properties of the basis functions. For the current case, the properties of particular relevance to the representation of orientation

information depend on the relationship of the hyperspherical harmonics to the three- and four-dimensional rotation groups. The investigation of these relationships is found to yield several results, including an addition formula for the hyperspherical harmonics that is useful when convolving orientation distribution functions, and a motivation for a self-consistent phase convention.

A further result of considerable practical importance is the derivation of formulas to convert from the generalized spherical harmonic expansion to the hyperspherical harmonic expansion of an orientation distribution function, and *vice-versa*. These follow directly from knowledge of the relationship of the generalized spherical harmonics and the hyperspherical harmonics to the three-dimensional rotation group. The conversion formulas not only allow analytical results derived in the context of the generalized spherical harmonic expansion to be used with little modification in our mathematical framework, but obviate the need to extensively modify existing implementations of the generalized spherical harmonic expansion to benefit from the advantages of working with the hyperspherical harmonics.

Apart from a series expansion for the orientation distribution function, Bunge contributed the observation that the orientation distribution function must reflect the symmetry of the crystallites and the symmetry of the microstructure that is introduced by the processing history. This suggests that the series expansion be performed using a set of basis functions that identically satisfy the crystal and sample point group symmetries. A procedure to calculate symmetrized hyperspherical harmonics consistent with these symmetries is presented, making use of the relationship of the hyperspherical harmonics to the four-dimensional rotation group. Moreover, the series expansion of an orientation distribution function is found to be significantly more efficient when the symmetrized hyperspherical harmonics are used as the basis functions.

Although the hyperspherical harmonic expansion is equivalent to the generalized spherical harmonic expansion in the sense that one may be converted into the other, the expression of orientation statistics by means of the hyperspherical harmonic expansion nevertheless simplifies certain calculations that are not otherwise practical. One instance of this is provided by the generalization of the Mackenzie distribution to materials with arbitrary textures. Essentially, finding the generalized Mackenzie distribution involves

integrating out the portion of the misorientation distribution function pertaining to the axis of rotation, and preserving only the rotation angle information. While this operation is difficult to perform within the generalized spherical harmonic expansion due to the complicated relationship of the axis of rotation to a triple of Euler angles, the axis information is completely contained in the portion of the hyperspherical harmonics that relates to the angles θ and ϕ. Writing the misorientation distribution function in the form of a hyperspherical harmonic expansion and integrating over the angles θ and ϕ results in a formula that is found to reduce to the Mackenzie distribution for the case of a random texture, and is in good agreement with experimental disorientation angle distributions presented in the literature.

Finally, some thoughts on further directions of research that may benefit from the use of the hyperspherical harmonic expansion of orientation information are presented. It is the hope of the author that the results presented in this thesis continue to motivate the study of the hyperspherical harmonic expansion, and eventually contribute to the wider field of texture analysis within the materials science community.

8. Directions for Further Research

This thesis research proposes and develops a novel mathematical framework for the analysis of orientation information based on the hyperspherical harmonic expansion. The development proceeds to the point where the hyperspherical harmonic expansion is a practicable method for the representation of experimental texture measurements, and is able to interface with and reproduce existing results in the field of texture analysis. The generalization of the Mackenzie distribution to arbitrary textures represents the beginning of the continuing trajectory of this line of research, that is, to provide a means to derive results not traditionally accessible by the generalized spherical harmonic expansion. Several avenues of further research that show potential in this regard include:

- the visual representation and interpretation of orientation and misorientation information. Considering a crystal orientation as parameterized by either a quaternion or by the angles ω, θ, and ϕ instead of by a triplet of Euler angles is a fundamental change of viewpoint that dramatically increases the potential to intuitively display orientation statistics. This is a direct result of the close relationship of a quaternion or the angles ω, θ, and ϕ to the parameterization of a rotation by an axis and an angle. By appropriately assigning colors to distinct points in the quaternion group space, it is expected that a color's shade and intensity will be indicative at a glance of the magnitude of a rotation and the direction of the rotation axis. Coloring a material surface by this scheme would reveal all of the orientation information at once, instead of the more restricted information that is accessible from, for instance, a traditional inverse pole figure map.
- the prediction of the fractions of coincident site lattice (CSL) boundaries of various types for a microstructure with a known MDF. This is, in effect, a generalization of the results presented by Warrington and Boon [108] to arbitrary textures, and is analogous to the generalization of the Mackenzie distribution as performed in Chapter 6. The necessary calculation for a given CSL misorientation involves integrating the MDF over the region of the

misorientation space defined by, e.g. the Brandon criterion [109]. While the shape and boundary of this region is difficult to describe in Euler angle space, the description is actually quite simple in the quaternion group space, being merely the collections of points on the surface of the unit sphere in four dimensions within a particular angular distance of the point representing the ideal misorientation. It is therefore expected that the necessary integration is practicable, but only within the current formalism.

- the prediction of triple junction types for uncorrelated materials with arbitrary ODFs. Analytical predictions for triple junction types in two-dimensional materials have only recently been found [97, 98, 107]. While the same ideas and techniques may in principle be applied to the more general situation of three-dimensional materials with arbitrary textures, there exist a number of purely practical mathematical barriers when these calculations are performed using the generalized spherical harmonic expansion of the ODF. On the other hand, the remarkable similarity of concepts underlying the hyperspherical harmonic expansion and the quantum theory of angular momentum raises the possibility of bringing the extensive mathematical machinery of quantum mechanics to bear on the question of predicting triple junction types. It is expected that this availability of results from the physics literature via the hyperspherical harmonic expansion will make the prediction of fractions of triple junction types achievable for the first time.

Appendix A: Definition of Functions[8]

Since the definitions of certain standard functions vary subtly with the field, we provide definitions consistent with the remainder of this paper. The associated Legendre functions P_l^m are defined using Rodrigues' formula as

$$P_l^m(x) = (-1)^m \frac{1}{2^l l!}\left(1-x^2\right)^{m/2} \frac{d^{l+m}}{dx^{l+m}}\left(x^2-1\right)^l . \tag{171}$$

Notice particularly the appearance of the Cordon-Shortly phase factor $(-1)^m$ in the definition of this function; this is occasionally inserted into the definition of the complex spherical harmonics directly instead. Meanwhile, the Gegenbauer polynomials C_n^v are defined as

$$C_n^v(x) = \frac{(-2)^n}{n!}\frac{\Gamma(v+n)\Gamma(2v+n)}{\Gamma(v)\Gamma(2v+2n)}\left(1-x^2\right)^{1/2-v} \frac{d^n}{dx^n}\left[\left(1-x^2\right)^{n+v-1/2}\right]. \tag{172}$$

Further properties and relationships of these functions are given in, e.g. Refs. [40, 41].

[8] The content of this appendix has previously been published in Ref. [47].

Appendix B: Conversions of the Hyperspherical Harmonic Expansion Coefficients

The majority of this document formulates probability distribution functions of rotations using the complex version of the hyperspherical harmonic expansion because of the notational simplicity that this affords. For reference, the definition of the complex hyperspherical harmonics

$$Z_{lm}^{n}(\omega,\theta,\phi)=(-i)^{l}\frac{2^{l+1/2}\,l!}{2\pi}\sqrt{(2l+1)\frac{(l-m)!}{(l+m)!}\frac{(n+1)(n-l)!}{(n+l+1)!}}\sin^{l}(\omega/2)C_{n-l}^{l+1}[\cos(\omega/2)] \times P_{l}^{m}(\cos\theta)e^{im\phi}, \tag{173}$$

and of the resulting hyperspherical harmonic expansion

$$f(\omega,\theta,\phi)=\sum_{n=0,2\ldots}^{\infty}\sum_{l=0}^{n}\sum_{m=-l}^{l}c_{lm}^{n}Z_{lm}^{n}, \tag{174}$$

are reproduced here. Nevertheless, the complex version of the expansion is not always the most convenient. For example, an expansion using the real hyperspherical harmonics and real expansion coefficients is often more suitable for a real-valued function. The real hyperspherical harmonics are defined in terms of the complex hyperspherical harmonics of Equation (173) as

$$\begin{aligned} Z_{l0c}^{n}(\omega,\theta,\phi)&=i^{l}Z_{l0}^{n}\\ Z_{lmc}^{n}(\omega,\theta,\phi)&=i^{l}\left[(-1)^{m}Z_{lm}^{n}+Z_{l-m}^{n}\right]/\sqrt{2}\\ Z_{lms}^{n}(\omega,\theta,\phi)&=i^{l-1}\left[(-1)^{m}Z_{lm}^{n}-Z_{l-m}^{n}\right]/\sqrt{2}, \end{aligned} \tag{175}$$

where the additional subscript c or s indicates whether the function is even or odd with respect to ϕ. Explicitly, these functions may be written as

$$
\begin{aligned}
Z^n_{l,0,c}(\omega,\theta,\phi) &= \frac{2^l l!}{\pi}\sqrt{\frac{(2l+1)}{2}\frac{(n+1)(n-l)!}{(n+l+1)!}}\sin^l(\omega/2)C^{l+1}_{n-l}[\cos(\omega/2)]P_l(\cos\theta) \\
Z^n_{l,m,c}(\omega,\theta,\phi) &= (-1)^m\frac{2^l l!}{\pi}\sqrt{(2l+1)\frac{(l-m)!}{(l+m)!}\frac{(n+1)(n-l)!}{(n+l+1)!}}\sin^l(\omega/2)C^{l+1}_{n-l}[\cos(\omega/2)] \\
&\quad\times P^m_l(\cos\theta)\cos(m\phi) \\
Z^n_{l,m,s}(\omega,\theta,\phi) &= (-1)^m\frac{2^l l!}{\pi}\sqrt{(2l+1)\frac{(l-m)!}{(l+m)!}\frac{(n+1)(n-l)!}{(n+l+1)!}}\sin^l(\omega/2)C^{l+1}_{n-l}[\cos(\omega/2)] \\
&\quad\times P^m_l(\cos\theta)\sin(m\phi).
\end{aligned}
\tag{176}
$$

The difference in phase of the complex hyperspherical harmonics of Equation (173) with respect to earlier publications [47] causes a difference in the phase of the real hyperspherical harmonics of Equation (176) as well. Nevertheless, we believe that the current phase of Equation (173) is preferable to earlier versions (as described in Section 3.2.4). Since the transformation relating the complex hyperspherical harmonics to the real hyperspherical harmonics is linear and invertible, the real hyperspherical harmonics provide an equally suitable basis for the expansion of a rotation distribution function that takes the form

$$
f(\omega,\theta,\phi) = \sum_{n=0,2\ldots}^{\infty}\sum_{l=0}^{n}\left[a^n_{l0}Z^n_{l0c} + \sum_{m=1}^{l}\left(a^n_{lm}Z^n_{lmc} + b^n_{lm}Z^n_{lms}\right)\right]. \tag{177}
$$

The expansion coefficients of Equation (177) may now be defined in terms of the complex expansion coefficients of Equation (174) by inverting Equations (175), substituting these relations into Equation (174), and comparing the resulting coefficients with those of Equation (177). This gives

$$
\begin{aligned}
a^n_{l0} &= (-i)^l c^n_{l0} \\
a^n_{lm} &= (-i)^l\left[(-1)^m c^n_{lm} + c^n_{l-m}\right]/\sqrt{2} \\
b^n_{lm} &= (-i)^{l-1}\left[(-1)^m c^n_{lm} - c^n_{l-m}\right]/\sqrt{2},
\end{aligned}
\tag{178}
$$

corresponding to Equations (175) above. Provided that the function f is real-valued, these coefficients will be real as well.

Often, the rotation distribution functions of interest characterize physical systems with certain symmetries. For example, the ODF of a single phase material exhibits the exact point group symmetry of the individual crystallites and the statistical point group

symmetry of the arrangement of crystallites within the sample. The expansion of any function that exhibits symmetries certainly requires a basis of only those functions that display the same symmetry. Roughly, this basis may be constructed by identifying all of the linear combinations of hyperspherical harmonics that satisfy the symmetry conditions and forming an orthonormal set of the linear combinations that span the symmetrized function space. The advantage of an expansion over the symmetrized basis functions is that the use of significantly fewer terms gives a comparable level of accuracy to the more general expansions given in Equation (174) or Equation (177). A description of the calculation of the coefficients of the linear combinations of hyperspherical harmonics that satisfy the symmetry conditions, and the subsequent orthogonalization procedure, is presented in Chapter 5. The symmetrized basis functions may be written in the form

$$\dddot{Z}_{\lambda}^{n}(\omega,\theta,\phi)=\sum_{l=0}^{n}\left[\dddot{a}_{\lambda l0}^{n}Z_{l0c}^{n}+\sum_{m=1}^{l}\left(\dddot{a}_{\lambda lm}^{n}Z_{lmc}^{n}+\dddot{b}_{\lambda lm}^{n}Z_{lms}^{n}\right)\right], \tag{179}$$

where $\dddot{a}_{\lambda lm}^{n}$ and $\dddot{b}_{\lambda lm}^{n}$ are the symmetrizing coefficients. By convention, the triplet of dots above the symmetrizing coefficients and the symmetrized harmonic indicates that the point group symmetries of the crystal and of the sample are both satisfied [4]. Provided that the rotation distribution function f displays symmetries equal to or higher than the symmetries of the symmetrized harmonics, the expansion of f may be written as

$$f(\omega,\theta,\phi)=\sum_{n=0,2,\ldots}^{\infty}\sum_{\lambda=1}^{\Lambda(n)}s_{\lambda}^{n}\dddot{Z}_{\lambda}^{n}, \tag{180}$$

where $\Lambda(n)$ is the number of symmetrized basis functions for a particular value of n.

While an arbitrary rotation distribution function does not, in general, exhibit the required symmetries and cannot be expanded in the form of Equation (180), a rotation distribution function that displays symmetry can certainly be expanded in the more general forms of either Equation (177) or Equation (174). Provided that the expansion coefficients of Equation (180) are known, the corresponding expansion coefficients of the more general expansions may easily be found. Substitution of Equation (179) into Equation (180) and comparison of the result with Equation (177) gives

$$
\begin{aligned}
a_{l0}^{n} &= \sum_{\lambda=1}^{\Lambda(n)} s_{\lambda}^{n} \ddot{a}_{\lambda l 0}^{n} \\
a_{lm}^{n} &= \sum_{\lambda=1}^{\Lambda(n)} s_{\lambda}^{n} \ddot{a}_{\lambda l m}^{n} \\
b_{lm}^{n} &= \sum_{\lambda=1}^{\Lambda(n)} s_{\lambda}^{n} \ddot{b}_{\lambda l m}^{n} ,
\end{aligned}
\tag{181}
$$

for the coefficients of the corresponding real hyperspherical harmonic expansion. Furthermore, inversion of Equations (178) and substitution of Equations (181) into these relations gives

$$
\begin{aligned}
c_{l0}^{n} &= i^{l} \sum_{\lambda=1}^{\Lambda(n)} s_{\lambda}^{n} \ddot{a}_{\lambda l 0}^{n} \\
c_{lm}^{n} &= i^{l} (-1)^{m} \sum_{\lambda=1}^{\Lambda(n)} s_{\lambda}^{n} \left(\ddot{a}_{\lambda l m}^{n} - i \ddot{b}_{\lambda l m}^{n} \right) \Big/ \sqrt{2} \\
c_{l-m}^{n} &= i^{l} \sum_{\lambda=1}^{\Lambda(n)} s_{\lambda}^{n} \left(\ddot{a}_{\lambda l m}^{n} + i \ddot{b}_{\lambda l m}^{n} \right) \Big/ \sqrt{2} ,
\end{aligned}
\tag{182}
$$

for the conversion formulas relating the coefficients of the symmetrized hyperspherical harmonic expansion to the coefficients of the complex hyperspherical harmonic expansion.

Appendix C: Clebsch-Gordan Coefficients

Although formulas for the Clebsch-Gordan coefficients may be found throughout the physics literature [8, 44, 45, 63], one of these is provided here for reference [110]:

$$C^{jm}_{j_1 m_1 j_2 m_2} = \delta_{m,m_1+m_2}\left[(2j+1)(j_1+j_2-j)!(j+j_1-j_2)!(j+j_2-j_1)!/(j_1+j_2+j+1)!\right]^{1/2}$$
$$\times \sum_z \frac{(-1)^z\left[(j_1+m_1)!(j_1-m_1)!(j_2+m_2)!(j_2-m_2)!(j+m)!(j-m)!\right]^{1/2}}{z!(j_1+j_2-j-z)!(j_1-m_1-z)!(j_2+m_2-z)!(j-j_2+m_1+z)!(j-j_1-m_2+z)!}. \tag{183}$$

The index z ranges over all integer values for which the factorials in the summation are finite. The Clebsch-Gordan coefficients vanish unless the indices satisfy the conditions $m = m_1 + m_2$ and $|j_1 - j_2| \le j \le j_1 + j_2$.

Appendix D: Euler Angles and the Angles ω, θ, and ϕ

One method to determine the relationships between different descriptions of a rotation is to compare the matrix elements of a single representative, expressed using the different descriptions. The simplest matrix that may be used for this purpose is one of the two-dimensional complex representatives of $SU(2)$. The requirements that this matrix be unitary and of unit determinant constrain the representative to be of the form

$$R^{1/2}(a,b)=\begin{pmatrix} a & b \\ -b^* & a^* \end{pmatrix}, \tag{184}$$

where the complex Cayley-Klein parameters a and b satisfy the condition $|a|^2+|b|^2=1$. The Cayley-Klein parameters may instead be written as simple functions of the rotation angle $0\le\omega\le\pi$ and the spherical coordinates $0\le\theta\le\pi$ and $0\le\phi<2\pi$ of the axis of rotation by Equation (38), giving the matrix

$$U^{1/2}(\omega,\theta,\phi)=\begin{pmatrix} \cos(\omega/2)-i\sin(\omega/2)\cos\theta & -i\sin(\omega/2)\sin\theta e^{-i\phi} \\ -i\sin(\omega/2)\sin\theta e^{i\phi} & \cos(\omega/2)+i\sin(\omega/2)\cos\theta \end{pmatrix} \tag{185}$$

for the same representative. This matrix describes an active rotation, which is interpreted as the rotation that brings a crystal aligned with the coordinate system to the observed orientation.

The construction of the corresponding matrix according to the conventions of Ref. [4] requires more consideration, since this matrix is interpreted following the passive convention. Independent of the rotation convention followed, the construction of rotation matrices reflects the apparent rotation of space from the perspective of an observer attached to the coordinate system. From this vantage point, sequential passive rotations by ϕ_1 about the z-axis, by Φ about the x'-axis, and by ϕ_2 about the z''-axis are indistinguishable from sequential active rotations by $-\phi_1$ about the z-axis, by $-\Phi$ about the x-axis, and by $-\phi_2$ about the z-axis. Since the apparent effect of these rotation sequences is the same, the corresponding matrices should be the same. That is, the matrix elements of the irreducible representatives describing the passive rotation sequence should be the same as those describing the active rotation sequence. Expressing the active rotation

sequence by repeated use of $U^{1/2}(\omega,\theta,\phi)$ allows the corresponding representative to be given as a function of the Euler angles $0 \le \phi_1 < 2\pi$, $0 \le \Phi \le \pi$, and $0 \le \phi_2 < 2\pi$ by

$$\begin{aligned} D^{1/2}(\phi_1,\Phi,\phi_2) &= \begin{pmatrix} e^{i\phi_2/2} & 0 \\ 0 & e^{-i\phi_2/2} \end{pmatrix} \begin{pmatrix} \cos(\Phi/2) & i\sin(\Phi/2) \\ i\sin(\Phi/2) & \cos(\Phi/2) \end{pmatrix} \begin{pmatrix} e^{i\phi_1/2} & 0 \\ 0 & e^{-i\phi_1/2} \end{pmatrix} \\ &= \begin{pmatrix} \cos(\Phi/2)e^{i(\phi_1+\phi_2)/2} & i\sin(\Phi/2)e^{-i(\phi_1-\phi_2)/2} \\ i\sin(\Phi/2)e^{i(\phi_1-\phi_2)/2} & \cos(\Phi/2)e^{-i(\phi_1+\phi_2)/2} \end{pmatrix}. \end{aligned} \tag{186}$$

This matrix describes an active rotation, with matrix elements that should be identical to those given by the construction in Ref. [4]. As for the interpretation of this matrix, recall that in the passive convention, a crystal orientation is described the passive rotation that brings the sample coordinate system into coincidence with the crystal coordinate system. From the perspective of an observer attached to the coordinate system, this operation is identical to the active rotation that brings the crystal from the observed orientation to the reference orientation, aligned with the sample coordinate system. Therefore, the rotation described by the matrix in Equation (186) is the inverse of the rotation described by the matrix in Equation (185), and these matrices are related by the complex conjugate transpose. The relationship of these matrices is outlined graphically in Figure 16.

Comparing the real and complex parts of Equation (185) with those of the complex conjugate transpose of Equation (186) provides a variety of formulas to convert from the angles ω, θ, and ϕ to the Euler angles ϕ_1, Φ, and ϕ_2 describing the equivalent rotation. For example, three of these formulas are

$$\begin{aligned} \tan\phi_1 &= \frac{\tan\phi + \tan(\omega/2)\cos\theta}{1 - \tan(\omega/2)\cos\theta\tan\phi} \\ \cos\Phi &= 1 - 2\sin^2(\omega/2)\sin^2\theta \\ \tan\phi_2 &= \frac{-\tan\phi + \tan(\omega/2)\cos\theta}{1 + \tan(\omega/2)\cos\theta\tan\phi}, \end{aligned} \tag{187}$$

though these do not uniquely determine the Euler angles as functions of the angles ω, θ, and ϕ due to the trigonometric functions involved. Nevertheless, these formulas are sufficient to calculate the Jacobian determinant relating the product of the differentials of the Euler angles to the product of the differentials of the angles ω, θ, and ϕ, or

$$d\phi_1 d\Phi d\phi_2 = \left|\frac{\partial(\phi_1,\Phi,\phi_2)}{\partial(\omega/2,\theta,\phi)}\right| d(\omega/2)d\theta d\phi\,. \tag{188}$$

This calculation is straightforward, though lengthy. We provide only the result, namely, that the Jacobian determinant is

$$\left|\frac{\partial(\phi_1,\Phi,\phi_2)}{\partial(\omega/2,\theta,\phi)}\right| = \frac{8\sin^2(\omega/2)\sin\theta}{\sin\Phi}\,. \tag{189}$$

Applying this result to Equation (188) and separating the terms that depend on the Euler angles from the terms that depend on the angles ω, θ, and ϕ gives

$$\sin\Phi d\phi_1 d\Phi d\phi_2 = 8\sin^2(\omega/2)\sin\theta d(\omega/2)d\theta d\phi\,, \tag{190}$$

which is useful when finding the formulas to convert from the coefficients of the generalized spherical harmonic expansion in Equation (94) to the coefficients of the hyperspherical harmonic expansion in Equation (96), and *vice-versa*.

Appendix E: Tables of the Symmetrizing Coefficients[9]

The tables below provide the coefficients necessary to construct the first thirty or more symmetrized hyperspherical harmonics for orthorhombic sample symmetry and crystals with the proper rotational symmetries of all the Laue groups. For the crystallographic point group 32, one of the two-fold axes is set on the x axis. Many of the harmonics appear more than once, i.e., harmonics for the crystallographic point group 2 satisfy the symmetry requirements of the crystallographic point group 1 as well.

The symbol $\dot{\ddot{Z}}^n_\lambda$ denotes the λ th linearly independent function with the required symmetry constructed from the real hyperspherical harmonics for a particular value of n, and is given by the equation

$$\dot{\ddot{Z}}^n_\lambda = \sum_{l=0}^{n}\left[\dot{\ddot{a}}^n_{l0\lambda} Z^n_{l0c} + \sum_{m=1}^{l}\left(\dot{\ddot{a}}^n_{lm\lambda} Z^n_{lmc} + \dot{\ddot{b}}^n_{lm\lambda} Z^n_{lms}\right)\right] \tag{191}$$

with the functions Z^n_{lmc} and Z^n_{lms} defined in Equation (29). We preset all symmetrized functions of this type for a given value of n, which is the reason that the number of harmonics provided for a particular crystallographic point group often exceeds thirty. The values of the coefficients $\dot{\ddot{a}}^n_{lm\lambda}$ and $\dot{\ddot{b}}^n_{lm\lambda}$ in this equation are found in the tables by the indices n and λ which appear in the left column, and by the indices l, m and i, which appear in that order in the parentheses following the coefficient. The index i stands for either c or s, and indicates the coefficients $\dot{\ddot{a}}^n_{lm\lambda}$ or $\dot{\ddot{b}}^n_{lm\lambda}$, respectively. As a particular example, the second harmonic listed for the crystallographic point group 1 is $0.63245553Z^4_{00c} + 0.59160798Z^4_{40c} + 0.50000000Z^n_{44c}$. Further information relating to the uses and properties of these functions is provided in Section 2.2 and in Chapter 5.

[9] The content of this appendix has previously been published in Ref. [47].

E.1. Cystallographic Point Group 1

n,λ	Coefficients of the Expansion of the Symmetrized Hyperspherical Harmonics
0,1	1.00000000(0,0,c)
4,1	0.63245553(0,0,c)+0.59160798(4,0,c)+0.50000000(4,4,c)
4,2	0.63245553(1,0,c)-0.31622777(3,0,c)-0.70710678(4,4,s)
4,3	0.63245553(1,1,c)+0.19364917(3,1,c)-0.25000000(3,3,c)+0.66143783(4,1,s)+0.25000000(4,3,s)
4,4	0.63245553(1,1,s)+0.19364917(3,1,s)+0.25000000(3,3,s)-0.66143783(4,1,c)+0.25000000(4,3,c)
4,5	0.75592895(2,0,c)+0.42257713(4,0,c)-0.50000000(4,4,c)
4,6	0.53452248(2,1,c)-0.55901699(3,1,s)+0.43301270(3,3,s)+0.16366342(4,1,c)+0.43301270(4,3,c)
4,7	0.53452248(2,1,s)+0.55901699(3,1,c)+0.43301270(3,3,c)+0.16366342(4,1,s)-0.43301270(4,3,s)
4,8	0.75592895(2,2,c)-0.65465367(4,2,c)
4,9	0.53452248(2,2,s)-0.70710678(3,2,c)-0.46291005(4,2,s)
4,10	1.00000000(3,2,s)
6,1	0.37796447(0,0,c)-0.56407607(4,0,c)-0.47673129(4,4,c)+0.19738551(6,0,c)-0.52223297(6,4,c)
6,2	0.37796447(1,0,c)+0.40824829(3,0,c)+0.47673129(4,4,s)-0.43643578(5,0,c)+0.52223297(6,4,s)
6,3	0.37796447(1,1,c)-0.25000000(3,1,c)+0.32274861(3,3,c)-0.44594129(4,1,s)-0.16854997(4,3,s)-0.21128856(5,1,c)+0.22821773(5,3,c)-0.30618622(5,5,c)+0.22613351(6,1,s)-0.35754847(6,3,s)-0.30618622(6,5,s)
6,4	0.37796447(1,1,s)-0.25000000(3,1,s)-0.32274861(3,3,s)+0.44594129(4,1,c)-0.16854997(4,3,c)-0.21128856(5,1,s)-0.22821773(5,3,s)-0.30618622(5,5,s)-0.22613351(6,1,c)-0.35754847(6,3,c)+0.30618622(6,5,c)
6,5	0.48795004(2,1,c)+0.32274861(3,1,s)-0.25000000(3,3,s)-0.04934638(4,1,c)-0.13055824(4,3,c)-0.38188131(5,1,s)-0.17677670(5,3,s)+0.39528471(5,5,s)-0.09731237(6,1,c)-0.27695585(6,3,c)-0.39528471(6,5,c)
6,6	0.48795004(2,1,s)-0.32274861(3,1,c)-0.25000000(3,3,c)-0.04934638(4,1,s)+0.13055824(4,3,s)+0.38188131(5,1,c)-0.17677670(5,3,c)-0.39528471(5,5,c)-0.09731237(6,1,s)+0.27695585(6,3,s)-0.39528471(6,5,s)
6,7	0.48795004(2,2,s)+0.40824829(3,2,c)+0.13957263(4,2,s)+0.57735027(5,2,c)-0.49236596(6,2,s)
8,1	0.57735027(0,0,c)+0.27097338(4,0,c)+0.22901431(4,4,c)-0.07784989(6,0,c)+0.20597146(6,4,c)+0.50383147(8,0,c)+0.26794565(8,4,c)+0.40824829(8,8,c)
8,2	0.57735027(1,0,c)-0.21320072(3,0,c)-0.17739372(4,4,s)+0.24806947(5,0,c)-0.15954481(6,4,s)-0.24428193(7,0,c)-0.20754981(8,4,s)-0.63245553(8,8,s)
8,3	0.57735027(1,1,c)+0.13055824(3,1,c)-0.16854997(3,3,c)+0.16593663(4,1,s)+0.06271815(4,3,s)+0.12009612(5,1,c)-0.12971863(5,3,c)+0.17403581(5,5,c)-0.06908493(6,1,s)+0.10923286(6,3,s)+0.09354143(6,5,s)+0.10098582(7,1,c)-0.10494754(7,3,c)+0.11602387(7,5,c)-0.15811388(7,7,c)+

	0.58539927(8,1,s)+0.20095924(8,3,s)+0.18708287(8,5,s)+0.15811388(8,7,s)
8,4	0.57735027(1,1,s)+0.13055824(3,1,s)+0.16854997(3,3,s)-0.16593663(4,1,c)+0.06271815(4,3,c)+ 0.12009612(5,1,s)+0.12971863(5,3,s)+0.17403581(5,5,s)+0.06908493(6,1,c)+0.10923286(6,3,c)- 0.09354143(6,5,c)+0.10098582(7,1,s)+0.10494754(7,3,s)+0.11602387(7,5,s)+0.15811388(7,7,s)- 0.58539927(8,1,c)+0.20095924(8,3,c)-0.18708287(8,5,c)+0.15811388(8,7,c)
8,5	0.67098171(2,0,c)-0.07591750(4,0,c)+0.08982680(4,4,c)+0.21374669(6,0,c)+0.08078865(6,4,c)+ 0.39823215(8,0,c)+0.10509693(8,4,c)-0.56044854(8,8,c)
8,6	0.50538229(2,1,c)-0.19003487(3,1,s)+0.14720038(3,3,s)+0.02070258(4,1,c)+0.05477388(4,3,c)+ 0.24472932(5,1,s)+0.11328766(5,3,s)-0.25331891(5,5,s)+0.03351900(6,1,c)+0.09539675(6,3,c)+ 0.13615482(6,5,c)-0.40569389(7,1,s)+0.09165423(7,3,s)-0.16887927(7,5,s)+0.32220112(7,7,s)+ 0.06024819(8,1,c)+0.17550449(8,3,c)+0.27230964(8,5,c)+0.32220112(8,7,c)
8,7	0.50538229(2,1,s)+0.19003487(3,1,c)+0.14720038(3,3,c)+0.02070258(4,1,s)-0.05477388(4,3,s)- 0.24472932(5,1,c)+0.11328766(5,3,c)+0.25331891(5,5,c)+0.03351900(6,1,s)-0.09539675(6,3,s)+ 0.13615482(6,5,s)+0.40569389(7,1,c)+0.09165423(7,3,c)+0.16887927(7,5,c)+0.32220112(7,7,c)+ 0.06024819(8,1,s)-0.17550449(8,3,s)+0.27230964(8,5,s)-0.32220112(8,7,s)
8,8	0.67098171(2,2,c)+0.11761089(4,2,c)+0.12773808(6,2,c)+0.18946619(6,6,c)-0.67255224(8,2,c)- 0.17722939(8,6,c)
8,9	0.50538229(2,2,s)-0.24037721(3,2,c)-0.05855574(4,2,s)-0.36999595(5,2,c)+0.16959422(6,2,s)- 0.43206218(7,2,c)-0.34444748(7,6,c)-0.46086633(8,2,s)
8,10	0.56853524(3,0,c)-0.35478744(4,4,s)+0.08268982(5,0,c)-0.31908961(6,4,s)-0.41222575(7,0,c)- 0.41509962(8,4,s)+0.31622777(8,8,s)
8,11	0.51480396(3,1,c)-0.08758414(3,3,c)-0.26882274(4,1,s)+0.03259043(4,3,s)+0.18171134(5,1,c)- 0.06740609(5,3,c)-0.25534521(5,5,c)+0.40227789(6,1,s)+0.05676101(6,3,s)-0.13724393(6,5,s)- 0.07292561(7,1,c)-0.05453421(7,3,c)-0.17023014(7,5,c)+0.29541786(7,7,c)+0.26318644(8,1,s)+ 0.10442507(8,3,s)-0.27448785(8,5,s)-0.29541786(8,7,s)
8,12	0.51480396(3,1,s)+0.08758414(3,3,s)+0.26882274(4,1,c)+0.03259043(4,3,c)+0.18171134(5,1,s)+ 0.06740609(5,3,s)-0.25534521(5,5,s)-0.40227789(6,1,c)+0.05676101(6,3,c)+0.13724393(6,5,c)- 0.07292561(7,1,s)+0.05453421(7,3,s)-0.17023014(7,5,s)-0.29541786(7,7,s)-0.26318644(8,1,c)+ 0.10442507(8,3,c)+0.27448785(8,5,c)-0.29541786(8,7,c)
8,13	0.47968488(3,2,c)-0.17040762(4,2,s)-0.42850416(5,2,c)+0.08498618(6,2,s)-0.49581583(6,6,s)+ 0.23768290(7,2,c)-0.17260774(7,6,c)+0.05292534(8,2,s)+0.46379324(8,6,s)
8,14	0.60302269(3,2,s)+0.58710899(7,2,s)+0.54006172(7,6,s)
8,15	0.52975071(3,3,c)+0.20372540(4,1,s)+0.20020250(4,3,s)+0.22116843(5,1,c)-0.12058217(5,3,c)- 0.15567313(5,5,c)+0.18175210(6,1,s)+0.34868204(6,3,s)+0.12796863(6,5,s)+0.16438861(7,1,c)- 0.29048154(7,3,c)+0.10950536(7,5,c)-0.09099430(7,7,c)+0.03743293(8,1,s)-0.46679245(8,3,s)- 0.14088853(8,5,s)+0.09099430(8,7,s)
8,16	0.52975071(3,3,s)+0.20372540(4,1,c)-0.20020250(4,3,c)-0.22116843(5,1,s)-0.12058217(5,3,s)+

	0.15567313(5,5,s)+0.18175210(6,1,c)-0.34868204(6,3,c)+0.12796863(6,5,c)-0.16438861(7,1,s)-0.29048154(7,3,s)-0.10950536(7,5,s)-0.09099430(7,7,s)+0.03743293(8,1,c)+0.46679245(8,3,c)-0.14088853(8,5,c)-0.09099430(8,7,c)
8,17	0.49090710(4,0,c)-0.31116917(4,4,c)+0.63466306(6,0,c)-0.27986010(6,4,c)+0.17114304(8,0,c)-0.36406645(8,4,c)+0.13867505(8,8,c)
8,18	0.35846409(4,1,c)+0.22581115(4,3,c)-0.38915589(5,1,s)+0.30024029(5,3,s)+0.04475718(5,5,s)+0.31980107(6,1,c)+0.39328325(6,3,c)-0.14433757(6,5,c)-0.28924923(7,1,s)+0.35255158(7,3,s)+0.15105548(7,5,s)-0.16010861(7,7,s)+0.06586495(8,1,c)+0.09367207(8,3,c)-0.06314769(8,5,c)-0.16010861(8,7,c)
8,19	0.35846409(4,1,s)-0.22581115(4,3,s)+0.38915589(5,1,c)+0.30024029(5,3,c)-0.04475718(5,5,c)+0.31980107(6,1,s)-0.39328325(6,3,s)-0.14433757(6,5,s)+0.28924923(7,1,c)+0.35255158(7,3,c)-0.15105548(7,5,c)-0.16010861(7,7,c)+0.06586495(8,1,s)-0.09367207(8,3,s)-0.06314769(8,5,s)+0.16010861(8,7,s)
8,20	0.64940905(4,2,c)-0.32387514(6,2,c)-0.48038446(6,6,c)-0.20169401(8,2,c)+0.44935852(8,6,c)
8,21	0.58536941(4,2,s)-0.33968311(5,2,c)-0.29193710(6,2,s)-0.14433757(6,6,s)-0.18180452(7,2,c)+0.59292706(7,6,c)-0.18180452(8,2,s)+0.13501543(8,6,s)
8,22	0.51095231(4,3,c)-0.33968311(5,3,s)+0.25318484(5,5,s)-0.15891043(6,3,c)+0.40824829(6,5,c)+0.41985956(7,3,s)-0.37977726(7,5,s)-0.07308817(8,3,c)-0.20412415(8,5,c)
8,23	0.51095231(4,3,s)+0.33968311(5,3,c)+0.25318484(5,5,c)-0.15891043(6,3,s)-0.40824829(6,5,s)-0.41985956(7,3,c)-0.37977726(7,5,c)-0.07308817(8,3,s)+0.20412415(8,5,s)
8,24	0.44249768(4,4,c)-0.85280287(6,4,c)+0.27735010(8,4,c)
8,25	0.31289311(4,4,s)-0.55470020(5,4,c)-0.60302269(6,4,s)+0.43852901(7,4,c)+0.19611614(8,4,s)
8,26	0.78446454(5,2,s)+0.41985956(7,2,s)-0.45643546(7,6,s)
8,27	0.78446454(5,4,s)-0.62017367(7,4,s)

E.2. Cystallographic Point Group 2

n,λ	Coefficients of the Expansion of the Symmetrized Hyperspherical Harmonics
0,1	1.00000000(0,0,c)
4,1	0.63245553(0,0,c)+0.59160798(4,0,c)+0.50000000(4,4,c)
4,2	0.63245553(1,0,c)-0.31622777(3,0,c)-0.70710678(4,4,s)
4,3	0.75592895(2,0,c)+0.42257713(4,0,c)-0.50000000(4,4,c)
4,4	0.75592895(2,2,c)-0.65465367(4,2,c)
4,5	0.53452248(2,2,s)-0.70710678(3,2,c)-0.46291005(4,2,s)
4,6	1.00000000(3,2,s)
6,1	0.37796447(0,0,c)-0.56407607(4,0,c)-0.47673129(4,4,c)+0.19738551(6,0,c)-0.52223297(6,4,c)
6,2	0.37796447(1,0,c)+0.40824829(3,0,c)+0.47673129(4,4,s)-0.43643578(5,0,c)+0.52223297(6,4,s)
6,3	0.48795004(2,2,s)+0.40824829(3,2,c)+0.13957263(4,2,s)+0.57735027(5,2,c)-0.49236596(6,2,s)
8,1	0.57735027(0,0,c)+0.27097338(4,0,c)+0.22901431(4,4,c)-0.07784989(6,0,c)+0.20597146(6,4,c)+ 0.50383147(8,0,c)+0.26794565(8,4,c)+0.40824829(8,8,c)
8,2	0.57735027(1,0,c)-0.21320072(3,0,c)-0.17739372(4,4,s)+0.24806947(5,0,c)-0.15954481(6,4,s)- 0.24428193(7,0,c)-0.20754981(8,4,s)-0.63245553(8,8,s)
8,3	0.67098171(2,0,c)-0.07591750(4,0,c)+0.08982680(4,4,c)+0.21374669(6,0,c)+0.08078865(6,4,c)+ 0.39823215(8,0,c)+0.10509693(8,4,c)-0.56044854(8,8,c)
8,4	0.67098171(2,2,c)+0.11761089(4,2,c)+0.12773808(6,2,c)+0.18946619(6,6,c)-0.67255224(8,2,c)- 0.17722939(8,6,c)
8,5	0.50538229(2,2,s)-0.24037721(3,2,c)-0.05855574(4,2,s)-0.36999595(5,2,c)+0.16959422(6,2,s)- 0.43206218(7,2,c)-0.34444748(7,6,c)-0.46086633(8,2,s)
8,6	0.56853524(3,0,c)-0.35478744(4,4,s)+0.08268982(5,0,c)-0.31908961(6,4,s)-0.41222575(7,0,c)- 0.41509962(8,4,s)+0.31622777(8,8,s)
8,7	0.47968488(3,2,c)-0.17040762(4,2,s)-0.42850416(5,2,c)+0.08498618(6,2,s)-0.49581583(6,6,s)+ 0.23768290(7,2,c)-0.17260774(7,6,c)+0.05292534(8,2,s)+0.46379324(8,6,s)
8,8	0.60302269(3,2,s)+0.58710899(7,2,s)+0.54006172(7,6,s)
8,9	0.49090710(4,0,c)-0.31116917(4,4,c)+0.63466306(6,0,c)-0.27986010(6,4,c)+0.17114304(8,0,c)- 0.36406645(8,4,c)+0.13867505(8,8,c)
8,10	0.64940905(4,2,c)-0.32387514(6,2,c)-0.48038446(6,6,c)-0.20169401(8,2,c)+0.44935852(8,6,c)
8,11	0.58536941(4,2,s)-0.33968311(5,2,c)-0.29193710(6,2,s)-0.14433757(6,6,s)-0.18180452(7,2,c)+ 0.59292706(7,6,c)-0.18180452(8,2,s)+0.13501543(8,6,s)
8,12	0.44249768(4,4,c)-0.85280287(6,4,c)+0.27735010(8,4,c)
8,13	0.31289311(4,4,s)-0.55470020(5,4,c)-0.60302269(6,4,s)+0.43852901(7,4,c)+0.19611614(8,4,s)

8,14	0.78446454(5,2,s)+0.41985956(7,2,s)-0.45643546(7,6,s)
8,15	0.78446454(5,4,s)-0.62017367(7,4,s)
10,1	0.42640143(0,0,c)-0.29268470(4,0,c)-0.24736372(4,4,c)+0.08010688(6,0,c)-0.21194288(6,4,c)-0.42469327(8,0,c)-0.22585869(8,4,c)-0.34412360(8,8,c)+0.21385976(10,0,c)-0.30476098(10,4,c)-0.36273813(10,8,c)
10,2	0.42640143(1,0,c)+0.23897606(3,0,c)+0.15644655(4,4,s)-0.28644595(5,0,c)+0.13404445(6,4,s)+0.30785681(7,0,c)+0.14284558(8,4,s)+0.43528575(8,8,s)-0.29025018(9,0,c)+0.19274777(10,4,s)+0.45883147(10,8,s)
10,3	0.28968273(2,0,c)+0.20906050(4,0,c)-0.24736372(4,4,c)-0.56074816(6,0,c)-0.21194288(6,4,c)-0.15872375(8,0,c)-0.22585869(8,4,c)+0.34412360(8,8,c)+0.18095826(10,0,c)-0.30476098(10,4,c)+0.36273813(10,8,c)
10,4	0.28968273(2,2,c)-0.32387514(4,2,c)-0.33511112(6,2,c)-0.49705012(6,6,c)+0.43515890(8,2,c)-0.07254763(8,6,c)-0.09760163(10,2,c)+0.49767260(10,6,c)
10,5	0.49707771(2,2,s)+0.16412943(3,2,c)+0.03145753(4,2,s)+0.26025182(5,2,c)-0.08679699(6,2,s)+0.33168904(7,2,c)+0.26442827(7,6,c)+0.19321769(8,2,s)+0.35426202(9,2,c)+0.31605223(9,6,c)-0.45503559(10,2,s)
10,6	0.27311550(3,0,c)+0.31289311(4,4,s)+0.50128041(5,0,c)+0.26808890(6,4,s)-0.12185999(7,0,c)+0.28569115(8,4,s)-0.21764288(8,8,s)-0.39909400(9,0,c)+0.38549554(10,4,s)-0.22941573(10,8,s)
10,7	0.45018358(3,2,c)+0.11010137(4,2,s)+0.04879722(5,2,c)+0.09154370(6,2,s)+0.47976040(6,6,s)-0.41392028(7,2,c)-0.09640614(7,6,c)-0.10377903(8,2,s)+0.07002408(8,6,s)+0.31788690(9,2,c)-0.11522738(9,6,c)-0.05391698(10,2,s)-0.48036122(10,6,s)
10,8	0.43452409(3,2,s)-0.49327022(7,2,s)-0.45374261(7,6,s)+0.26052505(9,2,s)-0.54232614(9,6,s)
10,9	0.40646007(4,2,s)+0.18014417(5,2,c)+0.33795090(6,2,s)-0.12995687(6,6,s)+0.35856101(7,2,c)-0.35590153(7,6,c)-0.38311996(8,2,s)-0.01896803(8,6,s)+0.17710135(9,2,c)-0.42538369(9,6,c)-0.19904474(10,2,s)+0.13011962(10,6,s)
10,10	0.35478744(4,4,s)+0.48038446(5,4,c)-0.25332020(6,4,s)+0.18421903(7,4,c)-0.49491340(8,4,s)-0.48507125(9,4,c)+0.25498133(10,4,s)

E.3. Cystallographic Point Group 3

n,λ	Coefficients of the Expansion of the Symmetrized Hyperspherical Harmonics
0,1	1.00000000(0,0,c)
4,1	0.44721360(0,0,c)+0.53452248(2,0,c)+0.71713717(4,0,c)
4,2	0.53452248(2,2,c)-0.70710678(3,2,s)-0.46291005(4,2,c)
6,1	0.23145502(1,1,c)+0.38575837(2,1,s)-0.40824829(3,1,c)-0.31209389(4,1,s)+0.17251639(5,1,c)-0.50000000(5,5,c)+0.06154575(6,1,s)-0.50000000(6,5,s)
6,2	0.23145502(1,1,s)-0.38575837(2,1,c)-0.40824829(3,1,s)+0.31209389(4,1,c)+0.17251639(5,1,s)-0.50000000(5,5,s)-0.06154575(6,1,c)+0.50000000(6,5,c)
6,3	0.48795004(2,2,s)+0.40824829(3,2,c)+0.13957263(4,2,s)+0.57735027(5,2,c)-0.49236596(6,2,s)
8,1	0.33333333(0,0,c)+0.37986859(2,0,c)+0.40229114(4,0,c)+0.44946657(6,0,c)+0.61703353(8,0,c)
8,2	0.30276504(1,1,c)+0.04909652(2,1,s)-0.34855072(3,1,c)+0.31642874(4,1,s)-0.11450715(5,1,c)+0.33187326(5,5,c)-0.37326273(6,1,s)+0.17837652(6,5,s)+0.15405792(7,1,c)+0.22124884(7,5,c)-0.30151134(7,7,c)+0.09020708(8,1,s)+0.35675303(8,5,s)+0.30151134(8,7,s)
8,3	0.30276504(1,1,s)-0.04909652(2,1,c)-0.34855072(3,1,s)-0.31642874(4,1,c)-0.11450715(5,1,s)+0.33187326(5,5,s)+0.37326273(6,1,c)-0.17837652(6,5,c)+0.15405792(7,1,s)+0.22124884(7,5,s)+0.30151134(7,7,s)-0.09020708(8,1,c)-0.35675303(8,5,c)+0.30151134(8,7,c)
8,4	0.44536177(2,1,c)-0.21956631(3,1,s)-0.19933137(4,1,c)+0.40394327(5,1,s)-0.25087260(5,5,s)-0.09958592(6,1,c)+0.13483997(6,5,c)-0.19652092(7,1,s)-0.16724840(7,5,s)+0.39886202(7,7,s)+0.04474978(8,1,c)+0.26967994(8,5,c)+0.39886202(8,7,c)
8,5	0.44536177(2,1,s)+0.21956631(3,1,c)-0.19933137(4,1,s)-0.40394327(5,1,c)+0.25087260(5,5,c)-0.09958592(6,1,s)+0.13483997(6,5,s)+0.19652092(7,1,c)+0.16724840(7,5,c)+0.39886202(7,7,c)+0.04474978(8,1,s)+0.26967994(8,5,s)-0.39886202(8,7,s)
8,6	0.44136741(2,2,c)-0.27524094(3,2,s)+0.24584459(4,2,c)-0.42365927(5,2,s)-0.49472744(7,2,s)-0.49472744(8,2,c)
8,7	0.42043748(3,3,c)+0.46933966(4,3,s)-0.09245003(5,3,c)+0.38924947(6,3,s)-0.56096819(7,3,c)-0.35805744(8,3,s)
8,8	0.42043748(3,3,s)-0.46933966(4,3,c)-0.09245003(5,3,s)-0.38924947(6,3,c)-0.56096819(7,3,s)+0.35805744(8,3,c)
8,9	0.31289311(4,4,c)-0.55470020(5,4,s)-0.60302269(6,4,c)+0.43852901(7,4,s)+0.19611614(8,4,c)
10,1	0.30895719(1,1,c)-0.00912415(2,1,s)-0.15003607(3,1,c)+0.17311854(4,1,s)-0.33493206(5,1,c)-0.27735010(5,5,c)+0.19359163(6,1,s)-0.10846523(6,5,s)+0.03512919(7,1,c)-0.20180184(7,5,c)+0.27500955(7,7,c)-0.41001963(8,1,s)-0.17770466(8,5,s)-0.15018785(8,7,s)+0.13645910(9,1,c)-0.15877684(9,5,c)+0.17751790(9,7,c)+0.11980362(10,1,s)-0.31545759(10,5,s)-0.29083753(10,7,s)

10,2	0.30895719(1,1,s)+0.00912415(2,1,c)-0.15003607(3,1,s)-0.17311854(4,1,c)-0.33493206(5,1,s)-0.27735010(5,5,s)-0.19359163(6,1,c)+0.10846523(6,5,c)+0.03512919(7,1,s)-0.20180184(7,5,s)-0.27500955(7,7,s)+0.41001963(8,1,c)+0.17770466(8,5,c)-0.15018785(8,7,c)+0.13645910(9,1,s)-0.15877684(9,5,s)-0.17751790(9,7,s)-0.11980362(10,1,c)+0.31545759(10,5,c)-0.29083753(10,7,c)
10,3	0.37928372(2,1,c)-0.14992506(3,1,s)+0.14992506(4,1,c)+0.24019223(5,5,s)-0.27749837(6,1,c)-0.09393364(6,5,c)+0.39549603(7,1,s)+0.17476552(7,5,s)-0.31755367(7,7,s)-0.05999194(8,1,c)-0.15389675(8,5,c)-0.17342199(8,7,c)-0.26665589(9,1,s)+0.13750477(9,5,s)-0.20498002(9,7,s)+0.05533492(10,1,c)-0.27319428(10,5,c)-0.33583025(10,7,c)
10,4	0.37928372(2,1,s)+0.14992506(3,1,c)+0.14992506(4,1,s)-0.24019223(5,5,c)-0.27749837(6,1,s)-0.09393364(6,5,s)-0.39549603(7,1,c)-0.17476552(7,5,c)-0.31755367(7,7,c)-0.05999194(8,1,s)-0.15389675(8,5,s)+0.17342199(8,7,s)+0.26665589(9,1,c)-0.13750477(9,5,c)-0.20498002(9,7,c)+0.05533492(10,1,s)-0.27319428(10,5,s)+0.33583025(10,7,s)
10,5	0.40394327(2,2,s)+0.20197163(3,2,c)+0.27097338(4,2,s)+0.32025631(5,2,c)+0.13351147(6,2,s)+0.40816431(7,2,c)-0.07430205(8,2,s)+0.43594180(9,2,c)-0.48995628(10,2,s)
10,6	0.35478744(4,4,s)+0.48038446(5,4,c)-0.25332020(6,4,s)+0.18421903(7,4,c)-0.49491340(8,4,s)-0.48507125(9,4,c)+0.25498133(10,4,s)
12,1	0.39223227(0,0,c)-0.12642791(2,0,c)+0.49598049(4,0,c)+0.10676525(6,0,c)+0.29367108(8,0,c)+0.27986801(10,0,c)+0.39775062(12,0,c)+0.50000000(12,12,c)
12,2	0.44474959(1,0,c)-0.45993311(3,0,c)+0.27967106(5,0,c)-0.10857496(7,0,c)+0.02542464(9,0,c)-0.00291641(11,0,c)-0.70710678(12,12,s)
12,3	0.30109690(1,1,c)-0.02382466(2,1,s)-0.02521365(3,1,c)+0.08056572(4,1,s)-0.28483698(5,1,c)+0.24590434(5,5,c)+0.20345976(6,1,s)+0.07687976(6,5,s)-0.22501531(7,1,c)+0.18465922(7,5,c)-0.25164810(7,7,c)+0.07194888(8,1,s)+0.11980846(8,5,s)+0.10125663(8,7,s)+0.11546539(9,1,c)+0.15877684(9,5,c)-0.17751790(9,7,c)-0.41858859(10,1,s)+0.17403079(10,5,s)+0.16044846(10,7,s)+0.11665626(11,1,c)+0.12878502(11,5,c)-0.13710212(11,7,c)+0.14543942(12,1,s)+0.29293746(12,5,s)+0.27863911(12,7,s)
12,4	0.30109690(1,1,s)+0.02382466(2,1,c)-0.02521365(3,1,s)-0.08056572(4,1,c)-0.28483698(5,1,s)+0.24590434(5,5,s)-0.20345976(6,1,c)-0.07687976(6,5,c)-0.22501531(7,1,s)+0.18465922(7,5,s)+0.25164810(7,7,s)-0.07194888(8,1,c)-0.11980846(8,5,c)+0.10125663(8,7,c)+0.11546539(9,1,s)+0.15877684(9,5,s)+0.17751790(9,7,s)+0.41858859(10,1,c)-0.17403079(10,5,c)+0.16044846(10,7,c)+0.11665626(11,1,s)+0.12878502(11,5,s)+0.13710212(11,7,s)-0.14543942(12,1,c)-0.29293746(12,5,c)+0.27863911(12,7,c)
12,5	0.56892559(2,0,c)-0.04065414(4,0,c)+0.36774696(6,0,c)+0.21390857(8,0,c)+0.29352011(10,0,c)+0.39689062(12,0,c)-0.50000000(12,12,c)
12,6	0.31318323(2,1,c)-0.10357562(3,1,s)+0.26231444(4,1,c)-0.09294310(5,1,s)-0.22447892(5,5,s)-0.05183233(6,1,c)+0.07018130(6,5,c)+0.14085253(7,1,s)-0.16857003(7,5,s)+0.27566668(7,7,s)-0.27654755(8,1,c)+0.10936966(8,5,c)+0.11092108(8,7,c)+0.33729599(9,1,s)-0.14494276(9,5,s)+

	0.19446112(9,7,s)-0.01930698(10,1,c)+0.15886764(10,5,c)+0.17576248(10,7,c)- 0.31148941(11,1,s)-0.11756410(11,5,s)+0.15018785(11,7,s)+0.05974534(12,1,c)+ 0.26741409(12,5,c)+0.30523385(12,7,c)
12,7	0.31318323(2,1,s)+0.10357562(3,1,c)+0.26231444(4,1,s)+0.09294310(5,1,c)+0.22447892(5,5,c)- 0.05183233(6,1,s)+0.07018130(6,5,s)-0.14085253(7,1,c)+0.16857003(7,5.c)+0.27566668(7,7,c)- 0.27654755(8,1,s)+0.10936966(8,5,s)-0.11092108(8,7,s)-0.33729599(9,1,c)+0.14494276(9,5,c)+ 0.19446112(9,7,c)-0.01930698(10,1,s)+0.15886764(10,5,s)-0.17576248(10,7,s)+ 0.31148941(11,1,c)+0.11756410(11,5,c)+0.15018785(11,7,c)+0.05974534(12,1,s)+ 0.26741409(12,5,s)-0.30523385(12,7,s)
12,8	0.38839304(2,2,c)-0.09146026(3,2,s)+0.17853236(4,2,c)-0.33755924(5,2,s)+0.26653969(6,2,c)- 0.24864709(7,2,s)+0.01282681(8,2,c)-0.39865719(9,2,s)-0.10299171(10,2,c)+ 0.09747754(10,10,c)-0.37245661(11,2,s)+0.13495155(11,10,s)-0.46610074(12,2,c)- 0.09332764(12,10,c)
12,9	0.10482848(2,2,s)-0.21926450(3,2,c)-0.31332712(4,2,s)+0.35275259(5,2,c)+0.32917948(6,2,s)- 0.25983856(7,2,c)-0.17425376(8,2,s)+0.09846921(9,2,c)+0.04579053(10,2,s)+ 0.36115756(10,10,s)-0.01662607(11,2,c)-0.50000000(11,10,c)-0.00410194(12,2,s)- 0.34578204(12,10,s)
12,10	0.25335246(3,2,s)-0.37544735(4,2,c)-0.27172884(5,2,s)+0.26715437(6,2,c)+0.33955076(7,2,s)- 0.18456544(8,2,c)+0.00948148(9,2,s)+0.07642462(10,2,c)+0.34775410(10,10,c)+ 0.12166870(11,2,s)+0.48144374(11,10,s)+0.12639077(12,2,c)-0.33294920(12,10,c)
12,11	0.39556103(3,3,c)+0.21706562(4,3,s)+0.07110372(5,3,c)+0.43882795(6,3,s)+0.02267913(7,3,c)+ 0.26210973(8,3,s)-0.32676784(9,3,c)-0.06625304(9,9,c)+0.16907972(10,3,s)+0.10965089(10,9,s)- 0.46456543(11,3,c)+0.10475525(11,9,c)-0.38426547(12,3,s)-0.05779109(12,9,s)
12,12	0.39556103(3,3,s)-0.21706562(4,3.c)+0.07110372(5,3,s)-0.43882795(6,3,c)+0.02267913(7,3,s)- 0.26210973(8,3,c)-0.32676784(9,3,s)+0.06625304(9,9,s)-0.16907972(10,3,c)+0.10965089(10,9,c)- 0.46456543(11,3,s)-0.10475525(11,9,s)+0.38426547(12,3,c)-0.05779109(12,9,c)
12,13	0.27648288(4,3,c)-0.34387124(5,3,s)-0.25992751(6,3,c)+0.34045481(7,3,s)+0.33385690(8,3,c)- 0.08646488(9,3,s)+0.25891911(9,9,s)-0.04473958(10,3,c)+0.42851938(10,9,c)+ 0.15404559(11,3,s)-0.40938706(11,9,s)-0.08885931(12,3,c)-0.22584954(12,9,c)
12,14	0.27648288(4,3,s)+0.34387124(5,3,c)-0.25992751(6,3,s)-0.34045481(7,3,c)+0.33385690(8,3,s)+ 0.08646488(9,3,c)+0.25891911(9,9,c)-0.04473958(10,3,s)-0.42851938(10,9,s)- 0.15404559(11,3,c)-0.40938706(11,9,c)-0.08885931(12,3,s)+0.22584954(12,9,s)
12,15	0.37384128(4,4,c)-0.32297388(5,4,s)-0.15346224(6,4,c)-0.40947817(7,4,s)-0.25380183(8,4,c)+ 0.05488623(8,8,c)+0.06546112(9,4,s)+0.10201378(9,8,s)-0.41763226(10,4,c)- 0.11620094(10,8,c)+0.45334140(11,4,s)-0.08834653(11,8,s)+0.28221985(12,4,c)+ 0.04119178(12,8,c)
12,16	0.10090092(4,4,s)-0.22310033(5,4,c)-0.32917948(6,4,s)+0.37085408(7,4,c)+0.33367054(8,4,s)+

	0.20335531(8,8,s)-0.24253563(9,4,c)-0.37796447(9,8,c)-0.14066741(10,4,s)-0.43052839(10,8,s)+ 0.06220908(11,4,c)+0.32732684(11,8,c)+0.01834446(12,4,s)+0.15261692(12,8,s)
12,17	0.32223077(5,4,s)-0.29885065(6,4,c)-0.27036871(7,4,s)+0.19580829(8,8,c)+0.41767335(8,4,c)+ 0.36393726(9,8,s)+0.23353452(9,4,s)-0.41455040(10,8,c)-0.02902433(10,4,c)- 0.31517891(11,8,s)-0.19168109(11,4,s)+0.14695293(12,8,c)-0.06005640(12,4,c)
12,18	0.26098171(6,6,c)-0.76088591(8,6,c)+0.58241841(10,6,c)-0.11717499(12,6,c)
12,19	0.18454194(6,6,s)-0.39147257(7,6,c)-0.53802759(8,6,s)+0.54232614(9,6,c)+0.41183200(10,6,s)- 0.22941573(11,6,c)-0.08285523(12,6,s)
12,20	0.55362582(7,6,s)-0.76696499(9,6,s)+0.32444284(11,6,s)

E.4. Cystallographic Point Group 4

n,λ	Coefficients of the Expansion of the Symmetrized Hyperspherical Harmonics
0,1	1.00000000(0,0,c)
4,1	0.44721360(0,0,c)+0.53452248(2,0,c)+0.71713717(4,0,c)
4,2	0.53452248(2,2,c)-0.70710678(3,2,s)-0.46291005(4,2,c)
6,1	0.48795004(2,2,s)+0.40824829(3,2,c)+0.13957263(4,2,s)+0.57735027(5,2,c)-0.49236596(6,2,s)
8,1	0.47140452(0,0,c)-0.10744306(2,0,c)+0.50571163(4,0,c)+0.25425669(6,0,c)+0.44254158(8,0,c)+ 0.50000000(8,8,c)
8,2	0.51639778(1,0,c)-0.44494921(3,0,c)+0.18490007(5,0,c)-0.03413944(7,0,c)-0.70710678(8,8,s)
8,3	0.64465837(2,0,c)+0.06321395(4,0,c)+0.38138504(6,0,c)+0.43007562(8,0,c)-0.50000000(8,8,c)
8,4	0.47445571(2,2,c)-0.13655775(3,2,s)+0.08316346(4,2,c)-0.52548465(5,2,s)+0.09032446(6,2,c)+ 0.13397283(6,6,c)-0.41420286(7,2,s)+0.18344985(7,6,s)-0.47556625(8,2,c)-0.12532010(8,6,c)
8,5	0.17407766(2,2,s)-0.32566947(3,2,c)-0.39666441(4,2,s)+0.35805744(5,2,c)+0.24618298(6,2,s)+ 0.36514837(6,6,s)-0.12543630(7,2,c)-0.50000000(7,6,c)-0.04181210(8,2,s)-0.34156503(8,6,s)
8,6	0.40394327(3,2,s)-0.45920154(4,2,c)-0.17764624(5,2,s)+0.22901431(6,2,c)+0.33968311(6,6,c)+ 0.29820379(7,2,s)+0.46513025(7,6,s)+0.14261920(8,2,c)-0.31774445(8,6,c)
8,7	0.44249768(4,4,c)-0.85280287(6,4,c)+0.27735010(8,4,c)
8,8	0.31289311(4,4,s)-0.55470020(5,4,c)-0.60302269(6,4,s)+0.43852901(7,4,c)+0.19611614(8,4,s)
8,9	0.78446454(5,4,s)-0.62017367(7,4,s)
10,1	0.30151134(0,0,c)-0.20483662(2,0,c)-0.35478744(4,0,c)+0.45315295(6,0,c)-0.18806885(8,0,c)- 0.48666426(8,8,c)+0.02326488(10,0,c)-0.51298918(10,8,c)
10,2	0.38138504(1,0,c)+0.09160572(3,0,c)-0.48038446(5,0,c)+0.32985294(7,0,c)+0.48666426(8,8,s)- 0.08112739(9,0,c)+0.51298918(10,8,s)
10,3	0.20483662(2,2,c)+0.30725493(3,2,s)-0.22901431(4,2,c)-0.23695935(6,2,c)-0.35146751(6,6,c)- 0.34879472(7,2,s)-0.32084447(7,6,s)+0.30770381(8,2,c)-0.05129892(8,6,c)+0.18421903(9,2,s)- 0.38348249(9,6,s)-0.06901477(10,2,c)+0.35190767(10,6,c)
10,4	0.45291081(2,2,s)+0.04117371(3,2,c)+0.13810082(4,2,s)+0.28563102(5,2,c)+0.01190766(6,2,s)- 0.15895716(6,6,s)+0.52178299(7,2,c)+0.14510737(7,6,c)+0.07289558(8,2,s)-0.02320081(8,6,s)+ 0.30549270(9,2,c)+0.17343648(9,6,c)-0.46819658(10,2,s)+0.15915623(10,6,s)
10,5	0.36538043(3,2,c)+0.32680619(4,2,s)+0.14484136(5,2,c)+0.27172275(6,2,s)+0.31346775(6,6,s)- 0.12648468(7,2,c)-0.28615560(7,6,c)-0.30804004(8,2,s)+0.04575261(8,6,s)+0.36146384(9,2,c)- 0.34202136(9,6,c)-0.16003799(10,2,s)-0.31386032(10,6,s)
10,6	0.35478744(4,4,s)+0.48038446(5,4,c)-0.25332020(6,4,s)+0.18421903(7,4,c)-0.49491340(8,4,s)- 0.48507125(9,4,c)+0.25498133(10,4,s)
12,1	0.39223227(0,0,c)+0.18964186(2,0,c)-0.03252331(4,0,c)+0.18980488(6,0,c)+0.57646546(8,0,c)+

	0.29083753(8,8,c)+0.09784004(10,0,c)+0.25085666(10,8,c)+0.42570066(12,0,c)+ 0.32013196(12,8,c)
12,2	0.29649973(1,0,c)+0.25087260(3,0,c)-0.22882178(5,0,c)-0.33888547(7,0,c)-0.41130637(8,8,s)+ 0.40679427(9,0,c)-0.35476488(10,8,s)-0.12832188(11,0,c)-0.45273496(12,8,s)
12,3	0.25285582(2,0,c)+0.48784967(4,0,c)+0.28470732(6,0,c)-0.06888581(8,0,c)-0.29083753(8,8,c)+ 0.47554808(10,0,c)-0.25085666(10,8,c)+0.36894057(12,0,c)-0.32013196(12,8,c)
12,4	0.44249768(2,2,c)-0.05666634(3,2,s)+0.10496854(4,2,c)-0.06077652(5,2,s)+0.10634073(6,2,c)+ 0.15772879(6,6,c)-0.41597078(7,2,s)+0.11153110(7,6,s)-0.03377538(8,2,c)+0.06569350(8,6,c)- 0.44322309(9,2,s)+0.14568039(9,6,s)+0.06508714(10,2,c)-0.01843781(10,6,c)+ 0.08555887(10,10,c)-0.22844730(11,2,s)+0.15406492(11,6,s)-0.11845089(11,10,s)- 0.45283924(12,2,c)-0.16692513(12,6,c)-0.08191638(12,10,c)
12,5	0.23652496(2,2,s)-0.14135070(3,2,c)-0.23565378(4,2,s)-0.28425614(5,2,c)-0.09284114(6,2,s)+ 0.29508355(6,6,s)+0.25475038(7,2,c)-0.20865558(7,6,c)-0.16148033(8,2,s)+0.12290129(8,6,s)+ 0.21820907(9,2,c)-0.27254305(9,6,c)+0.31118207(10,2,s)-0.03449399(10,6,s)- 0.16006598(10,10,s)-0.19158672(11,2,c)-0.28822906(11,6,c)-0.22160132(11,10,c)- 0.08362767(12,2,s)-0.31228832(12,6,s)+0.15325151(12,10,s)
12,6	0.31448545(3,2,c)-0.23302069(4,2,s)-0.25297199(5,2,c)+0.41311697(6,2,s)-0.14589321(6,6,s)+ 0.16391008(7,2,c)+0.10316208(7,6,c)-0.11455019(8,2,s)-0.06076402(8,6,s)-0.21773246(9,2,c)+ 0.13474889(9,6,c)-0.10277106(10,2,s)+0.01705428(10,6,s)-0.32374939(10,10,s)+ 0.11327017(11,2,c)+0.14250426(11,6,c)-0.44821073(11,10,c)+0.03677071(12,2,s)+ 0.15439948(12,6,s)+0.30996644(12,10,s)
12,7	0.37436021(3,2,s)+0.00847410(4,2,c)-0.00919965(5,2,s)-0.44312254(6,2,c)+0.25785185(6,6,c)+ 0.11689443(7,2,s)+0.18232879(7,6,s)+0.00416576(8,2,c)+0.10739441(8,6,c)-0.17090299(9,2,s)+ 0.23815536(9,6,s)+0.26374553(10,2,c)-0.03014176(10,6,c)-0.19858073(10,10,c)+ 0.29651121(11,2,s)+0.25186222(11,6,s)+0.27492258(11,10,s)+0.07080103(12,2,c)- 0.27288583(12,6,c)+0.19012658(12,10,c)
12,8	0.41641539(4,2,c)-0.45206900(5,2,s)-0.07533196(6,2,c)-0.13035791(6,6,c)+0.12112924(7,2,s)- 0.09217696(7,6,s)+0.20470484(8,2,c)-0.05429362(8,6,c)-0.13670900(9,2,s)-0.12040027(9,6,s)- 0.21897345(10,2,c)+0.01523827(10,6,c)-0.28927523(10,10,c)-0.25035837(11,2,s)- 0.12732983(11,6,s)+0.40048341(11,10,s)-0.17741818(12,2,c)+0.13795839(12,6,c)+ 0.27695994(12,10,c)
12,9	0.50907034(4,4,c)-0.09490244(6,4,c)-0.50503537(8,4,c)-0.55762317(10,4,c)+0.40723038(12,4,c)
12,10	0.35996709(4,4,s)-0.39795859(5,4,c)-0.06710616(6,4,s)-0.32130806(7,4,c)-0.35711394(8,4,s)- 0.39429912(10,4,s)+0.48825208(11,4,c)+0.28795537(12,4,s)
12,11	0.56279844(5,4,s)+0.45439821(7,4,s)-0.69049271(11,4,s)
12,12	0.18454194(6,6,c)-0.39147257(7,6,s)-0.53802759(8,6,c)+0.54232614(9,6,s)+0.41183200(10,6,c)- 0.22941573(11,6,s)-0.08285523(12,6,c)

E.5. Cystallographic Point Group 6

n,λ	Coefficients of the Expansion of the Symmetrized Hyperspherical Harmonics
0,1	1.00000000(0,0,c)
4,1	0.44721360(0,0,c)+0.53452248(2,0,c)+0.71713717(4,0,c)
4,2	0.53452248(2,2,c)-0.70710678(3,2,s)-0.46291005(4,2,c)
6,1	0.48795004(2,2,s)+0.40824829(3,2,c)+0.13957263(4,2,s)+0.57735027(5,2,c)-0.49236596(6,2,s)
8,1	0.33333333(0,0,c)+0.37986859(2,0,c)+0.40229114(4,0,c)+0.44946657(6,0,c)+0.61703353(8,0,c)
8,2	0.44136741(2,2,c)-0.27524094(3,2,s)+0.24584459(4,2,c)-0.42365927(5,2,s)-0.49472744(7,2,s)-0.49472744(8,2,c)
8,3	0.31289311(4,4,c)-0.55470020(5,4,s)-0.60302269(6,4,c)+0.43852901(7,4,s)+0.19611614(8,4,c)
10,1	0.40394327(2,2,s)+0.20197163(3,2,c)+0.27097338(4,2,s)+0.32025631(5,2,c)+0.13351147(6,2,s)+0.40816431(7,2,c)-0.07430205(8,2,s)+0.43594180(9,2,c)-0.48995628(10,2,s)
10,2	0.35478744(4,4,s)+0.48038446(5,4,c)-0.25332020(6,4,s)+0.18421903(7,4,c)-0.49491340(8,4,s)-0.48507125(9,4,c)+0.25498133(10,4,s)
12,1	0.39223227(0,0,c)-0.12642791(2,0,c)+0.49598049(4,0,c)+0.10676525(6,0,c)+0.29367108(8,0,c)+0.27986801(10,0,c)+0.39775062(12,0,c)+0.50000000(12,12,c)
12,2	0.44474959(1,0,c)-0.45993311(3,0,c)+0.27967106(5,0,c)-0.10857496(7,0,c)+0.02542464(9,0,c)-0.00291641(11,0,c)-0.70710678(12,12,s)
12,3	0.56892559(2,0,c)-0.04065414(4,0,c)+0.36774696(6,0,c)+0.21390857(8,0,c)+0.29352011(10,0,c)+0.39689062(12,0,c)-0.50000000(12,12,c)
12,4	0.38839304(2,2,c)-0.09146026(3,2,s)+0.17853236(4,2,c)-0.33755924(5,2,s)+0.26653969(6,2,c)-0.24864709(7,2,s)+0.01282681(8,2,c)-0.39865719(9,2,s)-0.10299171(10,2,c)+0.09747754(10,10,c)-0.37245661(11,2,s)+0.13495155(11,10,s)-0.46610074(12,2,c)-0.09332764(12,10,c)
12,5	0.10482848(2,2,s)-0.21926450(3,2,c)-0.31332712(4,2,s)+0.35275259(5,2,c)+0.32917948(6,2,s)-0.25983856(7,2,c)-0.17425376(8,2,s)+0.09846921(9,2,c)+0.04579053(10,2,s)+0.36115756(10,10,s)-0.01662607(11,2,c)-0.50000000(11,10,c)-0.00410194(12,2,s)-0.34578204(12,10,s)
12,6	0.25335246(3,2,s)-0.37544735(4,2,c)-0.27172884(5,2,s)+0.26715437(6,2,c)+0.33955076(7,2,s)-0.18456544(8,2,c)+0.00948148(9,2,s)+0.07642462(10,2,c)+0.34775410(10,10,c)+0.12166870(11,2,s)+0.48144374(11,10,s)+0.12639077(12,2,c)-0.33294920(12,10,c)
12,7	0.37384128(4,4,c)-0.32297388(5,4,s)-0.15346224(6,4,c)-0.40947817(7,4,s)-0.25380183(8,4,c)+0.05488623(8,8,c)+0.06546112(9,4,s)+0.10201378(9,8,s)-0.41763226(10,4,c)-0.11620094(10,8,c)+0.45334140(11,4,s)-0.08834653(11,8,s)+0.28221985(12,4,c)+0.04119178(12,8,c)

12,8	0.10090092(4,4,s)-0.22310033(5,4,c)-0.32917948(6,4,s)+0.37085408(7,4,c)+0.33367054(8,4,s)+ 0.20335531(8,8,s)-0.24253563(9,4,c)-0.37796447(9,8,c)-0.14066741(10,4,s)-0.43052839(10,8,s)+ 0.06220908(11,4,c)+0.32732684(11,8,c)+0.01834446(12,4,s)+0.15261692(12,8,s)
12,9	0.32223077(5,4,s)-0.29885065(6,4,c)-0.27036871(7,4,s)+0.41767335(8,4,c)+0.19580829(8,8,c)+ 0.23353452(9,4,s)+0.36393726(9,8,s)-0.02902433(10,4,c)-0.41455040(10,8,c)- 0.19168109(11,4,s)-0.31517891(11,8,s)-0.06005640(12,4,c)+0.14695293(12,8,c)
12,10	0.26098171(6,6,c)-0.76088591(8,6,c)+0.58241841(10,6,c)-0.11717499(12,6,c)
12,11	0.18454194(6,6,s)-0.39147257(7,6,c)-0.53802759(8,6,s)+0.54232614(9,6,c)+0.41183200(10,6,s)- 0.22941573(11,6,c)-0.08285523(12,6,s)
12,12	0.55362582(7,6,s)-0.76696499(9,6,s)+0.32444284(11,6,s)
14,1	0.25819889(0,0,c)-0.26986873(2,0,c)-0.16870346(4,0,c)+0.43800373(6,0,c)-0.34515908(8,0,c)+ 0.14198182(10,0,c)-0.02995934(12,0,c)-0.49065338(12,12,c)+0.00221038(14,0,c)- 0.50917508(14,12,c)
14,2	0.35856858(1,0,c)-0.06517949(3,0,c)-0.35168417(5,0,c)+0.42557555(7,0,c)-0.23907119(9,0,c)+ 0.07163761(11,0,c)+0.49065338(12,12,s)-0.00984467(13,0,c)+0.50917508(14,12,s)
14,3	0.13750477(2,2,c)+0.24753689(3,2,s)-0.27126499(4,2,c)-0.17668546(5,2,s)-0.18029903(7,2,s)+ 0.29293746(8,2,c)+0.31057362(9,2,s)-0.25335280(10,2,c)-0.35262987(10,10,c)- 0.16542735(11,2,s)-0.33166248(11,10,s)+0.08616254(12,2,c)-0.03475240(12,10,c)+ 0.03431933(13,2,s)-0.37416574(13,10,s)-0.00915182(14,2,c)+0.35276684(14,10,c)
14,4	0.37560552(2,2,s)+0.02648903(3,2,c)+0.14993895(4,2,s)+0.25465896(5,2,c)+0.19120613(6,2,s)+ 0.31987212(7,2,c)+0.22273124(8,2,s)+0.19241091(9,2,c)-0.08099842(10,2,s)- 0.12909366(10,10,s)+0.39970269(11,2,c)+0.12141774(11,10,c)-0.10791059(12,2,s)- 0.01272245(12,10,s)+0.31912320(13,2,c)+0.13697769(13,10,c)-0.44559984(14,2,s)+ 0.12914380(14,10,s)
14,5	0.27642349(3,2,c)+0.35048662(4,2,s)-0.08968362(5,2,c)+0.07522009(6,2,s)-0.06791204(7,2,c)- 0.22716815(8,2,s)+0.40943599(9,2,c)+0.24038793(10,2,s)+0.32815035(10,10,s)- 0.02052579(11,2,c)-0.30863851(11,10,c)-0.13504194(12,2,s)+0.03233990(12,10,s)+ 0.16242190(13,2,c)-0.34819120(13,10,c)-0.16546351(14,2,s)-0.32827781(14,10,s)
14,6	0.13910372(4,4,c)+0.26098171(5,4,s)-0.29072345(6,4,c)-0.18029903(7,4,s)-0.02620112(8,4,c)- 0.23952388(8,8,c)-0.22332067(9,4,s)-0.34802013(9,8,s)+0.32077105(10,4,c)+ 0.21816795(10,8,c)+0.29875904(11,4,s)-0.08451543(11,8,s)-0.20367028(12,4,c)+ 0.32837934(12,8,c)-0.10125076(13,4,s)+0.34891135(13,8,s)+0.03267854(14,4,c)- 0.19286801(14,8,c)
14,7	0.37997318(4,4,s)+0.21313292(5,4,c)-0.07368261(6,4,s)+0.38080015(7,4,c)-0.20585744(8,4,s)- 0.08768688(8,8,s)+0.25784294(9,4,c)+0.12740609(9,8,c)-0.22582792(10,4,s)+ 0.07986873(10,8,s)-0.20815996(11,4,c)+0.03094011(11,8,c)-0.36587056(12,4,s)+ 0.12021582(12,8,s)-0.40773386(13,4,c)-0.12773235(13,8,c)+0.29908077(14,4,s)-

	0.07060671(14,8,s)
14,8	0.36429660(5,4,c)+0.28342439(6,4,s)-0.04394309(7,4,c)-0.05282820(8,4,s)+0.22289617(8,8,s)-0.13854519(9,4,c)-0.32386062(9,8,c)-0.43354031(10,4,s)-0.20302276(10,8,s)+0.23915633(11,4,c)-0.07864838(11,8,c)+0.07493106(12,4,s)-0.30558329(12,8,s)-0.26920556(13,4,c)+0.32468997(13,8,c)+0.08254143(14,4,s)+0.17947913(14,8,s)
14,9	0.24296075(6,6,s)+0.42557555(7,6,c)-0.40936780(8,6,s)-0.14888045(9,6,c)-0.20999394(10,6,s)-0.45034100(11,6,c)+0.46241938(12,6,s)+0.30645235(13,6,c)-0.12433397(14,6,s)

E.6. Cystallographic Point Group 222

n,λ	Coefficients of the Expansion of the Symmetrized Hyperspherical Harmonics
0,1	1.00000000(0,0,c)
4,1	0.63245553(0,0,c)+0.59160798(4,0,c)+0.50000000(4,4,c)
4,2	0.75592895(2,0,c)+0.42257713(4,0,c)-0.50000000(4,4,c)
4,3	0.75592895(2,2,c)-0.65465367(4,2,c)
4,4	1.00000000(3,2,s)
6,1	0.37796447(0,0,c)-0.56407607(4,0,c)-0.47673129(4,4,c)+0.19738551(6,0,c)-0.52223297(6,4,c)
8,1	0.57735027(0,0,c)+0.27097338(4,0,c)+0.22901431(4,4,c)-0.07784989(6,0,c)+0.20597146(6,4,c)+ 0.50383147(8,0,c)+0.26794565(8,4,c)+0.40824829(8,8,c)
8,2	0.67098171(2,0,c)-0.07591750(4,0,c)+0.08982680(4,4,c)+0.21374669(6,0,c)+0.08078865(6,4,c)+ 0.39823215(8,0,c)+0.10509693(8,4,c)-0.56044854(8,8,c)
8,3	0.67098171(2,2,c)+0.11761089(4,2,c)+0.12773808(6,2,c)+0.18946619(6,6,c)-0.67255224(8,2,c)- 0.17722939(8,6,c)
8,4	0.60302269(3,2,s)+0.58710899(7,2,s)+0.54006172(7,6,s)
8,5	0.49090710(4,0,c)-0.31116917(4,4,c)+0.63466306(6,0,c)-0.27986010(6,4,c)+0.17114304(8,0,c)- 0.36406645(8,4,c)+0.13867505(8,8,c)
8,6	0.64940905(4,2,c)-0.32387514(6,2,c)-0.48038446(6,6,c)-0.20169401(8,2,c)+0.44935852(8,6,c)
8,7	0.44249768(4,4,c)-0.85280287(6,4,c)+0.27735010(8,4,c)
8,8	0.78446454(5,2,s)+0.41985956(7,2,s)-0.45643546(7,6,s)
8,9	0.78446454(5,4,s)-0.62017367(7,4,s)
10,1	0.42640143(0,0,c)-0.29268470(4,0,c)-0.24736372(4,4,c)+0.08010688(6,0,c)-0.21194288(6,4,c)- 0.42469327(8,0,c)-0.22585869(8,4,c)-0.34412360(8,8,c)+0.21385976(10,0,c)-0.30476098(10,4,c)- 0.36273813(10,8,c)
10,2	0.28968273(2,0,c)+0.20906050(4,0,c)-0.24736372(4,4,c)-0.56074816(6,0,c)-0.21194288(6,4,c)- 0.15872375(8,0,c)-0.22585869(8,4,c)+0.34412360(8,8,c)+0.18095826(10,0,c)- 0.30476098(10,4,c)+0.36273813(10,8,c)
10,3	0.28968273(2,2,c)-0.32387514(4,2,c)-0.33511112(6,2,c)-0.49705012(6,6,c)+0.43515890(8,2,c)- 0.07254763(8,6,c)-0.09760163(10,2,c)+0.49767260(10,6,c)
10,4	0.43452409(3,2,s)-0.49327022(7,2,s)-0.45374261(7,6,s)+0.26052505(9,2,s)-0.54232614(9,6,s)
12,1	0.55470020(0,0,c)+0.18781254(4,0,c)+0.15873057(4,4,c)-0.05032962(6,0,c)+0.13315966(6,4,c)+ 0.25380277(8,0,c)+0.13497638(8,4,c)+0.20565319(8,8,c)-0.10457949(10,0,c)+ 0.14903106(10,4,c)+0.17738244(10,8,c)+0.45182779(12,0,c)+0.20406918(12,4,c)+ 0.22636748(12,8,c)+0.35355339(12,12,c)
12,2	0.62578622(2,0,c)-0.09582272(4,0,c)+0.11337898(4,4,c)+0.25164810(6,0,c)+0.09511404(6,4,c)-

	0.02746783(8,0,c)+0.09641170(8,4,c)-0.02937903(8,8,c)+0.10871670(10,0,c)+ 0.10645076(10,4,c)-0.02534035(10,8,c)+0.38510913(12,0,c)+0.14576370(12,4,c)- 0.03233821(12,8,c)-0.55558390(12,12,c)
12,3	0.62578622(2,2,c)+0.14844793(4,2,c)+0.15038850(6,2,c)+0.22306220(6,6,c)-0.04776561(8,2,c)+ 0.09290464(8,6,c)+0.09204712(10,2,c)-0.02607500(10,6,c)+0.12099851(10,10,c)- 0.64041139(12,2,c)-0.23606778(12,6,c)-0.11584725(12,10,c)
12,4	0.53545615(3,2,s)+0.25149461(7,2,s)+0.23134139(7,6,s)-0.14516015(9,2,s)+0.30217494(9,6,s)+ 0.46295957(11,2,s)+0.31956640(11,6,s)+0.40949106(11,10,s)
12,5	0.58340853(4,0,c)-0.00953451(4,4,c)+0.15166192(6,0,c)-0.00799853(6,4,c)-0.16558015(8,0,c)- 0.00810766(8,4,c)-0.33044325(8,8,c)+0.41302841(10,0,c)-0.00895188(10,4,c)- 0.28501786(10,8,c)+0.22472726(12,0,c)-0.01225787(12,4,c)-0.36372695(12,8,c)+ 0.25484371(12,12,c)
12,6	0.58902222(4,2,c)-0.11926358(6,2,c)-0.17689648(6,6,c)+0.28955630(8,2,c)-0.07367677(8,6,c)- 0.30202226(10,2,c)+0.02067843(10,6,c)-0.41472611(10,10,c)-0.24881807(12,2,c)+ 0.18721037(12,6,c)+0.39707002(12,10,c)
12,7	0.58494024(4,4,c)-0.13280267(6,0,c)-0.10632148(6,4,c)-0.26382074(8,0,c)-0.23335193(8,4,c)+ 0.01465856(8,8,c)-0.16933267(10,0,c)-0.43328124(10,4,c)-0.19639934(10,8,c)- 0.03022304(12,0,c)+0.49841587(12,4,c)-0.00843598(12,8,c)+0.01590182(12,12,c)
12,8	0.64520508(5,2,s)-0.09470759(7,2,s)+0.10295800(7,6,s)+0.27994728(9,2,s)+0.13448232(9,6,s)+ 0.38541447(11,2,s)+0.14222236(11,6,s)-0.54672941(11,10,s)
12,9	0.64520508(5,4,s)+0.13989238(7,4,s)+0.16772893(9,4,s)+0.26138665(9,8,s)-0.64532342(11,4,s)- 0.22636748(11,8,s)
12,10	0.28053143(6,0,c)-0.28263207(6,4,c)+0.55729308(8,0,c)-0.34593719(8,4,c)+0.15044584(8,8,c)+ 0.35769714(10,0,c)-0.46510176(10,4,c)+0.03080415(10,8,c)+0.06384294(12,0,c)- 0.12005453(12,4,c)+0.15396757(12,8,c)-0.03359089(12,12,c)
12,11	0.62437262(6,2,c)-0.36833295(6,6,c)-0.15340941(8,6,c)-0.37921592(10,2,c)+ 0.04305652(10,6,c)+0.27245399(10,10,c)-0.10521198(12,2,c)+0.38980849(12,6,c)- 0.26085484(12,10,c)
12,12	0.42263864(6,4,c)-0.59067932(8,4,c)-0.27691474(8,8,c)+0.04104661(10,4,c)+ 0.58626279(10,8,c)+0.08493257(12,4,c)-0.20782282(12,8,c)
12,13	0.26098171(6,6,c)-0.76088591(8,6,c)+0.58241841(10,6,c)-0.11717499(12,6,c)
12,14	0.57490653(7,2,s)-0.21033293(7,6,s)+0.62389569(9,2,s)-0.27473398(9,6,s)+0.20663223(11,2,s)- 0.29054610(11,6,s)+0.18276769(11,10,s)
12,15	0.67968621(7,4,s)-0.29918901(9,4,s)-0.46625240(9,8,s)-0.26091723(11,4,s)+0.40378643(11,8,s)
12,16	0.55362582(7,6,s)-0.76696499(9,6,s)+0.32444284(11,6,s)

E.7. Cystallographic Point Group 32

n,λ	Coefficients of the Expansion of the Symmetrized Hyperspherical Harmonics
0,1	1.00000000(0,0,c)
4,1	0.44721360(0,0,c)+0.53452248(2,0,c)+0.71713717(4,0,c)
4,2	0.53452248(2,2,c)-0.70710678(3,2,s)-0.46291005(4,2,c)
6,1	0.23145502(1,1,c)+0.38575837(2,1,s)-0.40824829(3,1,c)-0.31209389(4,1,s)+0.17251639(5,1,c)-0.50000000(5,5,c)+0.06154575(6,1,s)-0.50000000(6,5,s)
8,1	0.33333333(0,0,c)+0.37986859(2,0,c)+0.40229114(4,0,c)+0.44946657(6,0,c)+0.61703353(8,0,c)
8,2	0.30276504(1,1,c)+0.04909652(2,1,s)-0.34855072(3,1,c)+0.31642874(4,1,s)-0.11450715(5,1,c)+0.33187326(5,5,c)-0.37326273(6,1,s)+0.17837652(6,5,s)+0.15405792(7,1,c)+0.22124884(7,5,c)-0.30151134(7,7,c)+0.09020708(8,1,s)+0.35675303(8,5,s)+0.30151134(8,7,s)
8,3	0.44536177(2,1,s)+0.21956631(3,1,c)-0.19933137(4,1,s)-0.40394327(5,1,c)+0.25087260(5,5,c)-0.09958592(6,1,s)+0.13483997(6,5,s)+0.19652092(7,1,c)+0.16724840(7,5,c)+0.39886202(7,7,c)+0.04474978(8,1,s)+0.26967994(8,5,s)-0.39886202(8,7,s)
8,4	0.44136741(2,2,c)-0.27524094(3,2,s)+0.24584459(4,2,c)-0.42365927(5,2,s)-0.49472744(7,2,s)-0.49472744(8,2,c)
8,5	0.42043748(3,3,c)+0.46933966(4,3,s)-0.09245003(5,3,c)+0.38924947(6,3,s)-0.56096819(7,3,c)-0.35805744(8,3,s)
8,6	0.31289311(4,4,c)-0.55470020(5,4,s)-0.60302269(6,4,c)+0.43852901(7,4,s)+0.19611614(8,4,c)
10,1	0.30895719(1,1,c)-0.00912415(2,1,s)-0.15003607(3,1,c)+0.17311854(4,1,s)-0.33493206(5,1,c)-0.27735010(5,5,c)+0.19359163(6,1,s)-0.10846523(6,5,s)+0.03512919(7,1,c)-0.20180184(7,5,c)+0.27500955(7,7,c)-0.41001963(8,1,s)-0.17770466(8,5,s)-0.15018785(8,7,s)+0.13645910(9,1,c)-0.15877684(9,5,c)+0.17751790(9,7,c)+0.11980362(10,1,s)-0.31545759(10,5,s)-0.29083753(10,7,s)
10,2	0.37928372(2,1,s)+0.14992506(3,1,c)+0.14992506(4,1,s)-0.24019223(5,5,c)-0.27749837(6,1,s)-0.09393364(6,5,s)-0.39549603(7,1,c)-0.17476552(7,5,c)-0.31755367(7,7,c)-0.05999194(8,1,s)-0.15389675(8,5,s)+0.17342199(8,7,s)+0.26665589(9,1,c)-0.13750477(9,5,c)-0.20498002(9,7,c)+0.05533492(10,1,s)-0.27319428(10,5,s)+0.33583025(10,7,s)
12,1	0.39223227(0,0,c)-0.12642791(2,0,c)+0.49598049(4,0,c)+0.10676525(6,0,c)+0.29367108(8,0,c)+0.27986801(10,0,c)+0.39775062(12,0,c)+0.50000000(12,12,c)
12,2	0.30109690(1,1,c)-0.02382466(2,1,s)-0.02521365(3,1,c)+0.08056572(4,1,s)-0.28483698(5,1,c)+0.24590434(5,5,c)+0.20345976(6,1,s)+0.07687976(6,5,s)-0.22501531(7,1,c)+0.18465922(7,5,c)-0.25164810(7,7,c)+0.07194888(8,1,s)+0.11980846(8,5,s)+0.10125663(8,7,s)+0.11546539(9,1,c)+0.15877684(9,5,c)-0.17751790(9,7,c)-0.41858859(10,1,s)+0.17403079(10,5,s)+0.16044846(10,7,s)+0.11665626(11,1,c)+0.12878502(11,5,c)-0.13710212(11,7,c)+

	0.14543942(12,1,s)+0.29293746(12,5,s)+0.27863911(12,7,s)
12,3	0.56892559(2,0,c)-0.04065414(4,0,c)+0.36774696(6,0,c)+0.21390857(8,0,c)+ 0.29352011(10,0,c)+0.39689062(12,0,c)-0.50000000(12,12,c)
12,4	0.31318323(2,1,s)+0.10357562(3,1,c)+0.26231444(4,1,s)+0.09294310(5,1,c)+0.22447892(5,5,c)- 0.05183233(6,1,s)+0.07018130(6,5,s)-0.14085253(7,1,c)+0.16857003(7,5,c)+0.27566668(7,7,c)- 0.27654755(8,1,s)+0.10936966(8,5,s)-0.11092108(8,7,s)-0.33729599(9,1,c)+0.14494276(9,5,c)+ 0.19446112(9,7,c)-0.01930698(10,1,s)+0.15886764(10,5,s)-0.17576248(10,7,s)+ 0.31148941(11,1,c)+0.11756410(11,5,c)+0.15018785(11,7,c)+0.05974534(12,1,s)+ 0.26741409(12,5,s)-0.30523385(12,7,s)
12,5	0.38839304(2,2,c)-0.09146026(3,2,s)+0.17853236(4,2,c)-0.33755924(5,2,s)+0.26653969(6,2,c)- 0.24864709(7,2,s)+0.01282681(8,2,c)-0.39865719(9,2,s)-0.10299171(10,2,c)+ 0.09747754(10,10,c)-0.37245661(11,2,s)+0.13495155(11,10,s)-0.46610074(12,2,c)- 0.09332764(12,10,c)
12,6	0.25335246(3,2,s)-0.37544735(4,2,c)-0.27172884(5,2,s)+0.26715437(6,2,c)+0.33955076(7,2,s)- 0.18456544(8,2,c)+0.00948148(9,2,s)+0.07642462(10,2,c)+0.34775410(10,10,c)+ 0.12166870(11,2,s)+0.48144374(11,10,s)+0.12639077(12,2,c)-0.33294920(12,10,c)
12,7	0.39556103(3,3,c)+0.21706562(4,3,s)+0.07110372(5,3,c)+0.43882795(6,3,s)+0.02267913(7,3,c)+ 0.26210973(8,3,s)-0.32676784(9,3,c)-0.06625304(9,9,c)+0.16907972(10,3,s)+0.10965089(10,9,s)- 0.46456543(11,3,c)+0.10475525(11,9,c)-0.38426547(12,3,s)-0.05779109(12,9,s)
12,8	0.27648288(4,3,s)+0.34387124(5,3,c)-0.25992751(6,3,s)-0.34045481(7,3,c)+0.33385690(8,3,s)+ 0.08646488(9,3,c)+0.25891911(9,9,c)-0.04473958(10,3,s)-0.42851938(10,9,s)- 0.15404559(11,3,c)-0.40938706(11,9,c)-0.08885931(12,3,s)+0.22584954(12,9,s)
12,9	0.37384128(4,4,c)-0.32297388(5,4,s)-0.15346224(6,4,c)-0.40947817(7,4,s)-0.25380183(8,4,c)+ 0.05488623(8,8,c)+0.06546112(9,4,s)+0.10201378(9,8,s)-0.41763226(10,4,c)- 0.11620094(10,8,c)+0.45334140(11,4,s)-0.08834653(11,8,s)+0.28221985(12,4,c)+ 0.04119178(12,8,c)
12,10	0.32223077(5,4,s)-0.29885065(6,4,c)-0.27036871(7,4,s)+0.41767335(8,4,c)+0.19580829(8,8,c)+ 0.23353452(9,4,s)+0.36393726(9,8,s)-0.02902433(10,4,c)-0.41455040(10,8,c)- 0.19168109(11,4,s)-0.31517891(11,8,s)-0.06005640(12,4,c)+0.14695293(12,8,c)
12,11	0.26098171(6,6,c)-0.76088591(8,6,c)+0.58241841(10,6,c)-0.11717499(12,6,c)
12,12	0.55362582(7,6,s)-0.76696499(9,6,s)+0.32444284(11,6,s)
14,1	0.25819889(0,0,c)-0.26986873(2,0,c)-0.16870346(4,0,c)+0.43800373(6,0,c)-0.34515908(8,0,c)+ 0.14198182(10,0,c)-0.02995934(12,0,c)-0.49065338(12,12,c)+0.00221038(14,0,c)- 0.50917508(14,12,c)
14,2	0.28970428(1,1,c)-0.02688710(2,1,s)+0.04940193(3,1,c)+0.03193759(4,1,s)-0.19415133(5,1,c)- 0.22422740(5,5,c)+0.14260138(6,1,s)-0.05880706(6,5,s)-0.27991425(7,1,c)-0.17106223(7,5,c)+ 0.23311852(7,7,c)+0.17620802(8,1,s)-0.08962978(8,5,s)-0.07575099(8,7,s)-0.11753027(9,1,c)-

	0.15194692(9,5,c)+0.16988182(9,7,c)-0.02767341(10,1,s)-0.12373722(10,5,s)-0.11408008(10,7,s)+0.15566414(11,1,c)-0.13478318(11,5,c)+0.14348765(11,7,c)-0.41013017(12,1,s)-0.17032279(12,5,s)-0.16200928(12,7,s)+0.09767017(13,1,c)-0.11038178(13,5,c)+0.11501518(13,7,c)+0.16703318(14,1,s)-0.27778806(14,5,s)-0.26836876(14,7,s)
14,3	0.26092069(2,1,s)+0.07426782(3,1,c)+0.28726816(4,1,s)+0.10483136(5,1,c)-0.21034395(5,5,c)+0.10185681(6,1,s)-0.05516591(6,5,s)-0.16047060(7,5,c)-0.24850518(7,7,c)-0.15945123(8,1,s)-0.08408019(8,5,s)+0.08075083(8,7,s)-0.21359588(9,1,c)-0.14253884(9,5,c)-0.18109463(9,7,c)-0.24431158(10,1,s)-0.11607581(10,5,s)+0.12160978(10,7,s)-0.26788769(11,1,c)-0.12643783(11,5,c)-0.15295835(11,7,c)+0.01352166(12,1,s)-0.15977694(12,5,s)+0.17270248(12,7,s)+0.34074575(13,1,c)-0.10354729(13,5,c)-0.12260660(13,7,c)+0.06104845(14,1,s)-0.26058830(14,5,s)+0.28608206(14,7,s)
14,4	0.13750477(2,2,c)+0.24753689(3,2,s)-0.27126499(4,2,c)-0.17668546(5,2,s)-0.18029903(7,2,s)+0.29293746(8,2,c)+0.31057362(9,2,s)-0.25335280(10,2,c)-0.35262987(10,10,c)-0.16542735(11,2,s)-0.33166248(11,10,s)+0.08616254(12,2,c)-0.03475240(12,10,c)+0.03431933(13,2,s)-0.37416574(13,10,s)-0.00915182(14,2,c)+0.35276684(14,10,c)
14,5	0.13406661(3,3,c)-0.25038670(4,3,s)-0.28273019(5,3,c)+0.18766118(6,3,s)+0.19134595(8,3,s)+0.30395938(9,3,c)+0.29001678(9,9,c)-0.30931494(10,3,s)-0.35661452(10,9,s)-0.23639449(11,3,c)-0.12344268(11,9,c)+0.13955100(12,3,s)-0.22700174(12,9,s)+0.06177480(13,3,c)-0.38813937(13,9,c)-0.01806374(14,3,s)+0.26701366(14,9,s)
14,6	0.13910372(4,4,c)+0.26098171(5,4,s)-0.29072345(6,4,c)-0.18029903(7,4,s)-0.02620112(8,4,c)-0.23952388(8,8,c)-0.22332067(9,4,s)-0.34802013(9,8,s)+0.32077105(10,4,c)+0.21816795(10,8,c)+0.29875904(11,4,s)-0.08451543(11,8,s)-0.20367028(12,4,c)+0.32837934(12,8,c)-0.10125076(13,4,s)+0.34891135(13,8,s)+0.03267854(14,4,c)-0.19286801(14,8,c)

E.8. Cystallographic Point Group 422

n,λ	Coefficients of the Expansion of the Symmetrized Hyperspherical Harmonics
0,1	1.00000000(0,0,c)
4,1	0.44721360(0,0,c)+0.53452248(2,0,c)+0.71713717(4,0,c)
4,2	0.53452248(2,2,c)-0.70710678(3,2,s)-0.46291005(4,2,c)
8,1	0.47140452(0,0,c)-0.10744306(2,0,c)+0.50571163(4,0,c)+0.25425669(6,0,c)+0.44254158(8,0,c)+ 0.50000000(8,8,c)
8,2	0.64465837(2,0,c)+0.06321395(4,0,c)+0.38138504(6,0,c)+0.43007562(8,0,c)-0.50000000(8,8,c)
8,3	0.47445571(2,2,c)-0.13655775(3,2,s)+0.08316346(4,2,c)-0.52548465(5,2,s)+0.09032446(6,2,c)+ 0.13397283(6,6,c)-0.41420286(7,2,s)+0.18344985(7,6,s)-0.47556625(8,2,c)-0.12532010(8,6,c)
8,4	0.40394327(3,2,s)-0.45920154(4,2,c)-0.17764624(5,2,s)+0.22901431(6,2,c)+0.33968311(6,6,c)+ 0.29820379(7,2,s)+0.46513025(7,6,s)+0.14261920(8,2,c)-0.31774445(8,6,c)
8,5	0.44249768(4,4,c)-0.85280287(6,4,c)+0.27735010(8,4,c)
8,6	0.78446454(5,4,s)-0.62017367(7,4,s)
10,1	0.30151134(0,0,c)-0.20483662(2,0,c)-0.35478744(4,0,c)+0.45315295(6,0,c)-0.18806885(8,0,c)- 0.48666426(8,8,c)+0.02326488(10,0,c)-0.51298918(10,8,c)
10,2	0.20483662(2,2,c)+0.30725493(3,2,s)-0.22901431(4,2,c)-0.23695935(6,2,c)-0.35146751(6,6,c)- 0.34879472(7,2,s)-0.32084447(7,6,s)+0.30770381(8,2,c)-0.05129892(8,6,c)+0.18421903(9,2,s)- 0.38348249(9,6,s)-0.06901477(10,2,c)+0.35190767(10,6,c)
12,1	0.39223227(0,0,c)+0.18964186(2,0,c)-0.03252331(4,0,c)+0.18980488(6,0,c)+0.57646546(8,0,c)+ 0.29083753(8,8,c)+0.09784004(10,0,c)+0.25085666(10,8,c)+0.42570066(12,0,c)+ 0.32013196(12,8,c)
12,2	0.25285582(2,0,c)+0.48784967(4,0,c)+0.28470732(6,0,c)-0.06888581(8,0,c)-0.29083753(8,8,c)+ 0.47554808(10,0,c)-0.25085666(10,8,c)+0.36894057(12,0,c)-0.32013196(12,8,c)
12,3	0.44249768(2,2,c)-0.05666634(3,2,s)+0.10496854(4,2,c)-0.06077652(5,2,s)+0.10634073(6,2,c)+ 0.15772879(6,6,c)-0.41597078(7,2,s)+0.11153110(7,6,s)-0.03377538(8,2,c)+0.06569350(8,6,c)- 0.44322309(9,2,s)+0.14568039(9,6,s)+0.06508714(10,2,c)-0.01843781(10,6,c)+ 0.08555887(10,10,c)-0.22844730(11,2,s)+0.15406492(11,6,s)-0.11845089(11,10,s)- 0.45283924(12,2,c)-0.16692513(12,6,c)-0.08191638(12,10,c)
12,4	0.37436021(3,2,s)+0.00847410(4,2,c)-0.00919965(5,2,s)-0.44312254(6,2,c)+0.25785185(6,6,c)+ 0.11689443(7,2,s)+0.18232879(7,6,s)+0.00416576(8,2,c)+0.10739441(8,6,c)-0.17090299(9,2,s)+ 0.23815536(9,6,s)+0.26374553(10,2,c)-0.03014176(10,6,c)-0.19858073(10,10,c)+ 0.29651121(11,2,s)+0.25186222(11,6,s)+0.27492258(11,10,s)+0.07080103(12,2,c)- 0.27288583(12,6,c)+0.19012658(12,10,c)
12,5	0.41641539(4,2,c)-0.45206900(5,2,s)-0.07533196(6,2,c)-0.13035791(6,6,c)+0.12112924(7,2,s)-

	0.09217696(7,6,s)+0.20470484(8,2,c)-0.05429362(8,6,c)-0.13670900(9,2,s)-0.12040027(9,6,s)-0.21897345(10,2,c)+0.01523827(10,6,c)-0.28927523(10,10,c)-0.25035837(11,2,s)-0.12732983(11,6,s)+0.40048341(11,10,s)-0.17741818(12,2,c)+0.13795839(12,6,c)+0.27695994(12,10,c)
12,6	0.50907034(4,4,c)-0.09490244(6,4,c)-0.50503537(8,4,c)-0.55762317(10,4,c)+0.40723038(12,4,c)
12,7	0.56279844(5,4,s)+0.45439821(7,4,s)-0.69049271(11,4,s)
12,8	0.18454194(6,6,c)-0.39147257(7,6,s)-0.53802759(8,6,c)+0.54232614(9,6,s)+0.41183200(10,6,c)-0.22941573(11,6,s)-0.08285523(12,6,c)
14.1	0.25819889(0,0,c)+0.04151827(2,0,c)-0.27684671(4,0,c)-0.26954076(6,0,c)+0.14373999(8,0,c)-0.36721654(8,8,c)+0.39227028(10,0,c)-0.30102799(10,8,c)-0.32322332(12,0,c)-0.31414766(12,8,c)+0.05746975(14,0,c)-0.41933925(14,8,c)
14,2	0.25169111(2,2,c)+0.05548112(3,2,s)-0.17410727(4,2,c)+0.25740645(5,2,s)-0.17437574(6,2,c)-0.25864102(6,6,c)+0.09850160(7,2,s)-0.15101382(7,6,s)-0.02051777(8,2,c)-0.13887740(8,6,c)-0.35457447(9,2,s)-0.20377149(9,6,s)-0.12901808(10,2,c)-0.04790284(10,6,c)-0.19264999(10,10,c)-0.10041873(11,2,s)-0.23567400(11,6,s)+0.18119501(11,10,s)+0.31546917(12,2,c)+0.06830252(12,6,c)-0.01898605(12,10,c)+0.18749459(13,2,s)-0.23561074(13,6,s)+0.20441554(13,10,s)-0.09666388(14,2,c)+0.28677626(14,6,c)+0.19272482(14,10,c)
14,3	0.33172883(3,2,s)+0.21030506(4,2,c)-0.04305082(5,2,s)-0.11373985(6,2,c)-0.16870346(6,6,c)-0.15101382(7,2,s)-0.09850160(7,6,s)-0.36312817(8,2,c)-0.09058539(8,6,c)+0.13952345(9,2,s)-0.13291378(9,6,s)+0.21832953(10,2,c)-0.03124553(10,6,c)+0.29535370(10,10,c)-0.26300769(11,2,s)-0.15372279(11,6,s)-0.27779195(11,10,s)+0.10289915(12,2,c)+0.04455160(12,6,c)+0.02910772(12,10,c)+0.16327154(13,2,s)-0.15368153(13,6,s)-0.31339159(13,10,s)-0.05212425(14,2,c)+0.18705520(14,6,c)-0.29546842(14,10,c)
16,1	0.42008403(0,0,c)-0.05245930(2,0,c)+0.28511260(4,0,c)-0.15313928(6,0,c)+0.17198292(8,0,c)+0.19431273(8,8,c)+0.30926235(10,0,c)+0.15568989(10,8,c)+0.37108806(12,0,c)+0.15434190(12,8,c)+0.00938434(14,0,c)+0.16841070(14,8,c)+0.34595886(16,0,c)+0.22909889(16,8,c)+0.40824829(16,16,c)
16,2	0.53498197(2,0,c)-0.20269253(4,0,c)+0.28745951(6,0,c)+0.05605603(8,0,c)+0.07621572(8,8,c)+0.26088383(10,0,c)+0.06106660(10,8,c)+0.25093613(12,0,c)+0.06053787(12,8,c)+0.13260978(14,0,c)+0.06605611(14,8,c)+0.31396898(16,0,c)+0.08985998(16,8,c)-0.56044854(16,16,c)
16,3	0.42375295(2,2,c)-0.04620774(3,2,s)+0.09611791(4,2,c)-0.07192806(5,2,s)+0.09559410(6,2,c)+0.14178897(6,6,c)+0.00434756(7,2,s)+0.07089449(7,6,s)+0.03422133(8,2,c)+0.08557827(8,6,c)-0.29589156(9,2,s)+0.09725485(9,6,s)+0.07730408(10,2,c)+0.04834222(10,6,c)+0.12079164(10,10,c)-0.45773762(11,2,s)+0.11626302(11,6,s)-0.08938737(11,10,s)-0.08708594(12,2,c)+0.00581170(12,6,c)+0.04433590(12,10,c)-0.27391043(13,2,s)+

	0.12716867(13,6,s)-0.11033136(13,10,s)+0.06228744(14,2,c)-0.05186054(14,6,c)-0.01936239(14,10,c)+0.06089190(14,14,c)-0.14639638(15,2,s)+0.12285661(15,6,s)-0.11190921(15,10,s)+0.08475794(15,14,s)-0.42931098(16,2,c)-0.16364360(16,6,c)-0.12552126(16,10,c)-0.05895833(16,14,c)
16,4	0.36192787(3,2,s)-0.02568830(4,2,c)-0.00918314(5,2,s)+0.11838469(6,2,c)+0.17559288(6,6,c)+0.08616018(7,2,s)+0.08779644(7,6,s)-0.38720420(8,2,c)+0.10598099(8,6,c)-0.08967022(9,2,s)+0.12044138(9,6,s)-0.16131976(10,2,c)+0.05986749(10,6,c)-0.20819168(10,10,c)+0.12864364(11,2,s)+0.14398129(11,6,s)+0.15406453(11,10,s)+0.21774103(12,2,c)+0.00719727(12,6,c)-0.07641559(12,10,c)-0.17735016(13,2,s)+0.15748695(13,6,s)+0.19016275(13,10,s)+0.14260284(14,2,c)-0.06422461(14,6,c)+0.03337225(14,10,c)+0.16558914(14,14,c)+0.25364233(15,2,s)+0.15214685(15,6,s)+0.19288227(15,10,s)+0.23049033(15,14,s)+0.02245931(16,2,c)-0.20265787(16,6,c)+0.21634346(16,10,c)-0.16033099(16,14,c)
16,5	0.38739174(4,0,c)+0.35670052(6,0,c)+0.27646503(8,0,c)-0.26401901(8,8,c)-0.03069989(10,0,c)-0.21154091(10,8,c)-0.04168882(12,0,c)-0.20970935(12,8,c)+0.50382928(14,0,c)-0.22882508(14,8,c)+0.25062322(16,0,c)-0.31128409(16,8,c)+0.13867505(16,16,c)
16,6	0.39868682(4,2,c)+0.08603557(5,2,s)-0.00650734(6,2,c)-0.00965195(6,6,c)-0.44959431(7,2,s)-0.00482598(7,6,s)+0.12311681(8,2,c)-0.00582554(8,6,c)-0.00848089(9,2,s)-0.00662039(9,6,s)-0.15126611(10,2,c)-0.00329078(10,6,c)-0.21143846(10,10,c)+0.00060700(11,2,s)-0.00791433(11,6,s)+0.15646718(11,10,s)+0.19085924(12,2,c)-0.00039562(12,6,c)-0.07760730(12,10,c)-0.27582279(13,2,s)-0.00865671(13,6,s)+0.19312836(13,10,s)-0.16934515(14,2,c)+0.00353028(14,6,c)+0.03389269(14,10,c)-0.22538833(14,14,c)-0.12433559(15,2,s)-0.00836317(15,6,s)+0.19589029(15,10,s)-0.31372727(15,14,s)-0.19750765(16,2,c)+0.01113965(16,6,c)+0.21971736(16,10,c)+0.21823131(16,14,c)
16,7	0.49189671(4,4,c)+0.07974594(6,4,c)-0.07028370(8,4,c)-0.43732843(10,4,c)-0.46518786(12,4,c)+0.04428275(12,12,c)-0.35172596(14,4,c)-0.09766847(14,12,c)+0.45008453(16,4,c)+0.03598866(16,12,c)
16,8	0.39066271(5,2,s)-0.41536004(6,2,c)+0.18377342(6,6,c)+0.03219942(7,2,s)+0.09188671(7,6,s)+0.11091844(8,6,c)+0.16147645(9,2,s)+0.12605251(9,6,s)-0.14367473(10,2,c)+0.06265660(10,6,c)+0.09462337(10,10,c)-0.14698549(11,2,s)+0.15068910(11,6,s)-0.07002251(11,10,s)+0.00294910(12,2,c)+0.00753257(12,6,c)+0.03473098(12,10,c)+0.10062619(13,2,s)+0.16482397(13,6,s)-0.08642920(13,10,s)+0.29232818(14,2,c)-0.06721671(14,6,c)-0.01516773(14,10,c)-0.21703634(14,14,c)+0.27866579(15,2,s)+0.15923508(15,6,s)-0.08766523(15,10,s)-0.30210180(15,14,s)+0.10238618(16,2,c)-0.21209931(16,6,c)-0.09832837(16,10,c)+0.21014454(16,14,c)
16,9	0.44083102(5,4,s)+0.21993970(7,4,s)+0.52475932(9,4,s)-0.18217503(13,4,s)+0.22964829(13,12,s)-0.59426107(15,4,s)-0.20700217(15,12,s)

16,10	0.34117845(6,4,c)-0.49356660(8,4,c)+0.30194134(10,4,c)-0.23724974(12,4,c)-0.27325335(12,12,c)-0.02048543(14,4,c)+0.60267796(14,12,c)+0.07006342(16,4,c)-0.22207343(16,12,c)
16,11	0.27748073(6,6,c)-0.36577006(7,6,s)-0.31972789(8,6,c)-0.13975100(9,6,s)-0.26183214(10,6,c)+0.02479605(10,10,c)+0.36754281(11,6,s)+0.05504819(11,10,s)-0.05511764(12,6,c)-0.07903718(12,10,c)+0.29759840(13,6,s)-0.08304548(13,10,s)+0.46309692(14,6,c)+0.06558258(14,10,c)-0.33416427(15,6,s)+0.03790490(15,10,s)-0.15284669(16,6,c)-0.01417182(16,10,c)
16,12	0.58529349(7,4,s)-0.24531108(9,4,s)+0.29019050(11,4,s)-0.18122473(13,4,s)-0.47235975(13,12,s)-0.27529859(15,4,s)+0.42577932(15,12,s)
16,13	0.23119572(7,6,s)-0.18605425(8,6,c)-0.30496168(9,6,s)+0.41627990(10,6,c)+0.11362978(10,10,c)+0.24061325(11,6,s)+0.25226249(11,10,s)-0.22852546(12,6,c)-0.36219388(12,10,c)-0.21533166(13,6,s)-0.38056220(13,10,s)-0.02439284(14,6,c)+0.30053715(14,10,c)+0.10318956(15,6,s)+0.17370208(15,10,s)+0.02529031(16,6,c)-0.06494343(16,10,c)
16,14	0.15426804(8,8,c)-0.59900757(10,8,c)+0.70693007(12,8,c)-0.33940244(14,8,c)+0.04946881(16,8,c)
16,15	0.37300192(9,8,s)-0.73029674(11,8,s)+0.54977166(13,8,s)-0.15901999(15,8,s)

E.9. Cystallographic Point Group 622

n,λ	Coefficients of the Expansion of the Symmetrized Hyperspherical Harmonics
0,1	1.00000000(0,0,c)
4,1	0.44721360(0,0,c)+0.53452248(2,0,c)+0.71713717(4,0,c)
4,2	0.53452248(2,2,c)-0.70710678(3,2,s)-0.46291005(4,2,c)
8,1	0.33333333(0,0,c)+0.37986859(2,0,c)+0.40229114(4,0,c)+0.44946657(6,0,c)+0.61703353(8,0,c)
8,2	0.44136741(2,2,c)-0.27524094(3,2,s)+0.24584459(4,2,c)-0.42365927(5,2,s)-0.49472744(7,2,s)-0.49472744(8,2,c)
8,3	0.31289311(4,4,c)-0.55470020(5,4,s)-0.60302269(6,4,c)+0.43852901(7,4,s)+0.19611614(8,4,c)
12,1	0.39223227(0,0,c)-0.12642791(2,0,c)+0.49598049(4,0,c)+0.10676525(6,0,c)+0.29367108(8,0,c)+0.27986801(10,0,c)+0.39775062(12,0,c)+0.50000000(12,12,c)
12,2	0.56892559(2,0,c)-0.04065414(4,0,c)+0.36774696(6,0,c)+0.21390857(8,0,c)+0.29352011(10,0,c)+0.39689062(12,0,c)-0.50000000(12,12,c)
12,3	0.38839304(2,2,c)-0.09146026(3,2,s)+0.17853236(4,2,c)-0.33755924(5,2,s)+0.26653969(6,2,c)-0.24864709(7,2,s)+0.01282681(8,2,c)-0.39865719(9,2,s)-0.10299171(10,2,c)+0.09747754(10,10,c)-0.37245661(11,2,s)+0.13495155(11,10,s)-0.46610074(12,2,c)-0.09332764(12,10,c)
12,4	0.25335246(3,2,s)-0.37544735(4,2,c)-0.27172884(5,2,s)+0.26715437(6,2,c)+0.33955076(7,2,s)-0.18456544(8,2,c)+0.00948148(9,2,s)+0.07642462(10,2,c)+0.34775410(10,10,c)+0.12166870(11,2,s)+0.48144374(11,10,s)+0.12639077(12,2,c)-0.33294920(12,10,c)
12,5	0.37384128(4,4,c)-0.32297388(5,4,s)-0.15346224(6,4,c)-0.40947817(7,4,s)-0.25380183(8,4,c)+0.05488623(8,8,c)+0.06546112(9,4,s)+0.10201378(9,8,s)-0.41763226(10,4,c)-0.11620094(10,8,c)+0.45334140(11,4,s)-0.08834653(11,8,s)+0.28221985(12,4,c)+0.04119178(12,8,c)
12,6	0.32223077(5,4,s)-0.29885065(6,4,c)-0.27036871(7,4,s)+0.41767335(8,4,c)+0.19580829(8,8,c)+0.23353452(9,4,s)+0.36393726(9,8,s)-0.02902433(10,4,c)-0.41455040(10,8,c)-0.19168109(11,4,s)-0.31517891(11,8,s)-0.06005640(12,4,c)+0.14695293(12,8,c)
12,7	0.26098171(6,6,c)-0.76088591(8,6,c)+0.58241841(10,6,c)-0.11717499(12,6,c)
12,8	0.55362582(7,6,s)-0.76696499(9,6,s)+0.32444284(11,6,s)
14,1	0.25819889(0,0,c)-0.26986873(2,0,c)-0.16870346(4,0,c)+0.43800373(6,0,c)-0.34515908(8,0,c)+0.14198182(10,0,c)-0.02995934(12,0,c)-0.49065338(12,12,c)+0.00221038(14,0,c)-0.50917508(14,12,c)
14,2	0.13750477(2,2,c)+0.24753689(3,2,s)-0.27126499(4,2,c)-0.17668546(5,2,s)-0.18029903(7,2,s)+0.29293746(8,2,c)+0.31057362(9,2,s)-0.25335280(10,2,c)-0.35262987(10,10,c)-0.16542735(11,2,s)-0.33166248(11,10,s)+0.08616254(12,2,c)-0.03475240(12,10,c)+

	0.03431933(13,2,s)-0.37416574(13,10,s)-0.00915182(14,2,c)+0.35276684(14,10,c)
14,3	0.13910372(4,4,c)+0.26098171(5,4,s)-0.29072345(6,4,c)-0.18029903(7,4,s)-0.02620112(8,4,c)-0.23952388(8,8,c)-0.22332067(9,4,s)-0.34802013(9,8,s)+0.32077105(10,4,c)+0.21816795(10,8,c)+0.29875904(11,4,s)-0.08451543(11,8,s)-0.20367028(12,4,c)+0.32837934(12,8,c)-0.10125076(13,4,s)+0.34891135(13,8,s)+0.03267854(14,4,c)-0.19286801(14,8,c)
16,1	0.34299717(0,0,c)+0.09637388(2,0,c)-0.01636829(4,0,c)+0.33157318(6,0,c)+0.40050356(8,0,c)-0.07264034(10,0,c)+0.39482075(12,0,c)+0.29523677(12,12,c)+0.22567494(14,0,c)+0.25044763(14,12,c)+0.37465184(16,0,c)+0.31640359(16,12,c)
16,2	0.28912165(2,0,c)+0.40920726(4,0,c)+0.07033370(6,0,c)+0.01483347(8,0,c)+0.50848236(10,0,c)+0.07439388(12,0,c)-0.29523677(12,12,c)+0.30737144(14,0,c)-0.25044763(14,12,c)+0.36772987(16,0,c)-0.31640359(16,12,c)
16,3	0.37013093(2,2,c)-0.02314463(3,2,s)+0.09995556(4,2,c)-0.10636681(5,2,s)+0.18970141(6,2,c)-0.36244578(7,2,s)+0.16231335(8,2,c)-0.21395260(9,2,s)+0.16949229(10,2,c)+0.13829111(10,10,c)-0.18035539(11,2,s)+0.10233720(11,10,s)-0.14676464(12,2,c)+0.05075898(12,10,c)-0.39160466(13,2,s)+0.12631540(13,10,s)-0.09949065(14,2,c)-0.02216748(14,10,c)+0.06971350(14,14,c)-0.26993630(15,2,s)+0.12812185(15,10,s)-0.09703708(15,14,s)-0.42220133(16,2,c)-0.14370591(16,10,c)-0.06749981(16,14,c)
16,4	0.30704815(3,2,s)-0.11236674(4,2,c)-0.13750541(5,2,s)-0.34726827(6,2,c)+0.01666412(7,2,s)+0.22772453(8,2,c)-0.01612728(9,2,s)+0.06847412(10,2,c)+0.27400450(10,10,c)+0.35869748(11,2,s)+0.20276686(11,10,s)-0.21106038(12,2,c)+0.10057182(12,10,c)-0.09046626(13,2,s)+0.25027632(13,10,s)+0.14486022(14,2,c)-0.04392176(14,10,c)-0.18076694(14,14,c)+0.13387134(15,2,s)+0.25385553(15,10,s)+0.25161692(15,14,s)+0.11486507(16,2,c)-0.28473319(16,10,c)+0.17502683(16,14,c)
16,5	0.38197496(4,2,c)-0.30626131(5,2,s)-0.13567619(6,2,c)+0.26645221(7,2,s)+0.19813538(8,2,c)-0.25786850(9,2,s)-0.14490959(10,2,c)-0.13187609(10,10,c)-0.17263812(11,2,s)-0.09759001(11,10,s)+0.13496999(12,2,c)-0.04840438(12,10,c)-0.05509514(13,2,s)-0.12045592(13,10,s)-0.11653783(14,2,c)+0.02113918(14,10,c)-0.30248240(14,14,c)-0.14013532(15,2,s)-0.12217856(15,10,s)+0.42103768(15,14,s)-0.16552630(16,2,c)+0.13703972(16,10,c)+0.29287732(16,14,c)
16,6	0.37871758(4,4,c)-0.14402102(5,4,s)-0.00712098(6,4,c)-0.30426666(7,4,s)-0.16926291(8,4,c)+0.10547532(8,8,c)-0.33898501(9,4,s)+0.12751344(9,8,s)-0.18843081(10,4,c)-0.03900479(10,8,c)-0.11523046(11,4,s)+0.08321910(11,8,s)-0.20997905(12,4,c)-0.11277897(12,8,c)+0.28568263(13,4,s)-0.01789938(13,8,s)-0.32671455(14,4,c)-0.10497700(14,8,c)+0.36380728(15,4,s)-0.14496573(15,8,s)+0.31146755(16,4,c)+0.09019348(16,8,c)
16,7	0.35490779(5,4,s)-0.23865376(6,4,c)+0.10658139(7,4,s)-0.11508301(8,4,c)+0.22659734(8,8,c)-0.11719072(9,4,s)+0.27394282(9,8,s)+0.23760841(10,4,c)-0.08379572(10,8,c)-

	0.03494890(11,4,s)+0.17878331(11,8,s)+0.38192568(12,4,c)-0.24228810(12,8,c)+ 0.20644141(13,4,s)-0.03845403(13,8,s)-0.11463622(14,4,c)-0.22552678(14,8,c)- 0.31563946(15,4,s)-0.31143635(15,8,s)-0.09409776(16,4,c)+0.19376667(16,8,c)
16,8	0.38339473(6,6,c)-0.38567009(8,6,c)-0.48728620(10,6,c)-0.00725295(12,6,c)+ 0.64721506(14,6,c)-0.21881336(16,6,c)
16,9	0.57509210(7,6,s)+0.10114435(9,6,s)-0.43528575(11,6,s)-0.47611622(13,6,s)+0.49282711(15,6,s)
16,10	0.10908397(8,8,c)-0.26375219(9,8,s)-0.42356231(10,8,c)+0.51639778(11,8,s)+ 0.49987505(12,8,c)-0.38874727(13,8,s)-0.23999377(14,8,c)+0.11244411(15,8,s)+ 0.03497973(16,8,c)
18,1	0.22941573(0,0,c)-0.05151401(2,0,c)-0.29947299(4,0,c)-0.04726000(6,0,c)+0.31637246(8,0,c)+ 0.05684638(10,0,c)-0.39346377(12,0,c)-0.37495107(12,12,c)+0.29427784(14,0,c)- 0.30205120(14,12,c)-0.08937307(16,0,c)-0.31185079(16,12,c)+0.00856571(18,0,c)- 0.41343179(18,12,c)
18,2	0.18927455(2,2,c)+0.08765295(3,2,s)-0.25214292(4,2,c)+0.16717565(5,2,s)-0.10163710(6,2,c)- 0.14341137(7,2,s)+0.10013128(8,2,c)-0.28061113(9,2,s)+0.03857101(10,2,c)- 0.26842588(10,10,c)+0.24457709(11,2,s)-0.16619298(11,10,s)+0.16484150(12,2,c)- 0.13121826(12,10,c)+0.12528823(13,2,s)-0.21210436(13,10,s)-0.28564403(14,2,c)- 0.03493165(14,10,c)-0.18675343(14,14,c)-0.18992696(15,2,s)-0.23544823(15,10,s)+ 0.17832408(15,14,s)+0.14009035(16,2,c)+0.07971938(16,10,c)-0.01390808(16,14,c)+ 0.05892784(17,2,s)-0.22802833(17,10,s)+0.19534424(17,14,s)-0.01909082(18,2,c)+ 0.28843556(18,10,c)+0.18678482(18,14,c)
18,3	0.28757317(3,2,s)+0.14189871(4,2,c)-0.16808028(5,2,s)-0.21429232(6,2,c)-0.11402575(7,2,s)- 0.13203666(8,2,c)+0.13309157(9,2,s)+0.36772305(10,2,c)-0.16732461(10,10,c)- 0.15846219(11,2,s)-0.10359722(11,10,s)-0.13558321(12,2,c)-0.08179556(12,10,c)+ 0.23526731(13,2,s)-0.13221631(13,10,s)-0.08883110(14,2,c)-0.02177482(14,10,c)+ 0.29959404(14,14,c)-0.16153463(15,2,s)-0.14676783(15,10,s)-0.28607147(15,14,s)+ 0.07000689(16,2,c)+0.04969347(16,10,c)+0.02231165(16,14,c)+0.04220239(17,2,s)- 0.14214259(17,10,s)-0.31337560(17,14,s)-0.01071907(18,2,c)+0.17979774(18,10,c)- 0.29964438(18,14,c)
18,4	0.17097154(4,4,c)+0.24748023(5,4,s)-0.15350305(6,4,c)+0.06062003(7,4,s)-0.21403821(8,4,c)- 0.25085666(8,8,c)-0.16772893(9,4,s)-0.26138665(9,8,s)-0.03572746(10,4,c)+0.01700967(10,8,c)- 0.21169921(11,4,s)-0.22555654(11,8,s)+0.20654324(12,4,c)+0.18067547(12,8,c)+ 0.02743408(13,4,s)-0.09453818(13,8,s)+0.18560165(14,4,c)+0.25891667(14,8,c)+ 0.29411257(15,4,s)+0.10882354(15,8,s)-0.26379619(16,4,c)+0.18978635(16,8,c)- 0.15771609(17,4,s)+0.33169449(17,8,s)+0.05848269(18,4,c)-0.22601170(18,8,c)

E.10. Cystallographic Point Group 23

n,λ	Coefficients of the Expansion of the Symmetrized Hyperspherical Harmonics
0,1	1.00000000(0,0,c)
6,1	0.37796447(0,0,c)-0.56407607(4,0,c)-0.47673129(4,4,c)+0.19738551(6,0,c)-0.52223297(6,4,c)
8,1	0.33333333(0,0,c)+0.36504196(4,0,c)+0.30851677(4,4,c)+0.22473329(6,0,c)-0.59458839(6,4,c)+ 0.36360905(8,0,c)+0.19337312(8,4,c)+0.29462783(8,8,c)
8,2	0.44946657(2,0,c)+0.04407382(4,0,c)-0.05214885(4,4,c)+0.55470020(5,4,s)+0.26590801(6,0,c)+ 0.10050378(6,4,c)-0.43852901(7,4,s)+0.29985590(8,0,c)-0.03268602(8,4,c)-0.34860834(8,8,c)
8,3	0.44946657(2,2,c)-0.06827887(4,2,c)-0.55470020(5,2,s)+0.15891043(6,2,c)+0.23570226(6,6,c)- 0.29688554(7,2,s)+0.32274861(7,6,s)-0.40484392(8,2,c)-0.22047928(8,6,c)
12,1	0.39223227(0,0,c)-0.09485966(4,0,c)-0.08017104(4,4,c)-0.14235366(6,0,c)+0.37663239(6,4,c)+ 0.14955472(8,0,c)+0.07953560(8,4,c)+0.12118230(8,8,c)-0.29579546(10,0,c)+ 0.42152349(10,4,c)+0.50171331(10,8,c)+0.22096659(12,0,c)+0.05170704(12,4,c)+ 0.18007423(12,8,c)+0.15625000(12,12,c)
12,2	0.35196040(2,0,c)-0.07058309(4,0,c)+0.08351504(4,4,c)-0.34384723(5,4,s)+0.04474308(6,0,c)+ 0.01691129(6,4,c)+0.24132897(7,4,s)-0.19437466(8,0,c)+0.32569833(8,4,c)+0.02611798(8,8,c)- 0.22843416(9,4,s)-0.35598892(9,8,s)-0.06855353(10,0,c)+0.17980615(10,4,c)- 0.19148454(10,8,c)+0.22265007(11,4,s)+0.30829545(11,8,s)+0.18912760(12,0,c)+ 0.11209021(12,4,c)+0.00359359(12,8,c)-0.30869661(12,12,c)
12,3	0.35196040(2,2,c)+0.10934685(4,2,c)+0.34384723(5,2,s)+0.02673910(6,2,c)+0.03966050(6,6,c)+ 0.16338049(7,2,s)-0.17761331(7,6,s)-0.01415456(8,2,c)+0.37992461(8,6,c)+0.38126709(9,2,s)+ 0.18315479(9,6,s)+0.07046470(10,2,c)-0.26078289(10,6,c)+0.02689195(10,10,c)+ 0.28226048(11,2,s)-0.12267422(11,6,s)-0.22338127(11,10,s)-0.36224302(12,2,c)- 0.10842997(12,6,c)-0.02574708(12,10,c)
12,4	0.51887452(3,2,s)+0.15860264(7,2,s)+0.14589321(7,6,s)-0.23302069(9,2,s)+0.48507125(9,6,s)+ 0.41803503(11,2,s)+0.28855641(11,6,s)+0.36975499(11,10,s)
12,5	0.40455600(4,0,c)-0.01668811(4,4,c)-0.19822379(5,4,s)-0.00610151(6,0,c)+0.26683570(6,4,c)- 0.28243066(7,4,s)-0.33586232(8,0,c)-0.07979529(8,4,c)-0.39259862(8,8,c)+0.05387300(9,4,s)+ 0.08395500(9,8,s)+0.14453240(10,0,c)+0.20469066(10,4,c)+0.00986666(10,8,c)+ 0.29018077(11,4,s)-0.07270716(11,8,s)+0.13051130(12,0,c)+0.06288932(12,4,c)- 0.39118051(12,8,c)+0.19004099(12,12,c)
12,6	0.41431120(4,2,c)-0.29985643(5,2,s)-0.07495130(6,2,c)-0.11117074(6,6,c)+0.28924120(7,2,s)- 0.31443834(7,6,s)+0.20367045(8,2,c)-0.10803854(8,6,c)+0.13601819(9,2,s)+0.06534103(9,6,s)- 0.21786696(10,2,c)+0.05651020(10,6,c)-0.28781349(10,10,c)-0.09098088(11,2,s)- 0.29368215(11,6,s)+0.33204978(11,10,s)-0.17652167(12,2,c)+0.12894241(12,6,c)+

	0.27556044(12,10,c)
12,7	0.40702507(4,4,c)+0.22499158(5,4,s)-0.17252518(6,0,c)+0.17191303(6,4,c)+0.32056959(7,4,s)-0.34273197(8,0,c)-0.29443672(8,4,c)-0.14099194(8,8,c)-0.06114791(9,4,s)-0.09529213(9,8,s)-0.21998164(10,0,c)-0.15262601(10,4,c)+0.08366972(10,8,c)-0.32936625(11,4,s)+0.08252541(11,8,s)-0.03926303(12,0,c)+0.41429801(12,4,c)-0.13106456(12,8,c)+0.02065820(12,12,c)
12,8	0.61205637(6,2,c)-0.41264832(6,6,c)-0.37173558(10,2,c)-0.07290334(10,6,c)+0.26707962(10,10,c)-0.10313659(12,2,c)+0.40527795(12,6,c)-0.25570927(12,10,c)
14,1	0.25819889(0,0,c)-0.02385706(4,0,c)-0.02016289(4,4,c)+0.15927408(6,0,c)-0.42139961(6,4,c)-0.29457543(8,0,c)-0.15665993(8,4,c)-0.23869075(8,8,c)-0.12817803(10,0,c)+0.18266018(10,4,c)+0.21740910(10,8,c)-0.16206879(12,0,c)-0.35636326(12,4,c)+0.32723714(12,8,c)-0.22488280(12,12,c)+0.17222506(14,0,c)-0.17910682(14,4,c)-0.19219716(14,8,c)-0.23337191(14,12,c)
14,2	0.24824313(2,0,c)+0.13323932(4,0,c)-0.15765088(4,4,c)+0.26098171(5,4,s)-0.25639398(6,0,c)-0.09690782(6,4,c)-0.18029903(7,4,s)+0.04653020(8,0,c)-0.11790505(8,4,c)+0.01996032(8,8,c)-0.22332067(9,4,s)-0.34802013(9,8,s)-0.24851092(10,0,c)-0.15274812(10,4,c)-0.01818066(10,8,c)+0.29875904(11,4,s)-0.08451543(11,8,s)-0.12152302(12,0,c)-0.12413624(12,4,c)-0.02736494(12,8,c)+0.24447338(12,12,c)-0.10125076(13,4,s)+0.34891135(13,8,s)+0.15639076(14,0,c)-0.19743286(14,4,c)+0.01607233(14,8,c)+0.25370201(14,12,c)
14,3	0.24824313(2,2,c)-0.20641346(4,2,c)-0.26098171(5,2,s)-0.15322471(6,2,c)-0.22726897(6,6,c)-0.12206302(7,2,s)+0.13269649(7,6,s)+0.03966392(8,2,c)-0.12203216(8,6,c)+0.37273246(9,2,s)+0.17905488(9,6,s)-0.16326565(10,2,c)-0.04209243(10,6,c)-0.23873155(10,10,c)+0.05565805(11,2,s)+0.20708776(11,6,s)-0.22453656(11,10,s)+0.29417351(12,2,c)+0.06001772(12,6,c)-0.02352749(12,10,c)-0.15799323(13,2,s)+0.20703217(13,6,s)-0.25331140(13,10,s)-0.08674138(14,2,c)+0.25199153(14,6,c)+0.23882428(14,10,c)
16,1	0.24253563(0,0,c)+0.25205881(4,0,c)+0.21302858(4,4,c)+0.01894607(6,0,c)-0.05012660(6,4,c)+0.17306592(8,0,c)+0.09203923(8,4,c)+0.14023313(8,8,c)+0.18548283(10,0,c)-0.26432242(10,4,c)-0.31460660(10,8,c)+0.21780861(12,0,c)-0.14258865(12,4,c)+0.45668536(12,8,c)+0.08698497(12,12,c)+0.14158322(14,0,c)-0.14724060(14,4,c)-0.15800194(14,8,c)-0.19185098(14,12,c)+0.28151346(16,0,c)+0.17753466(16,4,c)+0.08709763(16,8,c)+0.07069282(16,12,c)+0.23938511(16,16,c)
16,2	0.33074329(2,0,c)-0.07595849(4,0,c)+0.08987530(4,4,c)+0.09215524(5,4,s)+0.22315950(6,0,c)+0.08434636(6,4,c)-0.06307880(7,4,s)+0.06987654(8,0,c)-0.11378304(8,4,c)-0.01155750(8,8,c)+0.15540884(9,4,s)+0.24218719(9,8,s)+0.15737581(10,0,c)-0.01815374(10,4,c)+0.10803635(10,8,c)-0.05407081(11,4,s)-0.47417588(11,8,s)+0.14982585(12,0,c)-

	0.13351623(12,4,c)-0.10404093(12,8,c)-0.04779322(12,12,c)-0.00431613(13,4,s)+ 0.35696238(13,8,s)+0.13602188(13,12,s)+0.14617015(14,0,c)-0.06845402(14,4,c)+ 0.06677919(14,8,c)+0.10541104(14,12,c)-0.07293361(15,4,s)-0.10325042(15,8,s)- 0.12260847(15,12,s)+0.22603456(16,0,c)+0.09656469(16,4,c)+0.00786771(16,8,c)- 0.03884162(16,12,c)-0.32882073(16,16,c)
16,3	0.33074329(2,2,c)+0.11767439(4,2,c)-0.09215524(5,2,s)+0.13336331(6,2,c)+0.19780976(6,6,c)- 0.04270455(7,2,s)+0.04642474(7,6,s)+0.00208785(8,2,c)-0.13400944(8,6,c)-0.25938450(9,2,s)- 0.12460428(9,6,s)+0.04360387(10,2,c)+0.15563588(10,6,c)+0.10317330(10,10,c)- 0.32750357(11,2,s)+0.32770720(11,6,s)+0.11452436(11,10,s)-0.02496799(12,2,c)- 0.12707890(12,6,c)-0.19133903(12,10,c)-0.27429628(13,2,s)+0.08689615(13,6,s)- 0.25130326(13,10,s)+0.01005589(14,2,c)+0.10243519(14,6,c)+0.16434880(14,10,c)+ 0.06338764(14,14,c)-0.13508587(15,2,s)+0.03232437(15,6,s)+0.06272860(15,10,s)+ 0.08823186(15,14,s)-0.36699792(16,2,c)-0.16036683(16,6,c)-0.07705939(16,10,c)- 0.06137482(16,14,c)
16,4	0.17316517(4,0,c)-0.20489179(4,4,c)+0.14339438(5,4,s)+0.15944611(6,0,c)+0.06026496(6,4,c)+ 0.43644299(7,4,s)+0.12358063(8,0,c)-0.10596021(8,4,c)-0.08296968(8,8,c)+0.01775583(9,4,s)+ 0.02767047(9,8,s)-0.01372294(10,0,c)+0.26489326(10,4,c)-0.23064550(10,8,c)+ 0.18091894(11,4,s)-0.05417574(11,8,s)-0.01863502(12,0,c)+0.12876092(12,4,c)+ 0.06686396(12,8,c)-0.09331588(12,12,c)-0.17224260(13,4,s)+0.04078381(13,8,s)- 0.21979170(13,12,s)+0.22521307(14,0,c)+0.14089293(14,4,c)-0.17939292(14,8,c)+ 0.20581421(14,12,c)-0.36493701(15,4,s)-0.01179661(15,8,s)+0.19811756(15,12,s)+ 0.11202926(16,0,c)-0.16827842(16,4,c)-0.12790622(16,8,c)-0.07583796(16,12,c)+ 0.06198813(16,16,c)
16,5	0.26826632(4,2,c)+0.14339438(5,2,s)-0.09528728(6,2,c)-0.14133387(6,6,c)-0.29547330(7,2,s)+ 0.32121334(7,6,s)+0.08284220(8,2,c)+0.16285231(8,6,c)+0.02963530(9,2,s)+0.01423634(9,6,s)- 0.13322882(10,2,c)+0.30918514(10,6,c)-0.10103827(10,10,c)-0.03176185(11,2,s)- 0.12764092(11,6,s)+0.13551994(11,10,s)+0.12906984(12,2,c)-0.03658125(12,6,c)- 0.11003668(12,10,c)-0.16357045(13,2,s)-0.22604145(13,6,s)+0.04229893(13,10,s)- 0.04996707(14,2,c)-0.31226569(14,6,c)+0.07376775(14,10,c)-0.19916024(14,14,c)- 0.02267152(15,2,s)+0.27289069(15,6,s)+0.14399605(15,10,s)-0.27721933(15,14,s)- 0.11048896(16,2,c)+0.06555390(16,6,c)+0.11459159(16,10,c)+0.19283608(16,14,c)
18,1	0.32444284(0,0,c)-0.21705727(4,0,c)-0.18344687(4,4,c)-0.08454434(6,0,c)+0.22368331(6,4,c)- 0.02278519(8,0,c)-0.01211753(8,4,c)-0.01846255(8,8,c)+0.07872753(10,0,c)-0.11219072(10,4,c)- 0.13353367(10,8,c)-0.13069869(12,0,c)+0.04807753(12,4,c)-0.21997219(12,8,c)- 0.06517790(12,12,c)+0.23971486(14,0,c)-0.24929338(14,4,c)-0.26751342(14,8,c)- 0.32482332(14,12,c)-0.26617642(16,0,c)+0.14279781(16,4,c)-0.24327420(16,8,c)- 0.38283300(16,12,c)-0.10163592(16,16,c)+0.09429909(18,0,c)-0.08360100(18,4,c)-

	0.06557639(18,8,c)-0.10962766(18,12,c)-0.10458250(18,16,c)
18,2	0.21584035(2,0,c)+0.06109595(4,0,c)-0.07228971(4,4,c)-0.28374106(5,4,s)-0.23101905(6,0,c)-0.08731699(6,4,c)+0.19306134(7,4,s)-0.00792365(8,0,c)+0.08452636(8,4,c)-0.04569838(8,8,c)+0.08333198(9,4,s)+0.12986352(9,8,s)-0.13291633(10,0,c)+0.02938662(10,4,c)-0.10305327(10,8,c)-0.12876876(11,4,s)+0.11206221(11,8,s)+0.18118473(12,0,c)-0.21342447(12,4,c)-0.15080060(12,8,c)-0.01180751(12,12,c)+0.20842461(13,4,s)+0.04696896(13,8,s)+0.30426096(13,12,s)-0.04329424(14,0,c)-0.03726886(14,4,c)-0.17852419(14,8,c)+0.14367880(14,12,c)-0.23744920(15,4,s)-0.05406630(15,8,s)+0.05432561(15,12,s)-0.16546105(16,0,c)+0.01297944(16,4,c)-0.16802074(16,8,c)+0.17504492(16,12,c)+0.19439389(16,16,c)+0.09417951(17,4,s)-0.16479424(17,8,s)-0.30457370(17,12,s)+0.09852300(18,0,c)-0.08735331(18,4,c)-0.07971753(18,8,c)+0.00822272(18,12,c)+0.20002967(18,16,c)
18,3	0.21584035(2,2,c)-0.09464944(4,2,c)+0.28374106(5,2,s)-0.13806029(6,2,c)-0.20477650(6,6,c)+0.13070314(7,2,s)-0.14208930(7,6,s)-0.06529242(8,2,c)+0.07094175(8,6,c)-0.13908491(9,2,s)-0.06681423(9,6,s)-0.02951280(10,2,c)-0.14722541(10,6,c)-0.08126484(10,10,c)+0.02506124(11,2,s)-0.14568738(11,6,s)+0.08536072(11,10,s)+0.03104514(12,2,c)-0.16330240(12,6,c)-0.27134235(12,10,c)-0.27326643(13,2,s)-0.25154273(13,6,s)-0.01653319(13,10,s)-0.10209798(14,2,c)+0.18391951(14,6,c)-0.08806768(14,10,c)-0.06141288(14,14,c)-0.04944471(15,2,s)-0.13761907(15,6,s)-0.05161727(15,10,s)+0.19546977(15,14,s)+0.24563590(16,2,c)-0.00712571(16,6,c)+0.25258229(16,10,c)-0.00457360(16,14,c)+0.20185529(17,2,s)-0.19096043(17,6,s)+0.07570006(17,10,s)+0.21412640(17,14,s)-0.08643761(18,2,c)+0.18807089(18,6,c)+0.13098403(18,10,c)+0.06142320(18,14,c)
18,4	0.46658692(3,2,s)-0.13978274(7,2,s)-0.12858142(7,6,s)-0.12790739(11,2,s)-0.08829044(11,6,s)-0.11313500(11,10,s)+0.22047577(13,2,s)-0.21872825(13,6,s)-0.31628052(13,10,s)-0.34904243(15,2,s)-0.05544939(15,6,s)-0.39665971(15,10,s)-0.23207521(15,14,s)+0.22048401(17,2,s)-0.13603285(17,6,s)-0.21197250(17,10,s)-0.25422565(17,14,s)
18,5	0.18860259(4,0,c)-0.14126926(4,4,c)-0.10880359(5,4,s)+0.13402983(6,0,c)+0.10899634(6,4,c)-0.15990797(7,4,s)-0.32349420(8,0,c)-0.07793844(8,4,c)+0.04668319(8,8,c)+0.12904724(9,4,s)+0.20110561(9,8,s)-0.00547588(10,0,c)-0.11974085(10,4,c)-0.01165113(10,8,c)+0.28160992(11,4,s)+0.17353864(11,8,s)+0.13225675(12,0,c)+0.04444824(12,4,c)-0.04830880(12,8,c)+0.32466787(12,12,c)-0.13380474(13,4,s)+0.07273576(13,8,s)-0.15441905(13,12,s)-0.22626487(14,0,c)-0.18411262(14,4,c)-0.06622469(14,8,c)+0.05780579(14,12,c)-0.17993402(15,4,s)-0.08372663(15,8,s)-0.02757143(15,12,s)-0.00417484(16,0,c)+0.02066939(16,4,c)-0.05151353(16,8,c)+0.02416485(16,12,c)-0.14568218(16,16,c)+0.11331348(17,4,s)-0.25519904(17,8,s)+0.15457777(17,12,s)+0.07786968(18,0,c)-0.10262728(18,4,c)+0.03897839(18,8,c)+0.32973691(18,12,c)-

	0.14990573(18,16,c)
18,6	0.25902943(4,2,c)-0.12272906(5,2,s)-0.10335540(6,2,c)-0.15330083(6,6,c)+0.12211387(7,2,s)-0.13275178(7,6,s)-0.24102672(8,2,c)-0.12392048(8,6,c)+0.24295240(9,2,s)+0.11671056(9,6,s)+0.05808990(10,2,c)-0.05949348(10,6,c)+0.06461298(10,10,c)-0.24440014(11,2,s)-0.00709532(11,6,s)+0.28184940(11,10,s)-0.21823411(12,2,c)-0.01758887(12,6,c)+0.06014465(12,10,c)-0.10711192(13,2,s)-0.20864026(13,6,s)+0.06962153(13,10,s)+0.20615176(14,2,c)-0.01126063(14,6,c)+0.01796345(14,10,c)+0.27344741(14,14,c)+0.10900297(15,2,s)+0.07611023(15,6,s)+0.00037884(15,10,s)-0.18277350(15,14,s)+0.11787237(16,2,c)+0.08010360(16,6,c)-0.04735757(16,10,c)+0.02036443(16,14,c)+0.00600900(17,2,s)-0.06946066(17,6,s)+0.29095499(17,10,s)-0.20021834(17,14,s)-0.07314393(18,2,c)+0.19024558(18,6,c)-0.07481310(18,10,c)-0.27349336(18,14,c)
18,7	0.15691133(4,4,c)+0.05678204(5,4,s)-0.11698513(6,0,c)+0.06756851(6,4,c)+0.08345222(7,4,s)-0.24239836(8,0,c)-0.17802041(8,4,c)-0.35757118(8,8,c)-0.06734673(9,4,s)-0.10495229(9,8,s)+0.07917337(10,0,c)-0.04626371(10,4,c)-0.12336228(10,8,c)-0.14696560(11,4,s)-0.09056574(11,8,s)+0.38169793(12,0,c)+0.35296700(12,4,c)+0.00207409(12,8,c)+0.24302221(12,12,c)+0.06982955(13,4,s)-0.03795909(13,8,s)+0.08058768(13,12,s)+0.09956210(14,0,c)+0.11534431(14,4,c)+0.05522904(14,8,c)-0.00507183(14,12,c)+0.09390334(15,4,s)+0.04369496(15,8,s)+0.01438888(15,12,s)-0.13005623(16,0,c)-0.09965534(16,4,c)-0.01119235(16,8,c)-0.04024823(16,12,c)-0.03861591(16,16,c)-0.05913565(17,4,s)+0.13318238(17,8,s)-0.08067051(17,12,s)-0.04529146(18,0,c)+0.14132392(18,4,c)-0.37575550(18,8,c)+0.24011337(18,12,c)-0.03973544(18,16,c)
18,8	0.25582460(6,2,c)-0.17247691(6,6,c)-0.54499850(10,2,c)-0.10688300(10,6,c)+0.39156325(10,10,c)+0.02601278(12,2,c)-0.10221790(12,6,c)+0.06449417(12,10,c)+0.32735998(14,2,c)+0.10463604(14,6,c)+0.00849269(14,10,c)-0.24304537(14,14,c)-0.00881879(16,2,c)+0.02283584(16,6,c)+0.00889275(16,10,c)-0.01810030(16,14,c)-0.04762007(18,2,c)+0.17509730(18,6,c)-0.39682702(18,10,c)+0.24308622(18,14,c)
20,1	0.30860670(0,0,c)+0.10692591(4,0,c)+0.09036889(4,4,c)+0.03714749(6,0,c)-0.09828302(6,4,c)+0.01725994(8,0,c)+0.00917911(8,4,c)+0.01398551(8,8,c)-0.19286659(10,0,c)+0.27484465(10,4,c)+0.32713056(10,8,c)+0.08617657(12,0,c)+0.14664311(12,4,c)-0.11220149(12,8,c)+0.10473850(12,12,c)-0.09159011(14,0,c)+0.09524987(14,4,c)+0.10221137(14,8,c)+0.12410830(14,12,c)-0.03471280(16,0,c)+0.35160510(16,4,c)-0.20421064(16,8,c)-0.38862315(16,12,c)+0.12041342(16,16,c)-0.11958361(18,0,c)+0.07568431(18,4,c)+0.21322666(18,8,c)-0.00850202(18,12,c)+0.17727782(18,16,c)+0.23966156(20,0,c)+0.06328644(20,4,c)+0.09644250(20,8,c)+0.11474053(20,12,c)+0.13216473(20,16,c)+0.16601562(20,20,c)
20,2	0.35053725(2,0,c)-0.02186478(4,0,c)+0.02587075(4,4,c)+0.06978870(5,4,s)+0.07228427(6,0,c)+0.02732089(6,4,c)-0.04729098(7,4,s)-0.09437620(8,0,c)+0.08727756(8,4,c)+0.05918961(8,8,c)-

	0.12124603(9,4,s)-0.18894829(9,8,s)+0.07964932(10,0,c)+0.05164711(10,4,c)+ 0.00356666(10,8,c)+0.05925982(11,4,s)+0.29431297(11,8,s)-0.13771997(12,0,c)+ 0.16617974(12,4,c)+0.11652586(12,8,c)+0.00547550(12,12,c)+0.02352125(13,4,s)- 0.14941331(13,8,s)-0.02718092(13,12,s)+0.00651766(14,0,c)+0.18420576(14,4,c)- 0.08013918(14,8,c)-0.07056325(14,12,c)-0.08842723(15,4,s)+0.19814656(15,8,s)+ 0.37115597(15,12,s)-0.07229762(16,0,c)+0.16761426(16,4,c)+0.03788113(16,8,c)+ 0.11155041(16,12,c)-0.08601102(16,16,c)+0.09202859(17,4,s)-0.23107847(17,8,s)- 0.26882778(17,12,s)-0.04061394(17,16,s)-0.06309614(18,0,c)+0.12337954(18,4,c)+ 0.03279498(18,8,c)-0.03776827(18,12,c)-0.13649215(18,16,c)+0.00713361(19,4,s)+ 0.06272445(19,8,s)-0.05227723(19,12,s)+0.03744421(19,16,s)+0.20861601(20,0,c)+ 0.05848529(20,4,c)+0.06519505(20,8,c)-0.00352024(20,12,c)-0.09505955(20,16,c)- 0.28321854(20,20,c)
20,3	0.35053725(2,2,c)+0.03387277(4,2,c)-0.06978870(5,2,s)+0.04319811(6,2,c)+0.06407316(6,6,c)- 0.03201615(7,2,s)+0.03480522(7,6,s)+0.05749033(8,2,c)+0.12931555(8,6,c)+0.20236519(9,2,s)+ 0.09721309(9,6,s)+0.05372779(10,2,c)+0.01047046(10,6,c)+0.07763925(10,10,c)+ 0.21277827(11,2,s)-0.19101281(11,6,s)-0.09149518(11,10,s)-0.02825759(12,2,c)+ 0.12485992(12,6,c)+0.20928990(12,10,c)+0.09016904(13,2,s)-0.06369569(13,6,s)+ 0.10690552(13,10,s)+0.07992799(14,2,c)-0.02449760(14,6,c)-0.17348645(14,10,c)+ 0.09104689(14,14,c)+0.28364683(15,2,s)-0.23917610(15,6,s)-0.21719653(15,10,s)+ 0.00176882(15,14,s)-0.11704211(16,2,c)-0.00654495(16,6,c)+0.15781088(16,10,c)+ 0.12630079(16,14,c)+0.23020271(17,2,s)-0.13808150(17,6,s)+0.02704592(17,10,s)+ 0.25098429(17,14,s)+0.07675479(18,2,c)-0.10470569(18,6,c)-0.11438020(18,10,c)- 0.09626379(18,14,c)+0.03363876(18,18,c)+0.01736304(19,2,s)+0.02970861(19,6,s)- 0.06713229(19,10,s)+0.04133877(19,14,s)-0.02684227(19,18,s)-0.32194583(20,2,c)- 0.10936078(20,6,c)-0.11421302(20,10,c)-0.10355924(20,14,c)-0.03278701(20,18,c)
20,4	0.20851441(3,2,s)+0.34400370(7,2,s)+0.31643738(7,6,s)+0.05925242(9,2,s)-0.12334375(9,6,s)+ 0.17037471(11,2,s)+0.11760429(11,6,s)+0.15069765(11,10,s)-0.08698030(13,2,s)+ 0.08629088(13,6,s)+0.12477640(13,10,s)+0.01496693(15,2,s)+0.36039503(15,6,s)- 0.37603127(15,10,s)+0.15822169(15,14,s)+0.12124201(17,2,s)-0.07480314(17,6,s)- 0.11656162(17,10,s)-0.13979621(17,14,s)+0.30612521(19,2,s)+0.23733290(19,6,s)+ 0.15430446(19,10,s)+0.13606844(19,14,s)+0.28433458(19,18,s)
20,5	0.30739555(4,0,c)-0.04216267(4,4,c)+0.05604690(5,4,s)-0.15031300(6,0,c)+0.17813815(6,4,c)- 0.12866275(7,4,s)+0.07014134(8,0,c)+0.05953192(8,4,c)-0.06438866(8,8,c)-0.05997538(9,4,s)- 0.09346488(9,8,s)+0.15826749(10,0,c)-0.07389257(10,4,c)+0.03670440(10,8,c)- 0.09919828(11,4,s)+0.02673559(11,8,s)-0.19673798(12,0,c)+0.05491651(12,4,c)- 0.23173425(12,8,c)-0.18836313(12,12,c)+0.00857445(13,4,s)+0.28763904(13,8,s)+ 0.12612022(13,12,s)+0.01936822(14,0,c)+0.18394210(14,4,c)+0.19696950(14,8,c)+

	0.22830071(14,12,c)-0.04733037(15,4,s)-0.05934859(15,8,s)-0.06725873(15,12,s)- 0.07787541(16,0,c)-0.07623106(16,4,c)-0.06797752(16,8,c)-0.07214721(16,12,c)- 0.19857047(16,16,c)+0.14308718(17,4,s)-0.19552245(17,8,s)+0.07396372(17,12,s)+ 0.06889338(17,16,s)+0.06926878(18,0,c)+0.12901359(18,4,c)-0.03766574(18,8,c)+ 0.23447827(18,12,c)-0.17207688(18,16,c)+0.06585236(19,4,s)+0.03791770(19,8,s)- 0.10876601(19,12,s)-0.06351656(19,16,s)+0.10702618(20,0,c)+0.04495160(20,4,c)- 0.06587844(20,8,c)-0.15053777(20,12,c)-0.20996729(20,16,c)+0.23154952(20,20,c)
20,6	0.33140192(4,2,c)+0.08053781(5,2,s)+0.06235437(6,2,c)+0.09248648(6,6,c)+0.12516754(7,2,s)- 0.13607146(7,6,s)+0.15271195(8,2,c)-0.00971961(8,6,c)-0.14384324(9,2,s)-0.06910006(9,6,s)- 0.04121460(10,2,c)-0.19424246(10,6,c)-0.11038602(10,10,c)+0.02779190(11,2,s)+ 0.09738445(11,6,s)-0.10741950(11,10,s)+0.10698042(12,2,c)+0.00063542(12,6,c)- 0.04214190(12,10,c)+0.33726383(13,2,s)-0.07882514(13,6,s)+0.28961565(13,10,s)- 0.10072026(14,2,c)-0.08926523(14,6,c)-0.10965708(14,10,c)-0.17792327(14,14,c)+ 0.11074713(15,2,s)-0.02067183(15,6,s)-0.04851812(15,10,s)-0.07869874(15,14,s)+ 0.11581606(16,2,c)+0.07104721(16,6,c)+0.04920921(16,10,c)+0.05738413(16,14,c)+ 0.04044778(17,2,s)+0.06469281(17,6,s)+0.28397958(17,10,s)-0.23631810(17,14,s)- 0.18834503(18,2,c)+0.15817212(18,6,c)+0.05189256(18,10,c)-0.06611706(18,14,c)- 0.15618356(18,18,c)+0.08510509(19,2,s)-0.13293121(19,6,s)-0.00807971(19,10,s)- 0.11590170(19,14,s)+0.07917938(19,18,s)-0.20253351(20,2,c)-0.05879517(20,6,c)+ 0.12108955(20,10,c)+0.17102010(20,14,c)+0.15222891(20,18,c)
20,7	0.31160203(4,4,c)-0.05783669(5,4,s)-0.00036929(6,0,c)+0.22754086(6,4,c)+0.13277143(7,4,s)- 0.02117700(8,0,c)-0.03420177(8,4,c)+0.10793496(8,8,c)+0.06189062(9,4,s)+0.09644956(9,8,s)- 0.09513539(10,0,c)-0.02091651(10,4,c)-0.15353045(10,8,c)+0.10236605(11,4,s)- 0.02758935(11,8,s)-0.21844143(12,0,c)-0.04449253(12,4,c)-0.26415037(12,8,c)- 0.06527373(12,12,c)-0.00884827(13,4,s)-0.29682444(13,8,s)-0.13014771(13,12,s)- 0.29170262(14,0,c)+0.09275706(14,4,c)+0.09996599(14,8,c)+0.13259481(14,12,c)+ 0.04884180(15,4,s)+0.06124382(15,8,s)+0.06940655(15,12,s)-0.21993970(16,0,c)- 0.08136711(16,4,c)-0.03796611(16,8,c)-0.03081449(16,12,c)-0.03866808(16,16,c)- 0.14765650(17,4,s)+0.20176622(17,8,s)-0.07632566(17,12,s)-0.07109341(17,16,s)- 0.08361088(18,0,c)-0.04834930(18,4,c)-0.27013890(18,8,c)+0.13218452(18,12,c)+ 0.08204324(18,16,c)-0.06795527(19,4,s)-0.03912856(19,8,s)+0.11223932(19,12,s)+ 0.06554488(19,16,s)-0.01066830(20,0,c)+0.36275618(20,4,c)+0.04291719(20,8,c)- 0.04364674(20,12,c)-0.03321840(20,16,c)-0.00038403(20,20,c)
20,8	0.35835701(5,2,s)+0.09508115(6,2,c)+0.14102814(6,6,c)-0.02557322(7,2,s)+0.02780102(7,6,s)- 0.05568802(8,2,c)-0.25864373(8,6,c)+0.23953680(9,2,s)+0.11506976(9,6,s)+0.01264681(10,2,c)+ 0.11408703(10,6,c)+0.04874425(10,10,c)-0.04007385(11,2,s)+0.02523733(11,6,s)+ 0.02561122(11,10,s)-0.03770717(12,2,c)-0.03633689(12,6,c)-0.04238231(12,10,c)+

	0.12291815(13,2,s)+0.16160493(13,6,s)-0.02607523(13,10,s)-0.00574301(14,2,c)+ 0.13825671(14,6,c)-0.37411358(14,10,c)+0.03871446(14,14,c)-0.01255876(15,2,s)+ 0.10006259(15,6,s)+0.05426451(15,10,s)-0.09776751(15,14,s)+0.05230422(16,2,c)- 0.21060168(16,6,c)+0.18296858(16,10,c)-0.20129131(16,14,c)+0.09553091(17,2,s)+ 0.12793964(17,6,s)-0.00711988(17,10,s)+0.02032943(17,14,s)-0.02216420(18,2,c)+ 0.15496060(18,6,c)+0.17650828(18,10,c)+0.17218010(18,14,c)+0.07019728(18,18,c)+ 0.26967647(19,2,s)+0.09868386(19,6,s)+0.01957189(19,10,s)-0.09449283(19,14,s)- 0.33811658(19,18,s)-0.01967032(20,2,c)-0.05576575(20,6,c)-0.02375874(20,10,c)- 0.01775177(20,14,c)-0.06841985(20,18,c)
20,9	0.35835701(5,4,s)-0.15910119(6,0,c)-0.06013460(6,4,c)+0.03777415(7,4,s)-0.16190808(8,0,c)+ 0.19700543(8,4,c)+0.07051502(8,8,c)+0.14351720(9,4,s)+0.22365540(9,8,s)-0.08909906(10,0,c)+ 0.03341262(10,4,c)-0.08060241(10,8,c)+0.02299269(11,4,s)+0.04868375(11,8,s)- 0.04833616(12,0,c)+0.01791377(12,4,c)+0.02146805(12,8,c)+0.03768682(12,12,c)+ 0.12423930(13,4,s)-0.02310906(13,8,s)+0.16104505(13,12,s)+0.07817405(14,0,c)- 0.22646196(14,4,c)+0.31968873(14,8,c)-0.03178983(14,12,c)-0.13008890(15,4,s)- 0.00096983(15,8,s)+0.07582417(15,12,s)-0.07572089(16,0,c)+0.00796601(16,4,c)+ 0.30747876(16,8,c)-0.14338407(16,12,c)+0.01360886(16,16,c)+0.06831740(17,4,s)+ 0.06830528(17,8,s)-0.02021224(17,12,s)+0.12734705(17,16,s)-0.20585604(18,0,c)+ 0.09908378(18,4,c)-0.00572225(18,8,c)-0.07932139(18,12,c)-0.17808405(18,16,c)- 0.33837982(19,4,s)-0.21865394(19,8,s)-0.17321531(19,12,s)-0.11740818(19,16,s)- 0.06369914(20,0,c)+0.01352495(20,4,c)+0.05257209(20,8,c)+0.02884363(20,12,c)+ 0.00178809(20,16,c)+0.03490182(20,20,c)
20,10	0.20865829(6,0,c)+0.07886542(6,4,c)+0.06858624(8,0,c)+0.27678287(8,4,c)-0.26630527(8,8,c)+ 0.09074973(9,4,s)+0.14142324(9,8,s)-0.10020897(10,0,c)-0.07194027(10,4,c)+ 0.00136165(10,8,c)-0.38524776(11,4,s)+0.19454818(11,8,s)+0.02273093(12,0,c)+ 0.05724576(12,4,c)+0.02147825(12,8,c)-0.07584297(12,12,c)-0.15652982(13,4,s)- 0.01648108(13,8,s)-0.22103167(13,12,s)-0.14728391(14,0,c)-0.12295979(14,4,c)- 0.00876887(14,8,c)-0.00710321(14,12,c)+0.21517453(15,4,s)+0.07235784(15,8,s)- 0.01166869(15,12,s)-0.10376367(16,0,c)-0.08487318(16,4,c)-0.01572707(16,8,c)- 0.00015682(16,12,c)+0.19073734(16,16,c)+0.15206132(17,4,s)-0.07956213(17,8,s)- 0.03777364(17,12,s)+0.14333506(17,16,s)+0.11855009(18,0,c)+0.18406167(18,4,c)+ 0.08258651(18,8,c)+0.00540018(18,12,c)-0.09768658(18,16,c)+0.02582884(19,4,s)- 0.20752869(19,8,s)+0.21811915(19,12,s)-0.13214840(19,16,s)+0.05593948(20,0,c)+ 0.08044285(20,4,c)-0.25337435(20,8,c)-0.07598285(20,12,c)+0.18423133(20,16,c)- 0.05838005(20,20,c)
20,11	0.35437360(6,2,c)-0.14425339(6,6,c)-0.12343669(8,2,c)+0.06010538(8,6,c)-0.05329775(9,2,s)- 0.02560341(9,6,s)+0.24027674(10,2,c)+0.05015177(10,6,c)-0.22603151(10,10,c)-

	0.00572851(11,2,s)-0.11642944(11,6,s)+0.09733791(11,10,s)+0.06479953(12,2,c)- 0.38789595(12,6,c)+0.25440403(12,10,c)+0.06704309(13,2,s)+0.06798371(13,6,s)- 0.00028007(13,10,s)-0.03603568(14,2,c)-0.01537902(14,6,c)+0.00210649(14,10,c)- 0.05508415(14,14,c)+0.02714301(15,2,s)+0.03680490(15,6,s)+0.00900296(15,10,s)- 0.06500472(15,14,s)-0.01091734(16,2,c)+0.25620012(16,6,c)+0.09229774(16,10,c)- 0.17831408(16,14,c)-0.01937349(17,2,s)-0.05942888(17,6,s)-0.02967787(17,10,s)+ 0.03974275(17,14,s)-0.22131894(18,2,c)-0.01012656(18,6,c)-0.28063484(18,10,c)+ 0.14340409(18,14,c)+0.25460258(18,18,c)-0.01149902(19,2,s)-0.03288947(19,6,s)+ 0.09213321(19,10,s)-0.05869253(19,14,s)+0.01792089(19,18,s)-0.09698626(20,2,c)+ 0.12063543(20,6,c)+0.16541605(20,10,c)+0.07315743(20,14,c)-0.24815589(20,18,c)
20,12	0.25182101(6,6,c)-0.32835653(8,2,c)+0.15988759(8,6,c)-0.14177848(9,2,s)-0.06810818(9,6,s)- 0.16641088(10,2,c)-0.02457668(10,6,c)-0.02249161(10,10,c)-0.01523852(11,2,s)- 0.30971641(11,6,s)+0.25893063(11,10,s)-0.12598437(12,2,c)+0.14055915(12,6,c)- 0.06298368(12,10,c)+0.17834274(13,2,s)+0.18084490(13,6,s)-0.00074502(13,10,s)- 0.09585926(14,2,c)-0.04091007(14,6,c)+0.00560351(14,10,c)-0.14653052(14,14,c)+ 0.07220368(15,2,s)+0.09790550(15,6,s)+0.02394898(15,10,s)-0.17292042(15,14,s)+ 0.23698837(16,2,c)-0.00734817(16,6,c)-0.02273753(16,10,c)+0.07168108(16,14,c)- 0.05153583(17,2,s)-0.15808801(17,6,s)-0.07894673(17,10,s)+0.10572054(17,14,s)+ 0.25589230(18,2,c)-0.04479837(18,6,c)+0.05049144(18,10,c)-0.07486187(18,14,c)+ 0.09862218(18,18,c)-0.03058878(19,2,s)-0.08748998(19,6,s)+0.24508550(19,10,s)- 0.15612924(19,14,s)+0.04767174(19,18,s)+0.05402543(20,2,c)-0.29080507(20,6,c)+ 0.03534201(20,10,c)+0.13832813(20,14,c)-0.09612501(20,18,c)

E.11. Cystallographic Point Group 432

n,λ	Coefficients of the Expansion of the Symmetrized Hyperspherical Harmonics
0,1	1.00000000(0,0,c)
8,1	0.33333333(0,0,c)+0.36504196(4,0,c)+0.30851677(4,4,c)+0.22473329(6,0,c)-0.59458839(6,4,c)+ 0.36360905(8,0,c)+0.19337312(8,4,c)+0.29462783(8,8,c)
8,2	0.44946657(2,0,c)+0.04407382(4,0,c)-0.05214885(4,4,c)+0.55470020(5,4,s)+0.26590801(6,0,c)+ 0.10050378(6,4,c)-0.43852901(7,4,s)+0.29985590(8,0,c)-0.03268602(8,4,c)-0.34860834(8,8,c)
8,3	0.44946657(2,2,c)-0.06827887(4,2,c)-0.55470020(5,2,s)+0.15891043(6,2,c)+0.23570226(6,6,c)- 0.29688554(7,2,s)+0.32274861(7,6,s)-0.40484392(8,2,c)-0.22047928(8,6,c)
12,1	0.27735010(0,0,c)-0.28171881(4,0,c)-0.23809585(4,4,c)-0.01677654(6,0,c)+0.04438655(6,4,c)+ 0.44415485(8,0,c)+0.23620867(8,4,c)+0.35989308(8,8,c)-0.18301410(10,0,c)+ 0.26080436(10,4,c)+0.31041927(10,8,c)+0.10535554(12,0,c)-0.19046457(12,4,c)+ 0.39614309(12,8,c)
12,2	0.11826248(2,0,c)+0.22817079(4,0,c)-0.26997532(4,4,c)-0.39795859(5,4,s)+0.13315966(6,0,c)+ 0.05032962(6,4,c)-0.32130806(7,4,s)-0.03221839(8,0,c)+0.26783545(8,4,c)-0.13602680(8,8,c)+ 0.22241725(10,0,c)+0.29572434(10,4,c)-0.11732746(10,8,c)+0.48825208(11,4,s)+ 0.17255615(12,0,c)-0.21596652(12,4,c)-0.14972801(12,8,c)
12,3	0.11826248(2,2,c)-0.35348067(4,2,c)+0.39795859(5,2,s)+0.07957812(6,2,c)+0.11803342(6,6,c)- 0.21752658(7,2,s)+0.23647633(7,6,s)-0.19658475(8,2,c)+0.22941573(8,6,c)+0.22887667(10,2,c)- 0.14085045(10,6,c)+0.28011547(10,10,c)+0.18053364(11,2,s)+0.23538707(11,6,s)- 0.38780230(11,10,s)+0.04454082(12,2,c)-0.15787909(12,6,c)-0.26819014(12,10,c)
12,4	0.36689969(3,2,s)-0.43278921(6,2,c)+0.29178643(6,6,c)+0.11214901(7,2,s)+0.10316208(7,6,s)- 0.16477051(9,2,s)+0.34299717(9,6,s)+0.26285675(10,2,c)+0.05155045(10,6,c)- 0.18885381(10,10,c)+0.29559541(11,2,s)+0.20404020(11,6,s)+0.26145626(11,10,s)+ 0.07292858(12,2,c)-0.28657478(12,6,c)+0.18081376(12,10,c)
16,1	0.24253563(0,0,c)+0.25205881(4,0,c)+0.21302858(4,4,c)+0.01894607(6,0,c)-0.05012660(6,4,c)+ 0.17306592(8,0,c)+0.09203923(8,4,c)+0.14023313(8,8,c)+0.18548283(10,0,c)- 0.26432242(10,4,c)-0.31460660(10,8,c)+0.21780861(12,0,c)-0.14258865(12,4,c)+ 0.45668536(12,8,c)+0.08698497(12,12,c)+0.14158322(14,0,c)-0.14724060(14,4,c)- 0.15800194(14,8,c)-0.19185098(14,12,c)+0.28151346(16,0,c)+0.17753466(16,4,c)+ 0.08709763(16,8,c)+0.07069282(16,12,c)+0.23938511(16,16,c)
16,2	0.33074329(2,0,c)-0.07595849(4,0,c)+0.08987530(4,4,c)+0.09215524(5,4,s)+0.22315950(6,0,c)+ 0.08434636(6,4,c)-0.06307880(7,4,s)+0.06987654(8,0,c)-0.11378304(8,4,c)-0.01155750(8,8,c)+ 0.15540884(9,4,s)+0.24218719(9,8,s)+0.15737581(10,0,c)-0.01815374(10,4,c)+ 0.10803635(10,8,c)-0.05407081(11,4,s)-0.47417588(11,8,s)+0.14982585(12,0,c)-

	0.13351623(12,4,c)-0.10404093(12,8,c)-0.04779322(12,12,c)-0.00431613(13,4,s)+ 0.35696238(13,8,s)+0.13602188(13,12,s)+0.14617015(14,0,c)-0.06845402(14,4,c)+ 0.06677919(14,8,c)+0.10541104(14,12,c)-0.07293361(15,4,s)-0.10325042(15,8,s)- 0.12260847(15,12,s)+0.22603456(16,0,c)+0.09656469(16,4,c)+0.00786771(16,8,c)- 0.03884162(16,12,c)-0.32882073(16,16,c)
16,3	0.33074329(2,2,c)+0.11767439(4,2,c)-0.09215524(5,2,s)+0.13336331(6,2,c)+0.19780976(6,6,c)- 0.04270455(7,2,s)+0.04642474(7,6,s)+0.00208785(8,2,c)-0.13400944(8,6,c)-0.25938450(9,2,s)- 0.12460428(9,6,s)+0.04360387(10,2,c)+0.15563588(10,6,c)+0.10317330(10,10,c)- 0.32750357(11,2,s)+0.32770720(11,6,s)+0.11452436(11,10,s)-0.02496799(12,2,c)- 0.12707890(12,6,c)-0.19133903(12,10,c)-0.27429628(13,2,s)+0.08689615(13,6,s)- 0.25130326(13,10,s)+0.01005589(14,2,c)+0.10243519(14,6,c)+0.16434880(14,10,c)+ 0.06338764(14,14,c)-0.13508587(15,2,s)+0.03232437(15,6,s)+0.06272860(15,10,s)+ 0.08823186(15,14,s)-0.36699792(16,2,c)-0.16036683(16,6,c)-0.07705939(16,10,c)- 0.06137482(16,14,c)
16,4	0.17316517(4,0,c)-0.20489179(4,4,c)+0.14339438(5,4,s)+0.15944611(6,0,c)+0.06026496(6,4,c)+ 0.43644299(7,4,s)+0.12358063(8,0,c)-0.10596021(8,4,c)-0.08296968(8,8,c)+0.01775583(9,4,s)+ 0.02767047(9,8,s)-0.01372294(10,0,c)+0.26489326(10,4,c)-0.23064550(10,8,c)+ 0.18091894(11,4,s)-0.05417574(11,8,s)-0.01863502(12,0,c)+0.12876092(12,4,c)+ 0.06686396(12,8,c)-0.09331588(12,12,c)-0.17224260(13,4,s)+0.04078381(13,8,s)- 0.21979170(13,12,s)+0.22521307(14,0,c)+0.14089293(14,4,c)-0.17939292(14,8,c)+ 0.20581421(14,12,c)-0.36493701(15,4,s)-0.01179661(15,8,s)+0.19811756(15,12,s)+ 0.11202926(16,0,c)-0.16827842(16,4,c)-0.12790622(16,8,c)-0.07583796(16,12,c)+ 0.06198813(16,16,c)
16,5	0.26826632(4,2,c)+0.14339438(5,2,s)-0.09528728(6,2,c)-0.14133387(6,6,c)-0.29547330(7,2,s)+ 0.32121334(7,6,s)+0.08284220(8,2,c)+0.16285231(8,6,c)+0.02963530(9,2,s)+0.01423634(9,6,s)- 0.13322882(10,2,c)+0.30918514(10,6,c)-0.10103827(10,10,c)-0.03176185(11,2,s)- 0.12764092(11,6,s)+0.13551994(11,10,s)+0.12906984(12,2,c)-0.03658125(12,6,c)- 0.11003668(12,10,c)-0.16357045(13,2,s)-0.22604145(13,6,s)+0.04229893(13,10,s)- 0.04996707(14,2,c)-0.31226569(14,6,c)+0.07376775(14,10,c)-0.19916024(14,14,c)- 0.02267152(15,2,s)+0.27289069(15,6,s)+0.14399605(15,10,s)-0.27721933(15,14,s)- 0.11048896(16,2,c)+0.06555390(16,6,c)+0.11459159(16,10,c)+0.19283608(16,14,c)
18,1	0.22941573(0,0,c)-0.09178109(4,0,c)-0.07756918(4,4,c)-0.08926889(6,0,c)+0.23618327(6,4,c)- 0.27389653(8,0,c)-0.14566256(8,4,c)-0.22193490(8,8,c)+0.10350913(10,0,c)-0.14750574(10,4,c)- 0.17556695(10,8,c)+0.19012686(12,0,c)+0.26980337(12,4,c)-0.17004792(12,8,c)+ 0.21247228(12,12,c)+0.15789414(14,0,c)-0.16420327(14,4,c)-0.17620435(14,8,c)- 0.21395294(14,12,c)-0.27110993(16,0,c)+0.04526389(16,4,c)-0.19588976(16,8,c)- 0.28802885(16,12,c)-0.14373490(16,16,c)+0.06376261(18,0,c)-0.00409707(18,4,c)-

	0.26916934(18,8,c)+0.18087641(18,12,c)-0.14790199(18,16,c)
18,2	0.18731716(2,0,c)-0.03004842(4,0,c)+0.03555377(4,4,c)-0.18526992(5,4,s)-0.28641429(6,0,c)-0.10825443(6,4,c)+0.25716283(7,4,s)+0.07988926(8,0,c)+0.06676433(8,4,c)-0.14241317(8,8,c)-0.09474068(10,0,c)+0.06760915(10,4,c)-0.11265937(10,8,c)-0.26956980(11,4,s)+0.18672626(12,0,c)-0.12366417(12,4,c)-0.10911787(12,8,c)-0.09738651(12,12,c)+0.25586728(13,4,s)+0.35059143(13,12,s)+0.08497167(14,0,c)+0.07526245(14,4,c)-0.11306839(14,8,c)+0.09806517(14,12,c)-0.10523311(15,4,s)+0.06259789(15,12,s)-0.17165164(16,0,c)-0.02074667(16,4,c)-0.12570029(16,8,c)+0.13201781(16,12,c)+0.22399467(16,16,c)+0.01823143(17,4,s)-0.35095179(17,12,s)+0.04079452(18,0,c)+0.00187789(18,4,c)-0.17272299(18,8,c)-0.08290457(18,12,c)+0.23048861(18,16,c)
18,3	0.18731716(2,2,c)+0.04655082(4,2,c)+0.18526992(5,2,s)-0.17116528(6,2,c)-0.25387913(6,6,c)+0.17410006(7,2,s)-0.18926672(7,6,s)-0.17641225(8,2,c)+0.00324784(10,2,c)-0.15732751(10,6,c)-0.03842437(10,10,c)-0.09967478(11,2,s)-0.12996001(11,6,s)+0.21411028(11,10,s)-0.08148170(12,2,c)-0.15046067(12,6,c)-0.20560322(12,10,c)-0.29037033(13,2,s)-0.32195926(13,6,s)+0.02024141(13,10,s)+0.01381564(14,2,c)+0.15402008(14,6,c)-0.06750489(14,10,c)+0.08255841(14,14,c)+0.01124482(15,2,s)-0.08161929(15,6,s)-0.04460786(15,10,s)+0.07883203(15,14,s)+0.27173723(16,2,c)+0.03361345(16,6,c)+0.19567524(16,10,c)+0.00614837(16,14,c)+0.17816564(17,2,s)-0.20023493(17,6,s)+0.21025016(17,10,s)+0.08635616(17,14,s)-0.11135469(18,2,c)+0.25773625(18,6,c)+0.07650552(18,10,c)-0.08257228(18,14,c)
18,4	0.32992677(3,2,s)+0.18089531(6,2,c)-0.12195959(6,6,c)-0.09884132(7,2,s)-0.09092079(7,6,s)-0.38537213(10,2,c)-0.07557769(10,6,c)+0.27687703(10,10,c)-0.09044418(11,2,s)-0.06243077(11,6,s)-0.07999853(11,10,s)+0.01839381(12,2,c)-0.07227897(12,6,c)+0.04560426(12,10,c)+0.15589991(13,2,s)-0.15466423(13,6,s)-0.22364410(13,10,s)+0.23147846(14,2,c)+0.07398885(14,6,c)+0.00600524(14,10,c)-0.17185903(14,14,c)-0.24681027(15,2,s)-0.03920864(15,6,s)-0.28048077(15,10,s)-0.16410195(15,14,s)-0.00623583(16,2,c)+0.01614738(16,6,c)+0.00628812(16,10,c)-0.01279885(16,14,c)+0.15590574(17,2,s)-0.09618975(17,6,s)-0.14988720(17,10,s)-0.17976468(17,14,s)-0.03367248(18,2,c)+0.12381249(18,6,c)-0.28059908(18,10,c)+0.17188791(18,14,c)
20,1	0.21821789(0,0,c)-0.08048597(4,0,c)-0.06802306(4,4,c)+0.10277719(6,0,c)-0.27192289(6,4,c)-0.01299202(8,0,c)-0.00690936(8,4,c)-0.01052727(8,8,c)-0.16993041(10,0,c)+0.24215943(10,4,c)+0.28822738(10,8,c)+0.26832959(12,0,c)+0.09769994(12,4,c)+0.16831857(12,8,c)+0.20183119(12,12,c)+0.06894231(14,0,c)-0.07169711(14,4,c)-0.07693722(14,8,c)-0.09341962(14,12,c)+0.12322731(16,0,c)+0.32737136(16,4,c)-0.09119766(16,8,c)-0.22299882(16,12,c)+0.20500613(16,16,c)-0.07858940(18,0,c)+0.01179618(18,4,c)+0.30283079(18,8,c)-0.19012432(18,12,c)+0.17236223(18,16,c)+0.12036860(20,0,c)-

	0.15658146(20,4,c)+0.08052916(20,8,c)+0.17905392(20,12,c)+0.21642112(20,16,c)
20,2	0.18140661(2,0,c)+0.14698569(4,0,c)-0.17391582(4,4,c)+0.11985333(5,4,s)-0.13905627(6,0,c)-0.05255833(6,4,c)-0.15874456(7,4,s)-0.04147366(8,0,c)-0.01017195(8,4,c)+0.05786005(8,8,c)-0.15536067(9,4,s)-0.24211212(9,8,s)+0.20979806(10,0,c)+0.03256625(10,4,c)+0.09632966(10,8,c)+0.09019730(11,4,s)+0.10147000(11,8,s)-0.06940336(12,0,c)+0.11484118(12,4,c)+0.07367339(12,8,c)-0.02476130(12,12,c)+0.09607627(13,4,s)+0.23397880(13,8,s)+0.22467947(13,12,s)+0.23612360(14,0,c)+0.17767986(14,4,c)+0.03209228(14,8,c)+0.01146102(14,12,c)-0.19615508(15,4,s)+0.00866611(15,8,s)+0.13061506(15,12,s)+0.07828926(16,0,c)+0.12727434(16,4,c)+0.03215782(16,8,c)+0.02735821(16,12,c)-0.20623667(16,16,c)+0.13986010(17,4,s)-0.28913706(17,8,s)-0.04580441(17,12,s)-0.01671719(18,0,c)+0.08455748(18,4,c)+0.10570417(18,8,c)+0.02332506(18,12,c)-0.17339683(18,16,c)+0.03996431(19,4,s)+0.14610927(19,8,s)-0.24692998(19,12,s)+0.14071957(20,0,c)-0.17258191(20,4,c)+0.08805710(20,8,c)-0.02196691(20,12,c)-0.21772018(20,16,c)
20,3	0.18140661(2,2,c)-0.22770925(4,2,c)-0.11985333(5,2,s)-0.08310202(6,2,c)-0.12326021(6,6,c)-0.10747058(7,2,s)+0.11683283(7,6,s)+0.06934019(8,2,c)+0.01905933(8,6,c)+0.25930409(9,2,s)+0.12456566(9,6,s)+0.08767093(10,2,c)+0.14374718(10,6,c)+0.16126297(10,10,c)+0.09915581(11,2,s)-0.03222084(11,6,s)-0.08695778(11,10,s)-0.05088687(12,2,c)+0.06868274(12,6,c)+0.12938092(12,10,c)-0.29203601(13,2,s)-0.06749521(13,6,s)-0.15689792(13,10,s)+0.15973701(14,2,c)+0.06261062(14,6,c)+0.01402559(14,10,c)+0.24259645(14,14,c)+0.03295268(15,2,s)-0.15959975(15,6,s)-0.09100916(15,10,s)+0.14412351(15,14,s)-0.24229367(16,2,c)-0.07711025(16,6,c)+0.02817918(16,10,c)+0.03460993(16,14,c)+0.10612715(17,2,s)-0.05628782(17,6,s)-0.15988318(17,10,s)+0.25547056(17,14,s)+0.11200103(18,2,c)-0.16236757(18,6,c)-0.08763629(18,10,c)-0.00416653(18,14,c)+0.05107233(18,18,c)-0.05829180(19,2,s)+0.14675627(19,6,s)-0.14117876(19,10,s)+0.18429964(19,14,s)-0.07131863(19,18,s)-0.02238647(20,2,c)+0.08815827(20,6,c)-0.18584747(20,10,c)-0.24481606(20,14,c)-0.04977915(20,18,c)
20,4	0.14744196(3,2,s)-0.23455411(6,2,c)+0.15813635(6,6,c)+0.24324735(7,2,s)+0.22375501(7,6,s)+0.04189779(9,2,s)-0.08721720(9,6,s)-0.20044114(10,2,c)-0.03930974(10,6,c)+0.14401027(10,10,c)+0.12047311(11,2,s)+0.08315879(11,6,s)+0.10655933(11,10,s)-0.07423682(12,2,c)+0.29171553(12,6,c)-0.18405730(12,10,c)-0.06150436(13,2,s)+0.06101687(13,6,s)+0.08823024(13,10,s)+0.01058322(15,2,s)+0.25483777(15,6,s)-0.26589426(15,10,s)+0.11187963(15,14,s)+0.06619278(16,2,c)-0.17140303(16,6,c)-0.06674786(16,10,c)+0.13585866(16,14,c)+0.08573105(17,2,s)-0.05289381(17,6,s)-0.08242151(17,10,s)-0.09885085(17,14,s)+0.21015779(18,2,c)-0.00444400(18,6,c)+0.19831077(18,10,c)-0.11354375(18,14,c)-0.14397841(18,18,c)+0.21646321(19,2,s)+0.16781971(19,6,s)+0.10910973(19,10,s)+0.09621491(19,14,s)+0.20105491(19,18,s)+

	0.07763608(20,2,c)-0.15220390(20,6,c)-0.10069249(20,10,c)-0.01400330(20,14,c)+ 0.14033279(20,18,c)
20,5	0.07427138(4,0,c)-0.08787908(4,4,c)-0.26130464(5,4,s)+0.19180783(6,0,c)+0.07249654(6,4,c)- 0.09468225(7,4,s)+0.18566081(8,0,c)-0.00398492(8,4,c)-0.22651415(8,8,c)-0.10244875(9,4,s)- 0.15965484(9,8,s)+0.08604452(10,0,c)-0.07395114(10,4,c)+0.11286071(10,8,c)- 0.25195527(11,4,s)+0.06691188(11,8,s)+0.05679740(12,0,c)+0.03722921(12,4,c)+ 0.00279426(12,8,c)-0.09586249(12,12,c)-0.17073072(13,4,s)+0.15429152(13,8,s)- 0.17258701(13,12,s)-0.05600080(14,0,c)+0.14541978(14,4,c)-0.23957350(14,8,c)+ 0.04437093(14,12,c)+0.18411197(15,4,s)+0.00571465(15,8,s)-0.10033166(15,12,s)+ 0.04761059(16,0,c)-0.04507713(16,4,c)-0.26266366(16,8,c)+0.10591635(16,12,c)+ 0.04173020(16,16,c)+0.08883041(17,4,s)-0.19066427(17,8,s)+0.03518455(17,12,s)+ 0.26034270(18,0,c)+0.05111089(18,4,c)+0.10229643(18,8,c)+0.09030215(18,12,c)+ 0.03508535(18,16,c)+0.31832533(19,4,s)+0.09634814(19,8,s)+0.18967869(19,12,s)+ 0.10664089(20,0,c)-0.05210186(20,4,c)-0.19000680(20,8,c)-0.08504412(20,12,c)+ 0.04405379(20,16,c)
20,6	0.11506073(4,2,c)-0.26130464(5,2,s)-0.11462710(6,2,c)-0.17001947(6,6,c)+0.06410019(7,2,s)- 0.06968425(7,6,s)+0.26542859(8,2,c)+0.12386340(8,6,c)-0.17099166(9,2,s)-0.08214174(9,6,s)+ 0.00947979(10,2,c)-0.15697373(10,6,c)-0.02965383(10,10,c)+0.04976830(11,2,s)+ 0.17138987(11,6,s)-0.19001918(11,10,s)+0.11299003(12,2,c)+0.03190212(12,6,c)+ 0.00498933(12,10,c)-0.07307580(13,2,s)-0.25004350(13,6,s)+0.12198074(13,10,s)+ 0.01855295(14,2,c)-0.12173012(14,6,c)+0.26105566(14,10,c)-0.01829617(14,14,c)+ 0.01176552(15,2,s)-0.13787814(15,6,s)-0.07286125(15,10,s)+0.13978106(15,14,s)- 0.10607088(16,2,c)+0.15491337(16,6,c)-0.13595152(16,10,c)+0.18032914(16,14,c)- 0.03678720(17,2,s)-0.00019005(17,6,s)+0.14460470(17,10,s)-0.15237390(17,14,s)- 0.12466712(18,2,c)-0.04844967(18,6,c)-0.09988270(18,10,c)-0.15257716(18,14,c)- 0.19772471(18,18,c)-0.17253593(19,2,s)-0.08119238(19,6,s)-0.14359326(19,10,s)+ 0.11565786(19,14,s)+0.27610753(19,18,s)-0.06228964(20,2,c)+0.13427962(20,6,c)+ 0.01764158(20,10,c)-0.00039246(20,14,c)+0.19271821(20,18,c)
24,1	0.28284271(0,0,c)+0.03664076(4,0,c)+0.03096710(4,4,c)-0.04968430(6,0,c)+0.13145231(6,4,c)+ 0.20201592(8,0,c)+0.10743531(8,4,c)+0.16369096(8,8,c)+0.03487224(10,0,c)- 0.04969470(10,4,c)-0.05914852(10,8,c)-0.09514261(12,0,c)-0.11557284(12,4,c)+ 0.05705293(12,8,c)-0.09959180(12,12,c)+0.09105097(14,0,c)-0.09468919(14,4,c)- 0.10160971(14,8,c)-0.12337775(14,12,c)+0.35099402(16,0,c)+0.01513987(16,4,c)+ 0.21541201(16,8,c)+0.29789168(16,12,c)+0.21568883(16,16,c)-0.00059807(18,0,c)- 0.02676303(18,4,c)+0.11744976(18,8,c)-0.13204638(18,12,c)+0.04084228(18,16,c)+ 0.16953941(20,0,c)-0.20030099(20,4,c)+0.10997652(20,8,c)+0.23914778(20,12,c)+ 0.28870412(20,16,c)+0.00896113(20,20,c)-0.01171547(22,0,c)+0.03233190(22,4,c)-

	0.06574711(22,8,c)+0.02592305(22,12,c)+0.07966922(22,16,c)-0.02052303(22,20,c)+ 0.20155167(24,0,c)+0.09913791(24,4,c)+0.13953282(24,8,c)-0.11095195(24,12,c)+ 0.22333086(24,16,c)+0.00784151(24,20,c)+0.16682943(24,24,c)
24,2	0.29789301(2,0,c)-0.05650303(4,0,c)+0.06685529(4,4,c)-0.03946952(5,4,s)+0.19724399(6,0,c)+ 0.07455122(6,4,c)+0.00793207(7,4,s)-0.08392319(8,0,c)+0.02758243(8,4,c)+0.08546894(8,8,c)+ 0.06738839(9,4,s)+0.10501722(9,8,s)+0.06954640(10,0,c)+0.00355927(10,4,c)+ 0.03801213(10,8,c)+0.02765624(11,4,s)-0.07554288(11,8,s)+0.08653981(12,0,c)- 0.06554541(12,4,c)-0.05452961(12,8,c)-0.03784877(12,12,c)-0.00960339(13,4,s)+ 0.11006348(13,8,s)+0.03060495(13,12,s)+0.11898596(14,0,c)-0.05293321(14,4,c)+ 0.09850461(14,8,c)+0.04730971(14,12,c)-0.04313638(15,4,s)-0.21713158(15,8,s)- 0.32341712(15,12,s)+0.10126223(16,0,c)-0.05177283(16,4,c)+0.01141447(16,8,c)- 0.08078008(16,12,c)-0.06098462(16,16,c)+0.01478968(17,4,s)+0.06791755(17,8,s)+ 0.34241858(17,12,s)+0.08282285(17,16,s)+0.19555856(18,0,c)-0.06184758(18,4,c)+ 0.11539113(18,8,c)+0.12213715(18,12,c)+0.02538636(18,16,c)+0.05155777(19,4,s)+ 0.00896826(19,8,s)-0.27838801(19,12,s)-0.18344690(19,16,s)+0.08906762(20,0,c)- 0.09748700(20,4,c)+0.05106323(20,8,c)-0.02556599(20,12,c)-0.11791820(20,16,c)- 0.00953562(20,20,c)-0.06232500(21,4,s)+0.08623955(21,8,s)+0.14763612(21,12,s)+ 0.15451806(21,16,s)+0.01418374(21,20,s)+0.04371962(22,0,c)-0.00914056(22,4,c)- 0.00069381(22,8,c)+0.02959519(22,12,c)+0.00556189(22,16,c)+0.02183874(22,20,c)- 0.00762014(23,4,s)-0.06242130(23,8,s)+0.05460663(23,12,s)-0.04948795(23,16,s)- 0.01326768(23,20,s)+0.20080813(24,0,c)+0.09409078(24,4,c)+0.08991604(24,8,c)- 0.02942963(24,12,c)-0.05887724(24,16,c)-0.00834422(24,20,c)-0.31408220(24,24,c)
24,3	0.29789301(2,2,c)+0.08753412(4,2,c)+0.03946952(5,2,s)+0.11787583(6,2,c)+0.17483811(6,6,c)+ 0.00537003(7,2,s)-0.00583784(7,6,s)+0.09656326(8,2,c)+0.07605503(8,6,c)-0.11247432(9,2,s)- 0.05403092(9,6,s)+0.02529639(10,2,c)+0.05577500(10,6,c)+0.05043347(10,10,c)- 0.03876473(11,2,s)+0.06969442(11,6,s)-0.01056309(11,10,s)-0.02806156(12,2,c)- 0.07125716(12,6,c)-0.10161846(12,10,c)-0.07518662(13,2,s)+0.03720244(13,6,s)- 0.07813966(13,10,s)+0.02776472(14,2,c)+0.03238670(14,6,c)+0.15447342(14,10,c)+ 0.05673742(14,14,c)-0.29586015(15,2,s)+0.15347964(15,6,s)+0.17864610(15,10,s)+ 0.10296527(15,14,s)-0.06369172(16,2,c)-0.02894389(16,6,c)-0.11954505(16,10,c)- 0.06421758(16,14,c)-0.24937156(17,2,s)+0.12210836(17,6,s)-0.19316177(17,10,s)- 0.12055513(17,14,s)+0.06956519(18,2,c)-0.00207814(18,6,c)+0.11687606(18,10,c)+ 0.20591934(18,14,c)+0.10019439(18,18,c)-0.21124364(19,2,s)+0.17212018(19,6,s)+ 0.02329926(19,10,s)+0.19640807(19,14,s)-0.02287058(19,18,s)-0.02042619(20,2,c)+ 0.03749722(20,6,c)-0.09865843(20,10,c)-0.14834480(20,14,c)-0.03362327(20,18,c)- 0.15674146(21,2,s)+0.08923401(21,6,s)+0.00754570(21,10,s)-0.06942222(21,14,s)- 0.14067026(21,18,s)+0.00656403(22,2,c)+0.01124875(22,6,c)+0.03518644(22,10,c)+

	0.01229191(22,14,c)+0.03754080(22,18,c)+0.02027481(22,22,c)-0.02521138(23,2,s)- 0.00351961(23,6,s)-0.02374203(23,10,s)+0.07664500(23,14,s)-0.04086941(23,18,s)+ 0.02837267(23,22,s)-0.33130577(24,2,c)-0.19312418(24,6,c)-0.03085889(24,10,c)- 0.05002341(24,14,c)-0.09696775(24,18,c)-0.01984793(24,22,c)
24,4	0.31124766(3,2,s)-0.04461842(6,2,c)+0.03008173(6,6,c)-0.09992669(7,2,s)-0.09191918(7,6,s)- 0.04358693(9,2,s)+0.09073344(9,6,s)+0.22198799(10,2,c)+0.04353543(10,6,c)- 0.15949097(10,10,c)+0.01819741(11,2,s)+0.01256110(11,6,s)+0.01609574(11,10,s)- 0.02295591(12,2,c)+0.09020583(12,6,c)-0.05691518(12,10,c)-0.02234137(13,2,s)+ 0.02216429(13,6,s)+0.03204951(13,10,s)-0.34825186(14,2,c)-0.11131384(14,6,c)- 0.00903469(14,10,c)+0.25855636(14,14,c)+0.06698960(15,2,s)-0.00540771(15,6,s)+ 0.09374831(15,10,s)+0.03789389(15,14,s)+0.01767163(16,2,c)-0.04575985(16,6,c)- 0.01781982(16,10,c)+0.03627049(16,14,c)-0.12243116(17,2,s)+0.07553681(17,6,s)+ 0.11770486(17,10,s)+0.14116734(17,14,s)+0.20704101(18,2,c)+0.08911460(18,6,c)+ 0.00639151(18,10,c)+0.00486921(18,14,c)-0.15936355(18,18,c)+0.19344482(19,2,s)- 0.05181514(19,6,s)+0.14652315(19,10,s)+0.24529286(19,14,s)+0.07909555(19,18,s)+ 0.00067875(20,2,c)-0.00133068(20,6,c)-0.00088033(20,10,c)-0.00012243(20,14,c)+ 0.00122690(20,18,c)-0.20100861(21,2,s)+0.09834708(21,6,s)+0.10264816(21,10,s)+ 0.21785194(21,14,s)+0.18435362(21,18,s)-0.03459572(22,2,c)-0.02992165(22,6,c)+ 0.01094133(22,10,c)+0.00883331(22,14,c)-0.01449181(22,18,c)+0.03029068(22,22,c)+ 0.10275760(23,2,s)-0.01550126(23,6,s)+0.04460411(23,10,s)+0.08595817(23,14,s)+ 0.10266497(23,18,s)+0.04238892(23,22,s)+0.00079774(24,2,c)-0.03744958(24,6,c)+ 0.16937359(24,10,c)-0.26098341(24,14,c)+0.15866379(24,18,c)-0.02965291(24,22,c)
24,5	0.35534213(4,0,c)+0.08324150(4,4,c)-0.04647044(5,4,s)+0.00658191(6,0,c)-0.01690247(6,4,c)+ 0.04497559(7,4,s)-0.04514960(8,0,c)-0.02503581(8,4,c)+0.00378440(8,8,c)+0.07410784(9,4,s)+ 0.11548873(9,8,s)-0.00386580(10,0,c)+0.01454210(10,4,c)-0.01428397(10,8,c)+ 0.08289530(11,4,s)+0.06775289(11,8,s)+0.27129340(12,0,c)+0.03331795(12,4,c)+ 0.07895439(12,8,c)+0.08690697(12,12,c)-0.01955140(13,4,s)-0.13640505(13,8,s)- 0.08102705(13,12,s)+0.10130947(14,0,c)-0.01634197(14,4,c)-0.07104674(14,8,c)- 0.12558276(14,12,c)-0.03612239(15,4,s)-0.04281698(15,8,s)-0.04734835(15,12,s)- 0.12670222(16,0,c)-0.09103205(16,4,c)+0.06192186(16,8,c)+0.22039490(16,12,c)- 0.20892540(16,16,c)+0.01684595(17,4,s)-0.08491918(17,8,s)-0.07079018(17,12,s)- 0.03473871(17,16,s)+0.29526714(18,0,c)-0.07843128(18,4,c)-0.03672854(18,8,c)- 0.31145766(18,12,c)-0.24495882(18,16,c)+0.05953292(19,4,s)+0.09260374(19,8,s)+ 0.02006670(19,12,s)+0.07694385(19,16,s)+0.01571797(20,0,c)+0.02947965(20,4,c)+ 0.01266813(20,8,c)+0.07966034(20,12,c)-0.07784233(20,16,c)+0.00008663(20,20,c)- 0.09969734(21,4,s)+0.12284784(21,8,s)+0.04073624(21,12,s)-0.06481011(21,16,s)- 0.02053493(21,20,s)+0.11887382(22,0,c)-0.04546562(22,4,c)+0.01928123(22,8,c)-

	0.07150843(22,12,c)-0.23337201(22,16,c)-0.00019840(22,20,c)-0.03755817(23,4,s)- 0.10011782(23,8,s)+0.09735385(23,12,s)+0.02075692(23,16,s)+0.01920867(23,20,s)+ 0.16022627(24,0,c)+0.06069435(24,4,c)+0.00578285(24,8,c)+0.06528319(24,12,c)- 0.24006350(24,16,c)+0.00007580(24,20,c)+0.19931780(24,24,c)
24,6	0.30210831(4,2,c)-0.08467719(5,2,s)-0.00018426(6,2,c)-0.00027330(6,6,c)-0.05548265(7,2,s)+ 0.06031600(7,6,s)-0.06008845(8,2,c)-0.00569504(8,6,c)+0.22538350(9,2,s)+0.10827073(9,6,s)- 0.01137045(10,2,c)+0.03552908(10,6,c)-0.00612781(10,10,c)-0.13591550(11,2,s)+ 0.01928836(11,6,s)+0.13860978(11,10,s)+0.09966509(12,2,c)+0.11299534(12,6,c)+ 0.13888978(12,10,c)-0.23483376(13,2,s)+0.01189590(13,6,s)-0.17192688(13,10,s)- 0.07894746(14,2,c)+0.03586339(14,6,c)+0.03978474(14,10,c)-0.08950492(14,14,c)+ 0.10093163(15,2,s)-0.01611893(15,6,s)-0.04286027(15,10,s)-0.07469430(15,14,s)+ 0.16543664(16,2,c)+0.04024477(16,6,c)-0.21518523(16,10,c)-0.13555108(16,14,c)- 0.15269026(17,2,s)+0.02833056(17,6,s)-0.00150368(17,10,s)-0.14633028(17,14,s)- 0.17799842(18,2,c)+0.00673271(18,6,c)+0.03853606(18,10,c)+0.02318920(18,14,c)- 0.22523202(18,18,c)-0.16354811(19,2,s)-0.03949446(19,6,s)+0.10652768(19,10,s)+ 0.00973863(19,14,s)+0.14657633(19,18,s)+0.07206753(20,2,c)-0.09743603(20,6,c)+ 0.15282576(20,10,c)-0.04937495(20,14,c)-0.04081861(20,18,c)-0.00695235(21,2,s)+ 0.01829903(21,6,s)-0.19453980(21,10,s)-0.11635447(21,14,s)+0.22847428(21,18,s)- 0.01843706(22,2,c)-0.06999056(22,6,c)-0.09627907(22,10,c)+0.10565081(22,14,c)+ 0.01634283(22,18,c)-0.07840907(22,22,c)-0.04260023(23,2,s)+0.11262485(23,6,s)+ 0.04971930(23,10,s)-0.11038405(23,14,s)+0.17576802(23,18,s)-0.10972601(23,22,s)- 0.14497317(24,2,c)-0.01045015(24,6,c)-0.03083578(24,10,c)+0.11084532(24,14,c)+ 0.22785259(24,18,c)+0.07675816(24,22,c)
24,7	0.33066491(4,4,c)+0.07078647(5,4,s)+0.00395212(6,0,c)-0.01123566(6,4,c)-0.06850943(7,4,s)+ 0.00651140(8,0,c)+0.00502350(8,4,c)-0.05621562(8,8,c)-0.11288537(9,4,s)-0.17591914(9,8,s)+ 0.00575532(10,0,c)-0.02196141(10,4,c)+0.02198427(10,8,c)-0.12627094(11,4,s)- 0.10320513(11,8,s)+0.00207888(12,0,c)+0.10245984(12,4,c)+0.13739219(12,8,c)+ 0.18070746(12,12,c)+0.02978183(13,4,s)+0.20778009(13,8,s)+0.12342511(13,12,s)+ 0.00094177(14,0,c)-0.13657317(14,4,c)-0.06504473(14,8,c)-0.01909166(14,12,c)+ 0.05502373(15,4,s)+0.06522131(15,8,s)+0.07212376(15,12,s)+0.00080141(16,0,c)- 0.32055256(16,4,c)+0.02130084(16,8,c)-0.04017308(16,12,c)+0.01912516(16,16,c)- 0.02566074(17,4,s)+0.12935383(17,8,s)+0.10783171(17,12,s)+0.05291602(17,16,s)- 0.00262602(18,0,c)-0.30973038(18,4,c)-0.11440804(18,8,c)-0.20485667(18,12,c)- 0.07450133(18,16,c)-0.09068399(19,4,s)-0.14105939(19,8,s)-0.03056676(19,12,s)- 0.11720534(19,16,s)+0.00354903(20,0,c)+0.00174613(20,4,c)-0.01494496(20,8,c)- 0.13357430(20,12,c)+0.10235740(20,16,c)+0.03634837(20,20,c)+0.15186477(21,4,s)- 0.18712896(21,8,s)-0.06205181(21,12,s)+0.09872253(21,16,s)+0.03127999(21,20,s)+

	0.00829905(22,0,c)-0.15188194(22,4,c)+0.09311948(22,8,c)-0.09795966(22,12,c)- 0.05234676(22,16,c)-0.08324604(22,20,c)+0.05721078(23,4,s)+0.15250527(23,8,s)- 0.14829503(23,12,s)-0.03161815(23,16,s)-0.02925975(23,20,s)+0.00258059(24,0,c)+ 0.27986436(24,4,c)-0.03270100(24,8,c)+0.16847006(24,12,c)+0.01077491(24,16,c)+ 0.03180692(24,20,c)-0.00064469(24,24,c)
24,8	0.21917668(5,2,s)-0.07636419(6,2,c)-0.11326639(6,6,c)-0.07055967(7,2,s)+0.07670645(7,6,s)+ 0.19662563(8,2,c)+0.22987652(8,6,c)+0.03222453(9,2,s)+0.01548016(9,6,s)-0.13652115(10,2,c)- 0.00073673(10,6,c)-0.19021849(10,10,c)-0.07547170(11,2,s)+0.03614984(11,6,s)+ 0.05711498(11,10,s)-0.04407586(12,2,c)+0.06569898(12,6,c)+0.12190478(12,10,c)+ 0.09184151(13,2,s)+0.26582275(13,6,s)-0.11981173(13,10,s)-0.05149080(14,2,c)+ 0.03004312(14,6,c)+0.02856013(14,10,c)-0.05542126(14,14,c)-0.08464033(15,2,s)- 0.08125335(15,6,s)-0.01134930(15,10,s)+0.16611135(15,14,s)-0.09656341(16,2,c)+ 0.10276476(16,6,c)-0.09512740(16,10,c)+0.12996184(16,14,c)+0.06340358(17,2,s)- 0.20373661(17,6,s)+0.19316650(17,10,s)+0.00294370(17,14,s)+0.10711896(18,2,c)- 0.12677229(18,6,c)+0.00731948(18,10,c)+0.12424837(18,14,c)+0.07236616(18,18,c)+ 0.00107006(19,2,s)+0.05632524(19,6,s)+0.24018022(19,10,s)-0.08851256(19,14,s)- 0.13615129(19,18,s)+0.07209823(20,2,c)+0.08250365(20,6,c)+0.10662992(20,10,c)- 0.04068136(20,14,c)+0.12204641(20,18,c)-0.06576929(21,2,s)+0.07640682(21,6,s)- 0.05660303(21,10,s)-0.07587451(21,14,s)+0.00870624(21,18,s)+0.00165339(22,2,c)- 0.20399501(22,6,c)-0.14606927(22,10,c)-0.16664797(22,14,c)-0.09951870(22,18,c)- 0.14587419(22,22,c)+0.10018707(23,2,s)+0.10415914(23,6,s)+0.00855267(23,10,s)+ 0.15646562(23,14,s)-0.13498488(23,18,s)-0.20413702(23,22,s)+0.00309040(24,2,c)+ 0.01085502(24,6,c)+0.14951309(24,10,c)+0.02913377(24,14,c)-0.08244835(24,18,c)+ 0.14280281(24,22,c)
24,9	0.21917668(5,4,s)+0.12778172(6,0,c)+0.04829695(6,4,c)+0.10422354(7,4,s)+0.21052940(8,0,c)- 0.11941103(8,4,c)-0.18144760(8,8,c)+0.01930715(9,4,s)+0.03008803(9,8,s)+0.18608346(10,0,c)+ 0.14179495(10,4,c)-0.00942224(10,8,c)+0.05584266(11,4,s)+0.08453701(11,8,s)+ 0.06721527(12,0,c)-0.10680254(12,4,c)-0.06922650(12,8,c)+0.02007055(12,12,c)+ 0.18410325(13,4,s)-0.14970166(13,8,s)+0.19273519(13,12,s)+0.03044982(14,0,c)+ 0.06918014(14,4,c)+0.01136797(14,8,c)-0.03998469(14,12,c)+0.18884157(15,4,s)+ 0.07574667(15,8,s)+0.00944360(15,12,s)+0.02591151(16,0,c)-0.04227514(16,4,c)- 0.18886037(16,8,c)+0.07351536(16,12,c)+0.04788580(16,16,c)-0.02032203(17,4,s)- 0.09290311(17,8,s)+0.26382120(17,12,s)-0.06484585(17,16,s)-0.08490556(18,0,c)- 0.00153113(18,4,c)-0.14269707(18,8,c)-0.09201916(18,12,c)+0.11060064(18,16,c)- 0.21472546(19,4,s)+0.06081782(19,8,s)-0.12960214(19,12,s)+0.14362909(19,16,s)+ 0.11474886(20,0,c)+0.00908054(20,4,c)-0.12910959(20,8,c)+0.03197369(20,12,c)- 0.03566307(20,16,c)-0.08781818(20,20,c)-0.01738970(21,4,s)+0.04442606(21,8,s)-

	0.04761257(21,12,s)-0.12097936(21,16,s)+0.00460501(21,20,s)+0.26832880(22,0,c)- 0.00726865(22,4,c)-0.00659035(22,8,c)-0.01881619(22,12,c)+0.09490178(22,16,c)+ 0.20112365(22,20,c)-0.24620563(23,4,s)-0.04004003(23,8,s)-0.20394558(23,12,s)+ 0.03874641(23,16,s)-0.00430760(23,20,s)+0.08343687(24,0,c)+0.00524308(24,4,c)- 0.18233860(24,8,c)+0.01359179(24,12,c)+0.06131559(24,16,c)-0.07684599(24,20,c)- 0.02084433(24,24,c)
24,10	0.08388712(6,0,c)-0.22194445(6,4,c)+0.13820994(8,0,c)+0.07350226(8,4,c)+0.11198977(8,8,c)+ 0.12216148(10,0,c)-0.17408629(10,4,c)-0.20720413(10,8,c)+0.04412599(12,0,c)+ 0.30724605(12,4,c)-0.39231571(12,8,c)+0.13403094(12,12,c)+0.01998993(14,0,c)- 0.02078869(14,4,c)-0.02230806(14,8,c)-0.02708716(14,12,c)+0.01701058(16,0,c)+ 0.01804862(16,4,c)+0.00147064(16,8,c)-0.00317499(16,12,c)+0.01740380(16,16,c)- 0.05573944(18,0,c)-0.00001112(18,4,c)+0.25070549(18,8,c)-0.17559000(18,12,c)+ 0.13458051(18,16,c)+0.07533120(20,0,c)+0.20473917(20,4,c)-0.00117768(20,8,c)- 0.08309151(20,12,c)-0.10569595(20,16,c)+0.13400484(20,20,c)+0.17615453(22,0,c)- 0.03931797(22,4,c)-0.40496878(22,8,c)-0.07536620(22,12,c)+0.10626839(22,16,c)- 0.30690162(22,20,c)+0.05477527(24,0,c)-0.08811635(24,4,c)-0.00497883(24,8,c)+ 0.12320661(24,12,c)+0.03319172(24,16,c)+0.11726198(24,20,c)-0.01368405(24,24,c)
24,11	0.19957921(6,2,c)-0.13455628(6,6,c)+0.13848575(7,2,s)+0.12738836(7,6,s)-0.13336600(9,2,s)+ 0.27762347(9,6,s)+0.01977721(10,2,c)+0.00387863(10,6,c)-0.01420927(10,10,c)- 0.05426244(11,2,s)-0.03745565(11,6,s)-0.04799552(11,10,s)-0.08291048(12,2,c)+ 0.32579891(12,6,c)-0.20556213(12,10,c)-0.09343305(13,2,s)+0.09269248(13,6,s)+ 0.13403311(13,10,s)+0.05451770(14,2,c)+0.01742582(14,6,c)+0.00141435(14,10,c)- 0.04047616(14,14,c)-0.01768360(15,2,s)-0.17244316(15,6,s)+0.16613214(15,10,s)- 0.08201033(15,14,s)-0.05251590(16,2,c)+0.13598742(16,6,c)+0.05295629(16,10,c)- 0.10778729(16,14,c)+0.07372555(17,2,s)-0.04548673(17,6,s)-0.07087947(17,10,s)- 0.08500810(17,14,s)-0.00343395(18,2,c)-0.01456336(18,6,c)+0.02634355(18,10,c)- 0.01641826(18,14,c)+0.00509535(18,18,c)-0.11335160(19,2,s)-0.18155180(19,6,s)- 0.03438192(19,10,s)+0.02356973(19,14,s)-0.15197298(19,18,s)+0.10110578(20,2,c)- 0.19821577(20,6,c)-0.13113224(20,10,c)-0.01823656(20,14,c)+0.18275597(20,18,c)- 0.08774140(21,2,s)-0.00122685(21,6,s)+0.18801531(21,10,s)-0.05030596(21,14,s)+ 0.13189922(21,18,s)-0.09003566(22,2,c)-0.18636679(22,6,c)+0.15051635(22,10,c)+ 0.09906389(22,14,c)-0.15772502(22,18,c)+0.10331512(22,22,c)+0.01288541(23,2,s)+ 0.24431177(23,6,s)+0.03104566(23,10,s)-0.10044870(23,14,s)-0.13503030(23,18,s)+ 0.14457966(23,22,s)-0.06270920(24,2,c)+0.10226503(24,6,c)+0.06766872(24,10,c)+ 0.05878800(24,14,c)-0.02057873(24,18,c)-0.10113982(24,22,c)
24,12	0.16966889(7,2,s)-0.18444953(7,6,s)-0.17721338(8,2,c)+0.15185292(8,6,c)+0.10893088(9,2,s)+ 0.05232870(9,6,s)-0.10202311(10,2,c)+0.22009216(10,6,c)-0.08192376(10,10,c)+

	0.09141114(11,2,s)+0.21606364(11,6,s)-0.27196282(11,10,s)-0.08880913(12,2,c)+ 0.01395911(12,6,c)+0.05794390(12,10,c)-0.01691959(13,2,s)+0.11507478(13,6,s)- 0.09137604(13,10,s)+0.00446780(14,2,c)-0.13566655(14,6,c)+0.18927771(14,10,c)- 0.04577563(14,14,c)+0.03818836(15,2,s)+0.05480569(15,6,s)+0.01417542(15,10,s)- 0.09475858(15,14,s)+0.00680446(16,2,c)-0.14294978(16,6,c)+0.21897145(16,10,c)- 0.07608316(16,14,c)-0.01355475(17,2,s)-0.05601810(17,6,s)+0.07202647(17,10,s)- 0.04183660(17,14,s)-0.07031713(18,2,c)+0.13965806(18,6,c)+0.03077903(18,10,c)- 0.06412665(18,14,c)-0.01398362(18,18,c)-0.05343255(19,2,s)-0.01983759(19,6,s)+ 0.08375821(19,10,s)-0.02520598(19,14,s)+0.04069374(19,18,s)+0.10133642(20,2,c)+ 0.14367868(20,6,c)-0.19929464(20,10,c)+0.02054522(20,14,c)-0.04117840(20,18,c)+ 0.14769734(21,2,s)+0.30445529(21,6,s)+0.07501290(21,10,s)-0.02386259(21,14,s)- 0.01494560(21,18,s)+0.16123535(22,2,c)-0.19616744(22,6,c)-0.20274571(22,10,c)+ 0.08173359(22,14,c)+0.03445676(22,18,c)+0.05625725(22,22,c)+0.13027898(23,2,s)- 0.03929019(23,6,s)-0.27815075(23,10,s)-0.10361416(23,14,s)+0.03876501(23,18,s)+ 0.07872666(23,22,s)+0.04003686(24,2,c)-0.09106704(24,6,c)+0.04579580(24,10,c)+ 0.05976103(24,14,c)+0.01742434(24,18,c)-0.05507275(24,22,c)
24,13	0.25061756(7,4,s)+0.19510551(8,4,c)-0.12805362(8,8,c)-0.06526536(9,4,s)-0.10170871(9,8,s)- 0.19604127(10,4,c)+0.16470761(10,8,c)+0.35397531(11,4,s)-0.06086665(11,8,s)+ 0.07535705(12,4,c)+0.03623147(12,8,c)-0.06669340(12,12,c)-0.06929356(13,4,s)+ 0.12217410(13,8,s)-0.04636756(13,12,s)-0.12198083(14,4,c)+0.19289938(14,8,c)- 0.06524827(14,12,c)+0.11079088(15,4,s)+0.03615161(15,8,s)-0.00778393(15,12,s)+ 0.07234671(16,4,c)-0.20347288(16,8,c)+0.16370896(16,12,c)-0.02796787(16,16,c)- 0.00838500(17,4,s)+0.07605442(17,8,s)-0.05837095(17,12,s)+0.03159306(17,16,s)+ 0.00289320(18,4,c)-0.10597661(18,8,c)-0.05664466(18,12,c)+0.12351502(18,16,c)- 0.01346641(19,4,s)-0.08221152(19,8,s)+0.02680567(19,12,s)-0.06997646(19,16,s)- 0.10118506(20,4,c)-0.06433850(20,8,c)+0.13867131(20,12,c)-0.16399610(20,16,c)+ 0.11066362(20,20,c)-0.16767433(21,4,s)-0.10841220(21,8,s)+0.01408729(21,12,s)+ 0.05894145(21,16,s)-0.27818488(21,20,s)+0.02985467(22,4,c)+0.20825832(22,8,c)+ 0.02100128(22,12,c)+0.08762795(22,16,c)-0.25344489(22,20,c)-0.18941519(23,4,s)+ 0.08842181(23,8,s)+0.05054028(23,12,s)-0.01887735(23,16,s)+0.26021812(23,20,s)+ 0.02628372(24,4,c)-0.05880503(24,8,c)-0.07195183(24,12,c)-0.01407340(24,16,c)+ 0.09683706(24,20,c)
24,14	0.45561901(9,4,s)-0.29236568(9,8,s)+0.18110681(13,4,s)+0.05255548(13,8,s)- 0.13217467(13,12,s)-0.12256185(15,4,s)+0.33124247(15,8,s)-0.20603835(15,12,s)+ 0.07039568(17,4,s)+0.03347216(17,8,s)+0.00365695(17,12,s)-0.05513798(17,16,s)+ 0.08386855(19,4,s)-0.14033892(19,8,s)-0.06946531(19,12,s)+0.12212683(19,16,s)- 0.27864907(21,4,s)-0.27914402(21,8,s)+0.12797287(21,12,s)-0.10286792(21,16,s)+

	0.26142513(21,20,s)-0.18604964(23,4,s)+0.21766349(23,8,s)+0.19329241(23,12,s)+ 0.03294581(23,16,s)-0.24454082(23,20,s)

Appendix F: Correlated Grain Boundary Distributions in Two-Dimensional Networks[10]

Correlations relating grain boundary species arise in polycrystalline materials even in the absence of correlations relating grain orientations due to the requirement for crystallographic consistency among the misorientations of grain boundaries. Although this need for consistency substantially influences the connectivity of grain boundary networks, the nature of the resulting correlations are generally only appreciated in an empirical sense. Here a rigorous treatment of this problem is presented for a model two-dimensional polycrystal with uncorrelated grain orientations, or equivalently, a cross-section through a three-dimensional polycrystal in which each grain shares a common crystallographic direction normal to the plane of the network. The distribution of misorientations θ, boundary inclinations φ, and the joint distribution of misorientations about a triple junction are derived for arbitrary crystal symmetry and orientation distribution functions of the grains. From these, general analytical solutions for the fraction of low angle boundaries and the triple junction distributions within the same subset of systems are found. The results agree with existing analysis of a few specific cases in the literature, but nevertheless present a significant generalization.

F.1. Introduction

The properties and behaviour of polycrystalline materials are strongly influenced by granular crystalline nature of their microstructure. Generally, the more information that a particular function provides about the microstructure, the more difficult it is to measure and to relate to actual material behaviour. As a result, it is a continuing challenge to express the microstructure in terms of a simple function that still captures enough of the relevant crystallographic information to allow reasonable predictions of material properties. This is especially true for the broad range of properties that depend on the character of grain boundaries, for which the classical orientation distribution function [4, 74, 111, 112] does not directly apply. Many of the physical properties of

[10] The content of this appendix has previously been published in Ref. [107].

grain boundaries appear to be principally related to their misorientation [5, 14, 20, 21, 75, 90, 95, 96, 108, 112-115], and determination of the distribution of this quantity is often the focus of grain boundary characterization (for further discussion, refer to Section 6). The coincidence site lattice (CSL) theory provides a specific model to understand the relationship connecting misorientation to physical properties, and is frequently used in the literature [108, 109]. A more refined analysis of boundary properties reveals a dependence on the orientation of the interface as well; interest in the distributions of boundary normals [116-118], the indices of the crystallographic planes meeting at an internal interface [119-123], and joint distributions of the misorientation and plane of a boundary [124-126] is increasing.

While these distributions provide significant information about individual grain boundaries in a microstructure, a number of investigations suggest that this description is insufficient for certain applications. For example, the connection between orientation and misorientation distributions is ambiguous; materials sharing a single orientation distribution function may exhibit different CSL misorientation fractions [99, 127]. Some findings suggest that this is due to neglect of orientation correlations of adjoining grains [99, 125, 127, 128], or to differences in the connection length for boundaries of a distinct type [129]. The development of theories to satisfactorily explain these variations in grain boundary character necessarily involves structures more complicated than a single grain boundary; any analysis must begin with the structures within which the observed correlations occur. Since a triple junction is the smallest segment of the boundary network more inclusive than a single grain boundary, this structure is a natural candidate. Analyses of triple junctions within the CSL theory reveal that the granular nature of the material sharply constrains the sets of misorientations allowed at these junctions [130-134]. In other words, there are necessary correlations in the misorientation distributions, even when the grain orientations are completely uncorrelated. The experimental importance of this constraint upon the properties of polycrystals was first emphasized by Kumar et al. [135]. Gertsman presented a particularly rigorous analysis of these correlations for ideal CSL misorientations, and further extended his analysis to higher order structures including quadruple nodes [136-138]. Alternatively, triple junctions and their effect on the connectivity of boundaries in the network have been investigated using

percolation theory [97, 98, 139-142], although studies on correlations in structures more complicated than triple junctions remain, for the most part, empirical observations [143-145].

The purpose of this paper is to develop a methodology for analyzing correlations in the quantities that uniquely specify the states of grain boundaries, for which the correlations arise purely from the granular nature of polycrystalline materials. Our approach differs from the pertinent literature described above in the sense that we do not classify the boundaries (e.g. by the CSL model) prior to examining the strength of the correlations. Rather, we perform classification as a subsequent step, since boundary classification reduces the available information and thereby obscures the effects of correlations. This further allows our results to be interpreted using classification schemes other than the one used herein. The approach is worked out in detail for an arbitrary two-dimensional polycrystal with no spatial correlation in grain orientations.

F.2. Defining the System

Our system consists of a two-dimensional polycrystal, in which the orientation of each grain is fully specified by a single rotation in the plane, through an angle ω relative to a fixed reference orientation. This construct also applies to a cross-section through a three-dimensional polycrystal in which each grain shares a common crystallographic direction **n** normal to the plane of the network, with ω the rotation about **n**. The area orientation distribution function is, for a uniform grain size, identical to the distribution of orientations of the crystallites [4], and expresses the probability that the orientation of a given grain is defined by ω. Similarly, the distribution in the orientations of the boundary planes is specified as a function of the angle ϕ, measured with respect to the same reference orientation. Assuming that there are no correlations among grain orientations and none relating the grain orientations to the boundary normal, this information is sufficient to determine the distribution function describing the types of grain boundaries present in the material. While a two-dimensional polycrystal is a significant simplification from the three-dimensional polycrystals typically studied in practice, the majority of the literature on grain boundary correlations currently focuses on

grain boundary types in two-dimensional cross-sections. The present treatment therefore allows ready comparison with the existing literature.

We represent the orientation distribution function $f(\omega)$ as a Fourier series with periodicity $\omega_s = 2\pi/k$, where an axis of k-fold rotational symmetry coincides with the **n** direction. This yields, for an arbitrary distribution function of the appropriate symmetry,

$$f(\omega) = \frac{1}{\omega_s} + \sum_{n=1}^{\infty} a_n \cos(kn\omega) + b_n \sin(kn\omega), \tag{192}$$

where the Fourier coefficients a_n and b_n prescribe the details of the preferred orientation. Notice that $f(\omega)$ is normalized over $-\omega_s/2 \le \omega < \omega_s/2$, since this range contains all unique crystallite orientations. Meanwhile, we shall constrain our attention to simple systems based on a single triple junction schematically represented in Figure 30, with the grains and boundaries labeled as A, B, and C in the manner depicted. Grain orientations and grain boundary descriptors will be labeled with these subscripts in some cases, e.g., ω_A denotes the orientation of grain A.

A single boundary is completely specified by the rotations ω and ω' of the adjacent grains and by the inclination ϕ, each measured with respect to the reference orientation. Although ω is a natural variable of the orientation distribution function

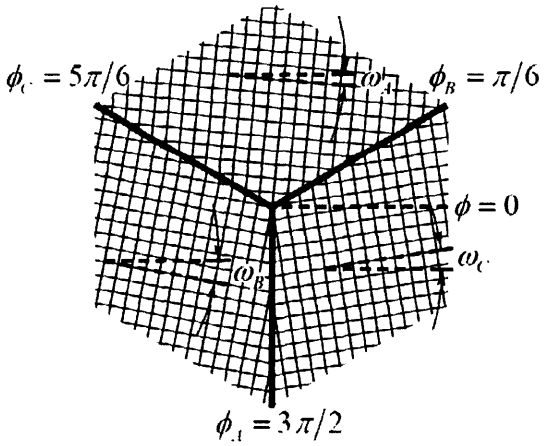

Figure 30: Representative triple junction depicting the physical significance of the quantities ω and ϕ. Grain A is rotated by the angle ω_A and is located opposite the boundary with orientation ϕ_A; a similar geometry applies for grains B and C.

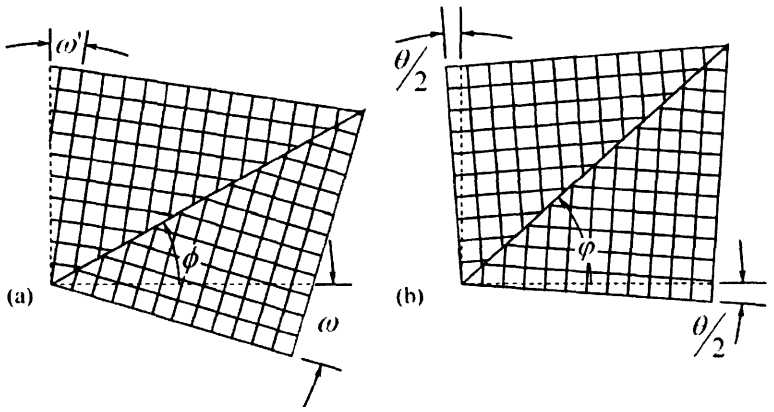

Figure 31: Comparison of the quantities used to define the state of a grain boundary. A single boundary is depicted in terms of (a) ω, ω' and ϕ and (b) θ and φ. Notice that in (b) the grains share the misorientation equally, resulting from a rotation of the system in (a).

describing the state of the grains, it is not a clear descriptor for a grain boundary. Since the properties of a grain boundary must remain invariant under an arbitrary rotation of the material, the natural quantities to describe a grain boundary must be defined with respect to the local crystal orientation. The misorientation of adjoining grains is given by

$$\theta = \omega' - \omega . \tag{193}$$

Meanwhile, following the notation of Read and Shockley [146], we define the orientation φ of the boundary plane in a manner that shares the misorientation equally between the grains, or

$$\varphi = \phi - \frac{\omega' + \omega}{2} . \tag{194}$$

These relationships may be derived from examination of Figure 31, which depicts a single boundary defined relative to the reference and crystal orientations.

Each grain orientation ω is symmetrically equivalent to the value $\omega + n\omega_s$ for any integer value of n, and similarly ω' is symmetrically equivalent to the value $\omega' + m\omega_s$ for any integer value of m. Then, according to Equation (194), θ is symmetrically equivalent to $\theta + \omega_s(m-n)$, and the distribution of θ displays a periodicity of ω_s. Similarly, φ is symmetrically equivalent to $\varphi - \omega_s(m+n)/2$, and the distribution of φ displays a

periodicity of $\omega_s/2$. However, when θ and φ refer to the same boundary and share values for the indices m and n, the periodicities change to $2\omega_s$ and ω_s, respectively. Since simple distributions, e.g. of the misorientation alone, display the periodicity corresponding to the first case, θ and φ shall be *defined* to fall within the ranges $-\omega_s/2 \le \theta < \omega_s/2$ and $-\omega_s/4+\phi \le \varphi < \omega_s/4+\phi$. As we shall see, in some cases this necessitates the application of further symmetries in order to enforce the required periodicity on joint distribution functions.

Crystallographic constraints impact the local grain boundary statistics only when considering the values of θ and φ for multiple boundaries simultaneously; in other words, the granular crystalline nature of the material generates spatial correlations in grain boundary character, despite the absence of correlations in grain orientations. For example, consider the grains and boundaries around a triple junction, as appears in Figure 32. The orientations ω of the three grains are specified independently. θ and φ for each boundary depend on the orientations of the adjoining grains, or alternatively, the orientation of a single grain influences the type of each of the adjoining boundaries. Therefore, the θ and φ for multiple boundaries may not be considered independently. Since these quantities uniquely specify the state of a grain boundary, and our purpose is to examine correlations in boundary character arising from the granular crystalline nature of the material, the remainder of this paper shall be devoted to finding distributions of

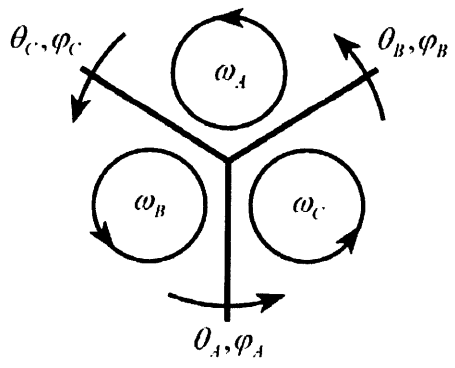

Figure 32: Labeling scheme for the grain rotations ω and the quantities θ and φ around a triple junction. The misorientations θ are the rotations that bring the grain at the tail of the arrow into coincidence with the grain at the head. Our labeling scheme differs in sense from some similar examples in the literature [97].

and correlations among the θ and φ given a set of grain orientations ω, each independently distributed according to the arbitrary orientation distribution function $f(\omega)$. The procedure for finding a joint distribution of a set of the quantities θ and φ is as follows:

i. Construct the function

$$F(\boldsymbol{\omega}) = f(\omega_1)f(\omega_2)\ldots f(\omega_n) \tag{195}$$

to provide the joint distribution of rotations ω_j of each of the n grains involved in the problem, where $\boldsymbol{\omega}$ is a vector quantity containing the n ω_j as elements. For example, $n = 2$ for a single grain boundary and $n = 3$ for a triple junction. Notice that this equation expressly forbids the introduction of correlations in grain orientations.

ii. State the equations relating the known grain rotations ω_j to the grain boundary character parameters; these desired quantities are called y_i, with each of the y_i denoting either a θ or a φ as in Equations (193) and (194). Examination of the definitions of θ and φ reveals that these are linear or affine functions of the grain rotations, suggesting a compact expression for the transformation equations as

$$\mathbf{y} = \boldsymbol{A}\boldsymbol{\omega}, \tag{196}$$

where $\mathbf{y}$ is a vector quantity containing the m y_i as elements and $\boldsymbol{A}$ is the m-by-n transformation matrix. Situations where $\boldsymbol{A}$ is affine will require the modification of $\boldsymbol{\omega}$ and $\mathbf{y}$ to conform with the use of homogenous coordinates by appending a constant term to these vectors.

iii. Determine the equations of the inverse transformation, relating the y_i to the ω_j. Provided the transformation matrix $\boldsymbol{A}$ is invertible, the equation containing the inverse transformation equations is

$$\boldsymbol{\omega} = \boldsymbol{A}^{-1}\mathbf{y}. \tag{197}$$

When the matrix $\boldsymbol{A}$ is not invertible, $\boldsymbol{A}$ must be decomposed by singular value decomposition (as discussed in Ref. [147]), and the noninvertible component removed by integration.

iv. Substitute the expressions for the ω_j in terms of the y_i into the joint probability distribution of the ω_j in Equation (195) to find the joint probability distribution of the desired quantities y_i. This amounts to a transformation of space, from one spanned by the ω_j to one spanned by the y_i, in which a single probability distribution function is embedded. Since this transformation generally includes a stretching component, the transformed probability density function must be multiplied by an appropriate factor to remain normalized; in situations where $\boldsymbol{A}$ is invertible, this factor is the magnitude of the determinant of $\boldsymbol{A}^{-1}$. Otherwise, the necessary multiplicative factor is found by multiplying the inverses of the singular values of $\boldsymbol{A}$.

v. Adjust the distribution function to account for symmetry defined to be present in the distributions of the y_i that is not captured by the inherent periodicity of the ω_j. Generally, this requires summing the derived distribution function with an equivalent distribution function shifted by an appropriate distance in the **y** space.

Since the full transformation procedure is often quite involved, a series of examples follow.

F.3. Distribution Functions for a Single Boundary

As defined above, a single boundary is uniquely specified by a pair of values θ and φ; the distribution function completely characterizing a single boundary is given by the joint probability distribution function of these quantities. We perform this derivation for the boundary type described by θ_A and φ_A, which depend exclusively on ω_B and ω_C, as indicated by Figure 32.

F.3.1. Joint Distribution of θ and φ

Step (*i*) is to construct the joint distribution function for ω_B and ω_C; reference to Equations (192) and (195) indicates that the relevant distribution function of the grain rotations is

$$F(\omega_B,\omega_C)=\frac{1}{\omega_s^2}+\frac{1}{\omega_s}\sum_{n=1}^{\infty}\left[a_n\{\cos(kn\omega_B)+\cos(kn\omega_C)\}+b_n\{\sin(kn\omega_B)+\sin(kn\omega_C)\}\right]$$
$$+\sum_{m=1}^{\infty}\sum_{n=1}^{\infty}\left[\{a_m\cos(km\omega_B)+b_m\sin(km\omega_B)\}\{a_n\cos(kn\omega_C)+b_n\sin(kn\omega_C)\}\right]. \tag{198}$$

To execute step (*ii*), we refer to Equations (193) and (194), which indicate that the desired quantities may be expressed in terms of the grain rotations as

$$\begin{pmatrix}\theta_A\\ \varphi_A\\ 1\end{pmatrix}=\begin{pmatrix}-1 & 1 & 0\\ -1/2 & -1/2 & \phi_A\\ 0 & 0 & 1\end{pmatrix}\begin{pmatrix}\omega_B\\ \omega_C\\ 1\end{pmatrix}. \tag{199}$$

Since the expression for φ_A includes a constant term, the transformation $\boldsymbol{A}$ contains a translational component; $\boldsymbol{A}$ is therefore affine instead of linear, and is expressed in matrix form using homogeneous coordinates. Since $\boldsymbol{A}$ is invertible, step (*iii*) is straightforward:

$$\begin{pmatrix}-1/2 & -1 & \phi_A\\ 1/2 & -1 & \phi_A\\ 0 & 0 & 1\end{pmatrix}\begin{pmatrix}\theta_A\\ \varphi_A\\ 1\end{pmatrix}=\begin{pmatrix}\omega_B\\ \omega_C\\ 1\end{pmatrix}. \tag{200}$$

from which we obtain $\omega_B=-\theta_A/2-\varphi_A+\phi_A$ and $\omega_C=\theta_A/2-\varphi_A+\phi_A$. Substitution of these equalities into Equation (198), and multiplication by the magnitude of the determinant of $\boldsymbol{A}^{-1}$ in Equation (200), completes step (*iv*). The joint distribution of θ and φ is

$$F(\theta,\varphi)=\frac{1}{\omega_s^2}+\frac{2}{\omega_s}\sum_{n=1}^{\infty}\left[\cos(kn\theta/2)\{a_n\cos(kn(\varphi-\phi))-b_n\sin(kn(\varphi-\phi))\}\right]$$
$$+\sum_{m=1}^{\infty}\sum_{n=1}^{\infty}\left[\{a_m\cos(km(\theta/2+\varphi-\phi))-b_m\sin(km(\theta/2+\varphi-\phi))\}\right.$$
$$\left.\times\{a_n\cos(kn(\theta/2-\varphi+\phi))+b_n\sin(kn(\theta/2-\varphi+\phi))\}\right] \tag{201}$$

where the subscript A has been dropped, since this result applies to any boundary with an arbitrary inclination ϕ in the external reference frame.

Recall that the periodicity of the ω implies the symmetric equivalence of θ with $\theta+\omega_s(m-n)$, and of φ with $\varphi-\omega_s(m+n)/2$. If these periodicities are independent of

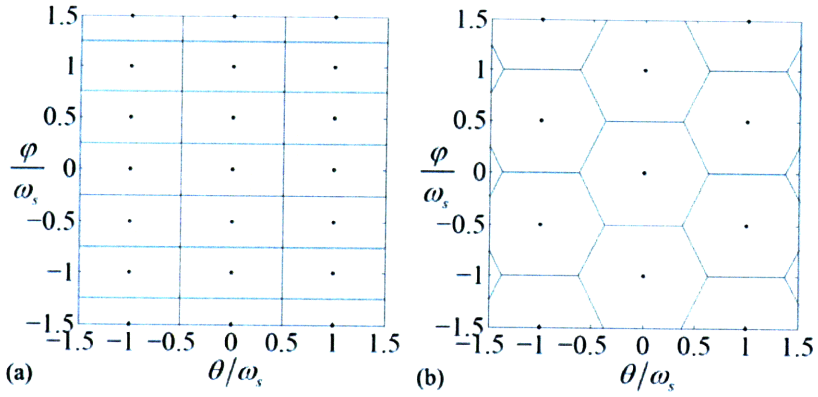

Figure 33: Lattices of symmetrically equivalent points and corresponding unit cells for θ and φ at a single grain boundary. (a) θ and φ display independent periodicities of ω_s and $\omega_s/2$, respectively, resulting in a rectangular lattice and simply described boundaries. (b) θ and φ display joint periodicities, leading to a sparser lattice, an extended range of unique quantity pairs, and more complicated boundaries.

one another (i.e., if m and n are independent), the symmetries of the system can be represented by the lattice of symmetrically equivalent points displayed in Figure 33a, which is consistent with the required boundary conditions on θ and φ. However, in the present case θ and φ refer to the same grain boundary, and the indices m and n are shared. Therefore, the symmetry of Equation (201) is represented by the lattice in Figure 33b; observe that this lattice misses some of the required symmetries in the definition of θ and φ, i.e., Figure 33b is of lower symmetry than is Figure 33a. Therefore, Equation (201) must be modified to incorporate the required symmetries. Examination of these figures indicates that the lattice in Figure 33a may be constructed by combining the lattice in Figure 33b with the equivalent lattice shifted in the θ direction by ω_s or in the φ direction by $\omega_s/2$; this leads to the equation

$$\mathcal{F}(\theta,\varphi)=F(\theta,\varphi)+F(\theta-\omega_s,\varphi)=F(\theta,\varphi)+F(\theta,\varphi-\omega_s/2), \tag{202}$$

where the symbol $\mathcal{F}$ denotes the final distribution function with the proper symmetry that is consistent with the specified periodicities. The conversion from the function F to $\mathcal{F}$ completes step (v) of the derivation.

F.3.2 Individual Distributions in θ and φ

The function $\mathcal{F}$ allows several sub-distributions to be determined. For example, the joint distribution function of θ and φ contains information specifying the distribution functions for θ and φ separately; these separate distributions may be found by integrating over the dependence of one or the other variable. The integration actually gives identical results for either F or $\mathcal{F}$, provided that the range of integration is specified as one period of the distribution in the dimension of the variable to be removed. While $\mathcal{F}$ is consistent with the preceding definitions of θ and φ, the integration is often simpler in F due to the nature of the trigonometric functions present.

The probability density function describing the distribution of misorientations θ is given by

$$\mathcal{F}(\theta) = \int_{-\omega_s/4+\phi}^{\omega_s/4+\phi} \mathcal{F}(\theta,\varphi)\,d\varphi = \frac{1}{2}\int_{-\omega_s/2+\phi}^{\omega_s/2+\phi} F(\theta,\varphi) + F(\theta-\omega_s,\varphi)\,d\varphi = \int_{-\omega_s/2+\phi}^{\omega_s/2+\phi} F(\theta,\varphi)\,d\varphi . \tag{203}$$

The trigonometric terms in this integral either vanish for all values of the indices m and n, or evaluate to constants for $m = n$ and vanish for other values, according to the relations provided in Appendix G. With simplification, this integral returns

$$\mathcal{F}(\theta) = \frac{1}{\omega_s} + \frac{\omega_s}{2}\sum_{n=1}^{\infty}\left(a_n^2 + b_n^2\right)\cos(kn\theta). \tag{204}$$

for the distribution of misorientation angles in the boundary network. Similarly, the distribution of boundary plane normals φ is found to be

$$\mathcal{F}(\varphi) = \int_{-\omega_s/2}^{\omega_s/2} \mathcal{F}(\theta,\varphi)\,d\theta = \frac{1}{2}\int_{-\omega_s}^{\omega_s} F(\theta,\varphi) + F(\theta,\varphi-\omega_s/2)\,d\theta = \int_{-\omega_s}^{\omega_s} F(\theta,\varphi)\,d\theta . \tag{205}$$

Following simplification with reference to Appendix G, this gives the function

$$\mathcal{F}(\varphi) = \frac{2}{\omega_s} + \omega_s\sum_{n=1}^{\infty}\left\{\left(a_n^2 - b_n^2\right)\cos(2kn(\varphi-\phi)) - 2a_n b_n \sin(2kn(\varphi-\phi))\right\}. \tag{206}$$

F.4. Triple Junction Misorientation Distribution

Within the literature, studies of the effects of crystallographic constraints on grain boundary networks frequently concentrate on the character and influence of the constraints on boundaries joining at triple junctions [97, 98, 130-133, 135-144, 148, 149]. The reason for this is probably related to the increasing difficulty of analysis with the extent of the boundary structure considered, and to the decrease in strength of the correlations in boundary character with the spatial separation of the boundaries [145]. Therefore, analyses of triple junctions provide descriptions of some of the more mathematically accessible correlations, and substantial information about the nature of the network. The analysis of correlations in grain boundary character around a triple junction is hence not only of practical interest, but provides an opportunity to compare the results derived using our method to those appearing in the literature. For the sake of simplicity, the joint distribution function of the three misorientations θ_A, θ_B and θ_C is determined, without consideration of the boundary plane inclinations.

Reference to Figure 32 reveals that the misorientations of the three boundaries around a triple junction depend on the rotations of the three grains meeting at the triple junction; that is, θ_A, θ_B and θ_C depend upon ω_A, ω_B and ω_C. The joint distribution function constructed in step (*i*) includes each of these grain rotations, and is found, as before, from Equations (192) and (195):

$$\begin{aligned}
F(\omega_A,\omega_B,\omega_C) = {} & \frac{1}{\omega_s^3} + \frac{1}{\omega_s^2}\sum_{n=1}^{\infty}\left[a_n\{\cos(kn\omega_A)+\cos(kn\omega_B)+\cos(kn\omega_C)\}\right. \\
& \left. + b_n\{\sin(kn\omega_A)+\sin(kn\omega_B)+\sin(kn\omega_C)\}\right] \\
& + \frac{1}{\omega_s}\sum_{m=1}^{\infty}\sum_{n=1}^{\infty}\left[\{a_m\cos(km\omega_A)+b_m\sin(km\omega_A)\}\{a_n\cos(kn\omega_B)+b_n\sin(kn\omega_B)\}\right. \\
& + \{a_m\cos(km\omega_B)+b_m\sin(km\omega_B)\}\{a_n\cos(kn\omega_C)+b_n\sin(kn\omega_C)\} \\
& \left. + \{a_m\cos(km\omega_C)+b_m\sin(km\omega_C)\}\{a_n\cos(kn\omega_A)+b_n\sin(kn\omega_A)\}\right] \\
& + \sum_{j=1}^{\infty}\sum_{m=1}^{\infty}\sum_{n=1}^{\infty}\left[\{a_j\cos(kj\omega_A)+b_j\sin(kj\omega_A)\}\{a_m\cos(km\omega_B)+b_m\sin(km\omega_B)\}\right. \\
& \left. \times\{a_n\cos(kn\omega_C)+b_n\sin(kn\omega_C)\}\right].
\end{aligned} \tag{207}$$

Transformation from a distribution of grain rotations to one of misorientations requires a description of the misorientations in terms of the grain rotations, as in step (*ii*). This appears in the form

$$\begin{pmatrix} \theta_A \\ \theta_B \\ \theta_C \end{pmatrix} = \begin{pmatrix} 0 & -1 & 1 \\ 1 & 0 & -1 \\ -1 & 1 & 0 \end{pmatrix} \begin{pmatrix} \omega_A \\ \omega_B \\ \omega_C \end{pmatrix}, \tag{208}$$

derived by use of Equation (193). Regrettably, the transformation matrix $\boldsymbol{A}$ is not invertible due to the linear dependence of the misorientations; a Frank-Nabarro circuit around the triple junction must start and finish in material of the same orientation, implying that the combination of the misorientations accumulated from grain to grain must be described by the identity operation [133]. Given two rotations, this constraint uniquely specifies the third. Since $\boldsymbol{A}$ is not invertible, we resort to singular value decomposition and piecewise application of the transformation components to perform steps (*iii*) and (*iv*), as outlined in Appendix H. This provides the probability distribution function

$$\begin{aligned} F(\theta_A,\theta_B,\theta_C) = \Bigg(& \frac{1}{\sqrt{3}\omega_s^2} + \frac{\sqrt{3}}{6}\sum_{n=1}^{\infty}\left[\left(a_n^2+b_n^2\right)\left\{\cos(kn\theta_A)+\cos(kn\theta_B)+\cos(kn\theta_C)\right\}\right] \\ & + \frac{\sqrt{3}\omega_s}{12}\sum_{m=1}^{\infty}\sum_{n=1}^{\infty}\left[\left\{a_{m+n}\left(a_m a_n - b_m b_n\right)+b_{m+n}\left(a_n b_m + a_m b_n\right)\right\}\right. \\ & \times\left\{\cos(km\theta_A - kn\theta_B)+\cos(km\theta_B - kn\theta_C)+\cos(km\theta_C - kn\theta_A)\right\} \\ & + \left\{a_{m+n}\left(a_n b_m + a_m b_n\right)-b_{m+n}\left(a_m a_n - b_m b_n\right)\right\} \\ & \left.\times\left\{\sin(km\theta_A - kn\theta_B)+\sin(km\theta_B - kn\theta_C)+\sin(km\theta_C - kn\theta_A)\right\}\right] \Bigg) \\ & \delta(\theta_A+\theta_B+\theta_C). \end{aligned} \tag{209}$$

Our definitions of θ_A, θ_B and θ_C require that the quantities display independent periodicities of period ω_s, as represented by the cubic lattice and cubic unit cell in Figure 34a. To perform step (*v*) and satisfy this requirement, we must initially determine the periodicity of F. As above, ω_A, ω_B and ω_C are symmetrically equivalent with $\omega_A + j\omega_s$, $\omega_B + m\omega_s$ and $\omega_C + n\omega_s$, respectively, where j, m and n are integers. From equation (17), this implies the symmetric equivalence of θ_A, θ_B and θ_C with $\theta_A + \omega_s(-m+n)$, $\theta_B + \omega_s(j-n)$ and $\theta_C + \omega_s(-j+m)$, respectively. Systematically varying the allowed

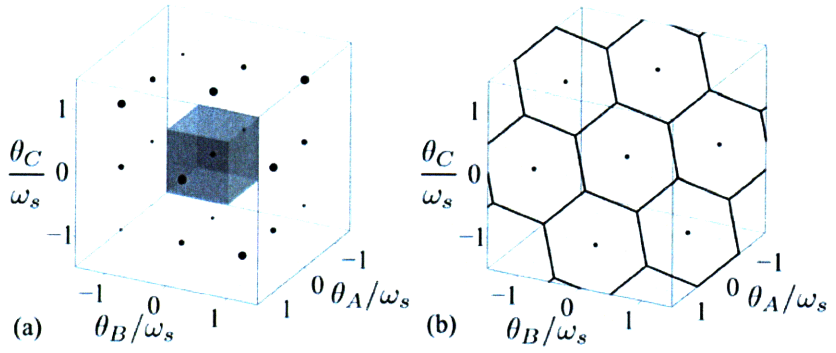

Figure 34: Lattices of symmetrically equivalent points and corresponding unit cells for θ_A, θ_B and θ_C at a triple junction. (a) θ_A, θ_B and θ_C each display independent periodicities of ω_s, resulting in a cubic lattice. The size of the markers indicates the relative positions of points residing in the three (111) type planes shown. (b) The three misorientations display joint periodicities, such that the lattice resides entirely in the (111) plane and each lattice point satisfies the constraint $\theta_A + \theta_B + \theta_C = 0$.

values of j, m, and n results in a lattice of symmetrically equivalent points in the (111) plane, i.e. the $\theta_A + \theta_B + \theta_C = 0$ plane, as displayed in Figure 34b. Examination of these figures indicates that the lattice in Figure 34a may be constructed by imposing the necessary infinite translational symmetry on the lattice in Figure 34b, or

$$\mathcal{F}(\theta_A, \theta_B, \theta_C) = \sum_{-\infty}^{\infty} F(\theta_A, \theta_B, \theta_C + n\omega_s). \tag{210}$$

Practically speaking, though, $\mathcal{F}$ need only include those terms that contribute probability density to the unit cell centered about the origin. Since the terms of Equation (210) represent distributions on parallel (111) planes, only those planes that pass through the cubic unit cell of edge length ω_s centered on the origin need be retained. Only three of the planes included in Equation (210) satisfy this condition, reducing the expression for $\mathcal{F}$ to

$$\mathcal{F}(\theta_A, \theta_B, \theta_C) = F(\theta_A, \theta_B, \theta_C - \omega_s) + F(\theta_A, \theta_B, \theta_C) + F(\theta_A, \theta_B, \theta_C + \omega_s), \tag{211}$$

giving the joint distribution function for the misorientations around a triple junction, for arbitrary textures described by Equation (192).

F.5. Derived Quantities

In order to better appreciate the correlations in grain boundary networks, the full information content of the distributions $\mathcal{F}$ may be reduced to a few, easily understood parameters by applying a classification criterion to separate the boundaries into discrete types. Although any classification scheme dependent on the boundary misorientation may be used with the above distributions, we restrict ourselves to two types of quantities appearing frequently in the literature pertaining to this problem. These are the special fraction p-the fraction of boundaries within the networks whose disorientation falls below a threshold value θ_t-and the triple junction fractions J_3, J_2, J_1 and J_0-the fractions of triple junctions coordinated by the subscripted number of special boundaries. In this section we derive these quantities from Equation (204) and Equation (211), respectively.

F.5.1. Special Fraction

The fraction of boundaries with disorientation less than the threshold angle θ_t is given by the integral

$$p = \int_{-\theta_t}^{\theta_t} \mathcal{F}(\theta) d\theta, \tag{212}$$

with the constraint $0 \le \theta_t < \omega_s/2$, since this spans the unique range of the disorientation θ. Performing this integral using Equation (204) for $\mathcal{F}(\theta)$ gives

$$p = \frac{2\theta_t}{\omega_s} + \frac{\omega_s^2}{2\pi} \sum_{n=1}^{\infty} \frac{1}{n} \left(a_n^2 + b_n^2\right) \sin(kn\theta_t). \tag{213}$$

F.5.2. Triple Junction Fractions

Determining the fractions of triple junctions is rather more involved, since the joint distribution of misorientations around a triple junction must be manipulated rather than the distribution of a single misorientation. The steps required to determine the triple junction populations are:

i. Specify the disorientation θ_t that separates low disorientation special boundaries from high disorientation general boundaries. θ_t is by definition unsigned, and must fall within the range $0 \le \theta_t < \omega_s/2$.

ii. Classify every region within the fundamental zone of the joint misorientation distribution in terms of the number of misorientations θ_A, θ_B and θ_C in that region smaller in magnitude than the threshold disorientation θ_t. Within a particular region this provides the number of special boundaries coordinating a given triple junction, or equivalently the subscript of the triple junction fraction to which probability density falling within this region contributes. An example of this classification is performed for Equation (211) in Figure 35a and for Equation (209) in Figure 35b for the case of $0 \le \theta_t < \omega_s/3$, where white regions containing no special boundaries contribute to J_0, and the three successive shades of grey

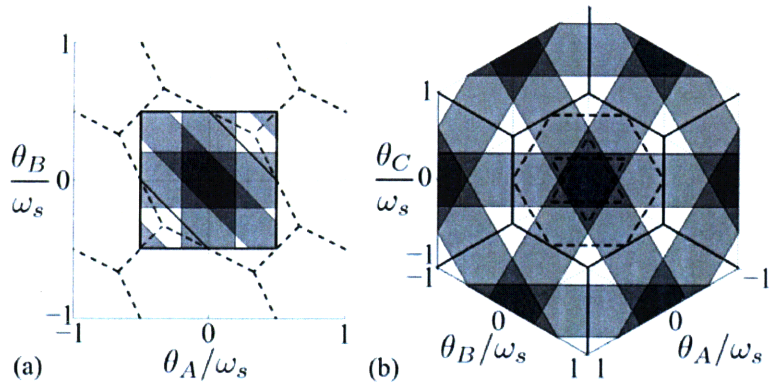

Figure 35: Representation of the distribution functions for misorientations about a triple junction. Triple junctions are classified by the number of misorientations smaller in magnitude than θ_t; for this figure, $0 \le \theta_t < \omega_s/3$. Darker shading corresponds to more special boundaries, e.g., white is a J_0 region, and dark grey is a J_3 region. Solid lines indicate unit cell borders in the current representation, and dashed lines in the alternate representation. (a) Classification of triple junctions as defined by Equation (211). For clarity of representation, the distribution is projected into the plane spanned by θ_A and θ_B. This representation is preferred for integration due to the simplicity of the equations of the region boundaries. (b) Classification of the triple junction distribution defined by Equation (209). Bands of special boundaries occur in a high symmetry configuration, and classification is continued outside of the fundamental zone to emphasize this symmetry. The three regions in dashed lines correspond to the three parallel planes that intersect the unit cell appearing in Figure 34a.

contribute to J_1, J_2 and J_3 respectively.

iii. Integrate the surface distribution function over the ranges specified above, and construct the triple junction fractions by summing the results from regions of the same special boundary coordination. Integration over a single region is performed by parameterizing the surface in θ_A and θ_B, or

$$\int_S \mathcal{F}(\mathbf{y})dA = \iint_{\theta} \mathcal{F}(\mathbf{y}(\theta_A,\theta_B))\left|\frac{\partial \mathbf{y}}{\partial \theta_A}\times\frac{\partial \mathbf{y}}{\partial \theta_B}\right| d\theta_A d\theta_B\,, \tag{214}$$

where $\mathbf{y} = \theta_A \mathbf{y}_1 + \theta_B \mathbf{y}_2 + \theta_C \mathbf{y}_3$ is expressed as a function of θ_A and θ_B alone using the equation of the surface, $\theta_A + \theta_B + \theta_C = 0$. The magnitude of the cross product of the partial derivatives of $\mathbf{y}$ appearing in Equation (225) is a numerical factor related to the ratio of a unit surface area to the projected area in the plane spanned by θ_A and θ_B, and in this case, is a constant equal to $\sqrt{3}$.

For the sake of brevity, we omit the equations for the boundaries of the regions within the fundamental zone, as well as the integral equations leading to the derivation of the triple junction fractions. The final results of this analysis appear in Appendix I, where we present a complete analytical solution for the triple junction distribution for arbitrary texture functions. The reader will notice that these expressions satisfy several physically necessary constraints; for example, since every triple junction must be one of J_3, J_2, J_1 or J_0, the sum of these quantities must be unity, or

$$J_3 + J_2 + J_1 + J_0 = 1\,. \tag{215}$$

A further constraint arises when each boundary in the system may be uniquely assigned to a single triple junction, namely, that the triple junction fractions must be consistent with the fraction of special boundaries around that junction, i.e.,

$$J_3 + 2J_2/3 + J_1/3 = p\,. \tag{216}$$

F.6. Comparison with Prior Literature

The majority of investigations into correlated grain boundary structures consider two-dimensional networks similar to our system [97, 98, 139, 142-145]; this restriction is

due principally to the complexity of the three-dimensional case. Of these, only the works of Frary and Schuh [97] and Van Siclen [98] provide analytical solutions for the special fraction and triple junction fractions of correlated networks. The present solution is exact for arbitrary two-dimensional polycrystals, and therefore more general as compared with these studies. When specific simplifying assumptions are used, the results of [97, 98] can be recovered. In this section, we demonstrate agreement with their results by simplifying our expression for the special fraction to a form that corresponds with their solutions, and further by numerical evaluation and comparison of triple junction fractions.

F.6.1. Simplification for Sharp Textures

Our decision to represent $f(\omega)$ in Equation (192) as a Fourier series allows us to predict grain boundary character distributions for arbitrary orientation distribution functions, and naturally captures the effect of the k-fold rotational axis consistent with any chosen crystal symmetry. For certain situations, the above distributions may be converted to integrals, and potentially evaluated to provide simple, closed-form expressions. The necessary, though not sufficient, conditions for this to be done while maintaining accurate distributions are:

i. A closed-form analytic expression for $f(\omega)$, the orientation distribution function, exists and is readily available.
ii. The texture is sufficiently sharp that any distributions of probability density arising from symmetrically equivalent points do not impinge on the fundamental zone of the distribution being converted.

As an example of the procedure, we shall convert the orientation distribution function in Equation (192) to integral form. By condition (*i*), the Fourier coefficients may be calculated as analytic functions of n; that is, a_n and b_n in Equation (192) may be expressed as $a(n)$ and $b(n)$, respectively. This allows the Fourier series representation of the orientation distribution function to be written as

$$f(\omega) = \frac{k}{2\pi} + \sum_{n=1}^{\infty} \{a(n)\cos(kn\omega) + b(n)\sin(kn\omega)\}\Delta n, \tag{217}$$

where Δn is the difference in magnitude of successive values of n, in this case unity. We then perform the substitution $kn = m$, giving the equation

$$f(\omega) = \frac{k}{2\pi} + \sum_{m=k}^{\infty} \left\{ \frac{1}{k} a\left(\frac{m}{k}\right) \cos(m\omega) + \frac{1}{k} b\left(\frac{m}{k}\right) \sin(m\omega) \right\} \Delta m, \tag{218}$$

where m is an integer multiple of k. Now, allow the period of the function to approach infinity, or equivalently, allow k to approach arbitrarily small values. While this effectively removes any symmetrically equivalent points, the distribution within the fundamental zone of $-\omega_s/2 \le \omega < \omega_s/2$ remains unchanged by condition (*ii*). Δm, of magnitude k, becomes a differential quantity, and $f'(\omega) = \lim_{k \to 0} f(\omega)$ becomes the integral

$$f'(\omega) = \int_0^{\infty} a'(n) \cos(n\omega) + b'(n) \sin(n\omega) dn, \tag{219}$$

where the index m is relabeled as n, and we define $a'(n)$ and $b'(n)$ in terms of the Fourier coefficients $a(n)$ and $b(n)$ as $a'(n) = \lim_{k \to 0} a(n/k)/k$ and $b'(n) = \lim_{k \to 0} b(n/k)/k$. The existence of nonzero values of $a'(n)$ and $b'(n)$ for some value of n is implied by the normalization of $f(\omega)$, i.e., that $f'(\omega)$ is nonzero somewhere in the range $-\omega_s/2 \le \omega < \omega_s/2$. Notice that neither k nor ω_s appear explicitly in Equation (219); by removing all symmetrically equivalent points, the distribution function is made independent of crystal symmetry.

Although the above example is circular, deriving an integral form for $f'(\omega)$ given the existence and availability of a closed-form analytic expression for $f(\omega)$, the utility of this procedure lies in the ability to derive integral forms for other distribution functions in terms of $a'(n)$ and $b'(n)$. For instance, applying this procedure to Equation (213) gives an expression for the special fraction of the network:

$$p' = 2\pi \int_0^{\infty} \left\{ a'(n)^2 + b'(n)^2 \right\} \frac{1}{n} \sin(n\theta_t) dn, \tag{220}$$

where the prime symbol denotes quantities derived for sharp textures. Comparison of this result with the expressions provided by Frary and Schuh or Van Siclen requires the evaluation of Equation (220) using the Fourier coefficients that describe their orientation

distribution functions. Since they define ω to be uniformly distributed on the interval $-\omega_{\max} \le \omega < \omega_{\max}$, the appropriate Fourier coefficients are

$$a(n) = \frac{1}{\pi n \omega_{\max}} \sin(kn\omega_{\max}) \qquad (221)$$
$$b(n) = 0 .$$

Evaluation and simplification of Equation (220) using these Fourier coefficients provides the piecewise function

$$p' = \begin{cases} 1 & 0 \le \omega_{\max} < \theta_t/2 \\ \dfrac{\theta_t}{\omega_{\max}} - \dfrac{1}{4}\left(\dfrac{\theta_t}{\omega_{\max}}\right)^2 & \theta_t/2 < \omega_{\max} \end{cases}, \qquad (222)$$

which is quite similar to the results in the literature. For comparison, our Equation (213) and the simplification Equation (222) appear along with the solutions by Frary and Schuh [97] and Van Siclen [98] in Figure 36.

The three regions of Figure 36 separated by vertical dashed lines correspond to three distinct physical situations, and are identifiable by considering the limiting values of the misorientation. Equation (193) and the orientation distribution function reveal that misorientations exist only from -2$\omega_{\max}$ to 2$\omega_{\max}$, or equivalently within 2$\omega_{\max}$ of any of the symmetrically equivalent points occurring at integer multiples of ω_s. For sharp textures where 2$\omega_{\max}$ is smaller than the threshold disorientation θ_t, or $0 \le \omega_{\max} < \theta_t/2$, every boundary in the network is special. The upper limit of this region is denoted by the vertical dashed line at small values of $\omega_{\max}$. For weak textures, the distributions centered on other multiples of ω_s begin to contribute to the probability that a misorientation is smaller than θ_t, and the symmetry of the crystal influences the special fraction. This occurs when $\omega_s - 2\omega_{\max}$ is less than θ_t, or for $\omega_s/2 - \theta_t/2 < \omega_{\max}$; the lower bound of the region is denoted by the vertical dashed line at higher values of $\omega_{\max}$.

Frary and Schuh [97] and Van Siclen [98] separately derived the expression for p shown by the dashed grey line in Figure 36. This solution is accurate for $\theta_t/2 \le \omega_{\max} < \omega_s/2 - \theta_t/2$, and within this range the special fraction is independent of crystal symmetry exactly as claimed by Frary and Schuh [97]. However, Frary and

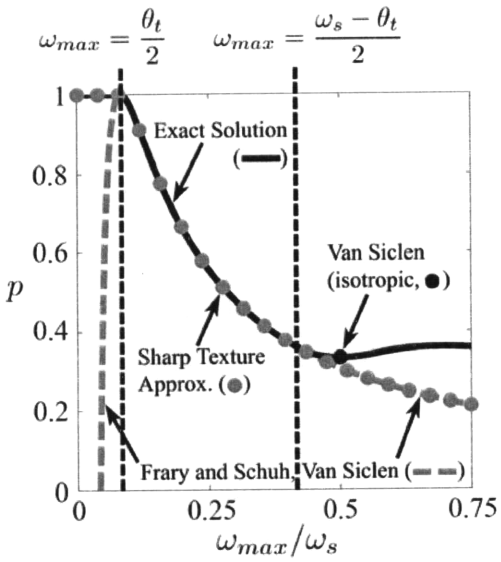

Figure 36: Analytic solutions for the special fraction of boundaries in correlated boundary networks, for the specific case where ω is uniformly distributed on the interval $-\omega_{\max} \le \omega < \omega_{\max}$, and $\theta_t = \omega_s/6$ with ω_s the angle of rotational symmetry of the crystallites. Our exact solution (Equation (213)) is given by the solid black line, and is valid over the full range of $\omega_{\max}/\omega_s$. The vertical dashed lines appear at $\omega_{\max} = \theta_t/2$ and $\omega_{\max} = \omega_s/2 - \theta_t/2$. The solutions of Frary and Schuh [97] and Van Siclen [98] are represented by the dashed grey line, which deviates for $\omega_{\max} < \theta_t/2$ and excludes the effects of crystal symmetry for $\omega_s/2 - \theta_t/2 < \omega_{\max}$. A further result for $\omega_{\max} = \omega_s/2$, found by Van Siclen, is denoted by the black dot. Equation (222), our simplification for sharp textures, is shown by the series of grey points.

Schuh as well as Van Siclen neglected the component of the piecewise solution for $\omega_{\max} < \theta_t/2$, which Equation (222) includes. Furthermore, neither the solution by Frary and Schuh and Van Siclen nor Equation (222) consider contributions from symmetrically equivalent distributions, and hence deviate from the crystallographically consistent special fraction for $\omega_s/2 - \theta_t/2 < \omega_{\max}$. Van Siclen acknowledged this, and with an independent calculation found the value of the special fraction for $\omega_{\max} = \omega_s/2$, or in his terminology, for an isotropic polycrystal [98]. Notice that our exact solution, expressed in Equation (213) and given in Figure 36 by the dark solid line, is physically reasonable for $0 \le \omega_{\max} < \omega_s/2 - \theta_t/2$, incorporates the effects of crystal symmetry for

$\omega_s/2-\theta_t/2<\omega_{\max}$, and includes the result provided by Van Siclen for an isotropic crystal.

F.6.2. Numerical Evaluation of Triple Junction Fractions

Triple junction fractions contain significant information about the structure of special boundary clusters; in particular, the presence or absence of J_2 junctions in a boundary network influences the fraction of special boundaries necessary to develop a percolating cluster [97], and presumably affects a variety of intergranular phenomena.

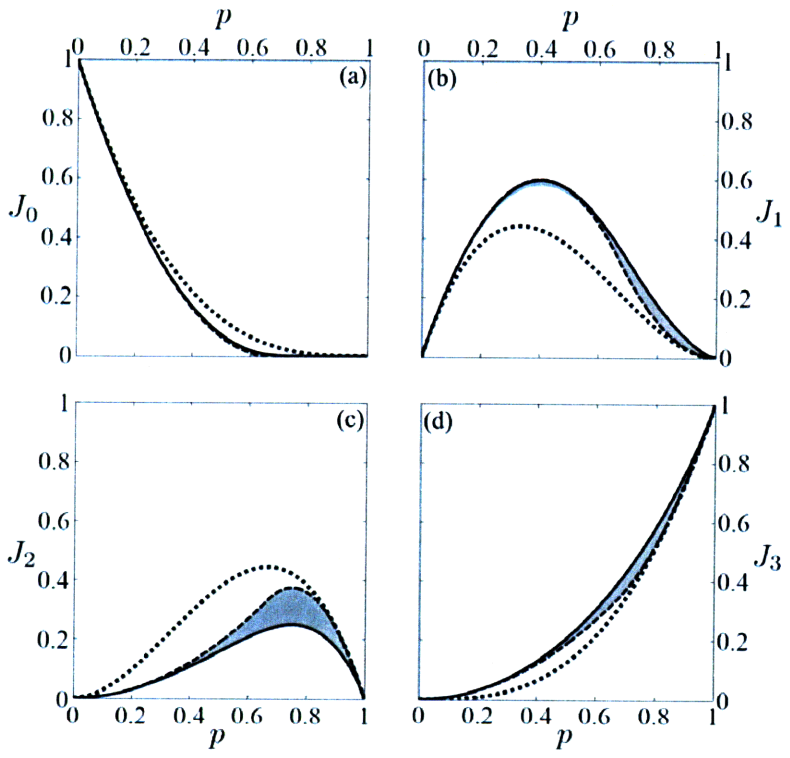

Figure 37: Triple junction fractions plotted as a function of the special boundary fraction in correlated boundary networks, for the specific case where ω is distributed uniformly on the interval $-\omega_{\max} \le \omega < \omega_{\max}$. For comparison, the dotted lines show the predicted triple junction fractions for a random (uncorrelated) spatial distribution of misorientations. Solutions by Frary and Schuh [97] and Van Siclen [98] for $\omega_{\max} < \omega_s/2-\theta_t/2$ appear as the solid lines, and the specific case derived by Van Siclen for $\omega_{\max} = \omega_s/2$ is given by the dashed lines. Our solutions, presented in Appendix I, migrate continuously over the regions shaded in grey with changes in the values of ω_s and θ_t.

Frary and Schuh [97] and Van Siclen [98] developed closed-form, analytical solutions for the triple junction fractions with an orientation distribution function distributed uniformly on the interval $-\omega_{\max} \le \omega < \omega_{\max}$. These author's results for $0 \le \omega_{\max} < \omega_s/2 - \theta_t/2$ are identical and appear in Figure 37 as the dark, solid line. A second solution found by Van Siclen for $\omega_{\max} = \omega_s/2$ is denoted by the heavy dashed line. For comparison, the fractions in a random polycrystal without crystallographic consistency are given as dotted lines. Imposing the requirement of crystallographic consistence clearly affects the triple junction fractions, and through them, the topology of the boundary network.

For comparison with our results, we use the Fourier coefficients of Equation (221) to numerically evaluate the equations presented in Appendix I. By independently varying the threshold disorientation θ_t over $0 \le \theta_t < \omega_s/2$ and $\omega_{\max}$ over $0 \le \omega_{\max} < 2\omega_s$, we find a continuous range of allowable triple junction fractions, shown in Figure 37 as the shaded grey region. Although Frary and Schuh and Van Siclen developed equations within the allowable range of values, they do not describe the boundaries of our results. While this subtle effect is difficult to see in Figure 37, our results for this specific texture include those of Frary and Schuh [97] and Van Siclen [98], the transitional solutions between theirs, and further allowable triple junction fractions outside of their equations.

F.7. Conclusions

The analysis of correlations in grain boundary distributions is critical to understanding intergranular and transgranular phenomena, and is presumably of interest for those investigating any material behaviour strongly affected by boundary character. Our contribution in this appendix is an analytical method to describe and determine correlations in grain boundary character arising solely from the requirement for crystallographic consistency in polycrystals with uncorrelated grain orientations. For the specific case of two-dimensional or two-dimensionally textured polycrystals, we present an exact solution for the misorientation correlations at triple junctions. Extension of the method to more complex structures, e.g. grain clusters of more than three boundaries, quadruple nodes in three dimensional structures with the required texture, etc., is possible using the same approach. Our results differ from prior analytical work along these lines

in a few respects. Most notably, our expression of distribution functions as Fourier series provides a general solution equally pertinent to all allowed textures and crystal systems, thereby avoiding the necessity of lengthy derivations for individual instances. Furthermore, the prior literature almost exclusively examines correlations in *classification* of boundaries arising from the granular nature of the material, particularly in terms of the triple junction fractions of "special" and "general" boundaries. Our analysis instead considers correlations among the *quantities* describing the boundaries, e.g. misorientation angles. This allows classification to be performed as a distinct, secondary step, and thereby clarifies the nature and extent of correlations in the structure.

Appendix G: Definite Trigonometric Integrals[11]

Integration of texture functions expressed using the Fourier series representation in Appendix F generally requires integration of trigonometric functions over intervals corresponding to a single period. The values of these definite integrals may be found by expansion of the trigonometric terms as complex exponentials, followed by evaluation of the integral of each exponential independently. A reference for integrals of trigonometric terms used in Appendix F follows, omitting the integrals of odd functions, which vanish identically:

$$\int_{-\pi}^{\pi} \cos(nx)dx = 0 \tag{223}$$

$$\int_{-\pi}^{\pi} \cos(mx)\cos(nx)dx = \pi\delta_{mn} \tag{224}$$

$$\int_{-\pi}^{\pi} \sin(mx)\sin(nx)dx = \pi\delta_{mn} \tag{225}$$

$$\int_{-\pi}^{\pi} \cos(jx)\cos(mx)\cos(nx)dx = \frac{\pi}{2}\left(\delta_{m+n,j} + \delta_{j+n,m} + \delta_{j+m,n}\right) \tag{226}$$

$$\int_{-\pi}^{\pi} \cos(jx)\sin(mx)\sin(nx)dx = \frac{\pi}{2}\left(-\delta_{m+n,j} + \delta_{j+n,m} + \delta_{j+m,n}\right) \tag{227}$$

where the indices j, m, and n are positive integers and δ is the Kronecker delta.

[11] The content of this appendix has previously been published in Ref. [107].

Appendix H: Singular Value Decomposition[12]

The matrix $\boldsymbol{A}$ in Equation (208) is not invertible due to the mutual dependence of the misorientations on the rotation angles. Performing singular value decomposition on $\boldsymbol{A}$ results in the factorization

$$\boldsymbol{A} = \boldsymbol{U}\boldsymbol{\Sigma}\boldsymbol{V}^T = \begin{pmatrix} 1/\sqrt{6} & -1/\sqrt{2} & 1/\sqrt{3} \\ 1/\sqrt{6} & 1/\sqrt{2} & 1/\sqrt{3} \\ -2/\sqrt{6} & 0 & 1/\sqrt{3} \end{pmatrix} \begin{pmatrix} \sqrt{3} & 0 & 0 \\ 0 & \sqrt{3} & 0 \\ 0 & 0 & 0 \end{pmatrix} \begin{pmatrix} 1/\sqrt{2} & -1/\sqrt{2} & 0 \\ 1/\sqrt{6} & 1/\sqrt{6} & -2/\sqrt{6} \\ 1/\sqrt{3} & 1/\sqrt{3} & 1/\sqrt{3} \end{pmatrix} \tag{228}$$

where the transformation $\boldsymbol{A}$ is expressed in terms of an orthogonal matrix $\boldsymbol{V}$, a matrix $\boldsymbol{\Sigma}$ that contains the singular values of $\boldsymbol{A}$ and performs a stretching of space, and a further orthogonal matrix $\boldsymbol{U}$; a single transformation $\boldsymbol{A}$ is now replaced by three component transformations. The columns of $\boldsymbol{V}$ and $\boldsymbol{U}$ form orthonormal bases for the $\boldsymbol{\omega}$ and $\mathbf{y}$ spaces, respectively.

We now consider these transformations in order. The initial component of the desired transformation in Equation (228) is a change in coordinates from ω_A, ω_B and ω_C to v_1, v_2 and v_3, the columns of $\boldsymbol{V}$. This transformation is performed by the matrix $\boldsymbol{V}^T$, and is given explicitly by

$$\begin{pmatrix} v_1 \\ v_2 \\ v_3 \end{pmatrix} = \begin{pmatrix} 1/\sqrt{2} & -1/\sqrt{2} & 0 \\ 1/\sqrt{6} & 1/\sqrt{6} & -2/\sqrt{6} \\ 1/\sqrt{3} & 1/\sqrt{3} & 1/\sqrt{3} \end{pmatrix} \begin{pmatrix} \omega_A \\ \omega_B \\ \omega_C \end{pmatrix}. \tag{229}$$

Inversion of this equation provides the functional relations $\omega_A = v_1/\sqrt{2} + v_2/\sqrt{6} + v_3/\sqrt{3}$, $\omega_B = -v_1/\sqrt{2} + v_2/\sqrt{6} + v_3/\sqrt{3}$, and $\omega_C = -2v_2/\sqrt{6} + v_3/\sqrt{3}$. Since $\boldsymbol{V}$ is an orthogonal matrix the distribution will remain normalized during direct substitution of the above equalities into Equation (207); this completes one component of the transformation $\boldsymbol{A}$.

The remaining components of the transformation $\boldsymbol{A}$ appear as

[12] The content of this appendix has previously been published in Ref. [107].

$$\begin{pmatrix}\theta_A\\ \theta_B\\ \theta_C\end{pmatrix}=\begin{pmatrix}1/\sqrt{6} & -1/\sqrt{2} & 1/\sqrt{3}\\ 1/\sqrt{6} & 1/\sqrt{2} & 1/\sqrt{3}\\ -2/\sqrt{6} & 0 & 1/\sqrt{3}\end{pmatrix}\begin{pmatrix}\sqrt{3} & 0 & 0\\ 0 & \sqrt{3} & 0\\ 0 & 0 & 0\end{pmatrix}\begin{pmatrix}v_1\\ v_2\\ v_3\end{pmatrix}. \tag{230}$$

Examination of $\boldsymbol{\Sigma}$ reveals that the nullspace of the transformation $\boldsymbol{A}$ is spanned by a unit vector pointing along v_3; the dependence of $F(v_1, v_2, v_3)$ on this quantity must be removed by integration before the remaining transformation may proceed. To determine the limits of integration, recall the symmetric equivalence of ω_A, ω_B and ω_C with $\omega_A + j\omega_s$, $\omega_B + m\omega_s$ and $\omega_C + n\omega_s$, respectively, where j, m and n are integers. From Equation (229), this implies the symmetric equivalence of v_1, v_2 and v_3 with $v_1 + (j-m)\omega_s/\sqrt{2}$, $v_2 + (j+m-2n)\omega_s/\sqrt{6}$ and $v_3 + (j+m+n)\omega_s/\sqrt{3}$, respectively. Notice that setting the values of j, m and n each to unity shifts the value of v_3 by the smallest amount that simultaneously leaves the values of v_1 and v_2 invariant; hence, the distribution is periodic in v_3 with a period of $\sqrt{3}\omega_s$, and the dependence on v_3 may be removed by integrating over this range. The appropriate integral is therefore

$$F(v_1, v_2) = \int_{-\sqrt{3}\omega_s/2}^{\sqrt{3}\omega_s/2} F(v_1, v_2, v_3)\,dv_3. \tag{231}$$

Performing this integral, with reference to the integrals of trigonometric functions in Appendix G, allows the joint distribution function of v_1 and v_2 to be expressed by

$$\begin{aligned}F(v_1, v_2) = {} & \frac{\sqrt{3}}{\omega_s^2} + \frac{\sqrt{3}}{2}\sum_{n=1}^{\infty}\Big[\left(a_n^2 + b_n^2\right)\Big\{\cos\left(\sqrt{2}knv_1\right) + \cos\left(kn\left(v_1 + \sqrt{3}v_2\right)/\sqrt{2}\right)\\ & + \cos\left(kn\left(v_1 - \sqrt{3}v_2\right)/\sqrt{2}\right)\Big\}\Big] + \frac{\sqrt{3}\omega_s}{4}\sum_{m=1}^{\infty}\sum_{n=1}^{\infty}\Big[\left\{a_{m+n}\left(a_m a_n - b_m b_n\right) + b_{m+n}\left(a_n b_m + a_m b_n\right)\right\}\\ & \times\Big\{\cos\left(\sqrt{2}kmv_1 + kn\left(v_1 + \sqrt{3}v_2\right)/\sqrt{2}\right) + \cos\left(\sqrt{2}kmv_1 + kn\left(v_1 - \sqrt{3}v_2\right)/\sqrt{2}\right)\\ & + \cos\left(km\left(v_1 + \sqrt{3}v_2\right)/\sqrt{2} - kn\left(v_1 - \sqrt{3}v_2\right)/\sqrt{2}\right)\Big\}\\ & + \left\{a_{m+n}\left(a_n b_m + a_m b_n\right) - b_{m+n}\left(a_m a_n - b_m b_n\right)\right\}\Big\{-\sin\left(\sqrt{2}kmv_1 + kn\left(v_1 + \sqrt{3}v_2\right)/\sqrt{2}\right)\\ & + \sin\left(\sqrt{2}kmv_1 + kn\left(v_1 - \sqrt{3}v_2\right)/\sqrt{2}\right) + \sin\left(km\left(v_1 + \sqrt{3}v_2\right)/\sqrt{2} - kn\left(v_1 - \sqrt{3}v_2\right)/\sqrt{2}\right)\Big\}\Big].\end{aligned} \tag{232}$$

At this point, the remaining v_1 and v_2 must be found in terms of the misorientations θ_A, θ_B and θ_C. Our procedure is similar to the construction of the pseudoinverse $\boldsymbol{A}^+$, as

explained in, e.g. Ref. [147]. Recall the decomposition of $\boldsymbol{A}$ and the subsequent completion of the transformation $\boldsymbol{V}^T$; this situation is expressed mathematically by

$$\mathbf{y} = \boldsymbol{A}\boldsymbol{\omega} = \boldsymbol{U}\boldsymbol{\Sigma}\boldsymbol{V}^T\boldsymbol{\omega} = \boldsymbol{U}\boldsymbol{\Sigma}\mathbf{v}. \tag{233}$$

Left multiplication of the sides of this equation by $\boldsymbol{U}^T$ and $\boldsymbol{\Sigma}^+$, defined as the matrix $\boldsymbol{\Sigma}^T$ with the nonzero diagonal values inverted, provides the equation

$$\boldsymbol{\Sigma}^+\boldsymbol{U}^T\mathbf{y} = \boldsymbol{\Sigma}^+\boldsymbol{U}^T\boldsymbol{U}\boldsymbol{\Sigma}\mathbf{v} = \boldsymbol{\Sigma}^+\boldsymbol{\Sigma}\mathbf{v}, \tag{234}$$

where $\boldsymbol{U}^T\boldsymbol{U} = \boldsymbol{I}$ since $\boldsymbol{U}$ is orthogonal. Explicit evaluation using the matrices provided in Equation (228) gives the matrix equation

$$\begin{pmatrix} \sqrt{2}/6 & \sqrt{2}/6 & -\sqrt{2}/3 \\ -1/\sqrt{6} & 1/\sqrt{6} & 0 \\ 0 & 0 & 0 \end{pmatrix}\begin{pmatrix} \theta_A \\ \theta_B \\ \theta_C \end{pmatrix} = \begin{pmatrix} 1 & 0 & 0 \\ 0 & 1 & 0 \\ 0 & 0 & 0 \end{pmatrix}\begin{pmatrix} v_1 \\ v_2 \\ v_3 \end{pmatrix}, \tag{235}$$

from which $v_1 = \sqrt{2}\,\theta_A/6 + \sqrt{2}\,\theta_B/6 - \sqrt{2}\theta_C/3$ and $v_2 = -\theta_A/\sqrt{6} + \theta_B/\sqrt{6}$. We point out that an expression for v_3 is not necessary, since integration already removed the dependence of F on this quantity. Substituting these relations into Equation (232), and multiplication by the product of the nonzero diagonal values of $\boldsymbol{\Sigma}^+$, in this case 1/3, results in the equation

$$\begin{aligned} F(\theta_A,\theta_B,\theta_C) = \Bigg(& \frac{\sqrt{3}}{3\omega_s^2} + \frac{\sqrt{3}}{6}\sum_{n=1}^{\infty}\Big[\left(a_n^2 + b_n^2\right)\Big\{\cos\left(kn\left(-2\theta_A + \theta_B + \theta_C\right)/3\right) \\ & + \cos\left(kn\left(\theta_A - 2\theta_B + \theta_C\right)/3\right) + \cos\left(kn\left(\theta_A + \theta_B - 2\theta_C\right)/3\right)\Big\}\Big] \\ & + \frac{\sqrt{3}\omega_s}{12}\sum_{m=1}^{\infty}\sum_{n=1}^{\infty}\Big[\Big\{a_{m+n}\left(a_m a_n - b_m b_n\right) + b_{m+n}\left(a_n b_m + a_m b_n\right)\Big\} \\ & \times \Big\{\cos\left(km\left(-2\theta_A + \theta_B + \theta_C\right)/3 - kn\left(\theta_A - 2\theta_B + \theta_C\right)/3\right) \\ & + \cos\left(km\left(\theta_A - 2\theta_B + \theta_C\right)/3 - kn\left(\theta_A + \theta_B - 2\theta_C\right)/3\right) \\ & + \cos\left(km\left(\theta_A + \theta_B - 2\theta_C\right)/3 - kn\left(-2\theta_A + \theta_B + \theta_C\right)/3\right)\Big\} \\ & + \Big\{a_{m+n}\left(a_n b_m + a_m b_n\right) - b_{m+n}\left(a_m a_n - b_m b_n\right)\Big\} \\ & \times \Big\{\sin\left(km\left(-2\theta_A + \theta_B + \theta_C\right)/3 - kn\left(\theta_A - 2\theta_B + \theta_C\right)/3\right) \\ & + \sin\left(km\left(\theta_A - 2\theta_B + \theta_C\right)/3 - kn\left(\theta_A + \theta_B - 2\theta_C\right)/3\right) \\ & + \sin\left(km\left(\theta_A + \theta_B - 2\theta_C\right)/3 - kn\left(-2\theta_A + \theta_B + \theta_C\right)/3\right)\Big\}\Big]\Bigg)\delta\left(\theta_A + \theta_B + \theta_C\right) \end{aligned} \tag{236}$$

for the joint probability distribution of the misorientations around a triple junction. The Dirac delta function reduces F from a volumetric probability distribution to a surface probability distribution; to understand appearance of this term, recall that for a circuit around a triple junction, the combination of the misorientations accumulated from grain to grain must be described by the identity operation. Mathematically, this is expressed in our current system as

$$\theta_A + \theta_B + \theta_C = 0 . \tag{237}$$

This requires the allowable sets of misorientations, considered as vectors in **y** space, to contain no component in the [111] direction. This is actually apparent directly from Equation (228); since the column vector of $\boldsymbol{U}$ spanning the left nullspace, or the subspace unreachable by the transformation $\boldsymbol{A}$, points in this direction, a surface probability density function must result. The constraint expressed by the Dirac delta function allows the expression for $F(\theta_A, \theta_B, \theta_C)$ to be considerably simplified, to the form appearing in Equation (209).

Appendix I: Triple Junction Fractions[13]

Following the procedure outlined in Section F.5.2 provides the equations for the triple junction fractions J_3, J_2, J_1 and J_0 in terms of the Fourier coefficients a_n and b_n, and the threshold angle θ_t. Due to the disappearance of certain regions and the appearance of others when $\theta_t = \omega_s/3$, the form of the equations depends to a certain extent on the choice of the threshold angle. For $0 \le \theta_t < \omega_s/3$,

$$\begin{aligned} J_3 = {} & \frac{3\theta_t^2}{\omega_s^2} + \frac{3\omega_s^2}{4\pi^2}\sum_{n=1}^{\infty}\left[\frac{1}{n^2}\left(a_n^2+b_n^2\right)\left\{1-\cos(kn\theta_t)+kn\theta_t\sin(kn\theta_t)\right\}\right] \\ & + \frac{3\omega_s^3}{4\pi^2}\sum_{m=1}^{\infty}\sum_{n=1}^{\infty}\left[\frac{1}{(m+n)m}\left\{a_{m+n}\left(a_m a_n - b_m b_n\right)+b_{m+n}\left(a_n b_m + a_m b_n\right)\right\}\right. \\ & \left.\times\left\{\cos(kn\theta_t)-\cos(k(m+n)\theta_t)\right\}\right] \end{aligned} \tag{238}$$

$$\begin{aligned} J_2 = {} & \frac{3\theta_t^2}{\omega_s^2} + \frac{3\omega_s^2}{4\pi^2}\sum_{n=1}^{\infty}\left[\frac{1}{n^2}\left(a_n^2+b_n^2\right)\left\{-2+3\cos(kn\theta_t)-\cos(2kn\theta_t)\right.\right. \\ & \left.+kn\theta_t\sin(kn\theta_t)\right\}] + \frac{3\omega_s^3}{4\pi^2}\sum_{m=1}^{\infty}\sum_{n=1}^{\infty}\left[\frac{1}{(m+n)m}\left\{a_{m+n}\left(a_m a_n - b_m b_n\right)\right.\right. \\ & \left.+b_{m+n}\left(a_n b_m + a_m b_n\right)\right\}\left\{-2\cos(kn\theta_t)+2\cos(k(m+n)\theta_t)+\cos(k(m-n)\theta_t)\right. \\ & \left.\left.-\cos(k(2m+n)\theta_t)\right\}\right] \end{aligned} \tag{239}$$

$$\begin{aligned} J_1 = {} & \frac{3\theta_t(2\omega_s-5\theta_t)}{\omega_s^2} + \frac{3\omega_s^2}{4\pi^2}\sum_{n=1}^{\infty}\left[\frac{1}{n^2}\left(a_n^2+b_n^2\right)\left\{1-3\cos(kn\theta_t)+2\cos(2kn\theta_t)+\right.\right. \\ & \left.n(2\pi-5k\theta_t)\sin(kn\theta_t)\right\}] + \frac{3\omega_s^3}{4\pi^2}\sum_{m=1}^{\infty}\sum_{n=1}^{\infty}\left[\frac{1}{(m+n)m}\left\{a_{m+n}\left(a_m a_n - b_m b_n\right)\right.\right. \\ & \left.+b_{m+n}\left(a_n b_m + a_m b_n\right)\right\}\left\{\cos(kn\theta_t)-\cos(k(m+n)\theta_t)-2\cos(k(m-n)\theta_t)\right. \\ & \left.\left.+2\cos(k(2m+n)\theta_t)\right\}\right] \end{aligned} \tag{240}$$

[13] The content of this appendix has previously been published in Ref. [107].

$$J_0 = \frac{(\omega_s - 3\theta_t)^2}{\omega_s^2} + \frac{3\omega_s^2}{4\pi^2}\sum_{n=1}^{\infty}\left[\frac{1}{n^2}(a_n^2 + b_n^2)\{\cos(kn\theta_t) - \cos(2kn\theta_t) + n(3k\theta_t - 2\pi)\sin(kn\theta_t)\} + \frac{3\omega_s^3}{4\pi^2}\sum_{m=1}^{\infty}\sum_{n=1}^{\infty}\left[\frac{1}{(m+n)m}\{a_{m+n}(a_m a_n - b_m b_n) + b_{m+n}(a_n b_m + a_m b_n)\}\{\cos(k(m-n)\theta_t) - \cos(k(2m+n)\theta_t)\}\right]\right] \quad (241)$$

Otherwise, when $\omega_s/3 \le \theta_t < \omega_s/2$, the equations

$$J_3 = 1 + \frac{6\theta_t(2\theta_t - \omega_s)}{\omega_s^2} + \frac{3\omega_s^2}{2\pi^2}\sum_{n=1}^{\infty}\left[\frac{1}{n^2}(a_n^2 + b_n^2)\sin(kn\theta_t)\{2kn\theta_t - n\pi + \sin(kn\theta_t)\}\right] + \frac{3\omega_s^3}{4\pi^2}\sum_{m=1}^{\infty}\sum_{n=1}^{\infty}\left[\frac{1}{(m+n)m}\{a_{m+n}(a_m a_n - b_m b_n) + b_{m+n}(a_n b_m + a_m b_n)\} \times \{\cos(kn\theta_t) - \cos(k(m+n)\theta_t) + \cos(k(m-n)\theta_t) - \cos(k(2m+n)\theta_t)\}\right] \quad (242)$$

$$J_2 = -3 + \frac{6\theta_t(3\omega_s - 4\theta_t)}{\omega_s^2} + \frac{3\omega_s^2}{2\pi^2}\sum_{n=1}^{\infty}\left[\frac{1}{n^2}(a_n^2 + b_n^2)\sin(kn\theta_t)\{-4kn\theta_t + 3n\pi - 2\sin(kn\theta_t)\}\right] + \frac{3\omega_s^3}{2\pi^2}\sum_{m=1}^{\infty}\sum_{n=1}^{\infty}\left[\frac{1}{(m+n)m}\{a_{m+n}(a_m a_n - b_m b_n) + b_{m+n}(a_n b_m + a_m b_n)\}\{-\cos(kn\theta_t) + \cos(k(m+n)\theta_t) - \cos(k(m-n)\theta_t) + \cos(k(2m+n)\theta_t)\}\right] \quad (243)$$

$$J_1 = \frac{3(\omega_s - 2\theta_t)^2}{\omega_s^2} + \frac{3\omega_s^2}{2\pi^2}\left[\sum_{n=1}^{\infty}\frac{1}{n^2}(a_n^2 + b_n^2)\sin(kn\theta_t)\{2kn\theta_t - 2n\pi + \sin(kn\theta_t)\}\right] + \frac{3\omega_s^3}{4\pi^2}\left[\sum_{m=1}^{\infty}\sum_{n=1}^{\infty}\frac{1}{(m+n)m}\{a_{m+n}(a_m a_n - b_m b_n) + b_{m+n}(a_n b_m + a_m b_n)\}\{\cos(kn\theta_t) - \cos(k(m+n)\theta_t) + \cos(k(m-n)\theta_t) - \cos(k(2m+n)\theta_t)\}\right] \quad (244)$$

$$J_0 = 0 \quad (245)$$

are used instead.

References

[1] Mason JK, Schuh CA. Representations of Texture. In: Schwartz AJ, Kumar M, Adams BL, Field DP, editors. Electron Backscatter Diffraction in Materials Science. Springer, 2009. p.35.

[2] Lewis AC, Jordan KA, Geltmacher AB. Determination of critical microstructural features in an austenitic stainless steel using image-based finite element modeling. Metallurgical and Materials Transactions A-Physical Metallurgy and Materials Science 2008;39A:1109.

[3] Morawiec A. Orientations and rotations: computations in crystallographic textures. Berlin ; New York: Springer, 2004.

[4] Bunge HJ. Texture analysis in materials science: mathematical methods. Gottingen: Cuvillier Verlag, 1993.

[5] Grimmer H. A Unique Description of the Relative Orientation of Neighboring Grains. Acta Cryst A 1980;36:382.

[6] Neumann P. The Role of Geodesic and Stereographic Projections for the Visualization of Directions, Rotations, and Textures. Physica Status Solidi a-Applied Research 1992;131:555.

[7] Wenk HR, Kocks UF. The Representation of Orientation Distributions. Metall Trans A 1987;18:1083.

[8] Wigner EP. Group theory and its application to the quantum mechanics of atomic spectra. New York,: Academic Press, 1959.

[9] Hopf H. Systeme symmetrischer Bilinearformen und euklidische Modelle der projektiven Räume. Vierteljschr Naturforsch Gesellschaft Zurich 1940;85:165.

[10] Stuelpnagel J. On the Parameterization of the Three-Dimensional Rotation Group. SIAM Rev 1964;6:422.

[11] Euler L. Formulae generales pro translatione quacunque corporum rigidorum. Novi Comm Acad Sci Imp Petrop 1776;20:189.

[12] Frank FC. Orientation Mapping. Metall Trans A 1988;19:403.

[13] Altmann SL. Rotations, quaternions, and double groups. Oxford: Clarendon Press, 1986.

[14] Morawiec A, Field DP. Rodrigues parameterization for orientation and misorientation distributions. Philos Mag A 1996;73:1113.

[15] Heinz A, Neumann P. Representation of Orientation and Disorientation Data for Cubic, Hexagonal, Tetragonal and Orthorhombic Crystals. Acta Cryst A 1991;47:780.

[16] Diamond R. A Note on the Rotational Superposition Problem. Acta Cryst A 1988;44:211.

[17] Morawiec A, Pospiech J. Some Information on Quaternions Useful in Texture Calculations. Texture Microstruct 1989;10:211.

[18] Neumann P. Representation of Orientation of Symmetrical Objects by Rodrigues Vectors. Texture Microstruct 1991;14-18:53.

[19] Meister L, Schaeben H. A concise quaternion geometry of rotations. Math Method Appl Sci 2005;28:101.

[20] Handscomb DC. On the Random Disorientation of Two Cubes. Canadian J Math 1957;10:85.
[21] Grimmer H. Disorientations and Coincidence Rotations for Cubic Lattices. Acta Cryst A 1974;30:685.
[22] Grimmer H. Comments on an Asymmetric Domain for Intercrystalline Misorientation in Cubic Materials in the Space of Euler Angles. Acta Cryst A 1989;45:Fc1.
[23] Becker R, Panchanadeeswaran S. Crystal Rotations Represented as Rodrigues Vectors. Texture Microstruct 1989;10:167.
[24] Humbert M, Gey N, Muller J, Esling C. Determination of a mean orientation from a cloud of orientations. Application to electron back-scattering pattern measurements. Journal of Applied Crystallography 1996;29:662.
[25] Glez JC, Driver J. Orientation distribution analysis in deformed grains. Journal of Applied Crystallography 2001;34:280.
[26] Sutton AP. Statistical representation and analysis of orientational data. Phil Mag Lett 1996;74:389.
[27] Schaeben H. Texture approximation or texture modelling with components represented by the von Mises-Fisher matrix distribution on SO(3) and the Bingham distribution on SO(4). Journal of Applied Crystallography 1996;29:516.
[28] Kunze K, Schaeben H. The Bingham distribution of quaternions and its spherical radon transform in texture analysis. Mathematical Geology 2004;36:917.
[29] Morawiec A. The Rotation Rate Field and Geometry of Orientation Space. Journal of Applied Crystallography 1990;23:374.
[30] Kumar A, Dawson PR. Polycrystal plasticity modeling of bulk forming with finite elements over orientation space. Computational Mechanics 1995;17:10.
[31] Grimmer H. Coincidence Rotations for Cubic Lattices. Scripta Metall Mater 1973;7:1295.
[32] Grimmer H. The Generating Function for Coincidence Site Lattices in the Cubic System. Acta Cryst A 1984;40:108.
[33] Pokorny A, Herzig P, Altmann SL. On the generation of point groups in spaces of various dimensions. Spectrochimica Acta Part a-Molecular and Biomolecular Spectroscopy 2001;57:1931.
[34] Funda J, Taylor RH, Paul RP. On Homogeneous Transforms, Quaternions, and Computational-Efficiency. IEEE Transactions on Robotics and Automation 1990;6:382.
[35] Siemens M, Hancock J, Siminovitch D. Beyond Euler angles: Exploiting the angle-axis parametrization in a multipole expansion of the rotation operator. Solid State Nucl Mag 2007;31:35.
[36] Gilmore R. Lie groups, Lie algebras, and some of their applications. New York: Wiley, 1974.
[37] Varshalovish DA, Moskalev AN, Khersonskii VK. Quantum Theory of Angular Momentum. Singapore: World Scientific, 2008.
[38] Adams BL, Lyon M, Henrie B. Microstructures by design: linear problems in elastic-plastic design. International Journal of Plasticity 2004;20:1577.

[39] Kalidindi SR, Houskamp JR, Lyons M, Adams BL. Microstructure sensitive design of an orthotropic plate subjected to tensile load. International Journal of Plasticity 2004;20:1561.
[40] Bateman H, Erdélyi A. Higher transcendental functions. New York: McGraw-Hill, 1953.
[41] Gradshtein IS, Ryzhik IM, Jeffrey A. Table of integrals, series, and products. San Diego: Academic Press, 2000.
[42] Gel'fand IM, Minlos RA, Shapiro ZY. Representations of the rotation and Lorentz groups and their applications. Oxford, New York: Pergamon Press; [distributed in the Western Hemisphere by Macmillan, 1963.
[43] Robinson AC. On the Use of Quaternions in Simulation of Rigid-Body Motion. WADC Technical Report 1958;58-17.
[44] Vilenkin NJ. Special functions and the theory of group representations. Providence: American Mathematical Society, 1968.
[45] Rose ME. Elementary theory of angular momentum. New York: Dover, 1995.
[46] Biedenharn LC, Louck JD. Angular momentum in quantum physics : theory and application. Reading, Mass.: Addison-Wesley Pub. Co., Advanced Book Program, 1981.
[47] Mason JK, Schuh CA. Hyperspherical harmonics for the representation of crystallographic texture. Acta Mater 2008;56:6141.
[48] Fock V. On the Theory of the Hydrogen Atoms. Z Phys 1935;98:145.
[49] Biedenharn LC. Wigner Coefficients for the R4 Group and Some Applications. J Math Phys 1961;2:433.
[50] Bander M, Itzykson C. Group Theory and the Hydrogen Atom (I). Rev Mod Phys 1966;38:330.
[51] Müller C. Spherical harmonics. Berlin, New York,: Springer-Verlag, 1966.
[52] Domokos G. Four-Dimensional Symmetry. Phys Rev 1967;159:1387.
[53] Hicks HR, Winternitz P. Relativistic Two-Variable Expansions for Three-Body Decay Amplitudes. Phys Rev D 1971;4:2339.
[54] Kalnins EG, Miller W, Winternitz P. Group O(4), Separation of Variables and Hydrogen-Atom. SIAM Journal on Applied Mathematics 1976;30:630.
[55] Avery J, Wen ZY. Angular Integrations in M-Dimensional Spaces and Hyperspherical Harmonics. International Journal of Quantum Chemistry 1982;22:717.
[56] Muljarov EA, Yablonskii AL, Tikhodeev SG, Bulatov AE, Birman JL. Hyperspherical theory of anisotropic exciton. J Math Phys 2000;41:6026.
[57] Santos MB, Ferreira PL. Gradient Formula for the Four-Dimensional Hyperspherical Harmonics. Rev Bras Fis 1975;5:61.
[58] Hanson A. Visualizing quaternions. San Francisco: Morgan Kaufmann, 2005.
[59] Meremianin AV. Multipole expansions in four-dimensional hyperspherical harmonics. Journal of Physics a-Mathematical and General 2006;39:3099.
[60] Kumar A, Dawson PR. Modeling crystallographic texture evolution with finite elements over neo-Eulerian orientation spaces. Computer Methods in Applied Mechanics and Engineering 1998;153:259.

[61] Mason JK. The Relationship of the Hyperspherical Harmonics to SO(3), SO(4) and the Orientation Distribution Function. Acta Cryst A. Cambridge, MA: Massachusetts Institute of Technology, 2009.
[62] Varshalovich DA, Moskalev AN, Khersonskii VK. Representation of the Rotation Group in Terms of the Variables ω, n(θ, ϕ). Bulletin of the Academy of Sciences of the USSR. Physical Series 1974;38:1711.
[63] Varshalovich DA, Moskalev AN, Khersonskii VK. Quantum Theory of Angular Momentum. Singapore: World Scientific, 2008.
[64] Alper JS. Analytical evaluation of multicenter molecular integrals. I. Two-center overlap and two-center coulombic integrals over hydrogenic orbitals of integral principal quantum number. J Chem Phys 1971;55:3770.
[65] Racah G. Four Dimensional Orthogonal Groups. Supplemento al Volume XIV, Serie X del Nuovo Cimento 1959;1:75.
[66] Roman P. Theory of elementary particles. Amsterdam: North-Holland Pub. Co., 1961.
[67] Sharp RT. Notes on O(4) Representations. J Math Phys Camb 1968;47:359.
[68] Dolginov AZ. Relativistic Spherical Functions. Sov Phys JEPT 1956;3:589.
[69] Emren F, Vonschlippenbach U, Lucke K. Investigation of the Development of the Recrystallization Textures in Deep Drawing Steels by Odf Analysis. Acta Metall 1986;34:2105.
[70] Clark JB, Garrett RK, Jungling TL, Vandermeer RA, Vold CL. Effect of Processing Variables on Texture and Texture Gradients in Tantalum. Metall Trans A 1991;22:2039.
[71] Nakamachi E, Xie CL, Morimoto H, Morita K, Yokoyama N. Formability assessment of FCC aluminum alloy sheet by using elastic/crystalline viscoplastic finite element analysis. International Journal of Plasticity 2002;18:617.
[72] Proust G, Kalidindi SR. Procedures for construction of anisotropic elastic-plastic property closures for face-centered cubic polycrystals using first-order bounding relations. J Mech Phys Solids 2006;54:1744.
[73] Bunge HJ. Einige Bemerkungen zur Symmetrie verallgemeinerter Kugelfunktionen. Mber Dt Akad Wiss 1965;7:351.
[74] Roe R-J. Description of Crystallite Orientation in Polycrystalline Materials. III. General Solution to Pole Figure Inversion. Journal of Applied Physics 1965;36:2024.
[75] Zhao JW, Adams BL. Definition of an Asymmetric Domain for Intercrystalline Misorientation in Cubic Materials in the Space of Euler Angles. Acta Cryst A 1988;44:326.
[76] Knapp AW. Representation theory of semisimple groups, an overview based on examples. Princeton, N.J.: Princeton University Press, 1986.
[77] Dahms M, Bunge HJ. A Positivity Method for the Determination of Complete Orientation Distribution-Functions. Texture Microstruct 1988;10:21.
[78] Dahms M, Bunge HJ. The Iterative Series-Expansion Method for Quantitative Texture Analysis .1. General Outline. Journal of Applied Crystallography 1989;22:439.
[79] Wagner F, Humbert M, Muller J, Esling C. Optimization of the Positivity Method in Quantitative Texture Analysis. Europhysics Letters 1990;11:479.

[80] Vanhoutte P. The Use of a Quadratic Form for the Determination of Non-Negative Texture Functions. Texture Microstruct 1983;6:1.
[81] Vanhoutte P. A Method for the Generation of Various Ghost Correction Algorithms - the Example of the Positivity Method and the Exponential Method. Texture Microstruct 1991;13:199.
[82] Schaeben H. Entropy Optimization in Quantitative Texture Analysis. Journal of Applied Physics 1988;64:2236.
[83] Wang F, Xu JZ, Liang ZD. Determination of the Odf of Hexagonal Symmetry Materials According to the Maximum-Entropy Method. Texture Microstruct 1989;10:217.
[84] Schaeben H. Entropy Optimization in Quantitative Texture Analysis .2. Application to Pole-to-Orientation Density Inversion. Journal of Applied Physics 1991;69:1320.
[85] Wang F, Xu JZ, Liang ZD. Determination of the Complete Odf of Cubic System Materials by the Maximum-Entropy Method. Texture Microstruct 1992;19:55.
[86] Altmann SL, Cracknell AP. Lattice Harmoncs I. Cubic Groups. Rev Mod Phys 1965;37:19.
[87] Mueller FM, Priestley MG. Inversion of Cubic de Hass-van Alphen Data, with an Application to Palladium. Phys Rev 1966;148:638.
[88] Altmann SL, Herzig P. Point-group theory tables. New York: Clarendon Press, 1994.
[89] Dillamore IL, Roberts WT. Preferred Orientation in Wrought and Annealed Metals. Metallurgical Reviews 1965;10:271.
[90] Mackenzie JK. Second Paper on Statistics Associated with the Random Disorientation of Cubes. Biometrika 1958;45:229.
[91] Hilgenkamp H, Mannhart J. Grain boundaries in high-T-c superconductors. Rev Mod Phys 2002;74:485.
[92] Roberts CG, Semiatin SL, Rollett AD. Particle-associated misorientation distribution in a nickel-base superalloy. Scripta Materialia 2007;56:899.
[93] Dalla Torre FH, Gazder AA, Gu CF, Davies CHJ, Pereloma EV. Grain size, misorientation, and texture evolution of copper processed by equal channel angular extrusion and the validity of the hall-petch relationship. Metallurgical and Materials Transactions a-Physical Metallurgy and Materials Science 2007;38A:1080.
[94] Kang JY, Bacroix B, Regle H, Oh KH, Lee HC. Effect of deformation mode and grain orientation on misorientation development in a body-centered cubic steel. Acta Mater 2007;55:4935.
[95] Grimmer H. Distribution of Disorientation Angles If All Relative Orientations of Neighboring Grains Are Equally Probable. Scripta Metall Mater 1979;13:161.
[96] Morawiec A. Misorientation-Angle Distribution of Randomly Oriented Symmetrical Objects. Journal of Applied Crystallography 1995;28:289.
[97] Frary M, Schuh CA. Percolation and statistical properties of low- and high-angle interface networks in polycrystalline ensembles. Phys Rev B 2004;69:134115.
[98] Van Siclen CD. Intergranular fracture in model polycrystals with correlated distribution of low-angle grain boundaries. Phys Rev B 2006;73:184118.

[99] Gertsman VY, Zhilyaev AP, Pshenichnyuk AI, Valiev RZ. Modeling of Grain-Boundary Misorientation Spectrum in Polycrystals with Crystallographic Texture. Acta Metall Et Mater 1992;40:1433.
[100] Garbacz A, Grabski MW. The Relationship between Texture and Csl Boundaries Distribution in Polycrystalline Materials .1. The Grain-Boundary Misorientation Distribution in Random Polycrystal. Acta Metall Et Mater 1993;41:469.
[101] Zhilyaev AP, Gertsman VY, Mishin OV, Pshenichnyuk AI, Aleksandrov IV, Valiev RZ. Grain-Boundary Misorientation Spectra (Gbms) Determined by Real Odf in Fcc-Materials Susceptible to Annealing Twinning. Acta Metall Et Mater 1993;41:2657.
[102] Zuo L, Watanabe T, Esling C. A Theoretical Approach to Grain-Boundary-Character-Distribution (Gbcd) in Textured Polycrystalline Materials. Zeitschrift Fur Metallkunde 1994;85:554.
[103] Morawiec A, Szpunar JA, Hinz DC. Texture Influence on the Frequency of Occurrence of Csl-Boundaries in Polycrystalline Materials. Acta Metall Et Mater 1993;41:2825.
[104] Zhao J, Adams BL, Morris PR. A Comparison of Measured and Texture-Estimated Misorientation Distributions in Type 304 Stainless Steel Tubing. Texture Microstruct 1988;8 & 9:493.
[105] Bunge HJ, Weiland H. Orientation Correlation in Grain and Phase Boundaries. Texture Microstruct 1988;7:231.
[106] Mishin OV, Gertsman VY, Gottstein G. Distributions of orientations and misorientations in hot-rolled copper. Mater Charact 1997;38:39.
[107] Mason JK, Schuh CA. Correlated grain-boundary distributions in two-dimensional networks. Acta Cryst A 2007;63:315.
[108] Warrington DH, Boon M. Ordered Structures in Random Grain-Boundaries - Some Geometrical Probabilities. Acta Metall 1975;23:599.
[109] Brandon DG. The Structure of High-Angle Grain Boundaries. Acta Metall 1966;14:1479.
[110] Racah G. Theory of Complex Spectra. II. Phys Rev 1942;62:438.
[111] Roe R-J. Inversion of Pole Figures for Materials Having Cubic Crystal Symmetry. Journal of Applied Physics 1966;37:2069.
[112] Haessner F, Pospiech J, Sztwiertnia K. Spatial Arrangement of Orientations in Rolled Copper. Mater Sci Eng 1983;57:1.
[113] Mackenzie JK, Thomson MJ. Some Statistics Associated with the Random Disorientation of Cubes. Biometrika 1957;44:205.
[114] Mackenzie JK. The Distribution of Rotation Axes in a Random Aggregate of Cubic Crystals. Acta Metall 1964;12:223.
[115] Adams BL, Zhao J, Grimmer H. Discussion of the Representation of Intercrystalline Misorientation in Cubic Materials. Acta Cryst A 1990;46:620.
[116] Hilliard JE. Specification and Measurement of Microstructural Anisotropy. T Metall Soc AIME 1962;224:1201.
[117] Philofsky EM, Hilliard JE. On the Measurement of the Orientation Distribution of Lineal and Areal Arrays. Q Appl Math 1969;27:79.
[118] Adams BL, Field DP. Measurement and Representation of Grain-Boundary Texture. Metall Trans A 1992;23:2501.

[119] Saylor DM, Morawiec A, Rohrer GS. Distribution of grain boundaries in magnesia as a function of five macroscopic parameters. Acta Mater 2003;51:3663.
[120] Saylor DM, Morawiec A, Rohrer GS. The relative free energies of grain boundaries in magnesia as a function of five macroscopic parameters. Acta Mater 2003;51:3675.
[121] Saylor DM, El Dasher BS, Rollett AD, Rohrer GS. Distribution of grain boundaries in aluminum as a function of five macroscopic parameters. Acta Mater 2004;52:3649.
[122] Saylor DM, El Dasher B, Pang Y, Miller HM, Wynblatt P, Rollett AD, Rohrer GS. Habits of grains in dense polycrystalline solids. J Am Ceram Soc 2004;87:724.
[123] Saylor DM, El Dasher B, Sano T, Rohrer GS. Distribution of grain boundaries in SrTiO3 as a function of five macroscopic parameters. J Am Ceram Soc 2004;87:670.
[124] Adams BL. Description of the Intercrystalline Structure Distribution in Polycrystalline Materials. Metall Trans A 1986;17:2199.
[125] Zhao JW, Koontz JS, Adams BL. Intercrystalline Structure Distribution in Alloy 304 Stainless-Steel. Metall Trans A 1988;19:1179.
[126] Morris PR, Zhao JW, Adams BL. Intercrystalline Structure Distribution in Polycrystalline Materials. Metall Trans A 1988;19:2611.
[127] Pan Y, Adams BL. On the CSL Grain-Boundary Distributions in Polycrystals. Scripta Metallurgica Et Materialia 1994;30:1055.
[128] Adams BL. Orientation Imaging Microscopy - Application to the Measurement of Grain-Boundary Structure. Materials Science and Engineering a-Structural Materials Properties Microstructure and Processing 1993;166:59.
[129] Adams BL, Wright SI, Kunze K. Orientation Imaging - the Emergence of a New Microscopy. Metall Trans A 1993;24:819.
[130] Miyazawa K, Iwasaki Y, Ito K, Ishida Y. Combination rule of Sigma values at triple junctions in cubic polycrystals. Acta Cryst A 1996;52:787.
[131] Miyazawa K, Ito K, Ishida Y. Branching rule of coincidence boundaries in cubic polycrystals. Mater Sci Forum 1996;207-209:301.
[132] Minich RW, Schuh CA, Kumar M. Role of topological constraints on the statistical properties of grain boundary networks. Phys Rev B 2002;66:052101.
[133] Frary M, Schuh CA. Combination rule for deviant CSL grain boundaries at triple junctions. Acta Mater 2003;51:3731.
[134] Reed BW, Kumar M. Mathematical methods for analyzing highly-twinned grain boundary networks. Scripta Materialia 2006;54:1029.
[135] Kumar M, King WE, Schwartz AJ. Modifications to the microstructural topology in f.c.c. materials through thermomechanical processing. Acta Mater 2000;48:2081.
[136] Gertsman VY. Geometrical theory of triple junctions of CSL boundaries. Acta Cryst A 2001;57:369.
[137] Gertsman VY. Coincidence site lattice theory of multicrystalline ensembles. Acta Cryst A 2001;57:649.

[138] Gertsman VY. On the auxiliary lattices and dislocation reactions at triple junctions. Acta Cryst A 2002;58:155.
[139] Frary M, Schuh CA. Nonrandom percolation behavior of grain boundary networks in high-T-c superconductors. Appl Phys Lett 2003;83:3755.
[140] Schuh CA, Kumar M, King WE. Analysis of grain boundary networks and their evolution during grain boundary engineering. Acta Mater 2003;51:687.
[141] Schuh CA, Kumar M, King WE. Connectivity of CSL grain boundaries and the role of deviations from exact coincidence. Zeitschrift Fur Metallkunde 2003;94:323.
[142] Schuh CA, Minich RW, Kumar M. Connectivity and percolation in simulated grain-boundary networks. Philosophical Magazine 2003;83:711.
[143] Frary M, Schuh CA. Grain boundary networks: Scaling laws, preferred cluster structure, and their implications for grain boundary engineering. Acta Mater 2005;53:4323.
[144] Frary M, Schuh CA. Connectivity and percolation behaviour of grain boundary networks in three dimensions. Philosophical Magazine 2005;85:1123.
[145] Schuh CA, Frary M. Correlations beyond the nearest-neighbor level in grain boundary networks. Scripta Materialia 2006;54:1023.
[146] Read W, Shockley W. Dislocation Models of Crystal Grain Boundaries. Phys Rev 1950;78:275.
[147] Strang G. Linear algebra and its applications. Belmont, CA: Thomson, Brooks/Cole, 2006.
[148] Kumar M, Schwartz AJ, King WE. Microstructural evolution during grain boundary engineering of low to medium stacking fault energy fcc materials. Acta Mater 2002;50:2599.
[149] Schuh CA, Kumar M, King WE. Universal features of grain boundary networks in FCC materials. J Mater Sci 2005;40:847.